UiT The Arctic University of Norway

Faculty of Engineering Science and Technology

Mathematical modelling of bioenergy systems for stability analysis and parametric sensitivity

Subhashis Das

A dissertation for the degree of Philosophiae Doctor; August 2020

Acknowledgement

I would like to take this opportunity to convey my sincere gratitude and deep regards to Prof Rajnish Kaur Calay, Department of Building, Energy and Material Technology and Prof Ranjana Chowdhury, Chemical Engineering Department, Jadavpur University for their constant advice, encouragement and support that they have provided me with throughout my study, and make it possible for me to shape this thesis in the present form.

I would like to extend my sincere gratitude to the Norwegian Government Quota scholarship for their financial assistance

My sincere thanks go to all my fellow scholars for their continuous support and help during the whole research period. I am also thankful to the Staff Members of the Department of Building, Energy and Material Technology, for their constant help throughout my study.

Above all, I am sincerely thankful to my parents, my wife, my sister and all other members of my family for their constant support and encouragement throughout the entire course of my research work.

Last but not least, I want to thank God for showing me the right direction.

Abstract

This thesis presents a research study on bioreactor design and biochemical processes for conversion of biomass into bioenergy and develops mathematical models that can be used for designing better reactors and control systems. Good design of the bioreactors and understanding of the biochemical process is essential to control the process for maximizing the yield. Improving the performance efficiency of bioreactors is necessary for large-scale biomass deployment to energy conversion systems and their economic viability.

Large scale production mostly deploys continuous stirred tank bioreactors (CSTBR) involving single, or polycultures. Many micro-environmental parameters in the reactor such as system pH, dilution rate, inlet substrate concentration etc. simultaneously affect the process and also the production of the desired output. Due to concurrent influence on many variable-limits, the process has multiple steady states, and the slight variation in one parameter leads to deviation from a steady-state operation and microbial growth is affected reactor may stall.

Bioprocesses within these reactors can be expresses as a set of nonlinear equations. The output variables (e.g. bioenergy products; gaseous or liquids) depend simultaneously upon a parametric range of a number of input variables such as pH, dilution rate, temperature, substrate concentration etc. It may be inferred that the biosystems are parametrically sensitive with respect to specific parameters. Thus, the sensitivity of a biosystem is studied for understanding the operation of a reactor. From the process engineering perspective, it is a challenge to determine a priori region of parametric sensitivity, i.e., to determine the set of values of system parameters beyond which the biosystem becomes highly sensitive.

Kinetics constants for the mathematical model need to be determined experimentally. Thus the experiments were performed using two types of lactic acid bacteria, namely, *Pediococcus acidilactici* and *Lactobacillus casei* using the batch reactor to find the optimum pH for microbial growth and other kinetic variables that define microbial growth characteristics. From the experiments, the kinetic constants for both bacteria strains were found. The maximum specific growth rate (μ_{max}) and substrate saturation constant (K_s) provide the guideline for a working range of feed stream flow rate and its concentration for designing continuous processes. For *Pediococcus acidilactici*, the optimum pH value, maximum specific growth rate (μ_{max}) and substrate saturation constant (k_s) to be 6.7, 1.0775 h^{-1} and 4.5017gL^{-1}, respectively. The kinetic constants for *Lactobacillus casei*, the optimum value of pH, maximum specific growth rate (μ_{max}) and substrate saturation constant (K_S) were found to be 6.75, 0.6 h^{-1} and 0.814gL^{-1}, respectively. Although both the strains are LAB and their optimum pH are quite similar, other kinetic parameters are different.

When the product is gaseous such as methane or hydrogen, that itself can retard the growth of bacteria and its own production if allowed to accumulate in the reactor headspace. In order to study the effect of accumulated hydrogen on the process in a reactor, the third series of batch experiments were conducted by using a hydrogen-producing bacteria, *Clostridium acetobutylicum*. From these experiments, the maximum specific microbe growth rate (μ_{max}), substrate saturation constant (k_s), a critical hydrogen concentration at which growth ceased (H_2^*) were determined, 0.976 h^{-1}, 0.63 ± 0.01 g/L, and 24.74 mM, respectively. The degree of inhibition was 0.4786.

Two models based on a set of ordinary differential equations were developed to derive a dimensionless multiplicity criterion, ω, that indicates a set of values of input parameters corresponding to multiple steady states in a reactor. Using the kinetic variables obtained experimentally model can quantitatively predicting the parametric range of operating variables for steady operation of the process and optimal yield for a reactor

Parametric sensitivity of pH with respect to input variables specifically dilution rates and concentrations of nutrient and alkali stream for pH control in the regions of multiple and unique steady states in a CSTBR was determined using the mathematical model. The parametric sensitivity of pH was observed over the entire region of operation under study, and the model estimation was in agreement with those of the experimental observations.

The first model studied the nonlinear behaviour of a CSTBR using *Lactobacillus casei*. Parameter space was determined where the system exhibits sensitive behaviour through normalized objective sensitivity. Parametric range of inputs for controlling optimal pH range conducive for the microbial growth was determined. The influence of input parameters, which are directly intricate pH of the system, is observed by determining normalized objective sensitivity of pH. A generalized criterion, i.e., a specific range of certain input parameters, e.g., θ, R and pH_0 corresponding to the system's maximum sensitivity was determined.

The second mathematical model studied the reactor process for producing biohydrogen. The multiplicity analysis of steady states was determined using the classical theory of bifurcation analysis with the help of local stability analysis. It was found that in a particular range of d_1 (a dimensionless form of dilution rate of feed stream), from 0.44 to 0.4453, the CSTBR operation becomes unstable as it comes across multiple steady states condition. On the other hand, CSTBR enters to instability due to another essential operating parameter X_{20} (a dimensionless form of feed substrate concentration) when the operating region of X_{20} within 9.5717 to 13.658 where steady-states of CSTBR system bifurcated to multiple steady states.

The present study also endorses some scope for further research works, such as more output variables namely, temperature, the concentration of byproducts needing to be analysed for designing and safe operation of a continuous stirred tank bioreactors. In the case of biohydrogen production, there are other metabolites such as volatile fatty acids (VFA) produce along with the hydrogen can alter the system pH, which can be unfavourable for microorganisms and shift the metabolic pathway of microbial reactions. So, the influence of the concentration of VFA and adopt a kinetic model is recommended to study further. The validation of the model-predicted data with the experimental study shows the critical value of input parameters for which the CSTBR becomes sensitive. The interaction between input parameters or the points corresponding to the limits of the region of instability is recommended to be investigated. Moreover, the impact of model kinetic parameters on system stability is the scope where further work is suggested.

The mathematical models presented in this thesis can be used to investigate the operation of similar processes in CSTBRs. Using the kinetic parameters, relevant to different microbial growth, the developed model can be used to perform a stability analysis of a CSBTR and obtain parametric sensitivity regions of the process. Such quantitative analysis of CSTBRs will benefit in selecting design and adopting strategies for safe, controlled and economical utilization of CSTBRs. The information

obtained from the present research study contributes to the general field of bioenergy conversion processes and the design and optimization of bioreactors, such as the production of biomethanol ethanol and biohydrogen.

List of symbols

A, B	constant of equation 2.14
C	inhibitor concentration, (gL^{-1})
C_{crit}	critical inhibitor concentration, (gL^{-1})
D	dilution rate, (h^{-1})
D_1	the dilution rate for the base feed stream, (h^{-1})
H	cumulative value for substate degradation, (h^{-1})
H_2^*	critical molar concentration of hydrogen at which microbial reaction ceases, (M)
H_{max}	maximum cumulative value for substate degradation, (h^{-1})
K	overall mass transfer coefficient
K_a, K_b	constants of equation 2.13
K_C	constant, (gL^{-1})
K_d	biomass decay constant, (h^{-1})
K_I	inhibition constant, (gL^{-1})
Ks	Monod constant or substrate saturation constant, (gL^{-1})
N	number of bacterial cell
P	product concentration, (gL^{-1})
R_{max}	maximum rate, (h^{-1})
S	substrate concentration, (gL^{-1})
S_0	initial substrate concentration, (gL^{-1})
S_{crit}	critical substrate concentration, (gL^{-1})
X	dry cell biomass concentration (gL^{-1})
X_{max}	maximum biomass concentration, (gL^{-1})
X_0	initial biomass concentration, (gL^{-1})
X_{20}	dimensionless form of feed substrate concentration
$Y_{P/X}$	product yield coefficient, (gg^{-1})
$Y_{X/S}$	biomass yield coefficient, (gg^{-1})
a, b, c	constant of the polynomial equation 2.12
k_c	apparent specific growth rate, (h^{-1})
m	degree of substrate inhibition
n	degree of cell inhibition
p	molar concentrations lactic acid
r_c	microbial growth rate, ($gL^{-1}h^{-1}$)
s_A	molar concentrations of sodium lactate
s_b	regulate the rate of neutralization of the acid

t	time, (h)
β	non-growth-associated product yield coefficient
μ	specific growth rate (h^{-1})
μ_{max}	maximum specific growth rate of cells, (h^{-1})
υ_0	reaction rate in the absence of inhibitor
υ_i	reaction rate in the presence of inhibitor
ϕ	vector containing the m system input parameters
ϕ_i	one element of the parameter vector, $\boldsymbol{\phi}$
λ	lag time, (h)
$_{obs}$	experimentally observed value

Table of Contents

Acknowledgement ii

Abstract iii

List of symbols vi

1 Introduction 1

1.1 Bioenergy 1

1.2 Bioprocesses 2

1.3 Bioreactors 3

1.3.1 Bioreactor design 5

1.4 Stability analysis and parametric sensitivity 5

1.5 Research Gaps 6

1.6 Aim 7

1.7 Thesis organization 7

2 Literature Review 8

2.1 Stability analysis of bioreactors 8

2.2 Influence of pH 11

2.2.1 Bioethanol production process 11

2.2.2 Biohydrogen production process 12

2.3 Effects of partial pressure 13

2.4 Kinetic models 13

2.4.1 Kinetic models describing the progress of the fermentation process 14

2.4.2 Kinetic models describing substrate inhibitions 15

2.4.3 Kinetic models describing product inhibitions 16

2.4.4 Kinetic models describing the effects of pH 17

2.4.5 Kinetic models describing the effect of dilution rates 18

2.4.6 Kinetic models describing the relationship among the substrate degradation, microbial growth and product formation rate 19

2.5 Gaps in existing knowledge & objectives 20

2.6 Objectives 21

3 Methodology 22

3.1 Theoretical background 22

3.1.1 Calculation of microbial growth rate 23

3.1.2 Microbial growth kinetics 23

3.2 Mathematical modelling of CSTBRs 28

3.2.1 Modelling of CSTBR 28

3.2.2 Stability analysis 30

3.3 Sensitivity analysis 32
3.3.1 Local sensitivity 33
3.3.2 Objective sensitivity 34
3.3.3 Computation of sensitivities 35
3.4 Nonlinear system analysis: Bifurcation theory 36
3.4.1 Saddle-node bifurcation: 36
3.4.2 Transcritical bifurcation (flip bifurcation): 37
3.4.3 Pitchfork bifurcation: 37
3.4.4 Fold bifurcation: 37
3.5 Experimental details 39
3.5.1 Chemicals 39
3.5.2 Microorganisms 40
3.5.3 Equipment 40
3.5.4 Preparation of seed culture 41
3.6 Analytical methods 42
3.6.1 Spectrophotometry 42
3.6.2 DNS method 42
3.6.3 GC- FID 43
3.6.4 HPLC 43
3.7 Experimental method 43
3.7.1 Batch experiments to examine pH influence on microbial growth 43
3.7.1 CSTBR operation 45
3.8 Case Studies 46
4 Case studies results and discussions 47
4.1 Case 1: Parametric sensitivity of pH and steady-state multiplicity in CSTBR 47
4.1.1 Determination of Growth Kinetics 47
4.1.2 Biochemical reactions in the CSTBR 48
4.1.3 Mathematical model for CSTBR for pH control 48
4.1.4 Generalized criterion for multiplicity 50
4.1.5 Theoretical parametric sensitivity analysis 52
4.1.6 Results 53
4.1.7 Discussion 69
4.2 Case 2: Parametric sensitivity of CSTBRs for *lactobacillus casei*: Normalized sensitivity analysis 71
4.2.1 Normalized objective sensitivity analysis 72
4.2.2 Calculation of sensitivities 73
4.2.3 Results 74
4.2.4 Discussions 81

4.3 Case 3: Kinetic modelling for determining inhibitory effects of products in the biohydrogen production process 83
4.3.2 Discussion 90
4.4 Case 4: Stability analysis of the biohydrogen production in a continuous bioreactor 93
4.4.1 Process model 93
4.4.2 Results and discussions 96
5 Conclusions 104
5.1 Microbial growth kinetics 104
5.2 Mathematical modelling and stability analysis 105
5.3 Parametric sensitivity analysis 105
5.4 General conclusions 106
5.5 Recommendations for further work 106
References 108
Appendix 1 116
List of papers 116
Appendix 2 161
Appendix 3 166

List of Tables

Table 1-1 Conversion technologies for biomass to biofuel 2
Table 3-1 Nature of Stability 32
Table 3-2 DeMan, Rogosa and Sharpe (MRS) media composition in 100mL solution 39
Table 3-3 Cooked meat (CM) medium in 100mL solution 40
Table 3-4 Chemicals used for DNS methods 40
Table 3-5 List of equipments used for experiments 41
Table 3-6: Details of case studies and corresponding objectives 46
Table 4-1 Definitions of the dimensionless variable used in the model 50
Table 4-2 Values of observed rate constants from experiments 57
Table 4-3 Values of kinetic parameters 58
Table 4-4 Summary of the results obtained from the present study 59
Table 4-5 Initial conditions for experiments on parametric sensitivity 60
Table 4-6 Definition of dimensionless variables 71
Table 4-7 Expressions of σi for various parameters ϕi, as defined in equation (4.57) 74
Table 4-8 Values of observed rate constants from experiments 75
Table 4-9 Values of kinetic parameters 76
Table 4-10 Different Critical values of input Parameters (From Figure 4-31 to 4-36) 81
Table 4-11 Values of observed rate constants from experiments 90
Table 4-12 Effects of added hydrogen on the specific growth rate, hydrogen production 91
Table 4-13 Values of kinetic and operating constants 94
Table 4-14 Definition of dimensionless variables 95
Table 4-15 Initial conditions and model parameters of equations 4.64 to 4.68 96

List of Figures

Figure 2-1 A curve for modified Gompertz model 15
Figure 2-2 A curve for modified Han-Levenspiel model 17
Figure 2-3 A curve for the Andrew model 18
Figure 3-1 Microbial growth curve 22
Figure 3-2 Variation of $\mu_{max,N}$ with respect initial pH 25
Figure 3-3 Evaluation procedure of $\mu_{max,obs}$ and $k_{s,obs}$ at various concentration of inhibitor 27
Figure 3-4 Evaluation procedure of u_{max}, n and H_2* for product inhibition 27
Figure 3-5 Schematic of Continuous Stirred tank bioreactor 29
Figure 3-6 Example of Saddle Node bifurcation, Stable (solid line), Unstable branch (dotted line) 36
Figure 3-7 Example of Transcritical bifurcation, Stable branch (solid line), Unstable branch (dotted line) 37
Figure 3-8 Example of Pitchfork bifurcation, Stable branch (solid line), Unstable branch (dotted line) 37
Figure 3-9 Example of Fold bifurcation, Stable branch (solid line), Unstable branch (dotted line) 39
Figure 3-10 Experimental setups for batch test (a); schematic diagram of the experimental setup (b) 44
Figure 3-11 The flow-sheet of the reactor set up 45
Figure 4-1 Schematic of a Continuous Stirred Tank Bioreactor 49
Figure 4-2 Experimental time histories of dry cell concentration (g/L) at an initial value of pH=4 53
Figure 4-3 Experimental time histories of dry cell concentration (g/L) at an initial value of pH=5 54
Figure 4-4 Experimental time histories of dry cell concentration (g/L) at an initial value of pH=6 55
Figure 4-5 Experimental time histories of dry cell concentration (g/L) at an initial value of pH=7 55
Figure 4-6 Experimental time histories of dry cell concentration (g/L) at an initial value of pH=8 56
Figure 4-7 Determination of μ_{max}, and k_s at different initial pH 57
Figure 4-8 Variation of normalized $\mu_{max,N}$ with initial pH 58
Figure 4-9 Time trajectories of Sensitivity variables, $S_{\varphi i}$ 59
Figure 4-10 Simulated (lines) and experimental (Points) time histories of pH in the region of multiplicity with D as a parameter 61
Figure 4-11: Simulated (lines) and experimental (Points) time histories of pH in the region of uniqueness with D as a parameter 61
Figure 4-12 Simulated (lines) and experimental (Points) time histories of pH in the region of multiplicity with D_1 as a parameter 62
Figure 4-13 Simulated (lines) and experimental (Points) time histories of pH in the region of uniqueness with D_1 as a parameter 63
Figure 4-14 Simulated (lines) and experimental (Points) time histories of pH in the region of multiplicity with sb as a parameter 63
Figure 4-15 Simulated (lines) and experimental (Points) time histories of pH in the region of uniqueness with s_b as a parameter 64
Figure 4-16 Time histories of all theoretical sensitivity variables in the region of multiplicity at D_1 =0.0045h^{-1} (D=0.1 h^{-1}; s_b = 0.008M) 65
Figure 4-17 Time histories of all theoretical sensitivity variables in the region of multiplicity at D_1 =0.0055h^{-1} (D=0.1 h^{-1}; s_b = 0.008M) 65
Figure 4-18 Time histories of theoretical sensitivity variable with respect to D in the region of multiplicity at D_1 =0.0045h^{-1} and D_1 =0.0055h^{-1} 66

Figure 4-19 Time histories of theoretical sensitivity variable with respect to D_1 in the region of multiplicity at D_1 =0.0045$h^{-1}$and D_1 =0.0055h^{-1} 66
Figure 4-20 Time histories of theoretical sensitivity variable with respect to sb in the region of multiplicity at D_1 =0.0045h^{-1} (D=0.1h^{-1}; s_b = 0.008M) and D_1 =0.0055h^{-1} (D=0.1h^{-1}; s_b = 0.008M).... 67
Figure 4-21 Time histories of all theoretical sensitivity variables in the region of uniqueness at D_1 =0.06h^{-1} (D=0.1h^{-1}; s_b = 0.002M) 67
Figure 4-22 Time histories of all theoretical sensitivity variables in the region of uniqueness at D_1 =0.065h^{-1} (D=0.1h^{-1}; s_b = 0.002M) 68
Figure 4-23 Determination of μ_{max} and k_s at different initial pH 75
Figure 4-24 Variation of $\mu_{max.N}$ with respect to initial pH 76
Figure 4-25 Normalized objective sensitivities S(γ*,ϕ_i) as a function of θ 77
Figure 4-26 Normalized objective sensitivities S(γ*,ϕi) as a function of R 77
Figure 4-27 Normalized objective sensitivities S(γ*,ϕi) as a function of pH_0 78
Figure 4-28 Normalized objective sensitivity S(γ*, θ) as a function of parameters R and θ. 78
Figure 4-29 Normalized objective sensitivity S(γ*, θ) as a function of parameters R and θ. 79
Figure 4-30 Normalized objective sensitivity S(γ*, R) as a function of parameters R and θ..... 79
Figure 4-31 Normalized objective sensitivity S(γ*, R) as a function of parameters R and pH_0. 80
Figure 4-32 Normalized objective sensitivity S(γ*, pH_0) as a function of parameters R and pH_0. 80
Figure 4-33 Normalized objective sensitivity S(γ*, pH_0) as a function of parameters pH_0 and θ..... 81
Figure 4-34 Experimental time histories of dry cell concentration with initial 0% H_2 in reactor headspace at different substrate concentration. 83
Figure 4-35 Experimental time histories of hydrogen concentration with an initial 0% H_2 in reactor headspace at different substrate concentration. 84
Figure 4-36 Experimental time histories of dry cell concentration with an initial 10% H_2 in reactor headspace at different substrate concentrations 84
Figure 4-37 Experimental time histories of hydrogen concentration with an initial 10% H_2 in reactor headspace at different substrate concentrations 85
Figure 4-38 Experimental time histories of dry cell concentration with an initial 20% H_2 in reactor headspace at different substrate concentrations 85
Figure 4-39 Experimental time histories of hydrogen concentration with an initial 20% H_2 in reactor headspace at different substrate concentrations 86
Figure 4-40 Experimental time histories of dry cell concentration with an initial 30% (v/v) H_2 in reactor headspace at different substrate concentrations 86
Figure 4-41 Experimental time histories of produced hydrogen concentration with an initial 30% (v/v) H_2 in reactor headspace at different substrate concentrations 87
Figure 4-42 Experimental time histories of dry cell concentration with an initial 40% H_2 in reactor headspace at different substrate concentrations 87
Figure 4-43 Experimental time histories of hydrogen concentration with an initial 40% H_2 in reactor headspace at different substrate concentrations 88
Figure 4-44 Experimental time histories of dry cell concentration with an initial 50% H_2 in reactor headspace at different substrate concentrations 88
Figure 4-45 Experimental time histories of hydrogen concentration with an initial 50% H_2 in reactor headspace at different substrate concentrations 89
Figure 4-46 Determination of $\mu_{max,obs}$ and $k_{s,obs}$ at different initial concentrations of H_2 89
Figure 4-47 Determination of $u_{max,\ n}$ and H_2* for product inhibition 90
Figure 4-48 Schematic of reactor setup 93

Figure 4-49 Steady-state dimensionless cell concentration (x_1) in CSTBR as function of feed stream dilution rate (d_1) at x_{20}=6 97
Figure 4-50 Steady-state dimensionless substrate concentration (x_2) in CSTBR as function of feed stream dilution rate (d_1) at x_{20}=6. 97
Figure 4-51 Steady-state dimensionless liquid phase H_2 concentration (x_3) in CSTBR as functions of feed stream dilution rate (d_1) at X_{20}=6..... 98
Figure 4-52 Steady-state dimensionless gas phase H_2 concentration (x_4) in CSTBR as functions of the dilution rate (d_1) at x_{20}=6 98
Figure 4-53 Eigenvalues of the stability matrix [Eq. (4.69)] for the steady-state solutions..... 99
Figure 4-54 Steady-state dimensionless cell concentration (x_1) in CSTBR as functions of feed substrate concentration(x_{20})at d_1=0.2..... 99
Figure 4-55 Steady-state dimensionless substrate concentration (x_2) in CSTBR as functions of feed substrate concentration(x_{20})at d_1=0.2 100
Figure 4-56 Steady-state dimensionless liquid phase H_2 concentration (x_3) in CSTBR as functions of feed substrate concentration(x_{20})at d_1=0.2..... 100
Figure 4-57 Steady-state dimensionless gas phase H_2 concentration (x_4) in CSTBR as functions of feed substrate concentration(x_{20})at d_1=0.2 101
Figure 4-58 Two parameter continuation diagrams showing the effects of initial substrate concentration (x_{20}) on the limits of the hysteresis region..... 102
Figure 4-59 Two parameter continuation diagrams showing the effects of gaseous phase dilution rate (d_2) on the limits of the hysteresis region. 103

1 Introduction

Human energy consumption can be grouped under three broad categories: heat, grid electricity, and transportation fuels until the twentieth-century humankind have been dependant primarily on fossil fuels to meet all kinds of energy demands. However, by the mid 20th century, it was widely acknowledged that the use of fossil fuels is associated with an increased level CO_2 of in the atmosphere leading to global warming and climate change. Energy consumption of energy worldwide has increased 13-fold in the twentieth century, tripling since 1960, which is faster than the increase in population size [1]. This increased consumption of fossil fuels has caused severe environmental pollution that is affecting the quality of life and health issues in urbanized worlds. Thus, alternative energy sources are needed, one for meeting the carbon emissions target to combat climate change and two to meet the increasing energy demand. Solar, wind, wave and bioenergy are alternative energy sources that are replenished on human time scale, unlike fossil fuels and are regarded as renewable energy sources.

1.1 Bioenergy

Plant sources are classified as renewable energy sources. From prehistoric times, humans burned biomass from plants and trees, to produce heat used for comfort, cooking, and in increasingly sophisticated industrial processes, such as ceramic firing to produce pottery and glass and then smelting to produce metals such as bronze and iron.

Biowaste, such as municipal solid waste, agricultural waste and forest waste is also a source of biomass, which can be biologically and chemically processed to produce bioenergy products in gaseous and liquid forms. These products can be combusted to generate electricity and heat. Thus bioenergy is an important renewable energy source. Still, there are two significant challenges for creating bioenergy: first, there must be a net energy gain during feedstock production, and second, greenhouse gas emissions from the green energy must be lower than those from fossil fuels. The targets can be met by increasing the yield of the feedstocks such as, target crops per unit land area, better collection and sorting systems of biowaste and improving the conversion technologies. The technologies should be capable of proper use of the lignocellulosic component of biomass and development of better pretreatment, extraction, and fermentation technologies to retrieve the energy captured in the biomass. The conversion technologies for biomass into energy forms are classified as first, second and third generation. Combustion and fermentation of sugars are humankind's earliest and most direct routes for obtaining bioenergy and biofuel from biomass. They have been classified as first-generation (1G) energy conversion technology, followed more complex and evolving conversion technologies, classified as second-generation (2G), third-generation (3G), and so forth (Table 1). Depending on the bioenergy feedstock and the energy processing platform (Table 1), there are three major biofuel products: bioethanol (1G and 2G), biogas (1G and 2G), and biodiesel (3G). Biogas, sometimes called synthesis gas or syngas, is currently used for electrical generation. Use of syngas to produce transportation biofuels is possible, but thus far, this technology is primarily at the demonstration and precommercial scale. Both bioethanol and biodiesel are currently used as transportation fuels. Ethanol is also an essential raw material in the chemical industry, capable of replacing petroleum. Therefore, sustainable economic production of bioethanol is particularly crucial for switching modern society from a petroleum-based to a biomass-based economy.

Table 1-1 Conversion technologies for biomass to biofuel

Biofuel Generation	Feedstock	Technology	Output
1ST Generation	Nonfood plants: lignocellulosic plants, e.g., trees & weedy grasses; sugarcane bagasse and trash	Conventional burning	Heat for steam for generating electricity
	Food crops: Starch (maize), sugar (sugarcane)	Conventional fermentation	Fermentation fuels (bioethanol, biodiesel)
2ND Generation	Nonfood crops: crop residues, plant stover sugarcane bagasse in the crop residues section	Pretreatment (physical & biological saccharification) & Fermentation	Fermentation fuels (bioethanol, biodiesel)
		Gasification & Fisher-Tropsch synthesis	Syngas, synthetic cellulosic fuels (alkanes and diesel), electrical generation
3RD Generation	Oilseed crops: (canola, oil palm, soybean), & algae	Conventional, currently existing	Biodiesel, aircraft fuel
4TH Generation	No biomass: waste CO2 in a photosynthetic reaction	Solar-to-fuel, bioengineered hydrocarbons	Liquid fuels

The critical challenge for developing the next generations of biofuels is acquiring economical feedstock. Feedstock cost contributes 80% to 90% of the final fuel price for most processes and is a serious issue to the economic viability of future generations of biofuels. There is probable space in the marketplace for all biofuel generations, with each generation broadening the feedstock and technology options and improving fuel economics and performance. Potential future biofuels, will not be based only on biomass but utilizing microorganisms, waste CO_2, sunlight, and water and therefore, will not compete with food production because they use nonarable land. Companies such as Amyris, LS9, Joule Unlimited, Algenol, and Naturally Scientific are involved in developing and deploying this 4G technology (Table 1). The electrofuels will also ultimately be classified as 4G.

1.2 Bioprocesses

Biomass conversion technologies can be broadly divided into two categories: thermochemical processes and biochemical processes. The thermochemical process is a method to convert biomass into biofuels using heat. These processes do not primarily produce useful energy directly, but under controlled temperature and oxygen conditions are employed to convert the original biomass feedstock into more valuable forms of energy carriers, such as producer gas, oils or methanol. The thermochemical processes include pyrolysis, torrefaction, combustion and gasification. These conversion processes can not be considered as energy-efficient as they need heat.

Biomass biochemical conversion technologies refer to the conversion of biomass into similar products through certain physical, chemical, and biological pretreatments. Pretreatments in the biochemical conversion technologies of biomass aim to help reach ideal conversion effects, not to produce final products, which is the essential difference between those mentioned above physical and chemical conversion of biomass.

Microbes utilize a variety of substrates (cellulose, hemicellulose, starch, glucose, xylose, etc.) to produce biofuels. By selecting different microorganisms in the biochemical conversions of biomass, different products, such as hydrogen, biogas, ethanol, acetone, butanol, organic acids (pyruvate, lactate, oxalic acid, levulinic acid, citric acid), 2,3-butanediol, 1,4-butanediol, isobutanol, xylitol, mannitol, and xanthan gum etc. can be produced [2]. Compared with other conversion technologies, biomass biochemical conversion technologies are clean and efficient. Moreover, biomass can be turned into various intermediate products by screening different enzymes or microorganisms through biochemical conversion technologies, thus providing many platform substances for the conversion of renewable materials, fuels, and chemicals. Therefore, various biochemical conversion technologies of biomass are being developed for bioenergy using multiple microbes. Different microbial cells require an optimal environment for growth within a bioreactor, which is a closed system where biological reactions take place, and microbial cell reproduction occur using enzymes or living cells as biocatalysts. Therefore, to maintain such favourable conditions for microbial growth and production of metabolites, the design and control bioreactors becomes critical in bioenergy production processes.

1.3 Bioreactors

Bioreactors are used in various biological conversion processes in a variety of fields, like food and agriculture, health and medicine. Especially closed bioreactors can provide the ideal environment for microbial growth and metabolism as well as bio-energy production. Biogas production by anaerobic digestion, hydrogen production by photo-fermentation or dark-fermentation, alcohol production by fermentation, and fatty acid production by microalgae all employ bioreactors.

Microbial biofuel conversion is a complex biochemical process that is much dependent on the configuration of a bioreactor. Microbial cells are sensitive to variations in their surroundings, and any instability is detrimental to their growth and product synthesis. The conversion process is mainly divided into an upstream treatment process that includes fermentation for microbial growth and product generation, and a downstream treatment process that provides for product purification, isolation, and collection [3]. In order to improve energy conversion efficiency, the specifications of the bioreactor should integrate not only the correct structural configuration but also precise operational control for optimized multiphase flow as well as heat and mass transfer in the reaction solution. During the microbial biofuel conversion process, product yields are affected by many factors including temperature, pH, nutrient content, organic loading rate, type of reactor, hydraulic retention time and solids retention time [4–6]. Therefore, the abovementioned environmental parameters within the bioreactors need to be maintained at near-optimal ranges to enhance microorganism growth and product accumulation and fine control of operating conditions for microorganism growth, metabolism, and product synthesis is essential for optimal production of biofuels.

Various methods are employed to control the operating environment within the reactor. For example, the pH can be maintained at suitable levels by adding buffer solutions, a thermostatic water bath can

control the temperature, and the hydraulic retention time (HRT) of wastewater can be controlled by regulating the inward feeding rate.

Research has developed various configurations of bioreactors with optimized operating conditions to maximize biofuel output [7]. So far, the most commonly used configurations include (i) conventional anaerobic reactors, such as the anaerobic sequencing batch reactor, the continuous stirred tank reactor, and the anaerobic plug-flow reactor; (ii) sludge retention reactors, such as the anaerobic contact reactor, the up-flow anaerobic sludge bed reactor, the up-flow anaerobic solid-state reactor, the anaerobic baffled reactor, and the internal circulation reactor; and (iii) anaerobic membrane reactors such as the anaerobic filter reactor, the anaerobic fluidized bed reactor, and the expanded granular sludge blanket.

The conventional anaerobic reactor is a single-tank system that utilizes the same tank for substrate treatment and fermentation [8]. All steps of microbial biofuel conversion take place in a single tank, which means that downstream treatment processes, as well as the intermediate byproducts, can have significant negative influences on the upstream treatment processes. Thus, efficient approaches to avoid the interactive effects of different reactions are essential to enhance bioreactor performance.

The configuration of sludge retention reactors is relatively complicated compared to conventional reactors. Sludge retention reactors usually contain two main components: the liquid-phase reaction module and the solid-phase recycling or gathering module. For example, the anaerobic contact reactor includes an agitated reactor module and a solid phase setting module to recycle the microorganisms. In contrast, the up-flow anaerobic sludge bed reactor contains the liquid-phase reaction module at the top of the reactor and a dense sludge bed located at the bottom of the reactor. Sludge retention reactors provide good contact between wastewater and biomass, which prevents washout of microorganisms. Sludge retention reactors are often used to process effluents containing high concentrations of suspended solids.

Anaerobic membrane reactors are constructed with a supporting membrane to enhance contact between wastewater and the bacterial microorganism. The bacterial biofilm accumulates and grows on this supporting membrane, causing a separation between bacterial biomass and the wastewater in the reactor. For example, the anaerobic filter reactor contains a filter on which the bacterial biofilm grows. In the anaerobic fluidized bed reactor, inert particles like fine sand and alumina are provided for the thin bacterial biofilm to grow on. The configurations of anaerobic membrane reactors enhance the resistance of the microbes to inhibitors, thereby improving biofuel production.

The function of conventional anaerobic reactors is to supply relatively stable operating conditions in an established temporal sequence. Owing to its simple structure, the anaerobic sequencing reactor has advantages of operational simplicity and low cost. However, the self-immobilization of the conventional anaerobic reactor is poor, and the channelling and clogging effects severe. These disadvantages limit reactor performance and biofuel conversion efficiency. The major function of sludge retention reactors is recycling of microbial biomass, thus avoiding biomass washout. These reactors rapidly achieve steady-state due to short hydraulic retention time [9]. In addition, some configurations of sludge retention reactors can have special functions. For example, in the anaerobic baffled reactor, the flow patterns of waste influents can be regulated by arranging the baffles, serving to separate acidogenesis and methanogenesis along the vertical axis of the reactor and allowing different bacterial communities to develop under independently suited conditions [10]. The function of the anaerobic membrane reactor is based on the supporting membrane material used for microbial biofilm formation, which serves to

separate influents from microbial biomass. By generating this microbial biofilm, biomass washout can be avoided, and the microbes have a longer retention time than the hydraulic retention time. As a result, the mechanical mixing and sludge settling that occur in sludge retention reactors can be avoided in anaerobic membrane reactors [11].

1.3.1 Bioreactor design

Bioreactor design is critical for various applications of biochemical engineering, including bioenergy. The design of a bioreactor includes determination of operating conditions, reactor size, mixing and mass transfer capabilities, temperature and sterility conditions, the means of feed introduction and product removal, and control of operating variables such as pH, oxygen concentration, and illumination [12]. Usually, watertight structure, high heat and mass transfer efficiency, good mixing performance, low energy investment, and high product output are essential considerations in the design of bioreactors. Presently, bioreactor design is based on empirical measures. The structural configuration of a bioreactor closely aligns with its functional advantages. For example, the leakage resistance of a bioreactor is critical when applied to biogas production.

Reactor size and shape usually influence biofuel output capacity. Increasing the size of the container can improve biofuel production to some extent, but can also cause biomass concentration gradients in the reactors, which hinders biofuel production. Bioreactors operated at low temperature are less prone to thermal instability and degradation. However, some thermophilic bacteria prefer high ambient temperatures of up to 65°C; bioreactors must maintain the standard for thermotolerance. Generated byproducts can dissolve and accumulate in the bioreactor over time, inhibiting microbial growth and metabolism. Thus, in order to maximize the efficiency of microbial biofuel conversion, bioreactor design must incorporate some mechanism to remove such byproducts quickly.

1.4 Stability analysis and parametric sensitivity

For biomass energy conversion a wide range of reactors are used depending on the requirement of different applications. Microorganisms play a vital role in case of bioreactors for biomass energy conversion. Therefore, a bioreactor needs to provide a precise environment condition to facilitate the growth of microorganism and produce metabolites. On the other hand, to perform a successful operation, different limitations occur due to complex interactions between microbe and the environment of the reactor system. Depending on the mode of operation, bioreactors are classified as batch, fed-batch and continuous type bioreactors. In the case of batch and fed-batch bioreactors, a proper operative environment is achieved by attaining a suitable reactor startup. Continuous type bioreactor, which are the most extensively used reactors designed for continuous production of products in large quantities, often encounters stability phenomena such as steady states multiplicity, oscillations of process variables, bifurcations and chaos. These phenomena unfavourably affect the productivity of industrial bioprocesses, and consequently, their profitability in most of the cases. Therefore, stability and consistency are the most crucial factor for a bioprocess in bioreactors. As the microorganisms are the participant for biochemical reaction in the bioreactor, sufficient knowledge of microbial growth dynamics and stability in needed in order to adapt the industrial requirements. These can be helpful to understand, optimize and control a bioprocess in a continuous type bioreactors.

On the other hand, bioprocesses for energy conversion in bioreactors are complex and are sensitive to disturbance in process parameters. The biochemical reactions inside of the reactors often show drastic changes in the output variables with small changes in one or more of the reactor input parameters. This

kind of occurrence in the reaction system is called parametric sensitivity behaviour of the reactor. Continuous type of bioreactors follows the nonlinear dynamic response due to the mechanism of microbial growth and generation of secondary metabolic products. The impact of operating conditions on microbial growth and generation of secondary metabolic products directly affect continuous type bioreactors. In bioreactors, the growth of microorganisms is subjected to changes in the environment such as temperature, pH, the concentration of metabolic products, partial pressure and dissolved oxygen. In order to understand the influence of these environmental parameters, parametric sensitivity analysis comes into the picture. The parametric sensitivity analysis is a mathematical tool to analyze any system behaviour concerning changes in system parameters. Therefore, to design, optimize bioreactor for bioenergy conversion, a competent knowledge on processes design through stability and parametric sensitivity analysis is essential.

1.5 Research Gaps

The above discussions infer that for an efficient bioenergy conversion process, especially in continuous reactors type, there is a need for having an optimal design of a reactor maintaining an optimized environment within the reactor. Although studies on stability and parametric sensitivity of continuous type chemical reactors are well advanced in this field, there is limited information available in case of continuous type bioreactors. As it is mentioned in the previous section above, the stability of continuous bioreactors is susceptible to many system parameters such as pH, temperature, hydraulic retention time, the concentration of metabolites, oxygen loading rate and partial pressure of the reactor. For a better bioreactor design, the simultaneous influences of all these parameters on the reaction system and how these parameters affect the microbial growth in the bioreactors, need to be taken into account, which warrants a thorough investigation of these influencing factors.

In many cases, the mechanisms behind the growth of microorganisms and generation of metabolic products, and their correlation with conditions of operating variables are not well understood. Also, the development of kinetic models, which mathematically explain the influence of system parameters on microbial reactions and provide essential information for designing continued type bioreactors, are desirable. For instance, every bioreactor for biofuel production, which involve microbial reactions is affected by system pH. However, according to the author's knowledge, no such article dealing simultaneously with both parametric sensitivity of pH and multiplicity of steady states in continuous type bioreactors is currently available. Since a priori determination of both phenomena, i.e. parametric sensitivity and multiplicity may save the continuous type bioreactors from 'out of control situations', such studies are also required for bioreactors. The experimental verifications of parametric sensitivity and stability analysis also lack for continuous type bioreactors.

Secondly, in the case of biohydrogen production in bioreactors, one of the vital parameter other than pH and soluble metabolites, is partial pressure exerted by gaseous hydrogen. In this case, produced hydrogen itself restrict the microbial growth as well as the hydrogen production rate. Therefore, in order to adopt control strategies for biohydrogen production processes, development of the kinetic model is essential to examine the adverse influence produced hydrogen on microbial growth, which is not well described in the previous studies.

1.6 Aim

Motivated by the research gaps discussed above, the present thesis aims to develop a mathematical model of a continuous stirred tank bioreactor (CSTBR) for the analysis of stability and parametric sensitivity for bioenergy production.

1.7 Thesis organization

The thesis is divided into five chapters which are included as follows:

Chapter 1 describes the general background, statement of the problem, research gaps, significance of the study, aims of the research, and organization of the thesis.

Chapter 2 deals with the state of the art review of literature related to the present research areas. In the background of existing knowledge, the objectives to achieve the aim of the research are also presented

Chapter 3 provides the research methodology adopted for the study to be carried out. This chapter presents the theoretical analysis, which includes the development of mathematical models and simulation processes. Information about the different experimental procedures, which are performed to fulfil the objectives of the present study, also provided in this chapter

Chapter 4 presented the results from the theoretical research as well as the experimental observations. This chapter presents the analysis of the obtained results through discussions as well.

Chapter 5 summarises the present investigation through concluding remarks followed by recommendations for future works.

2 Literature Review

This chapter reviews the previous research work relevant to the topic of the thesis. Primarily, economic viability bioenergy conversion and biological waste treatment processes are dependent upon the overall process efficiency.

Several technical aspects influence the efficiency of the bioprocesses. They can be divided into the technology of the feedstocks, the fermentation, the separation processes, and technology of the use and treatment of waste. Complete knowledge of static and dynamic behaviour of bioreactor is required to be understood, in order to operate, control and optimize the bioprocess.

Mathematical models are essential for correctly reproducing the dynamic behaviour of the process and analyzing the stability of the bioreactor system, and good knowledge of the system is vital to develop a suitable design of the operations. Several research studies already described the various features of bioreactor stability analysis of bioreactor used for bioprocesses. The review of available research studies is presented in the following sections.

2.1 Stability analysis of bioreactors

The stability analysis of the conditions in the bioreactors provides insight into the control environment and processes for the production of metabolites and growth of microorganisms in a bioreactor. Stability analysis of bioreactors also offers information on the limitations for carrying out a successful process due to complex biological reaction mechanisms in the bioreactors. There are various mathematical models such as, based on physical laws, statistical, empirical data that can describe the dynamic behaviour of biochemical networks. In general, a bioreactor can be modelled by a differential equations system. If uniformity (perfect mixture) inside the bioreactor is assumed, solely variations concerning the time occur, and the system can be defined by a set of first-order ordinary differential equations. These equations result from material balances formulation for components considered in the system

For the stability analysis of bioreactors [13] formulated mathematical models for microbial growth in batch and continuous bioreactors. The models were referred to as distributed models since the microbial population in the reactor is observed upon as mass distributed uniformly throughout the culture. Growth was observed as the increase in this mass by the conversion of medium components into biological mass and metabolic products. Two sets of models were presented. The first arises from introducing additional considerations into the model proposed by Monod to account for the stationary phase and the phase of decline in batch culture. These were referred to as unstructured, distributed models since they do not recognize any form of structure in the protoplasmic mass. The models in the second set were referred to as structured, distributed models. The arrangement was introduced by considering the protoplasmic mass to be composed of two groups of substances which relate to each other and with elements in the environment to harvest growth. The structured models subject to the dependence of growth on cell growth; thus, they predict all growth phases detected in batch cultures, whereas the unstructured models do mot predict a lag phase. The full implications of the models are discussed for continuous propagation, as determined by the method of stability analysis and transient calculations. Using the observation form Ramkrishna et al. [13] the transient behaviour of a single-vessel continuous fermentation was studied theoretically by Yano et al. [14]. In this study, the microbial growth in the bioreactor inhibited by its products. By the stability analysis, the occurrence of diverging as well as damped oscillations was found when the product formation was negatively growth-associated; otherwise, no oscillation was observed,

the product formation was either completely growth-associated, completely non-growth associated, or partially growth associated. The dynamic behaviour of isothermal biological continuous type bioreactors modelled by idealized cell and substrate balance equations has been investigated by Agrawal et al. [15] adopting the model developed by Ramkrishna et al. [13]. The stability of the bioreactor model was analyzed theoretically in terms of multiplicity and stability of steady states and existence and stability character of limit cycles. Various types of dynamic behaviour have been classified in terms of a Damkdhler number and two other system parameters. The predicted examples of behaviour have been illustrated by numerical computation of cell and substrate concentration trajectories.

Fermentation processes in Continuous type bioreactors often face the occurrence of oscillation or cycling of the substrate, biomass, and product concentrations under certain fermentation conditions [16–19]. The mechanism causing oscillation in continuous ethanol fermentation by *Zymomonas mobilis* under certain operating conditions was examined by Daugulis et al. [20]. In this study, forced oscillation fermentation experiments were performed, in which exogenous ethanol was added at a controlled rate to generate oscillatory behaviour, in order to obtain estimates for the model parameters and to validate the proposed model. From this study, the lag in the cells' response to a changing environment was shown to be the significant factor contributing to the oscillatory behaviour in continuous fermentation under certain operating conditions. Skupin et al. [21] studied the stability analysis of Continuous fermentation processes where the continuous fermentation processes involving yeast Saccharomyces cerevisiae or bacterium *Zymomonas mobilis* often exhibit oscillatory behaviour. In this research study, two substrates were fed to a continuous type bioreactor, and an unstructured mathematical model described the kinetics of fermentation process with product inhibition on cell growth was considered. From the bifurcation analysis for stability, it was found that an appropriate ration of both substrates to the mixture allows for the induction and elimination of oscillatory behaviours.

Several researchers studied the stability analysis of bioreactors for biofuel production, such as bioethanol and biohydrogen [22–26]. A mathematical model for continuous ethanol fermentation to study the mechanisms of the self-sustained oscillations of ethanol concentration was analyzed by Skupin et al. [26]. The model was considered on the assumption that microorganism cells response to the inhibitory effect of product (ethanol) concentration with a delay. From the stability analysis, it was observed that the delay time is one of the crucial factors for the occurrence of oscillations. For critical delay time, the fermentation process undergoes a Hopf bifurcation. The analysis showed the operating variables and kinetic parameters have a significant effect on the dynamical behaviour of the fermentation system. The oscillatory behaviour can be avoid by proper manipulation of the operating variables. On another study, the dynamic responses of bioethanol fermentors to sinusoidal periodic perturbations of the feed concentration have been investigated by Abashar et al. [25]. It was shown that the steady-state autonomous model of the unforced fermentor could be reduced analytically to a cubic polynomial. This analytical form enables to implement the global bifurcation analysis to divide the parameter space into regions with a different number of steady-state solutions; moreover, the discriminant of the cubic polynomial is used for the study of the nature of the steady-state solutions. It was shown that within the parameters range studied, the best policy for the production of bioethanol is to operate the forced fermentors in the frequency locking regions at small forcing amplitudes.

The stability analysis becomes sometimes challenging when the microbial growth kinetics undergoes metabolic overflow and certain inhibition phenomena due to substrate, product, and some toxic chemicals. One of the often observed mechanisms of microorganisms is the so-called metabolic

overflow [27–31]. This term is used to describe the phenomena of excessive uptake of the substrate and corresponding overflow of intermediate metabolite(s) under conditions of high extracellular substrate concentration. In general, the substrate consumption rate and product formation rate of many microorganisms are dependent on the nature of growth limitation and growth rate and the extracellular substrate concentration in a relatively wide range [31]. In a continuous culture of *Klebsiella pneumoniae* anaerobically grown on glycerol, it has been experimentally shown that the extracellular substrate concentration also strongly affects cells' dynamic behaviour, leading to sustained oscillation and multiplicity under certain conditions [32]. On the other hand, using extended forms of the Monod model which separately took substrate and product inhibition into account, Yano et al. [14] showed that although substrate inhibition does not give rise to sustained oscillation, the product inhibition can lead to both damped and sustained oscillations depending on the nature of products.

Lorencez et al. [33] considered the interactions of the substrate and product inhibition and their effects on the stability of the growth of *Methylomonas clara*. No oscillation was reported for this culture. The result of product inhibition on the occurrence of multiple steady states was considered by Axelsson et al. [34] for Saccharomyces cerevisiae. The combined influences of enhanced rates of substrate consumption and product formation, together with inhibition by substrate and product on the dynamic behaviour of culture, are not clear. In general, little is known about the multiplicity of bioreactions [35].

One of the most popular applications of bioreactors is in the field of wastewater treatment. The stability of activated sludge reactors with substrate inhibition kinetics and solid recycle studied by Bertucci et al. [36]. In this study, an analytical relationships were developed for the continuous stirred tank reactor; numerical simulation was performed for other bioreactors. The occurrence of multiple solutions and hysteresis behaviour is examined as a function of spacetime, recycle ratio, recycle solids concentration, and sludge age. The sensitivity of the outlet substrate conversion as a function of the degree of substrate inhibition and hydraulic mixing is calculated. Criteria were suggested to operate such bioreactors and to prevent washout occurrence. In another study, a continuous bioreactor with cell recycle involving the biodegradation of mixed wastes is analyzed by Ajbar et al. [37]. The biodegradation of the different substrates follows Andrew's inhibitory kinetic models. The stability analysis revealed that the model exhibits a number of singularities, including hysteresis and pitchfork, that occur at clean feed conditions. The effect of the growth kinetic and operating parameters on its stability behaviour was also examined. A similar type of study on stability analysis of the biodegradation of mixed wastes in a continuous bioreactor with cell recycle was observed by Ajbar et al. [38]. The continuous bioreactors system involves a pure culture of *Pseudomonas putida* and media containing phenol and glucose as carbon and energy sources. The stability analysis carried out using the bifurcation theory's elementary principles shows rich dynamics characteristics of the reactor model, including steady-state multiplicity and hysteresis. The effect of the bioreactor operating parameters on the stability behaviour of the model was observed. A practical criterion was derived for the safe operation of the unit and to prevent the occurrence of washout conditions. Most of the time, the kinetic model for microbial growth with or without inhibition are gererally adopted from Monod model by incorporating inhibition term. But Ajbar et al. [39] investigated the static and dynamic behaviour of a continuous flow bioreactor for the aerobic biodegradation of municipal and industrial waste where, the kinetic model for the bioreactor was described by the biomass-dependent Contois model. This kinetic model is known to explain the aerobic biodegradation of solid municipal organic waste well. In this investigation the analysis of the unsteady-state model was conducted for both analytically and through numerical simulations. The results show the ability of the model to predict a wide range of behavior, including oscillations for some range of

kinetic and operating parameters. The analysis also showed that the inconsistency of the yield coefficient is essential for the presence of Hopf points in the model. The influences of the operating variable on the performance of the bioreactor were also examined.

2.2 Influence of pH

The microbial reactions in the bioreactors are controlled by a wide range of environmental variables, including pH, temperature, salinity, nutrient availability [40,41]. Among these environmental factors, pH appears as a primary control [42–44]. pH correlates strongly with microbial communities across a wide range of biochemical conditions.

2.2.1 Bioethanol production process

Ethanol is considered to be one of the biofuels that can be used as a fuel supplement for the internal combustion engine. Ther are research articles that reflect ethanol can produce biological processes using a different kind of organic waste material as feedstocks. For the production of ethanol from sugar cane molasses using *Zymomonas mobilis* and *Saccharomyces cerevisiae strain* Vuuren et al. [45] found, pH plays an important role. This study concludes pH had a noticeable effect on ethanol production if the reaction system maintains the optimum range of pH for those particular strains. In the case of continuous fermentation for ethanol, pH also shows an important role. The effects of temperature and inlet pH of the medium on the ethanol productivity and activity of the immobilized *Z. mobilis* cells during continuous fermentation of glucose was studied at various temperatures and pH by Bajpai et al. [46]. On changing the temperature from one steady-state level to a new one, 6-8h was required in order to experience the effect of a change in temperature entirely, whereas 8-20 h was needed to alter the pH. In order to obtain maximum ethanol productivity and ethanol yield, the optimum temperature of 37°C was required whereas, pH range was broad as 4.4-6.0. The fastest growth of yeast *Zymomonas mobilis* for bioethanol production was 5.5-6.5, with an apparent optimum at 6.5 was observed by Lawford et al. [47]. From this study, it was observed that the specific rates of glucose utilization and ethanol production were relatively unaffected by pH over the range 7.0-5.5 but increased sharply as the pH was further decreased below 5.5 to 4.0. Under these conditions, the ethanol yield was unaffected by pH over the range 4.0-6.5 but decreased markedly at a pH of 7. The formation of ethanol by the polymorphic fungus *Aureobasidium pullulans* was examined by Madi et al. [48] under a range of culture pH values and aeration conditions. Although culture pH had a profound effect on fungal morphology, with a significantly increased proportion of the biomass in the unicellular form at pH 6.5, there appeared to be no direct link between morphological structure and ethanol formation. The levels of ethanol noted may have influenced the morphology. The effects of lactic and acetic acids on ethanol production by *Saccharomyces cerevisiae* in corn mash, as controlled by pH were examined by Graves et al. [49]. In this study pH of corn mash was adjusted by acetic acid and lactic acid, and the growth inhibition of *Saccharomyces cerevisiae* with the variation of pH range was examined. Results from this study suggest that the inhibitory effects of lactic acid and acetic acid on ethanol production in corn mash fermentation when setting at a pH of 5.0–5.5 are not as great as that reported thus far using laboratory media. Sweet sorghum has the potential to be used as a renewable energy crop and is a viable candidate for ethanol production. In this respect, the influence of temperature, pH, and yeast on in-field production of ethanol from unsterilized sweet sorghum juice was studied by Kundiyana et al. [50]. The main objective of this study was to evaluate the effects of pH and nutrients on fermentation process efficiency. *Saccharomyces cerevisiae,* an ethanol-producing yeast, was used in this study. Results indicated that both strains of Saccharomyces cerevisiae tested were able to perform fermentation within a wide ambient temperature

range, and maximum ethanol produced was 7.9% wv^{-1} in 12h under ambient temperature conditions. Other process variables, such as lowering pH, did not significantly improve the sugar to the ethanol conversion efficiency of yeasts. Results indicate that in-field fermentation of sweet sorghum juice to ethanol is possible with minimal or no process controls and is a feasible process for ethanol production. The influence of pH was observed for the production of ethanol and glycerol by *Saccharomyces cerevisiae* in cassava mash by Zhang et al. [51]. The pH was varied from 4.0 to 6.0. Inhibition of microbial growth was observed as the pH of the reaction medium declined. Complete inhibition of ethanol fermentation was observed in mashes at pH 4.0. Glycerol production linearly decreased with an increased undissociated propionic acid concentration in all mashes at all pH levels, which partly contributed to increased final ethanol production when the propionic acid concentration in mashes was low. Waste gases containing carbon monoxide (CO) can be utilized for generating valuable fuels like ethanol by biological conversion using acetogens.[52,53]. Several bioreactors can be used for gas treatment or bioconversion [54,55]. The bioconversion of carbon monoxide to ethanol and acetic acid by *Clostridium autoethanogenum* was investigated by Abubackar et al. [56] by varying pH in the range of 4.75-5.75. A maximum ethanol concentration of 0.65 gL^{-1} was obtained under the following conditions: pH = 4.75. Such maximum ethanol concentration is considerably higher than that achieved (0.06 and 0.25 gL^{-1}) with *C. autoethanogenum* in previous studies [57,58].

2.2.2 Biohydrogen production process

The operational pH is one of the most critical parameters that determine the ideal metabolic pathways for hydrogen production as well as the inhibition of the hydrogen consuming processes, which may coincide [59–61]. An acidic operational pH (below 6) mainly inhibits the methanogenic activity under both mesophilic and thermophilic conditions. Still, the inhibition of hydrogen consuming homo-acetogenic activity can only be achieved under thermophilic conditions at the initial pH of 5.5 [62]. Thus, the control of the process pH plays a vital role in achieving high biohydrogen conversion rates by minimizing the activity of hydrogen consumers. The pH is one of the critical parameters that can influence the metabolic pathways as it may directly affect the hydrogenase activity, an iron-containing enzyme which plays a significant role in DF [63,64]. An acidic pH affects the activity of the hydrogenase enzyme, although it is one of the essential parameters for the inhibition of methanogenic activities in a mixed culture system [59,65]. The optimum pH range for biohydrogen production varies from pH 4.5 [59] to 9 [66] in DF of sucrose. The conceivable justifications for the disagreements in optimum pH in the different studies can be differences in inoculum sources, inoculum enrichment methods, substrate types and applied oxygen loading rate [6]. The operational pH influences the metabolic by-products and biohydrogen yields.

In most of the studies, for favourable hydrogen production, acetate and butyrate are the major end products. However, Khanal et al. [59] concluded the independence of the acetate and butyrate levels from different initial pH ranges studied (4.5–7.5). Similarly, Luo et al. [67] reported butyrate as a significant VFA in the DF of cassava stillage in both BHP tests carried at the initial pH 5 and 7. Luo et al. [62] found acetate as a primary metabolic product when the operational pH was 7. In contrast, butyrate dominated at an initial pH 5.5 in the BHP tests carried under mesophilic (37°C) conditions using an acid pre-treated inoculum. Luo et al. [62] further reported the inhibition of homo-acetogenesis could be achieved at pH 5.5 and thermophilic temperatures (55°C). The dark fermentation of cheese whey from mozzarella production at different pH ranges (5.5–7.7) and a temperature of 39°C, De Gioannis et al.[68] reported, pH 6 as the optimal pH and acetate levels were higher in all the tests except at pH 6.5 where butyrate and propionate levels exceeded those of acetate. A lower pH (64.5) favours

the solvent production [69]. In the DF of glucose by *C. pasteurianum*, a pH below 5 favours the butanol and acetone production [63]. The selection of the operational pH is also substrate type and OLR dependent, which determines the VFA concentrations and thus the pH of the solution. The optimum pH for organic food waste varies from 4.5 to 7, for the lignocellulosic waste, it varies from 6.5 to 7, whereas a neutral pH is optimal for animal manure [70]. However, Tang et al. [71] reported an optimum pH of 5.5 at 45°C for the DF of cattle wastewater. Thus, it is crucial to determine the optimum pH conditions for the DF of a selected substrate type at a particular loading rate and operational temperature.

2.3 Effects of partial pressure

High concentrations H_2 in the liquid phase, which is corresponding to the high partial pressure of H_2 according to Henry's law, results in process inhibition and decreases bio-hydrogen production Bio-hydrogen is produced from the dark fermentation process mainly through the reduction of protons by Fd_{red} or NADH. At high H_2 concentrations in the liquid phase, the reduction of protons to H_2 is thermodynamically unfavourable [72]. Instead, the reduction of F_{dox} is favoured, resulting in the oxidation of H_2 to proton and a decrease in H_2 production. On the other hand, Dong et al. [73] reported that high H_2 partial pressure might inhibit the conversion of long-chain fatty acids into acetate and H_2 while van Niel et al. [74] revealed that high H_2 partial pressure could result in a metabolic shift to favour lactate, ethanol, acetone and butanol formation at the expense of H_2.

Several strategies have been employed to decrease the H_2 partial pressure during dark fermentation processes and increase biohydrogen production. These include continuous gas release [75–77], larger headspace volume [78], vacuum stripping [79], or sparging with an inert gas like N_2 or CO_2 [80,81]. Logan et al. [75] compared an alternate release method with a continuous release method and reported higher H_2 production with the continuous gas release technique. Similarly, Chang et al. [76] reported higher H_2 production with a continuous gas release method as compared to the intermittent release method. The same authors also reported that the continuous release method could be further enhanced, bypassing the gas released through an alkaline solution of NaOH [76]. Kim et al. [82] compared N_2 and CO_2 sparging on biohydrogen production and reported increased gas production for the N_2 and CO_2 sparging systems relative to the control. The authors also observed that CO_2 sparging resulted in higher H_2 production than N_2 sparging [82]. Likewise, Nguyen et al. [80] reported an increase in H_2 yield of 78% (with glucose as substrate) and 56% (with xylose as substrate) for N_2 sparged system as compared to the control setup. In the same study, Nguyen et al. [80] also studied the potential of using large volume headspace to decrease H_2 partial pressure and reported a headspace: liquid volume ratio of 2:1 in the reactor as the optimum value for maximum biohydrogen production. Similarly, Oh et al. [83] compared the use of a high volume headspace of 81%by intermittent gas release method with that of a continuous release method and reported an H_2 yield 14% higher for the intermittent release as opposed to the continuous release method. Besides, Beckers et al. [84] studied the influence of H_2 partial pressure on biohydrogen production using *Clostridium sp*. and reported an increase in H_2 production of 9.2% and 22.5% when the pressure was decreased from 1.18 bar to 1 bar and 0.89 bar respectively.

2.4 Kinetic models

There are mathematical expressions to define the bio-reaction kinetics. The microbial growth, perhaps, is the process that has generated more difficulty for its modelling due to the multiple interactions between cells and the environment, and to the significant amount of biochemical reactions affecting the microbial activity.

Kinetic models provide useful information to adopt control strategies for any bioprocess processes. Kinetic models are also helpful in describing the influence of substrate overdose, temperature, pH, dilution rate (in case of the continuous operation), and soluble metabolites, which are produced during fermentation [85].

2.4.1 Kinetic models describing the progress of the fermentation process

Monod model is the most popular and simplest model for describing the microbial reaction of microbial growth within a single substrate. The reaction kinetics are expressed as:

$$\text{Substrate(S)} \xrightarrow{\text{Cell(X)}} \text{more Cells(X)} + \text{Product } (H_2) \tag{2.1}$$

$$r_c = \frac{dX}{dt} = \frac{\mu_{max} S}{K_S + S} X \tag{2.2}$$

According to Monod:

$$\mu = \frac{1}{X}\frac{dX}{dt} = \frac{\mu_{max} S}{K_S + S} \tag{2.3}$$

where,

r_c microbial growth rate, ($gL^{-1}h^{-1}$);

X cell biomass concentration (gL^{-1});

t incubation time, (h);

μ_{max} maximum specific growth rate of cells, (h^{-1});

S substrate concentration, (gL^{-1});

K_S Monod constant or substrate saturation constant, (gL^{-1});

Some kinetic models have been proposed to describe such changes in substrate concentrations, microbial growth rate, hydrogen, and some soluble metabolites. Among them, the modified Gompertz model (Eq. (2.4)) developed by Zwieteringet al. [86] was widely used to describe the progress of substrate degradation, HPB growth, hydrogen production and some soluble metabolite production in a batch fermentative process [87–93].

$$H = H_{max} \exp\left\{-\exp\left[\frac{R_{max} e}{H_{max}}(\lambda - t) + 1\right]\right\} \tag{2.4}$$

Where,

H cumulative value for substate degradation, (h^{-1});

H_{max} maximum cumulative value for substate degradation, (h^{-1});

R_{max} maximum rate, (h^{-1});

λ lag time, (h);

t time, (h);

When Equation (2.4) was used to describe the progress of substrate degradation in batch tests, H and H_{max} denote the cumulative degraded substrate value and the maximum degraded substrate value, respectively. As shown in Figure 2-1, in a batch test, H increases very slowly with increasing cultivation time from 0 to λ, and then increases rapidly almost at the rate of R_{max} and finally reaches an asymptotic value H_{max} with further growing the cultivation time.

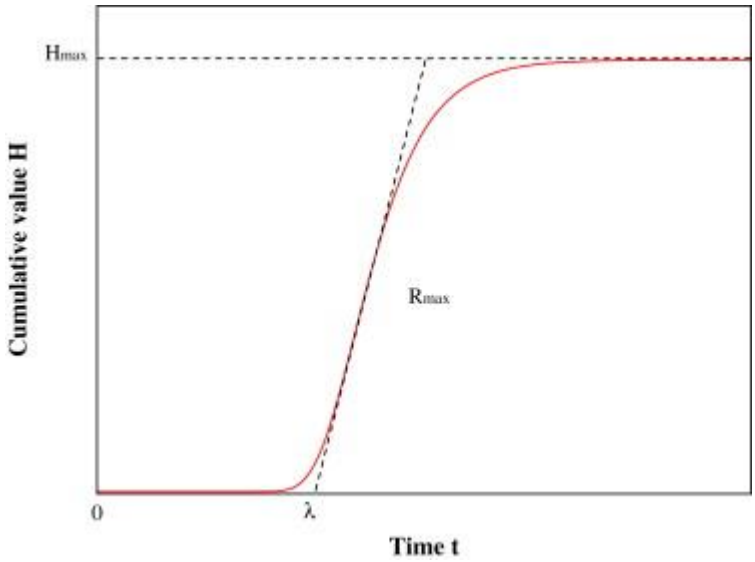

Figure 2-1 A curve for modified Gompertz model

Besides, a Logisticmodel (Eq.(2.5)) was also used by Mu et al. [94] to describe the progress of microbial growth in the batch tests.

$$X = \frac{X_0 \exp(k_c t)}{1-\left(\frac{X_0}{X_{max}}\right)(1-\exp(k_c t))} \tag{2.5}$$

Where,

X_0 initial biomass concentration, (gL^{-1});

X_{max} maximum biomass concentration, (gL^{-1});

k_c apparent specific growth rate, (h^{-1});

2.4.2 Kinetic models describing substrate inhibitions

A substrate is usually carbohydrates that can provide carbon and energy sources for microorganisms. Thus it is of great importance to microbial growth and thus for the fermentation process. Some kinetic models have been proposed to describe the effects of substrate concentrations on the rates of substrate degradation, microbial growth, and product formation. Among them, the classical Monod model (or Michaelis–Menten model) (Eq. (2.3)) was widely used. When a substrate inhibits a microbial growth at much higher concentrations, the classical Monod model becomes unsatisfactory. In this case, modified

Monod models with the item of substrate inhibition can be used to describe the effects of substrate concentrations on microbial growth and product formation. Among these models, the Andrew model (Eq. (2.6)) was the most widely used [95–98].

$$\mu = \frac{\mu_{max} S}{K_S + S \pm \frac{S^2}{K_I}} \tag{2.6}$$

where,

K_I inhibition constant, (gL^{-1});

Moreover, Wang and Wan [99] used the Han–Levenspiel model (Eq. (2.7)), an extended Monod model, to describe the effects of glucose concentrations on hydrogen production rate in batch tests. Besides, Wang and Wan [99] also compared the ability of the Andrew model and the Han–Levenspiel model to describe the effects of glucose concentrations on hydrogen production rate in batch tests and concluded that the Han–Levenspiel model was the most suitable one [95].

$$R = \frac{R_{max} S \left(1 - \frac{S}{S_{Crit}}\right)^m}{S + K_S \left(1 - \frac{S}{S_{Crit}}\right)^n} \tag{2.7}$$

Where,

C inhibitor concentration, (gL^{-1});

C_{crit} critical inhibitor concentration, (gL^{-1});

S_{crit} critical substrate concentration, (gL^{-1});

m, n degree of inhibition;

2.4.3 Kinetic models describing product inhibitions

It has been found that some volatile fatty acids or salts may change the intracellular pH of bacterial strains, increase the maintenance energy requirement of bacteria or inhibit some specific enzymes related to product formation and thus, they can inhibit bacterial growth and then inhibit the product formation. So far, some kinetic models have been proposed to describe the inhibitory effects of some volatile fatty acids, salts or hydrogen on the fermentative hydrogen production. Among them, the modified Han–Levenspiel model (Eq. (2.8)) was widely used.

$$R = R_{max} \left(1 - \frac{C}{C_{Crit}}\right)^n \tag{2.8}$$

$$R = \frac{R_{max}}{1 + \left(\frac{C}{K_C}\right)^n} \tag{2.9}$$

$$R = \frac{R_{max} K_C}{K_C + C} \tag{2.10}$$

$$R = R_{max} \frac{S}{K_S + S} \left(1 - \frac{S}{S_{Crit}}\right)^m \left(1 - \frac{C}{C_{Crit}}\right)^n \tag{2.11}$$

Where,

K_C constant, (gL^{-1});

The value of R decreases from R_{max} to zero with increasing inhibitor concentrations from 0 to C_{Crit} which is shown in Figure 2-2.

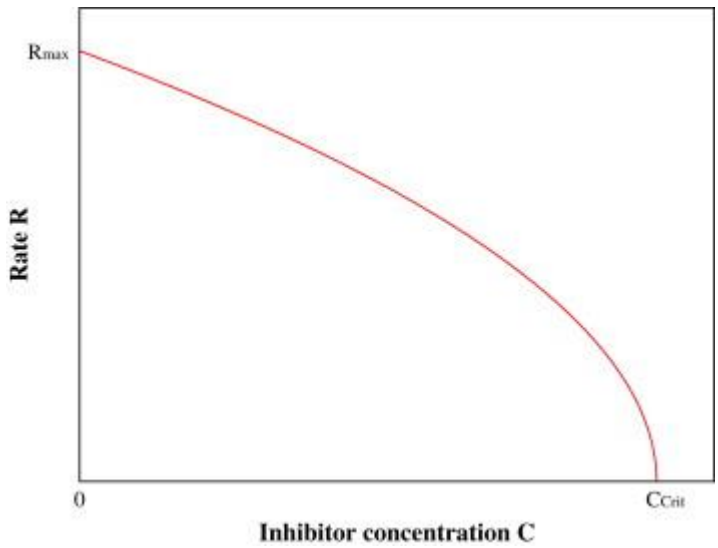

Figure 2-2 A curve for modified Han-Levenspiel model

Besides, Wang et al. used Eq. (2.9) to describe the inhibitory effects of sodium acetate concentrations on the specific rates of sucrose degradation and hydrogen production in batch tests [100]. Moreover, Liu et al. used Eq. (2.10) to describe the inhibitory effects of butyrate concentrations on specific growth rates of wild *Clostridium tyrobutyricum ack* and deleted mutant of *C. tyrobutyricum* in fed-batch tests [101]. Furthermore, van Niel et al. used Eq. (2.11) to describe the combined inhibitory effects of sucrose and sodium acetate concentrations on the specific growth rate of *Caldicellulosiruptor saccharolyticus* in batch tests [74]. Also, van Niel et al. also developed a model incorporating cell lysis to describe the inhibitory effects of sodium acetate concentrations on the specific growth rate of *C. saccharolyticus* in batch tests [74].

2.4.4 Kinetic models describing the effects of pH

pH is another critical factor influencing fermentative hydrogen production because it can affect the activity of microorganisms considerably by changing the ionization states of the active components of the cells and substrates [102].

In general terms, the addition of the pH effect in the growth rate equation can take several forms, as reviewed by Andreyeva and Biryukov[103]. Here a polynomial equation (Eq.(2.12) is used to describe the influence of pH on the growth rate of pure cultures

$$\mu = a(pH)^2 + b(pH) + c \tag{2.12}$$

where,

μ specific growth rate, (h^{-1});

a, b, c constant of the polynomial equation 2.12

Lallai et al. [104] studied the effect of pH on specific growth rate μ, yield factor Y and specific substrate consumption rate U for two mixed microbial populations in a batch reactor with a limiting substrate (phenol). In other studies, Andrew model (Eq. (2.13)) was adopted to describe the effects of H^+ concentration on the specific hydrogen production rate [11,55]. In addition, using it to describe the effects of H^+ concentration on the rates of substrate degradation, microbial growth and some soluble metabolite production is recommended.

$$R = \frac{R_{max}[H^+]}{K_a + [H^+] + \frac{[H^+]^2}{K_b}} \tag{2.13}$$

$[H^+]$ molar hydrogen ion concentration

K_a, K_b constants of equation 2.13

As shown in Figure 2-2, R-value increases first and then decreases with increasing H^+ concentration.

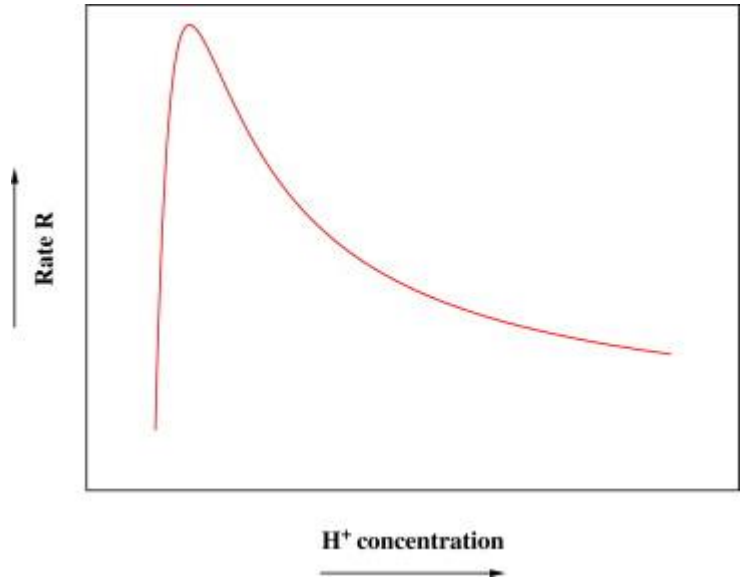

Figure 2-3 A curve for the Andrew model

In practice, it is convenient to use pH rather than H^+ concentration in the model. In addition, the Ratkowsky model (Eq. (2.14)) may also be a good candidate to describe the effects of pH on R.

$$R = [A(pH - pH_{min})]^2\{1 - \exp[B(pH - pH_{min})]^2\} \tag{2.14}$$

A, B constant of equation 2.14

2.4.5 Kinetic models describing the effect of dilution rates

Dilution rate is a significant factor influencing fermentation processes in a continuous type bioreactors because it can affect the capability of microorganisms to degrade substrate and thus can influence the fermentation processes. Some models have been proposed to describe the effects of dilution rates on

hydrogen production rate, hydrogen production, and concentrations of substrate, biomass, and some soluble metabolites in a continuous fermentative hydrogen production process [105,106]. Chen et al. [105] used the single-substrate models without biomass decay (based on Eqs. (2.15), (2.17) and (2.18)) to describe the effects of dilution rates on hydrogen production and concentrations of sucrose, biomass, acetate, propionate, butyrate and ethanol in a continuous stirred tank reactor for hydrogen production.

$$S = \frac{DK_S}{R_{max} - D} \tag{2.15}$$

Considering death rate,

$$S = \frac{(D + k_d)K_S}{R_{max} - D - k_d} \tag{2.16}$$

$$X = Y_{X/S}(S_0 - S) \tag{2.17}$$

$$P = Y_{P/X}X \tag{2.18}$$

Where,

D dilution rate, (h^{-1});

P product concentration, (gL^{-1});

$Y_{P/X}$ product yield coefficient, (gg^{-1})

$Y_{X/S}$ biomass yield coefficient, (gg^{-1})

K_d biomass decay constant, (h^{-1});

Moreover, Chang and Lin [107] used Eq. (19) to describe the effects of dilution rates on the specific sucrose degradation rate in an up-flow anaerobic sludge blanket reactor for hydrogen production.

$$R = \frac{D + k_d}{Y_{X/S}} \tag{2.19}$$

2.4.6 Kinetic models describing the relationship among the substrate degradation, microbial growth and product formation rate

Luedeking–Piret model (Eq. (20)) and its modified form (Eq. (21)) were widely used to describe the relationship between microbial growth rate and product formation rate [108].

$$\frac{dP}{dt} = Y_{P/X}\frac{dX}{dt} + \beta X \tag{2.20}$$

Where,

β non-growth-associated product yield coefficient

$$\frac{dP}{dt} = Y_{P/X}\frac{dX}{dt} \tag{2.21}$$

$$\frac{dP}{dt} = Y_{P/S} \frac{dS}{dt} \tag{2.22}$$

to describe the relationship between the rate of substrate degradation and the rates of hydrogen production, acetate production and butyrate production Mu et al. [94] used Eq. (22), while van Niel et al. [109] used Eq. (33) to describe the relationship between substrate degradation rate and the growth rates of *C. saccharolyticus and Thermotoga elfii*.

2.5 Gaps in existing knowledge & objectives

From the above literature review, it is apparent that there is a need for having an improved design of a reactor and maintaining an optimized environment within the reactor for the efficient bioenergy conversion process. This requirement becomes more critical in case of continuous type reactors. The stability and parametric sensitivity analysis studies are well advanced in the field of chemical processes; however, in the case of bioprocesses, such analyses of bioreactors are not explicitly available in the literature.

From the research studies, it is well understood that the performance of bioreactors depends upon several system variables such as pH, temperature, hydraulic retention time, the concentration of metabolites, oxygen loading rate and partial pressure of the reactor. The stability and parametric sensitivity analysis of these variables can help to inspect the performance of bioreactors. The influences of operating parameters on the behaviour of bioreactor can also lead to better control of bioprocesses within the reactor. The parametric sensitivity of batch type bioreactor is adequately investigated, and the studies are reported in the literature. However, the continuous type bioreactors, which are mostly used in industry, the comprehensive studies are not available.

A good design of a bioreactor requires the knowledge of the impact of operating parameters on the reaction system. A thorough investigation of the influencing factors and how their operating parametric range affects the microbial growth in the reactors need to be taken into account. In many cases, the mechanisms behind the growth of microorganisms and the generation of metabolic products, and their correlations with operating variables conditions are not well understood. The development of kinetic models that mathematically explain the influence of system parameters on microbial reactions is desirable for providing essential information for designing these bioreactors. The experimental verifications of parametric sensitivity and stability analysis also lack for continuous type bioreactors.

For instance, every bioreactor for biofuel production, which involve microbial reactions is affected by system pH. pH is an important factor for most microorganisms as it affects cell metabolism and its structured integrity by a small pH variation. At the same time, the temperature is generally an essential factor for temperature-sensitive bacteria. Naturally, a large group of bacteria can grow at optimum room temperature, but there is no optimum pH value where a large number of bacteria can grow. Each type of bacteria responds uniquely at different pH value. According to the author's knowledge, no such information dealing simultaneously with both parametric sensitivity of pH and multiplicity of steady states in continuous type bioreactors is currently available. Since a priori determination of both phenomena, i.e. parametric sensitivity and multiplicity may save the continuous type bioreactors from 'out of control situations'. Therefore such studies are required for bioreactors.

Furthermore, in the case of biohydrogen production in bioreactors, one of the vital parameter other than pH and soluble metabolites, is partial pressure exerted by gaseous hydrogen. In this case, produced

hydrogen itself restrict the microbial growth as well as the hydrogen production rate. Therefore, in order to adopt control strategies for biohydrogen production processes, development of the kinetic model is essential to examine the adverse influence produced hydrogen on microbial growth, which is not well described in the previous studies. In the case of the biohydrogen production process in a continuous type bioreactor system, one of the critical issues generally appears that the reacting system distributed in two phases, because of gaseous production. The design of the reaction system becomes complicated as the mass transfer mechanism comes into the picture, along with biochemical reactions. Although there are some articles which investigate the stability analysis of continuous type bioreactor in the application of biodegradation of mixed waste, activated sludge processes and other biofuel production processes, but research studies on the stability analysis of steady-state to investigate the performance of continuous type bioreactor involving biohydrogen production is still lacking. In the background of the existing knowledge and above discussion regarding gaps in understanding, the following objectives will be achieved in this thesis:

2.6 Objectives

- To investigate the influence of pH on microbial growth experimentally in a batch reactor, and develop a kinetic model to determine constants which will describe the nature of microbial growth.
- To develop a mathematical model of a continuous stirred tank bioreactor (CSTBR) system with the help of the kinetic parameters to derive a simple dimensionless steady-state multiplicity criterion for the CSTBR. The approach should be able to identify the set of values of input variables, which lead to multiple steady-states.
- To derive an expression for theoretical sensitivity functions of pH concerning different input variables, namely dilution rates of nutrient and base streams and concentrations of substrate and base stream for pH control.
- To conduct experiments to study the parametric sensitivity for sets of input parameters belonging to the regimes of multiple and unique steady states as determined using multiplicity criterion. The experimental and simulated transient behaviours of pH will be analyzed and compared to verify the existence of parametric sensitivity under both multiple and unique steady-state conditions.
- To develop a generalized criterion for sensitivity with the help of normalized sensitivity analysis, which does not depend upon the topology of pH contour for recognizing the extent of input parameters where a CSTBR exhibits sensitive behaviour.
- To explore the influence of hydrogen on microbial growth and evaluates how the produced hydrogen in the reactor headspace hinders the rate of production of hydrogen.
- To examine the adverse effects of produced hydrogen on microbial growth experimentally and to develop kinetic models to explain how the produced hydrogen influences the bacterial growth and hydrogen production rate simultaneously.
- To investigate the effects of the operating parameters on the stability behaviour of a CSTBR for biohydrogen production. The stability analysis will be carried out using elementary principles of bifurcation theory shows the dynamics characteristics of the reactor model, including a steady-state multiplicity analysis.

3 Methodology

The methodology followed in the research work consists of theoretical, numerical and experimental methods to describe, simulate microbial growth and kinetic reactions for in bioreactors. In this chapter, the underpinning theoretical basis of microbial growth reactions and developing of the mathematical models is presented. The details of experimental that are conducted for calibrating the mathematical models are also described. The developed model was then used to study various cases studies to predict performance variables for better design and performance of bioenergy conversion processes.

3.1 Theoretical background

Microbial growth mechanism, which includes different microbial population phases, is an important aspect in biochemical processes, and the Microbial growth rate, can be determined theoretically by considering the simplest population growth model defined by Monod.

First of all, the bacterial growth curve is considered. When bacterial cultures are allowed to grow into a suitable liquid medium, its growth follows a specific course [1]. If bacterial counts are made at intervals after inoculation and plotted with time, a growth curve is obtained (Figure 3-1)

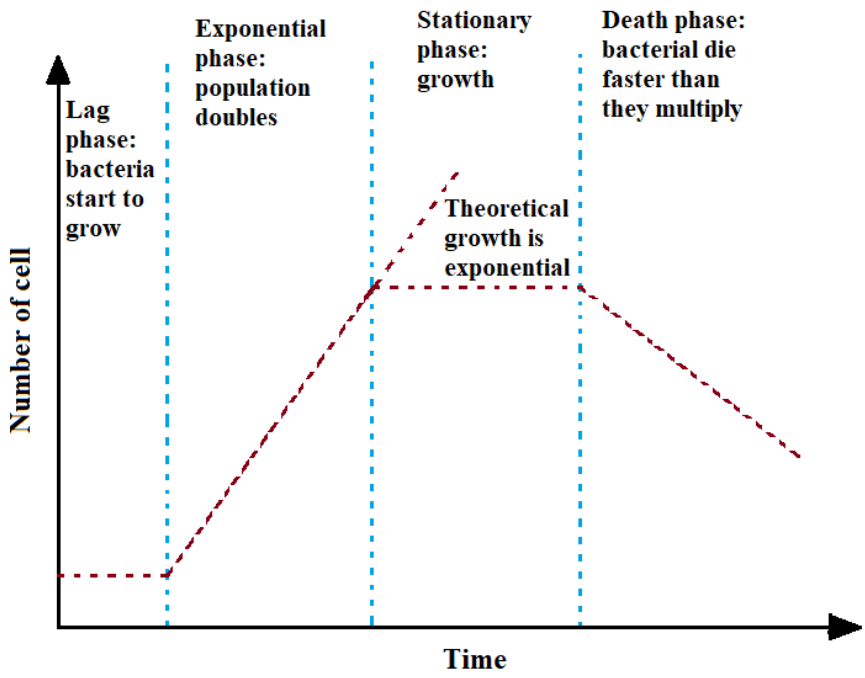

Figure 3-1 Microbial growth curve

After adding the bacterial culture in the growth medium, there is no apparent increase in number; however, there may be an increase in the size of the cells. This initial period is the time required by the cells for the adaptation to the new environment, during which the necessary enzymes and metabolic intermediates are built up in adequate quantities for multiplication to proceed. The period of the lag phase differs with the species, size of the inoculums, the composition of the growth medium and environmental factors such as temperature. After the lag phase, the cells start growing, and their numbers rise exponentially or by geometric progression with time. If the logarithm of the cell number is plotted against time, a straight line will be obtained.

After the end of exponential growth, cell division ceases due to the reduction of nutrients and accumulation of toxic products. The number of progeny cells formed is just enough to replace the number of cells that die. The viable count remains stationary as equilibrium exists between the dying cells and the newly formed cells.

The phase of decline or death Phase is the phase at which the bacterial cells decrease due to cell death. Besides, nutritional exhaustion and toxic accumulation, cell death may also be caused by autolytic enzymes.

3.1.1 Calculation of microbial growth rate

In the exponential phase, a typical microbial cell uptakes the nutrients from the culture media and converts them into complex cellular matter through cell metabolism. The growth rate is directly related to cell concentration, and cell reproduction is the usual outcome of this reaction. The rate of microbial growth is expressed as specific growth rate and is defined as follows:

$$\mu = \frac{1}{X}\frac{dX}{dt} \tag{3.1}$$

Where,

X bacterial cell concentration (gL^{-1})

t incubation time (h)

μ specific growth rate (h^{-1})

When the specific growth rate is expressed in terms of cell number, it is represented through the following equation (3.2),

$$\mu = \frac{1}{N}\frac{dN}{dt} \tag{3.2}$$

Where,

N number of bacterial cell

3.1.2 Microbial growth kinetics

A wide range of well established kinetic models viz. unstructured and structured, non-segregated and segregated is available to predict the microbial growth kinetics. Among these models, the structured and segregated models are the most realistic ones, but they are computationally complex [110]. In the present study, a simple Monod model is considered to explain the process kinetics and to predict microbial growth.

Monod model is an unstructured, non-segregated growth model. Monod equation describes substrate-limited growth when the microbial growth is slow, and the population density is low. This is applicable in case of uninhibited growth, and it resembles Langmuir- Hinshelwood kinetics in classical chemical engineering system or Michaelis- Menten kinetics for enzymatic reactions in biochemical systems.

Monod equation (3.3) can be described as follows,

$$\mu = \frac{\mu_{max} S}{K_S + S} \quad (3.2)$$

At very high substrate concentration,

i.e. $S \gg K_S$

The eq. (3.2) becomes

$$\mu = \mu_{max}$$

Therefore, a zero-order correlation exists between μ and S.

Where μ_{max} is the maximum specific growth rate at saturating substrate concentration.

At a low range of substrate concentration,

i.e. $S \ll K_S$

The eq. (3.2) becomes

$$\mu = \left(\frac{\mu_{max}}{K_S}\right) S$$

Therefore, the 1st order correlation exists between μ and S.

3.1.2.1 Determination of Kinetic parameters

The kinetic parameters μ_{max} and K_S for the Monod model can be determined by taking reciprocal of both sides of Eq. (3.2) as follows:

$$\frac{1}{\mu} = \frac{K_S}{\mu_{max}} \frac{1}{S} + \frac{1}{\mu_{max}} \quad (3.5)$$

If the Monod model is valid, the plot of 1/μ versus 1/S should be linear in nature and $\mu_{max,}$ and K_S can be determined from the intercept and slope of the linear plot. The kinetic parameters may also be determined through the regression analysis of the data on μ against different substrate concentrations. During the determination of μ_{max} and K_S, initial values of μ against each concentration of limiting substrate have been used to avoid the inhibitory effect of metabolic products on growth kinetics.

3.1.2.2 The kinetic model describing pH influence

In general terms, the addition of the pH effect in the growth rate equation can take several forms. Here is a polynomial equation (Eq. (3.6)) used to describe the influence of pH on the growth rate of pure cultures

$$\mu_{max,N} = A + BpH + CpH^2 \quad (3.6)$$

Here, the normalized $\mu_{max,}$ i.e. $\mu_{max,N}$ is expressed as a function of pH in terms of a second-order polynomial.

Where,

$$\mu_{max,N} = \frac{\mu_{max}}{\mu_{max,opt}} \tag{3.7}$$

In the above equation (Eq. (3.7) $\mu_{max,opt}$ specify the value of μ_{max} at optimum pH. Therefore, eq. (3.2) can be written as:

$$\mu = \frac{\mu_{max,opt}\left(A+BpH+CpH^2\right)S}{K_S+S} \tag{3.8}$$

The value of $\mu_{max,opt}$ can be experimentally determined with the varying pH. pH at which the μ_{max} reaches its maximum is considered as optimum pH for particular microorganism. After the determination of $\mu_{max,opt}$ a plot of $\mu_{max,N}$ versus pH can be obtained using Eq. (3.6). From the plot, the constants of the second-order polynomial of Eq. (3.6) can be evaluated shown in Figure 3-2.

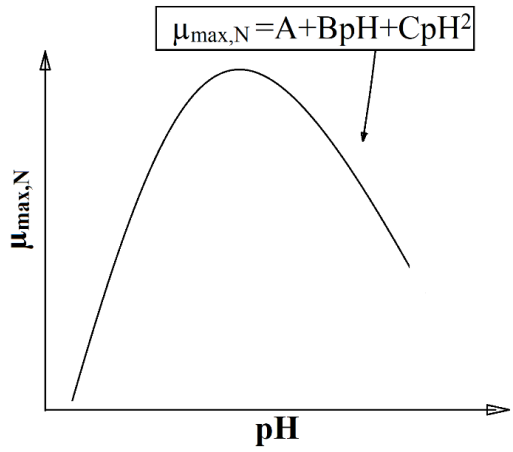

Figure 3-2 Variation of $\mu_{max,N}$ with respect initial pH

3.1.2.3 The kinetic model describing the influence of partial pressure

In the case of microbial reactions where gaseous hydrogen formed, one of the essential factor influencing microbial growth is the partial pressure. For hydrogen-producing bacteria, the microbial reaction can be expressed as follows:

$$\text{Substrate(S)} \xrightarrow{\text{Cell(X)}} \text{more Cells(X)} + \text{Product } (H_2) \tag{3.9}$$

and the rate of reaction will be:

$$r_c = \frac{dX}{dt} = \frac{\mu_{max}S}{K_S+S}X \tag{3.10}$$

where,

r_c microbial growth rate, ($gL^{-1}h^{-1}$);

X dry cell concentration, (gL^{-1});

t time, (h);

μ_{max} maximum specific growth rate of cells, (h^{-1});

S substrate concentration, (gL^{-1});

Ks Monod constant or substrate saturation constant, (gL^{-1});

A situation is considered that gaseous H_2 is forming and accumulated in the reactor headspace. In order to investigate the influence of accumulated H_2 in the reactor headspace on microbial growth; the headspace gas concentration is varied. Microbial growth inhibition occurs typically due to the excess presence of substrate, product, or other inhibitory substance in the cell growth medium. Hans and Levenspiel [111] express the inhibition of microbial growth model as:

$$\frac{dX}{dt} = \mu_{max}\left(1 - \frac{H_2}{H_2^*}\right)^n \left(\frac{S \cdot X}{S + k_s\left(1 - \frac{X}{X^*}\right)^m}\right) \tag{3.11}$$

Where,

H_2^* critical molar concentration of hydrogen at which microbial reaction ceases, (M);

n degree of cell inhibition;

m degree of substrate inhibition.

The degree of inhibition is defined as below,

$$\text{Degree of inhibition} = \frac{\upsilon_0 - \upsilon_i}{\upsilon_0}$$

Where,

υ_0 reaction rate in the absence of inhibitor

υ_i reaction rate in the presence of inhibitor

3.1.2.4 Evaluation of the growth associated kinetic constants

Taking inhibition of microbial growth Equation (3.11) into account, Equation (3.2) can be expressed as a generalized Monod model:

$$\mu = \frac{\mu_{max,obs} \cdot S}{K_{s,obs} + S} \tag{3.12}$$

where,

obs experimentally observed value.

$$\mu = \frac{1}{X} \cdot \frac{dX}{dt} \tag{3.13}$$

$$\mu_{max,obs} = \mu_{max}\left(1 - \frac{H_2}{H_2^*}\right)^n \tag{3.14}$$

$$K_{S,obs} = K_s\left(1 - \frac{X}{X^*}\right)^m \tag{3.15}$$

By reciprocating Equation (3.12), the following equation is obtained

$$\frac{1}{\mu} = \frac{K_{S,obs}}{\mu_{max,obs}} \cdot \frac{1}{S} + \frac{1}{\mu_{max,obs}} \tag{3.16}$$

1/μ and 1/S can be plotted for each initial hydrogen concentration in reactor headspace, which is shown in Figure 3-3. $\mu_{max,obs}$ and $K_{s,obs}$ at each headspace H_2 concentration can be calculated by evaluating the intercepts and abscissas on Figure 3-3.

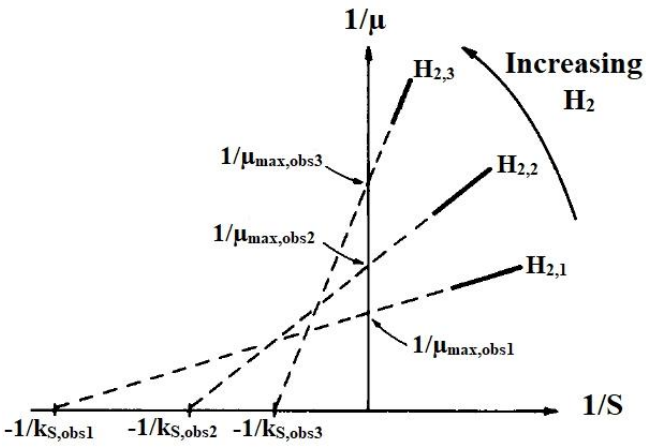

Figure 3-3 Evaluation procedure of $\mu_{max,obs}$ and $k_{S,obs}$ at various concentration of inhibitor

After determining the values of $\mu_{max,obs}$ and $K_{S,obs}$ at different headspace H_2 concentration, constants in Equation (3.11) can be evaluated. On taking logarithms of Equation (3.14), i.e.,

$$\ln(\mu_{max,obs=}) = n \cdot \ln\left(1 - \frac{H_2}{H_2^*}\right) + \ln(\mu_{max}) \tag{3.17}$$

The plot of $\ln(\mu_{max,obs})$ and $\ln(1-H_2/H_2^*)$ provides the values of μ_{max} and n. If the values of H_2^* is not evaluated from the experiments, then a guessed value of H_2^* has to be considered. A corrected value of H_2^* can be calculated until a straight line is obtained, which is shown in Figure 3-4.

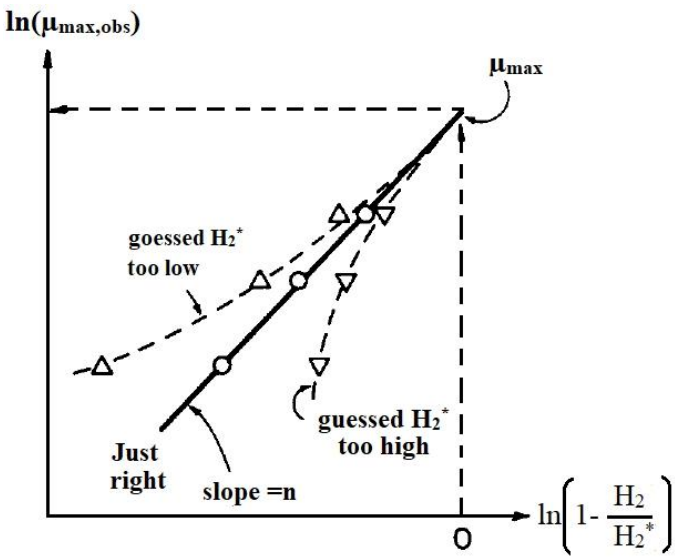

Figure 3-4 Evaluation procedure of u_{max}, n and H_2 for product inhibition*

3.2 Mathematical modelling of CSTBRs

Mathematical models are an essential part of establishing a real-life case for reactor operation. In this section, mathematical modelling is examined, and it is seen how vital modelling is. Main features and process of mathematical modelling will be mentioned in this section.

3.2.1 Modelling of CSTBR

One of the more critical features of modelling is the frequent need to review both the basic theory (physical model) and the mathematical equations, representing the physical model (mathematical model), in order to achieve agreement, between the model prediction and actual process behaviour (experimental data).

3.2.1.1 Material balance

One of the basic principles of modelling is that of the conservation of mass or matter. For a steady-state flow process, this can be expressed by the statement:

$$\begin{pmatrix}\text{Rate of mass flow}\\ \text{into the system}\end{pmatrix} = \begin{pmatrix}\text{Rate of mass flow}\\ \text{out the system}\end{pmatrix} \tag{3.18a}$$

Most real situations are, however, such that conditions change with respect to time. Under these circumstances, a steady-state material balance is inappropriate and must be replaced by a dynamic or unsteady-state material balance, expressed as,

$$\begin{pmatrix}\text{Rate of accumulation}\\ \text{of mass in the system}\end{pmatrix} = \begin{pmatrix}\text{Rate of mass flow}\\ \text{into the system}\end{pmatrix} - \begin{pmatrix}\text{Rate of mass flow}\\ \text{out the system}\end{pmatrix} \tag{3.18b}$$

Here the rate of accumulation term represents the rate of change in the total mass of the system, with respect to time, and at steady state, this is equal to zero. Thus, the steady-state material balance is seen to be a simplification of the more general dynamic balance. At steady state

$$\begin{pmatrix}\text{Rate of accumulation}\\ \text{of mass in the system}\end{pmatrix} = 0 = \begin{pmatrix}\text{Rate of mass flow}\\ \text{into the system}\end{pmatrix} - \begin{pmatrix}\text{Rate of mass flow}\\ \text{out the system}\end{pmatrix} \tag{3.18c}$$

therefore, when steady state is reached the above equation (3.18c) reduced to equation (3.18a)

3.2.1.2 Component balance

The previous discussion was in terms of the total mass of the system, but most processes streams, faced in general, comprise with more than one chemical component. If no chemical reaction occurs, the generalized equation for the conservation of mass can also be implemented to each chemical component of the system. Therefore, for any particular component

$$\begin{bmatrix}\text{Rate of accumulation}\\ \text{of mass of component}\\ \text{in the system}\end{bmatrix} = \begin{bmatrix}\text{Rate of mass flow}\\ \text{of component}\\ \text{into the system}\end{bmatrix} - \begin{bmatrix}\text{Rate of mass flow}\\ \text{of component}\\ \text{out of the system}\end{bmatrix} \tag{3.19}$$

Where a biochemical reaction occurs, the change can be taken into account by adding a reaction rate term into the component balance equation. Thus in the case of material balance will be

$$\begin{bmatrix}\text{Rate of}\\ \text{accumulation}\\ \text{of mass of}\\ \text{component}\\ \text{in the system}\end{bmatrix} = \begin{bmatrix}\text{Rate of mass}\\ \text{flow of}\\ \text{component into}\\ \text{the system}\end{bmatrix} - \begin{bmatrix}\text{Rate of mass}\\ \text{flow of}\\ \text{component out}\\ \text{of the system}\end{bmatrix} \pm \begin{bmatrix}\text{Rate of production}\\ \text{/consumption}\\ \text{of the component}\\ \text{by the reaction}\end{bmatrix} \tag{3.20}$$

While the principle of the material balance is straightforward, its application can often be quite tricky. Therefore, it is important to have a clear understanding of the nature of the system (physical model), which is to be modelled by the material balance equations and also of the methodology of modelling.

In the case of a microbial reaction in a CSTBR, bacterial cell consumes nutrients (substrate) increases its population and yields products. The flow rate of feed into and out of the reaction mixture's reactor and volume are F_{in}, F_{out} and V, respectively shown in Figure 3-5.

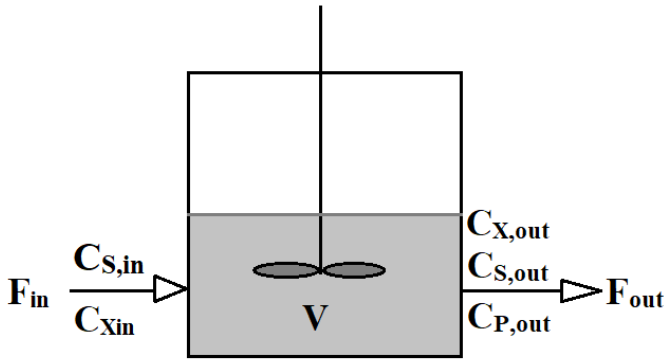

Figure 3-5 Schematic of Continuous Stirred tank bioreactor

The general biochemical reaction is as follows:

$$\text{Substrate (S)} \xrightarrow{\text{Cell(X)}} \text{more cell (X)} + \text{product (p)} \tag{3.21}$$

Therefore, the mass balance for each component can be expressed as

For substrate:

$$\begin{pmatrix}\text{Rate of}\\ \text{accumulation}\\ \text{of substrate}\\ \text{in the system}\end{pmatrix} = \begin{pmatrix}\text{Rate of}\\ \text{mass flow}\\ \text{of substrate}\\ \text{in the system}\end{pmatrix} - \begin{pmatrix}\text{Rate of}\\ \text{mass flow}\\ \text{of substrate out}\\ \text{of the system}\end{pmatrix} - \begin{pmatrix}\text{Rate of}\\ \text{consumption}\\ \text{of substrate}\\ \text{by biochemical}\\ \text{reaction}\end{pmatrix} \tag{3.22}$$

$$V\frac{dS}{dt} = F_{in}S_0 - F_{out}S - (-r_S).V \tag{3.23}$$

For cell:

$$\begin{pmatrix}\text{Rate of}\\ \text{accumulation}\\ \text{of cell}\\ \text{in the system}\end{pmatrix} = \begin{pmatrix}\text{Rate of}\\ \text{mass flow}\\ \text{of cell}\\ \text{in the system}\end{pmatrix} - \begin{pmatrix}\text{Rate of}\\ \text{mass flow}\\ \text{of cell out}\\ \text{of the system}\end{pmatrix} + \begin{pmatrix}\text{Rate of}\\ \text{formation}\\ \text{of cell}\\ \text{by biochemical}\\ \text{reaction}\end{pmatrix} \tag{3.24}$$

$$V\frac{dX}{dt} = F_{in}X_0 - F_{out}X + (r_X).V \tag{3.25}$$

For product:

$$\begin{pmatrix}\text{Rate of}\\ \text{accumulation}\\ \text{of product}\\ \text{in the system}\end{pmatrix} = \begin{pmatrix}\text{Rate of}\\ \text{mass flow}\\ \text{of product}\\ \text{in the system}\end{pmatrix} - \begin{pmatrix}\text{Rate of}\\ \text{mass flow}\\ \text{of substrate out}\\ \text{of the system}\end{pmatrix} + \begin{pmatrix}\text{Rate of}\\ \text{generation}\\ \text{of product}\\ \text{by biochemical}\\ \text{reaction}\end{pmatrix} \tag{3.26}$$

$$V\frac{dp}{dt} = 0 - F_{out}p + (r_P).V \tag{3.27}$$

There are several computational tools available to solve the above equations numerically. The solution of these design equations can be solved by knowing the biochemical reaction kinetics.

3.2.2 Stability analysis

An important criterion for good modelling of bioprocesses is the ability of the model to describe the static and dynamic behaviour of the industrial process dependably. In this regard, it is known that depending on the kinetic and operating parameters continuous bioreactors can exhibit a variety of nonlinear behaviour, including unique steady states, the coexistence of non-trivial steady-states with wash-out conditions, and the hysteresis phenomenon, as well as sustained oscillations.

Therefore, stability analysis of steady-states becomes essential to be analyzed in order to avoid the unfavourable situation for bioreactor operation. In general microbial reactions inside the bioreactor characterize by a nonlinear equation. Considering governing equations of a CSTBR through ordinary differential equations.

$$\frac{dx}{dt} = F(x) \leftrightarrow \begin{cases}\frac{dx_1}{dt} = F_1(x_1, x_2, \ldots\ldots x_n)\\ \frac{dx_2}{dt} = F_2(x_1, x_2, \ldots\ldots x_n)\\ \qquad . \\ \qquad . \\ \frac{dx_n}{dt} = F_n(x_1, x_2, \ldots\ldots x_n)\end{cases} \qquad \text{for } t \geq 0 \tag{3.28}$$

With the initial condition: $X(t = 0) = X_0$, and F(x) is a matrix nonlinear function of X. Then Taylor's Expansion:

$$F(x) \approx \underbrace{F(x^*)}_{=0} + \left.\underbrace{\frac{\partial x}{\partial t}}_{J(X)}\right|_{x=x^*} (x - x^*) + \cdots \tag{3.29}$$

The fixed points are:

$$\underbrace{F(x^*)}_{=0} \rightarrow \begin{cases}F_1(x_1, x_2, \ldots\ldots x_n) = 0\\ F_2(x_1, x_2, \ldots\ldots x_n) = 0\\ \qquad . \\ \qquad . \\ F_n(x_1, x_2, \ldots\ldots x_n) = 0\end{cases} \tag{3.30}$$

The Jacobian matrix will be as below:

$$J(x) = \begin{bmatrix} \frac{\partial F_1}{\partial x_1} & \cdots & \frac{\partial F_1}{\partial x_n} \\ \vdots & \ddots & \vdots \\ \frac{\partial F_n}{\partial x_1} & \cdots & \frac{\partial F_n}{\partial x_n} \end{bmatrix} \tag{3.31}$$

Let's consider a very small perturbation from x^* and it is given by $\delta x = x - x^*$. Then equation (3.28) will be

$$\frac{d(\partial x)}{dt} = J(x^*) \text{ for } t \geq 0 \tag{3.32}$$

With the initial conditions, $\delta x(t = 0) = x_0 - x^*$, and $J(x^*)$ is a constant matrix independent of x.

The general solution of the above equation (3.30) close to the fixed points is

$$x(t) = x^* + \sum_{i=1}^{n} a_i \mathbf{V_i} e^{\lambda_i t}; \quad \left.\begin{matrix} \lambda_i = \text{eigenvalues} \\ \mathbf{V_i} = \text{eigenvector} \end{matrix}\right\} \text{ of } J(x^*) \tag{3.33}$$

the characteristics equation is

$$\det|J(x^*) - \lambda \mathbf{1}| = 0 \tag{3.34}$$

a_i are the constants determined by using initial conditions.

The procedure for stability analysis of fixed-point are as below:

- Determine the fixed points vector, x^* by solving equation (3.30), $F(x^*) = 0$
- Construct the Jacobian matrix, $J(x) = \frac{\partial F(x)}{\partial x}$
- Compute eigenvalues of $J(x^*)$ by solving equation (3.34).
- Determine the nature of fixed point, i.e., whether it is a stable or unstable fixed point based on eigenvalues' real part.

If all eigenvalues have real parts less than zero, then the fixed point x* is stable. If at least one of the eigenvalues has a real part greater than zero then the fixed point x* is stable. Otherwise, there is no conclusion and require an investigation of higher-order terms.

Table 3-1 Nature of Stability

Eigenvalues	Graph
All real and negative	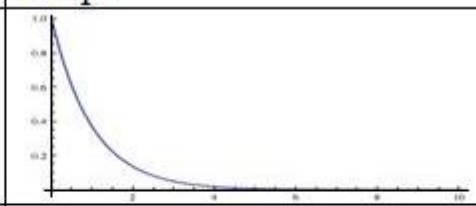
All real and one or more are positive	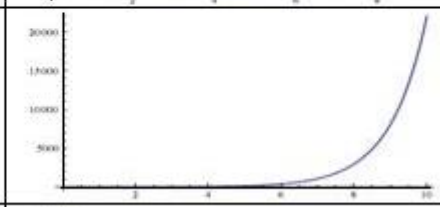
All real eigenvalues are negative and there are imaginary parts	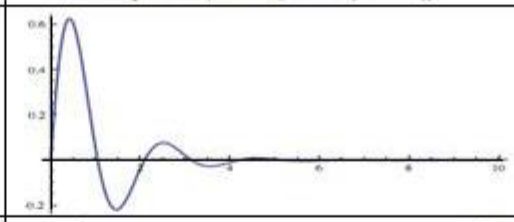
One or more eigenvlaues have a positive real part and there are imaginary parts	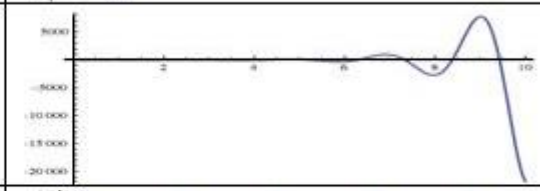
Real parts of the eigenvlaues are zero and there are imaginary parts	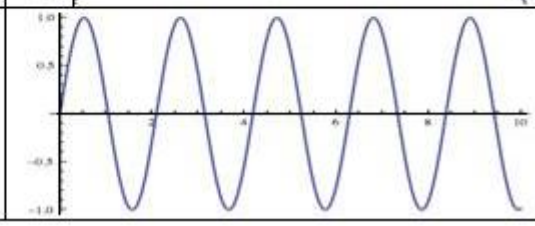

3.3 Sensitivity analysis

The concept of sensitivity has now generated a useful mathematical tool, called sensitivity analysis, which is widely practised in various fields in science and engineering. Systems control, process optimization, chemical and reactor design, cell biology, and ecology are the areas where generally it is used. The wide applications arise as the concept of sensitivity determines a relation between system behaviour and a parameter, and the sensitivity value determines this relationship.

In general mathematical models provides an explicit or implicit relationship between the system behaviour and the input parameters. This behaviour is described by the state or output variables, which is indicated in general as *dependent variables* that change in time and space. The physicochemical parameters of the systems (such as those related to reaction kinetics, thermodynamic equilibria, and transport properties) as well as initial conditions, operating conditions, and geometric parameters are considered as the *input parameters*. The physicochemical parameters are measured experimentally or calculated theoretically. Therefore, these parameters are always subject to uncertainties.

On the other hand, the initial and operating conditions may change in time for a variety of reasons. Both of these affect system behaviour. In particular, parametric sensitivity specifies the effect of variations of the input parameters on the system behaviour.

3.3.1 Local sensitivity

Considering a chemical system for a single variable y, which changes in time according to the following general differential equation,

$$\frac{dy}{dt} = f(y, \phi, t) \tag{3.35}$$

With initial condition

$$y(0) = y^{i} \tag{3.36}$$

where,

y dependent variable,

t time,

ϕ vector containing the m system input parameters

The function, f is considered to be continuous and continuously differentiable in all its arguments. They confirm that the above equation has a unique solution called the nominal solution, which is continuous in t and ϕ, represented by

$$y = y(t, \phi) \tag{3.37}$$

By changing the yth parameter in the parameter vector ϕ, from ϕ_j to $\phi_j + \Delta\ \phi_j$. Then, the corresponding solution for y, the current solution, becomes

$$y = y(t, \phi_j + \Delta\phi_j) \tag{3.38}$$

where for shortness, only ϕ_j, the parameter changed only. Since y is a continuous function of ϕ_j, the solution of equation (3.38) can be expanded into a Taylor series as follows:

$$y(t, \phi_j + \Delta\phi_j) = y(t, \phi_j) + \frac{\partial y(t,\phi_j)}{\partial \phi_j} \cdot \Delta\phi_j + \frac{\partial^2 y(t,\phi_j + \theta \cdot \Delta\phi_j)}{\partial \phi_j^2} \cdot \frac{\Delta\phi_j^2}{2} \tag{3.39}$$

where $0 < \theta < 1$. If $\Delta\ \phi_j$ is sufficiently small, *i.e.*, $\Delta\phi_j << \phi_j$ the Taylor series can be reduced after the linear term, leading to

$$\Delta y = y(t, \phi_j + \Delta\phi_j) - y(t, \phi_j) \approx \frac{\partial y(t,\phi_j)}{\partial \phi_j} \cdot \Delta\phi_j \tag{3.40}$$

where Δy represents the variation of y due to the change of the input parameter ϕ_j, given by $\Delta\phi_j$. If an infinitesimal variation is considered ($\Delta\phi_j \rightarrow 0$), it follows from Equation. (3.40) that

$$s(y; \phi_j) = \frac{\partial y(t,\phi_j)}{\partial \phi_j} = \lim_{\Delta\phi_j \rightarrow 0} \frac{y(t,\phi_j + \Delta\phi_j) - y(t,\phi_j)}{\Delta\phi_j} \tag{3.41}$$

This is defined as the first-order local sensitivity, of the dependent variable, y, with respect to the input parameter, ϕ_j. Although higher-order local sensitivities can be represented in a similar fashion, the treatment will be limited to first-order local sensitivities, since most applications are based on linear sensitivity analysis. The local sensitivity, $s(y; \phi_j)$, is also called the absolute sensitivity.
Another quantity related to local sensitivity, commonly used in sensitivity analysis, is the normalized sensitivity. The normalized sensitivity of y with respect to ϕ_j, $S(y; \phi_j)$ is defined as

$$S(y;\phi_j) = \frac{\phi_j}{y} \cdot \frac{\partial y}{\partial \phi_j} = \frac{\partial \ln(y)}{\partial \ln(\phi_j)} = \frac{\phi_j}{y} \cdot s(y;\phi_j) \tag{3.42}$$

which serves to normalize the magnitudes of the input parameter ϕ_j and the variable y. In the literature, the normalized sensitivity is sometimes also referred to as the relative sensitivity. Once the local sensitivity $s(y; \phi_j)$, is known, the calculation of $S(y; \phi_j)$ is straightforward.
When the sensitivity of y with respect to each parameter of ϕ vector is considered, m sensitivity indices will be obtained which can be defined as the row sensitivity vector,

$$s^T(\mathbf{y};\phi_j) = \frac{\partial \mathbf{y}}{\partial \phi} = \left[\frac{\partial y}{\partial \phi_1}\ \frac{\partial y}{\partial \phi_2}\ \cdots\ \frac{\partial y}{\partial \phi_m}\right] = [s(y;\phi_1)s(y;\phi_2)\cdots s(y;\phi_m)] \tag{3.43}$$

In the case of a system described by *n* dependent variables, the dynamics are in general given by a set of differential equations,

$$\frac{\partial y}{\partial t} = f(\mathbf{y}, \phi, t), \qquad \mathbf{y}(0) = \mathbf{y}^i \tag{3.44}$$

For a biochemical system, the n vector of the dependent variables, y, may include the involved biochemical species and other state variables. At the same time, ϕ_j is the m vector containing the system input parameters. For a selected input parameter, ϕ_j, each variable's local sensitivity, y_i, can be computed, based on equation (3.41). Thus, there will be n sensitivity indices with respect to the same input parameter, which constitutes the column sensitivity vector,

$$s(\mathbf{y};\phi_j) = \frac{\partial \mathbf{y}}{\partial \phi_j} = \left[\frac{\partial y_1}{\partial \phi_j}\ \frac{\partial y_2}{\partial \phi_j}\ \cdots\ \frac{\partial y_n}{\partial \phi_j}\right]^T = \left[s(y_1;\phi_j)\ s(y_2;\phi_j)\ \cdots\ s(y_n;\phi_j)\right]^T \tag{3.45}$$

Now combining all the row and column sensitivity vectors, an n×m matrix of the sensitivity indices is obtained, which is usually referred to as the sensitivity matrix,

$$S(\mathbf{y};\phi) = \begin{bmatrix} \frac{\partial y_1}{\partial \phi_1} & \cdots & \frac{\partial y_1}{\partial \phi_m} \\ \vdots & \ddots & \vdots \\ \frac{\partial y_n}{\partial \phi_1} & \cdots & \frac{\partial y_n}{\partial \phi_m} \end{bmatrix} = \begin{bmatrix} s(y_1;\phi_1) & \cdots & s(y_1;\phi_m) \\ \vdots & \ddots & \vdots \\ s(y_n;\phi_1) & \cdots & s(y_n;\phi_m) \end{bmatrix} \tag{3.46}$$

3.3.2 Objective sensitivity

In general, the sensitivity analysis is performed, when a specific behaviour of the system is the objective of interest, then it is referred to as the objective or objective function. This can be one of the system-independent variables which can be determined from the system-independent variables, such as, the conversion of a reactant at a specific time or position; the magnitude of the pH minimum in time or space; the time required by a reactant to reach a particular conversion value; concentration maximum of

an intermediate product in a complex reaction network; selectivity of the desired product at the reactor outlet.

The first four performance indices can be obtained from a direct solution of the relevant model equations. At the same time, the latter three are computed, through a proper definition, from the model solution. Assuming that the objective function, I, is a continuous function of a chosen j^{th} parameter, ϕ_j in the parameter vector, ϕ, the corresponding sensitivity with respect to ϕ_j, $s(I; \phi_j)$, is defined as

$$s(I;\phi_j) = \frac{\partial I}{\partial \phi_j} = \lim_{\Delta\phi_j \to 0} \frac{I(\phi_j + \Delta\phi_j) - I(\phi_j)}{\Delta\phi_j} \tag{3.47}$$

which will be denoted as the objective sensitivity. Similar to Equation. (3.42), the normalized objective sensitivity, $S(I; \phi_j)$, is defined as

$$S(I;\phi_j) = \frac{\phi_j}{I} \cdot \frac{\partial I}{\partial \phi_j} = \frac{\partial \ln(I)}{\partial \ln(\phi_j)} = \frac{\phi_j}{I} \cdot s(I;\phi_j) \tag{3.48}$$

3.3.3 Computation of sensitivities

For the single-variable system (3.35), to compute the local sensitivity of y for the jth input parameter, ϕ_j, both sides of system equation (3.35) is first differentiated with respect to ϕ_j. Then, considering the definition (3.41) for the local sensitivity leads to

$$\frac{d(\partial y/\partial \phi_j)}{dt} = \frac{ds(y;\phi_j)}{dt} = \frac{\partial f}{\partial y} \cdot \frac{\partial y}{\partial \phi_j} + \frac{\partial f}{\partial \phi_j} = \frac{\partial f}{\partial y} \cdot s(y;\phi_j) + \frac{\partial f}{\partial \phi_j} \tag{3.49}$$

which represents the local sensitivity equation. The initial condition can be obtained by differentiating the initial condition (3.36). Depending on which input parameter in the vector ϕ is chosen, then

$$s(y;\phi_j)\big|_{t=0} = \begin{cases} 0, & \phi_j \neq y^i \\ 1, & \phi_j = y^i \end{cases} \tag{3.50a}$$

Or in more concise form

$$s(y;\phi_j)\big|_{t=0} = \delta(\phi_j - y^i) \tag{3.50b}$$

where δ is the Kronecker delta function. By simultaneously solving the model equation (3.33) and the sensitivity equation (3.47), along with initial conditions (3.34) and (3.48), Both of the dependent variable y and the corresponding local sensitivity $s(y; \phi_j)$, are functions of time. This method is called the direct differential method (DDM) for computing local sensitivities.

For the model given by equation (3.42), have n dependent variables, then in order to obtain the sensitivity of the ith variable, y_i, to the jth input parameter, ϕ_j; computation of the sensitivities is needed for all the n variables to ϕ_j, as they may interact with each other. Thus, in this case, n sensitivity equations needed to be solved together with the n model equations. The n sensitivity equations can be presented in the form

$$\frac{ds(y;\phi_j)}{dt} = \mathbf{J}(t) \cdot s(\mathbf{y};\phi_j) + \frac{\partial \mathbf{f}(t)}{\partial \phi_j} \tag{3.41}$$

Where, $s(y; \phi_j;)$ is the column sensitivity vector defined by equation (3.43), and

$$\mathbf{J}(t) = \frac{\partial \mathbf{f}}{\partial \mathbf{y}} = \begin{bmatrix} \frac{\partial f_1}{\partial y_1} & \cdots & \frac{\partial f_1}{\partial y_n} \\ \vdots & \ddots & \vdots \\ \frac{\partial f_n}{\partial y_1} & \cdots & \frac{\partial f_n}{\partial y_n} \end{bmatrix}, \quad \frac{\partial \mathbf{f}(t)}{\partial \phi_j} = \begin{bmatrix} \frac{\partial f_1}{\partial \phi_j} \\ \frac{\partial f_2}{\partial \phi_j} \\ \vdots \\ \frac{\partial f_n}{\partial \phi_j} \end{bmatrix} \tag{3.52}$$

are usually referred to as the n × n Jacobian matrix and the n × 1 nonhomogeneous term, respectively.

3.4 Nonlinear system analysis: Bifurcation theory

A model for dynamical systems may contain one or more parameters. In general, the dynamics of a system is affected by the magnitude of the parameters. Typically, this effect is continuous, and the nature of dynamics is unchanged. However, in some cases, the changes are discontinuous, and the character of the dynamical behaviour transforms. The value of the parameter at which such a change occurs is called the bifurcation point. The phenomenon itself is called the bifurcation. It can be stated that bifurcation has happened if the topological structure of the phase plane changes. Some of the changes are listed below

a. Change in the number of fixed points (steady states)
b. Changes in the stability of fixed points
c. Formation or destruction of closed orbits
d. Formation or destruction of closed path joining a saddle point (homoclinic bifurcation)
e. Formation or destruction of saddle connection (heteroclinic bifurcation)

A variety of bifurcation phenomena have been identified and classified. They are typically classified as below:

3.4.1 Saddle-node bifurcation:

This bifurcation is characterized by the fact that at this point of bifurcation, fixed points are either generated or destroyed.

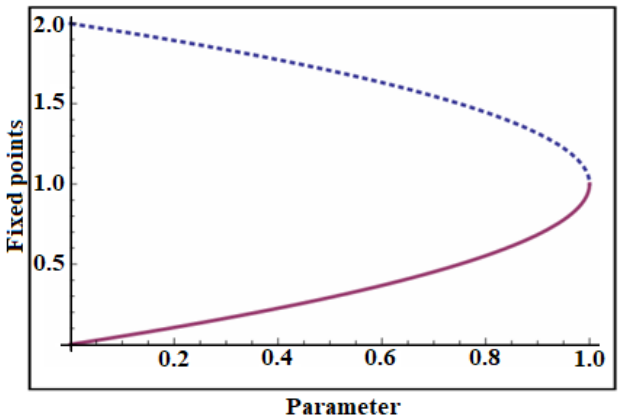

Figure 3-6 Example of Saddle Node bifurcation, Stable (solid line), Unstable branch (dotted line)

3.4.2 Transcritical bifurcation (flip bifurcation):

In this case, the number of fixed points does not change. But they exchange their characters at the critical value of the parameter. In another way, there is an exchange of stability at the bifurcation point in the case of transcritical bifurcation.

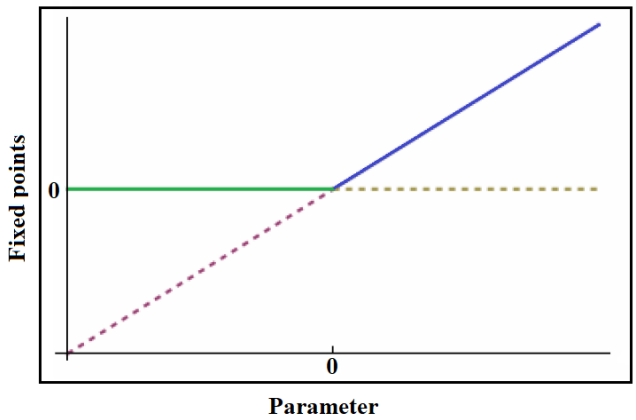

Figure 3-7 Example of Transcritical bifurcation, Stable branch (solid line), Unstable branch (dotted line)

3.4.3 Pitchfork bifurcation:

Pitchfork bifurcation is characterized by splitting of a single fixed point into three (including the original fixed point). The two new fixed points are symmetrically placed about the original fixed point. The original fixed point also changes its stability at the critical point. This bifurcation arises in cases where the system has symmetry.

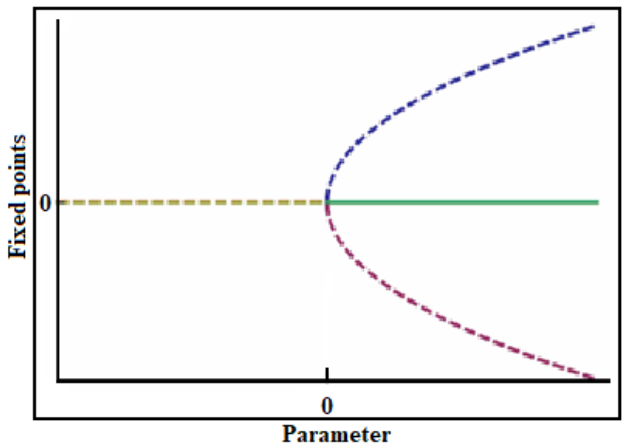

Figure 3-8 Example of Pitchfork bifurcation, Stable branch (solid line), Unstable branch (dotted line)

3.4.4 Fold bifurcation:

Consider the following equation,

$$\dot{x} = x(1 - x)^2 + a \tag{3.53}$$

The fixed points are given as solutions of

$$x(1-x)^2 + a = 0 \text{ or } x^3 - 2x^2 + x + a = 0 \tag{3.54}$$

For a cubic equation of the form $x^3 + bx^2 + cx + d = 0$, we define,

$$p = \frac{1}{3}(3c - b^2), q = \frac{1}{27}(27d - 9bc + 2b^3), R = \left(\frac{p}{3}\right)^3 + \left(\frac{q}{2}\right)^3$$

If R > 0, there is only one real root. If R = 0, there are three real roots, two of which are equal. If R < 0, there are three real and unequal roots. For the present case, b = -2c, c = 1 and d = a. Hence,

$$p = -\frac{1}{3}, q = a + \frac{1}{27} \text{ and } R = \frac{a^2}{4} + \frac{a}{27}$$

It can be observed that if a > 0, R > 0 and there is only one fixed point. If a = 0, and there are two fixed points. If -4/27 < a < 0 , R < 0 and there are three fixed points. If a −< -4/27, and there is only one fixed point.

Case 1: a = 0 : In this case, the fixed points are $x_f = 0$ and $x_f = 0$

$$\left.\frac{dX_a}{dx}\right|_{x_f} = (1-x_f)^2 - 2x_f(1-x_f) = (1-x_f)(1-3x_f)$$

Note that

$$\left.\frac{dX_{a_0=0}(x)}{dx}\right|_{x_f=1} = 0$$

Thus a=0 is a bifurcation point

Case 2: a > 0: There is a single fixed point, $x_f < 0$. In this case, bifurcation cannot occur since

$(1-x_f)(1-3x_f)$ cannot become zero for negative values of x_f.

Case 3: -4/27 < a <0, there are three fixed points now.

Case 4: a<-4/27: there is only one fixed point now.

Therefore, the critical values of the parameters are a = 0 and a = −4/27. The fixed point at which bifurcation can occur are: x_f =1for a = 0 and x_f = 1/3 for a = −4/27.

$$X_a(x_f) = x_f(1-x_f)^2 + a = 0 \tag{3.55}$$

The corresponding value of a is

$$a = x_f(1-x_f)^2 = \frac{1}{3}\left(1-\frac{1}{3}\right)^2 = -\frac{4}{27} \tag{3.56}$$

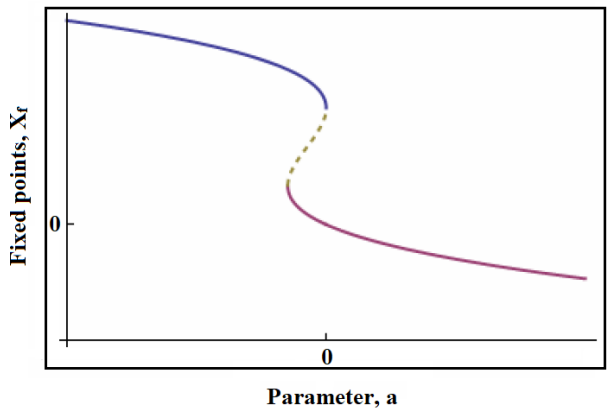

Figure 3-9 Example of Fold bifurcation, Stable branch (solid line), Unstable branch (dotted line)

From the above Figure 3-9, it can be observed there are two bifurcation points, 0=a and -4/27=μ. As the bifurcation diagram folds back and hence this bifurcation is called the fold bifurcation. Such a system shows a phenomenon called hysteresis.

3.5 Experimental details

General information on materials and equipment used for experiments is described below. Later the description of analytical methods applied for quantification of products is given.

3.5.1 Chemicals

Different chemicals were used for the preparation of bacterial growth, medium and solutions methods as listed in Tables 3-2 to 3-4

Table 3-2 DeMan, Rogosa and Sharpe (MRS) media composition in 100mL solution

CHEMICALS	AMOUNT (g)
Peptone	1.0
Beef extract	0.8
Yeast extract	0.4
Glucose	2.0
Sodium acetate trihydrate	0.5
Polysorbate 80 (also known as Tween 80)	0.1
Dipotassium hydrogen phosphate	0.2
Triammonium citrate	0.2
Magnesium sulfate heptahydrate	0.02
Manganese sulfate tetrahydrate	0.005

Table 3-3 Cooked meat (CM) medium in 100mL solution

CHEMICALS	AMOUNT (g)
Beef extract	4.5
Glucose	0.2
Peptone	2.0
NaCl	0.5

Table 3-4 Chemicals used for DNS methods

Chemicals
Sodium hydroxide
3,5-dinitro salicylic acid
Sodium-potassium tartrate
Deionized water

3.5.2 Microorganisms

There are three microorganisms used in this research study, two of them are probiotic lactic acid bacteria and one hydrogen-producing bacteria. The details are given below:

1. Pediococcus acidilactici (NCIM-2292),
2. Lactobacillus casei (NCIM-2360),
3. Clostridium acetobutylicum (NCIM 2337)

All of these microorganisms were procured from NCIM, Pune, India.

3.5.3 Equipment

The list of equipment used in a different stage of experiments are presented in Table 3-5

Table 3-5 List of equipments used for experiments

Equipment	Manufacturer
BOD incubator shaker	G. B. Enterprises, Kolkata, India
Autoclave	G. B. Enterprises, Kolkata, India
Ultracentrifuge	Superspin R-V/ FM, Plasto Crafts, India)
Hot Air Oven	G. B. Enterprises, Kolkata, India
Laminar Air Flow	G. B. Enterprises, Kolkata, India
Magnetic Stirrer	Remi; 5MLH,India
Fermenter	B. Braun Biotech International
Peristaltic pump	Enertech electronics Pvt. Ltd, India
UV-visible spectrophotometer	Varian. India
Reverse Phase HPLC (YL9100)	Technolab Systems
pH meter.	Sartorius, PB-11
ORSAT apparatus	G. B. Enterprises, Kolkata, India
GC FID	GC-2014, Shimadzu Analytical Pvt. Ltd

3.5.4 Preparation of seed culture

3.5.4.1 Seed culture for lactic acid bacteria

An autoclaved 250ml conical flask containing 100ml sterile MRS broth was taken. Syringe filtered Glucose substrate is added to the conical flask and shaken well to dissolve the glucose completely in the medium. A slant test tube culture of chosen bacteria was taken, and a loopful of the bacteria was carefully taken out from the test tube with the help of a sterile inoculating loop. The cotton plug of the conical flask is removed, and the loopful of the bacterial inoculum is inserted into the flask. The sterile MRS broth was then inoculated with the bacterial culture by dipping the loop containing the inoculum and transferred it to the media by gentle shaking. The loop was taken out from the flask, and the cotton plug is placed to the mouth of the flask and sealed tightly with the parafilm strip. The flask is kept in the incubator at 37 ºC and incubated for 24h. The total procedure was performed in the laminar airflow bench, maintaining strictly sterile conditions. From the 24h old broth culture, several subcultures were prepared as required for the experiment.

3.5.4.2 Seed culture for *clostridium acetobutylicum*

An autoclaved 250ml conical flask containing 100ml sterile CM (Cooked meat) media broth was taken. Syringe filtered Glucose substrate is added to the conical flask and shaken well to dissolve the glucose

entirely in the medium. A slant test tube culture of chosen bacteria was taken, and a loopful of the bacteria was carefully taken out from the test tube with the help of a sterile inoculating loop. The cotton plug of the conical flask is removed, and the loopful of the bacterial inoculum is inserted into the flask. The sterile CM broth was then inoculated with the bacterial culture by dipping the loop containing the inoculum and transferred it to the CM media. As this bacteria is strictly anaerobic an inert gas Argon was purged for 3min to remove oxygen from the headspace of the conical flask. After proper purging, a rubbed stopper was used to seal the whole system tightly. The neck of the flask was also sealed with the parafilm strip. The flask was kept in the incubator at 37ºC and incubated for 72h. The total procedure was performed in the laminar airflow bench, maintaining strictly sterile conditions. From the 72h old broth culture, several subcultures were prepared in the same manner as described above as required for the experiment.

3.6 Analytical methods

In order to determine the quality and quantity of the product, several analytical procedures were adopted. The adopted analytical methods are described below.

3.6.1 Spectrophotometry

The spectrophotometric method was used for the determination of bacterial cell concentration. For the generation of the standard plot, the dry cell weight method was followed. In this method, the optical density versus its corresponding known cell concentrations was plotted. For measuring the dry cell weight, 15mL of bacterial cultures of different incubation period were centrifuged at 10,000×g, at 4ºC for 15 minutes. The supernatant was discarded, and the cell precipitate was washed with distilled water and transferred to aluminium cups of known weight. The cups containing the cell mass were dried in a hot air oven for 24h at 80ºC. The weight of the dry biomass was calculated by subtracting the weight of the aluminium cup. The biomass concentration was determined using the sample volume and weight of the dry cell. The samples were analyzed spectrophotometrically at 600nm, and the optical densities were plotted against the corresponding biomass concentration determined through dry cell weight method. The standard plot was used for the measurement of the biomass concentration from their corresponding optical density.

3.6.2 DNS method

The amount of glucose consumed by the bacteria was determined by the used of DNS method. For this analysis, each liquid sample was centrifuged at 10,000 rpm, and the supernatant was collected to find out the reducing sugar concentration using the dinitrosalicylic (DNS) acid reagent [20]. For analysis 1ml DNS was added to each test tubes containing supernatant. The test tubes were cotton plugged and were placed in a boiling water bath for exactly 15min and cooled on ice to room temperature. Finally, 9mL of deionized water was added, mixed well by inversion and the concentration of glucose was determined through analyzing the optical density obtained from spectrophotometry at 540nm, against blank. The preparation of DNS acid reagent is described as below.

3.6.2.1 Preparation of DNS solution

In order to prepare DNS a colouring reagent solution (Solution 1) was prepared by dissolving 12g of sodium-potassium tartrate in 8mL of 2M NaOH by direct heating and constant stirring. Another solution was prepared (solution 2) by dissolving 0.1 M of 3,5- dinitrosalicylic acid in 20mL of deionized water by direct heating and continuous stirring. Solution 1 was then added slowly into solution 2 and mixed

well by stirring. Deionized water was added to the mixture of solution 1 and 2 to make up the volume to 100mL. The prepared DNS was then stored in a coloured bottle at room temperature and was stored in the refrigerator.

3.6.3 GC- FID

The gaseous products were analysed in this study by the use of Gas Chromatography Flame Ionization Detection Method (GC-FID). In this study, the gaseous products were mainly CO_2 and Hydrogen. The analytical method was used only for the detection of hydrogen. Therefore each time the produced gases were first passed through the ORSAT instrument containing 1N (normal) potassium hydroxide to remove CO_2. The remaining gas composition was then analyzed by gas chromatography. On a molecular sieve column (13×, 180 cm by 1⁄4 inch, 60–80 mesh), the gases were separated where argon was the carrier gas at 100 ◦C. A 406 Packard GC equipped with a thermal conductivity detector (TCD) of 100 mA was used to measure hydrogen concentration.

3.6.4 HPLC

Reversed-phase HPLC analysis was done using a YL9100 HPLC system which consists of YL9101 vacuum degasser, YL9110 quarternary pump, YL9131 column compartment, YL9120 UV/Vis detector with manual sample injector Rheodyne 9725i. The analytical column was a Tracer Excel 120 ODSA, 250 mm×4.6 mm, and with particle size five µm. Chromatographic separation was carried out at the column oven temperature 40ºC ± 2ºC with a flow rate 1.0 mL/min of isocratic elution using two solvents: A – ($3\cdot10^{-2}$ mol/L H_3PO_4 in water) and B – acetonitrile HPLC grade in ratio 88:12 v/v. The injected sample volume was 20 µL. The quantitation wavelength was set at 200 nm. For optimization of separation of analytes, aqueous solutions of H_3PO_4 in three different concentrations were tested: 1st – $1.2\cdot10^{-2}$ mol/L, 2nd – $2.1\cdot10^{-2}$ mol/L and 3rd – $3.1\cdot10^{-2}$ mol/L.

3.7 Experimental method

There are several batches, and continuous type experiments were conducted in order to achieve the aim of this study. The detailed procedure of the experiments is provided below.

3.7.1 Batch experiments to examine pH influence on microbial growth

There are two types of Lactic acid bacteria which were used to perform the batch experiments in order to investigate the influence of pH on bacterial growth. Moreover, Batch experiments were conducted to determine the kinetic parameters of bacterial growth.

3.7.1.1 Growth study for *pediococcus acidilactici*

The bacterial strain was maintained in MRS medium. Composition of MRS medium is provided in **Error! Reference source not found.** The growth kinetics of *Pediococcus acidilactici* were determined b y conducting batch experiments in Erlenmeyer flask using 50mL modified MRS (MMRS) medium. The temperature was maintained at an optimum value of 37°C. Initial pH was varied in the range of 4.0-8.0. At each initial pH, experiments were conducted by varying the MMRS medium's initial glucose concentration in the range of 5.0-30.0g/L. The concentrations of all components other than glucose in mMRS medium were always the same as those of MRS medium. At each initial substrate concentration, the microbial growth pattern was studied for 24h. Samples were withdrawn at 2h interval during incubation. Each sample's biomass concentration was determined using the spectrophotometric method [112], and glucose concentration was determined using the DNS method [113]. Each sample was

centrifuged at 10000rpm, and the supernatant was analyzed for Lactic acid using HPLC. Each experimental run was repeated three times to ensure the repeatability and the statistical accuracy of the results.

3.7.1.2 Growth study for *lactobacillus casei*

The procedure of batch experiments was the same as for described for *Pediococcus acidilactici*. The differences were the bacteria was *lactobacillus casei*, the range of variation of glucose concentration was from 10g/L to 50g/L, and the pH was varied from 3 to 8, respectively.

3.7.1.3 Growth study for c*lostridium acetobutylicum*

Batch experiments were conducted in 250 mL cork fitted Erlenmeyer flask having an outlet port at the bottom. A cork was fitted to a glass tube and connected to a gas measuring tube for gas sampling. The batch experimental setup is shown in Figure 2a, and the whole system is presented schematically in Figure 2b.

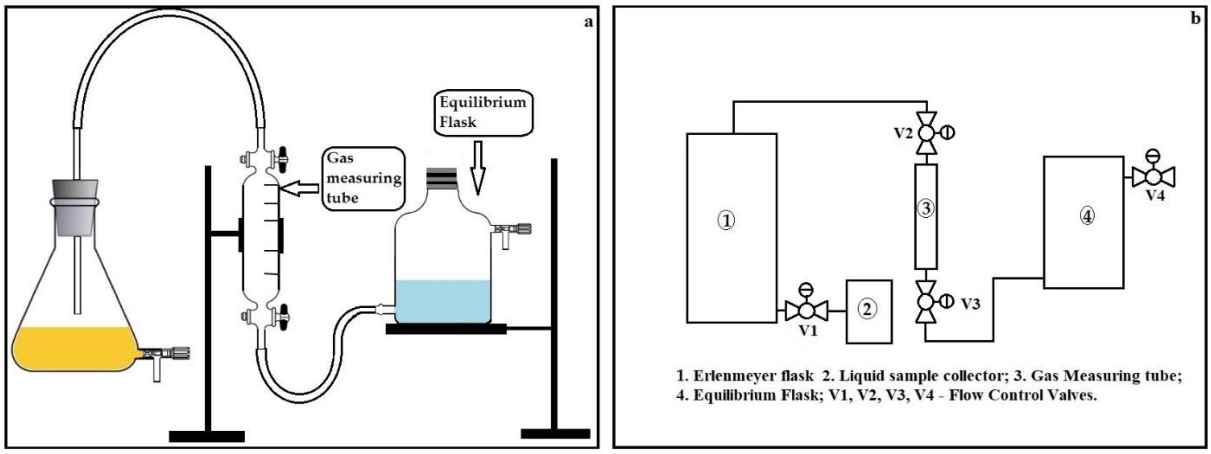

Figure 3-10 Experimental setups for batch test (a); schematic diagram of the experimental setup (b)[114]

An Erlenmeyer flask was half-filled with the CM medium and 1% (v/v) of inoculum into the medium then the remaining void was filled completely with the CM medium. The composition of CM medium is provided in Table 3-3. The flask was then firmly sealed with the cork, and 150 mL of argon gas was passed through the flask by a glass tube for displacing the CM media from the bottom of the flask. Thus, the flask was left with 100 mL of CM medium with bacterial culture, and a mixture of argon and hydrogen occupied 150 mL headspace. The whole setup was then kept in the incubator at maintaining the temperature of 37 ◦C and pH of 7.2, which are the ideal conditions for this bacteria. Initial hydrogen concentration in the reactor headspace were varied in the range of 0% (v/v) to 50% (v/v). Initially, H_2 experiments were performed by varying the modified CM medium's glucose concentration in the range of 2 g/L to 5 g/L. At each initial substrate concentration, microbial growth pattern was observed for 30 h. An interval of 3h, samples were collected. The produced gas was accumulated in the reactor headspace and was taken out from the flask using a gas sampling tube, connected with the flask for examining the gas composition after each interval. Each experimental run was repeated three times to ensure the repeatability and the statistical accuracy of the results.

Each sample's biomass concentration was determined in terms of optical density with a spectrophotometer at 600 nm wavelength. The spectrophotometry method is described above. Each liquid sample was centrifuged at 10,000 rpm, and the supernatant was collected in order to find out the

reducing sugar concentration using the dinitrosalicylic (DNS) acid reagent [20]. Next, 100 mL of gas was collected after every 3h interval from the batch reactor's headspace using a gas sampling tube. Collected gas was then passed through an ORSAT apparatus for the removal of CO_2 gas present in the gas sample. Furthermore, the remaining gas composition was analyzed by gas chromatography which is described in Chapter 3.6.3.

3.7.1 CSTBR operation

Continuous flow reactor operations were conducted in a 2L Braun bioreactor. The total bioreactor set up was autoclaved to make it free from any contamination prior to adding microbial growth. 10g of the substrate (glucose) was sterilized and added to the reactor. The media was inoculated with the bacteria by adding a previously calculated amount of inoculums of the bacteria, maintaining a biomass's desired concentration. A feed tank is prepared by adding 2L of fresh MRS medium in a conical flask with an outlet near its bottom. UV-sterilized glucose (20 g) was added to the feed tank media, and a rubber pipe fitted with a flow control valve was attached to the outlet. Another feed tank was prepared by adding 2L of fresh distilled water in a conical flask having an outlet port. Sodium hydroxide (1.6g) was added to this feed tank, and a rubber pipe fitted with a flow control valve was attached to the outlet. The flow rate of the feed stream was adjusted to the desired value as per the optimized values of the dilution rate (D) and the dilution rate for the base feed stream (D_1).

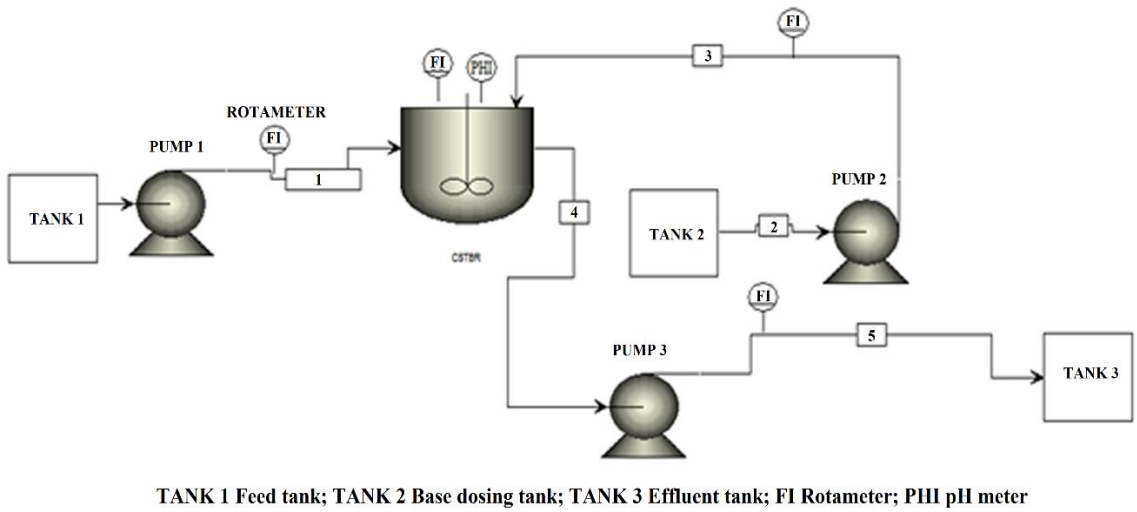

Figure 3-11 The flow-sheet of the reactor set up[115]

After adding the substrate and bacterial inoculum to the bioreactor, the connecting pipe from the feed tank and base dosage tank was connected with the bioreactor through the input channel. The control valves were used for maintaining the flow rate of the feed tank and the base tank. The feed tank and the base dosage tank were connected to the peristaltic pump. The product outlet was connected to the sample outlet channel through a peristaltic pump to continuously draw effluent from the reactor vessel. The effluent was collected in a 1000ml conical flask. After connecting all of the parts of the entire set up the feed and output flow streams are started. The flow rates of the inlet the feed stream, as well as base feed stream and the outlet stream, are adjusted to same values according to the dilution rate (D) and dilution rate for base feed stream (D_1) of the system so that the working volume of the reactor must be maintained at a constant value. The reactor's sample is collected after every one hour from the outlet stream and kept in sample vials in the refrigerator for further analysis. The reactor is operated up to a specific

estimated time. The samples are used to obtain the growth of the Biomass as well as to check the pH of each of the sample. The reactor system was maintained at 37°C, and the pH of the reactor medium was kept at 6.7. The flow-sheet of the reactor set up has been represented in Figure 3-11.

3.8 Case Studies

Four case studies were conducted to fulfil the research objectives set at the beginning to achieve the overall aim of the thesis. Table 3-6 lists the Case study and the objectives that each case study address

Table 3-6: Details of case studies and corresponding objectives

Case	Objective number	Objectives
Case 1 Case 2 Case 4	**1**	To investigate the influence of pH on microbial growth experimentally in a batch reactor, and develop a kinetic model to determine constants which will describe the nature of microbial growth.
	2	To develop a mathematical model of a continuous stirred tank bioreactor (CSTBR) system with the help of the kinetic parameters.
Case 1	**2**	To derive a simple dimensionless steady-state multiplicity criterion for the CSTBR. The approach should be able to identify the set of values of input variables, which lead to multiple steady-states.
	3	To derive an expression for theoretical sensitivity function of pH concerning different input variables
	4	To conduct experiments to study the parametric sensitivity for sets of input parameters belonging to the regimes of multiple and unique steady states as determined using multiplicity criterion.
Case 2	**5**	To develop a generalized criterion for sensitivity with the help of normalized sensitivity analysis which does not depend upon the topology of pH contour for recognizing the extent of input parameters where a CSTBR exhibits sensitive behaviour.
Case 3	**6**	To explore the influence of hydrogen in the reactor headspace on microbial growth Experimentally in a batch reactor.
	7	To develop kinetic models to explain how the produced hydrogen influences the bacterial growth and hydrogen production rate simultaneously.
Case 4	**8**	To investigate the effects of the operating parameters on the stability behaviour of a CSTBR for biohydrogen production. The stability analysis will be carried out using elementary principles of bifurcation theory shows the dynamics characteristics of the reactor model, including a steady-state multiplicity analysis.

4 Case studies results and discussions

In this chapter, the details of the four case studies, along with the procedure of obtaining the mathematical results are described. Other calculation details are given in the Appendix section.

The results obtained and their discussions are presented in the following sections.

4.1 Case 1: Parametric sensitivity of pH and steady-state multiplicity in CSTBR

In the first case study, an anti-pathogenic bacteriocin production process called pediocin from lactic acid bacteria *pediococcus acidilactici* was considered. Experiments were conducted in a batch reactor, and the experimental data is analysed to determine the kinetic parameters of microbial growth and their dependence on pH. Using the fundamental knowledge of microbial growth and dimensionless variables unstructured mathematical model for the CSTBR is derived.

The mathematical model is then used to derive a simple dimensionless steady-state multiplicity criterion for the CSTBR. This criterion then identifies the set of values of input variables which lead to multiple steady states. Different input variables, namely dilution rates of nutrient and base streams and concentrations of substrate and base stream for pH control, influence the pH within the reactor. Theoretical expressions are derived for pH sensitivity to all these input variables. The parametric sensitivity for sets of input parameters belonging to the regimes of multiple and unique steady states as determined using multiplicity criterion. The experimental and simulated transient behaviours of pH are also analyzed and compared to verify the existence of parametric sensitivity under both multiple and unique steady-state conditions.

4.1.1 Determination of Growth Kinetics

The growth kinetics of *Pediococcus acidilactici* has been determined using classical Monod type growth model, which was described in chapter 3.1.2. Kinetic parameters of the Monod model, were determined using the initial specific growth rate at each initial glucose concentration obtained at each initial pH. Eq. (3.2) can be linearized in the form of Eq. (4.1) to find out the kinetic parameters (μ_{max} and K_s) by making double reciprocal plots of μ versus S at each initial pH.

$$\frac{1}{\mu} = \frac{K_S}{\mu_{max} S} + \frac{1}{\mu_{max}} \tag{4.1}$$

Regression analysis is used to find the best fit for a straight line on a plot of 1/ μ vs 1/S and the values of μ_{max} and K_S are determined. The variation of μ_{max} with initial pH would determine an optimum value of pH at which μ_{max} is maximum, thus describing optimum conditions for the microbial growth. By plotting the values of normalized μ_{max}, i.e. $\mu_{max,N}$ versus initial pH, a second-order correlation was then obtained, as given in Eq. (4.2)

$$\mu_{max,N} = (A + B \cdot pH + C \cdot pH^2) \tag{4.2}$$

Where,

$$\mu_{max,N} = \frac{\mu_{max}}{\mu_{max,opt}} \tag{4.3}$$

Therefore, Eq. (3.2) was written as

$$\mu = \frac{\mu_{max,opt}(A+B\cdot pH+C\cdot pH^2)S}{K_S+S} \tag{4.4}$$

This correlation defines the influence of pH on the specific microbial growth rate. To establish a mathematical model of a CSTBR, design equations for mass or molar balance for each component are expressed with the help of the kinetic model (Eq. 4.4). The constants were obtained from the batch experiments.

4.1.2 Biochemical reactions in the CSTBR

The biochemical reaction occurring in the system is represented as follows:

$$X + Glucose(S) \rightarrow nX + CH_3CH(OH)COOH\ (p) \tag{4.5}$$

The desired product is pediocin, and its formation is influenced by the system pH. To control pH, NaOH has been fed to the system. The acid-base neutralization reaction may be written as follows,

$$CH_3CH(OH)COOH\ (p) + NaOH(s_b) \rightarrow CH_3CH(OH)COONa(s_A) + H_20 \tag{4.6}$$

The pH is correlated to the concentrations of salt and lactic acid according to the Henderson-Hasselbalch equation [116] equation as follows

$$pH = pK_a + \log\frac{s_A}{p} \tag{4.7}$$

Where,

K_a Equilibrium dissociation constant for lactic acid,

s_A molar concentrations of sodium lactate

p molar concentrations lactic acid

4.1.3 Mathematical model for CSTBR for pH control

The continuous bioreactor setup is schematically represented in Figure 4-1.

The mathematical model for the CSTBR was developed using the following assumptions:

1. The bioreactor is uniformly stirred, i.e., concentration within the reactor is spatially uniform.
2. Temperature effect of the reaction is negligible.

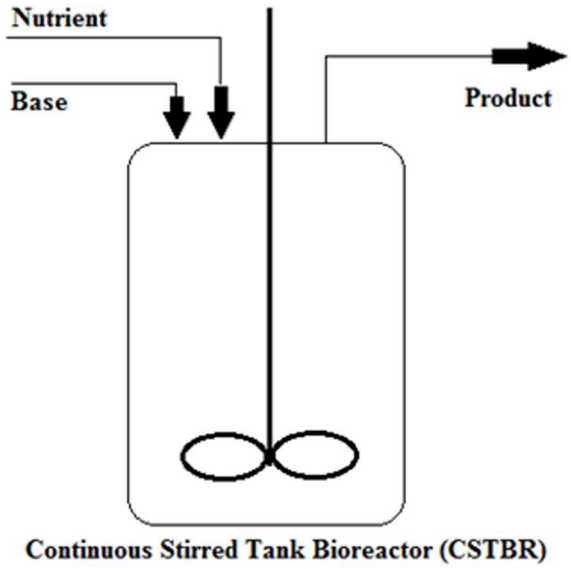

Figure 4-1 Schematic of a Continuous Stirred Tank Bioreactor

The differential mass and mole balance equations for different components, namely biomass, substrate, lactic acid and sodium lactate are as follows:

Mass balance Equations:

Biomass:

$$\frac{dX}{dt} = (\mu - D - D_1) \tag{4.8}$$

Substrate:

$$\frac{dX}{dt} = D(S_0 - S) - D_1 S - \frac{1}{Y_{X/S}} \mu X \tag{4.9}$$

Mole balance equations:

Lactic acid:

$$\frac{dp}{dt} = -D_p + \frac{Y_{P/X} \mu X}{M_a} - D_1(s_b + p) \tag{4.10}$$

Sodium Lactate:

$$\frac{dS_A}{dt} = D_1(s_b - s_A) - Ds_A \tag{4.11}$$

pH dynamics:

Differentiating equation (4.7), with respect to time,

$$\frac{dpH}{dt} = \frac{1}{S_A}\frac{ds_A}{dt} - \frac{1}{p}\frac{dp}{dt} \tag{4.12}$$

Since bacteriocin is a growth-related product [117,118], the influence of the sensitivity of pH towards bacteriocin formation is expected to be similar to that of biomass. For the model's simplicity, the mass balance of bacteriocin has been excluded from the mathematical analysis.

4.1.4 Generalized criterion for multiplicity

In order to obtain a generalized criterion for multiplicity the mass, molar and pH balances equations (Eq (4.8) to (4.12)) are suitability transform dimensionless where initial substrate concentration S_0 and the dilution rate of feed concentration D_1 are considered as scaling parameters for concentration and time, respectively. The detailed definition of each dimensionless variables are provided in Table 4-1.

Table 4-1 Definitions of the dimensionless variable used in the model

Parameter	definition	Parameter	definition
x	$\frac{X}{S_0\, Y_{X/S}}$	τ	tD
y	$\frac{S}{S_0}$	θ	$\frac{\mu}{D}$
z	$\frac{pM_a}{S_0 Y_{P/S}}$	θ_1	$\frac{D_1}{D}$
R	$\frac{s_b\, M_b}{S_0}$	m	$\frac{\mu_m}{D}$
L	$\frac{s_A M_c}{S_0}$	n	$\frac{K_s}{S_o}$

In dimensionless form, the system equations (4.8) through (4.12) were written as follows:

$$\frac{dx}{d\tau} = (\theta - \theta_1 - 1)x \tag{4.13}$$

$$\frac{dy}{d\tau} = (1 - y) - \theta x - \theta_1 y \tag{4.14}$$

$$\frac{dz}{d\tau} = -z + \theta x - \theta_1 \left[\frac{M_a}{M_b\, Y_{P/S}} R + z\right] \tag{4.15}$$

$$\frac{dL}{d\tau} = \left[\frac{M_c}{M_b} R - L\right] \theta_1 - L \tag{4.16}$$

$$\frac{dpH}{d\tau} = \frac{1}{L}\frac{dL}{d\tau} - \frac{1}{z}\frac{dz}{d\tau} \tag{4.17}$$

And

$$\theta = \frac{my}{n+y} H \tag{4.18}$$

And

$$H = A + BpH + CpH^2 \tag{4.19}$$

When a process or system has a single steady-state for a particular value or a set of input or manipulated variables, it is defined as uniqueness. On the other hand, if the system offers more than one solution or multiple solutions for a set of input parameters, then its called multiplicity.

Under steady-state, the left-hand sides of equations (4.13) - (4.17) become zero. After further mathematical operations, the following condition with respect to pH has been obtained,

$$\mathrm{In}(\alpha + \beta pH + \gamma pH^2) = -\frac{pH}{2.303} \tag{4.20}$$

Where,

$$\alpha = (M + n(1 + mMA) - p_m)\frac{K_a}{p_m}; \tag{4.21}$$

$$\beta = (nmMB)\frac{K_a}{p_m}; \tag{4.22}$$

$$\gamma = (nmMC)\frac{K_a}{p_m}; \tag{4.23}$$

The details of mathematical operations have been provided in **Appendix 2**. Equation (4.20) was represented in the following form:

$$f(pH, \alpha, \beta, \gamma) = \mathrm{In}(\alpha + \beta pH + \gamma pH^2) + \frac{pH}{2.303} = 0 \tag{4.24}$$

The multiplicity of solutions of the transcendental equation (4.24) is dependent only on the values of α, β and γ. The number of solutions was obtained as the number of intersecting points of the function, f(pH α β and γ) with the abscissa of pH-f system of coordinate. This was obtained by setting

$$\frac{\partial f}{\partial pH} = 0 \tag{4.25}$$

This leads to the following roots,

$$pH_{1/2} = \frac{4.606\gamma + \beta}{2\gamma}(-1 \pm \sqrt{1 - \omega}) \tag{4.26}$$

Where,

$$\omega = \frac{4\gamma(2.303\beta + \alpha)}{(4.606 + \beta)^2}; \tag{4.27}$$

For a higher value of ω (>1), the radicand in equation (4.27) is negative. Using the same principles, as cited by Kauschus et al. [119], one steady state at the most is obtainable for $\omega \geq 1$, and more than one steady states are possible for $\omega < 1$. Therefore, it is understandable that the nature of steady states is extremely influenced by ω and hence the values of *α*, β and γ.

4.1.5 Theoretical parametric sensitivity analysis

The parametric sensitivity analysis was done on the basis of the differential equations (4.8) - (4.12). The generalized form of the model equations is as follows:

$$\frac{\mathbf{dy}}{\mathbf{dx}} = F(x, y, \phi) \tag{4.28}$$

Where **y** is a vector of dependent variables, in the present investigation, 'y' may be concentrations of biomass, substrate, product and salt, **x** is an independent variable namely time, and **ϕ** represents the vector of input parameters of the system.

The first order local sensitivity or only local sensitivity with respect to vector **ϕ** is given by,

$$s_{j\phi_i} = \frac{dy_j(t,\phi_i)}{d\phi_i} \tag{4.29}$$

Where,

j any output variable

i any input vector

by differentiating equation (4.29), the following equation, is obtained

$$\frac{ds_{\phi_i}}{dt} = Js_{\phi_i} + \frac{\partial F(t,y,\phi_i)}{\partial \phi_i} \tag{4.30}$$

Where J is the jacobian matrix of the system. The initial conditions for the above equation (4.30) is $s_{\phi i}$= 0 at t = 0. For the CSTBR under consideration,

$$y_1 = X, y_2 = S, y_3 = p, y_4 = s_A, y_5 = pH$$

$$F_1 = \frac{dX}{dt}, \qquad F_2 = \frac{dS}{dt}, F_3 = \frac{dp}{dt}, F_4 = \frac{ds_A}{dt} \text{ and } F_5 = \frac{dpH}{dt}$$

and

$$\phi_1 = D, \phi_2 = D_1, \phi_3 = s_b, \phi_4 = S_0$$

The dynamic equations for the parametric sensitivity in a CSTBR for any variable y_i become,

$$\frac{d}{dt}\left[s_{j\phi i}\right] = \left[\frac{\partial F_j}{\partial X}\frac{\partial F_j}{\partial S}\frac{\partial F_j}{\partial p}\frac{\partial F_j}{\partial s_A}\frac{\partial F_j}{\partial pH}\right]\left[\frac{dX}{d\phi_i}\frac{dS}{d\phi_i}\frac{dp}{d\phi_i}\frac{ds_A}{d\phi_i}\frac{dpH}{d\phi_i}\right]^T + \left[\frac{\partial F_1}{\partial \phi_i}\frac{\partial F_2}{\partial \phi_i}\frac{\partial F_3}{\partial \phi_i}\frac{\partial F_4}{\partial \phi_i}\frac{\partial F_5}{\partial \phi_i}\right]^T \tag{4.31}$$

Equation (4.31) may be written with respect to D as follows:

$$\frac{d}{dt}\left[\frac{dX}{dD}\right] = \left[\frac{\partial F_1}{\partial X}\frac{\partial F_1}{\partial S}\frac{\partial F_1}{\partial p}\frac{\partial F_1}{\partial s_A}\frac{\partial F_1}{\partial pH}\right]\left[\frac{dX}{dD}\frac{dS}{dD}\frac{dp}{dD}\frac{ds_A}{dD}\frac{dpH}{dD}\right]^T + \left[\frac{\partial F_1}{\partial D}\right] \tag{4.32}$$

$$\frac{d}{dt}\left[\frac{dS}{dD}\right] = \left[\frac{\partial F_2}{\partial X}\frac{\partial F_2}{\partial S}\frac{\partial F_2}{\partial p}\frac{\partial F_2}{\partial s_A}\frac{\partial F_2}{\partial pH}\right]\left[\frac{dX}{dD}\frac{dS}{dD}\frac{dp}{dD}\frac{ds_A}{dD}\frac{dpH}{dD}\right]^T + \left[\frac{\partial F_2}{\partial D}\right] \tag{4.33}$$

$$\frac{d}{dt}\left[\frac{dp}{dD}\right] = \left[\frac{\partial F_3}{\partial X}\ \frac{\partial F_3}{\partial S}\ \frac{\partial F_3}{\partial p}\ \frac{\partial F_3}{\partial s_A}\ \frac{\partial F_3}{\partial pH}\right]\left[\frac{dX}{dD}\ \frac{dS}{dD}\ \frac{dp}{dD}\ \frac{ds_A}{dD}\ \frac{dpH}{dD}\right]^T + \left[\frac{\partial F_3}{\partial D}\right] \tag{4.34}$$

$$\frac{d}{dt}\left[\frac{ds_A}{dD}\right] = \left[\frac{\partial F_4}{\partial X}\ \frac{\partial F_4}{\partial S}\ \frac{\partial F_4}{\partial p}\ \frac{\partial F_4}{\partial s_A}\ \frac{\partial F_4}{\partial pH}\right]\left[\frac{dX}{dD}\ \frac{dS}{dD}\ \frac{dp}{dD}\ \frac{ds_A}{dD}\ \frac{dpH}{dD}\right]^T + \left[\frac{\partial F_4}{\partial D}\right] \tag{4.35}$$

$$\frac{d}{dt}\left[\frac{dpH}{dD}\right] = \left[\frac{\partial F_5}{\partial X}\ \frac{\partial F_5}{\partial S}\ \frac{\partial F_5}{\partial p}\ \frac{\partial F_5}{\partial s_A}\ \frac{\partial F_5}{\partial pH}\right]\left[\frac{dX}{dD}\ \frac{dS}{dD}\ \frac{dp}{dD}\ \frac{ds_A}{dD}\ \frac{dpH}{dD}\right]^T + \left[\frac{\partial F_5}{\partial D}\right] \tag{4.36}$$

The overall set of dynamic equations for the parametric sensitivities of different output variables with respect to all input variables are provided in the **Appendix 2**.

4.1.6 Results

4.1.6.1 Influence of pH on microbial growth

The influence of initial pH on the microbial growth was studied by conducting batch experiments, and the results were presented in Figures 4-2 to 4-6. In these figures, the time history of dry cell concentrations was showed when pH at each batch reaction was varied initially. From these figures, it was observed that initially altered pH has a significant impact on microbial growth.

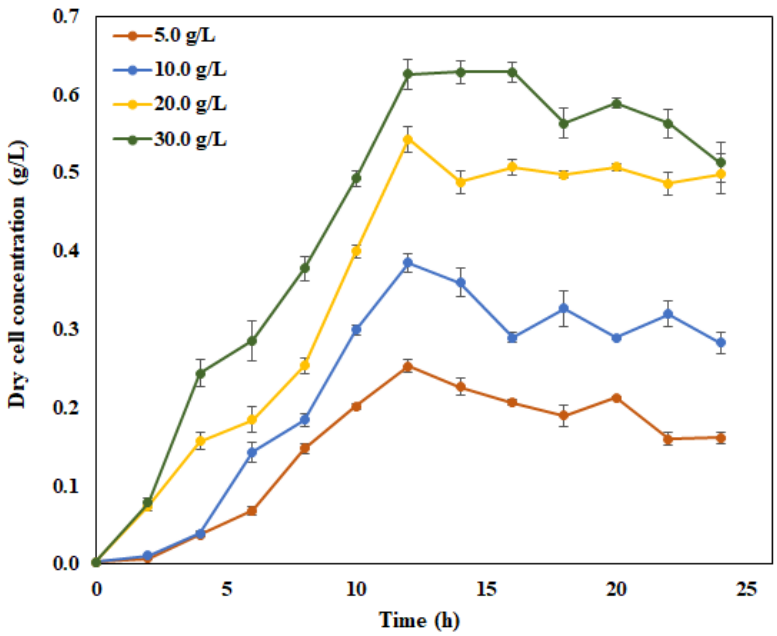

Figure 4-2 Experimental time histories of dry cell concentration (g/L) at an initial value of pH=4

At first, when the batch experiments were started the initial pH of the reaction medium was 4, and the initial glucose concentration was varied in the range of 5.0g/L to 30 g/L. At each variation of glucose, the microbial growth pattern was observed for 24h. The time histories of microbial growth were presented in Figure 4-2. From this figure, it can be seen that the microbial growth was started immediately for 20g/L and 30g/L initial glucose concentration. Whereas, in the case of 5g/L and 10g/L initial glucose concentration, the microbial growth started after 2h of inoculation. The maximum dry cell concentration was observed for 30g/L glucose which was 0.625g/L.

As the initial pH of the batch reactor was changed to 5 there was no significant change in Lag phase of microbial growth observed. On the other hand, a substantial shift in the microbial growth rate was seen. The time histories in this initial pH=5 were shown in Figure 4-3. The trend of microbial growth, in this case, was the same as pH= 4 as the exponential growth was ended at 12h. The Maximum dry cell of 1.46g/L was obtained in this case when initial glucose concentration was 30g/L.

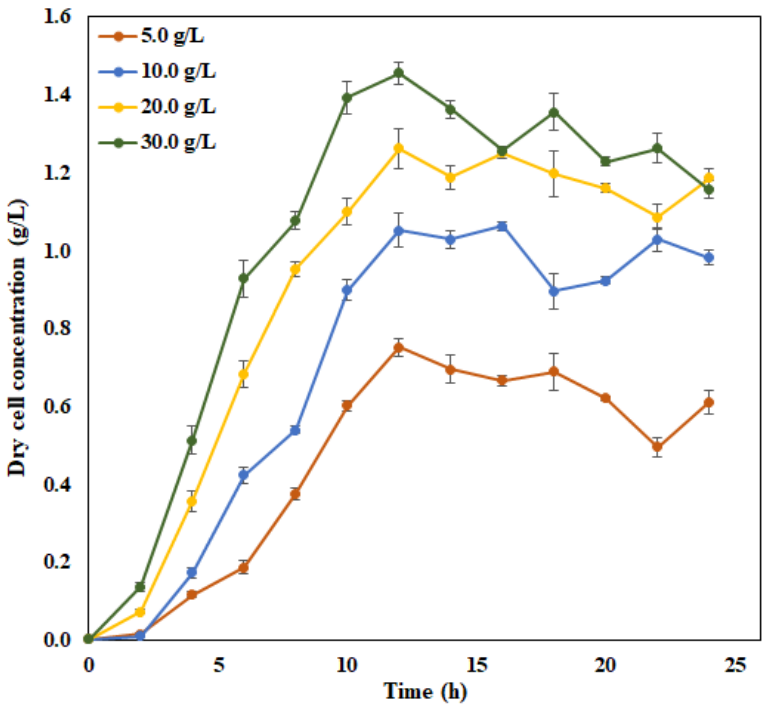

Figure 4-3 Experimental time histories of dry cell concentration (g/L) at an initial value of pH=5

No substantial change in microbial growth was observed when the pH of the reaction medium altered initially to 6. In this case, almost the same phenomenon was observed compare to pH= 5 conditions. The time histories of microbial growth with the variation of glucose concentration at initial pH=6 were presented in Figure 4-4. Here also the microbial growth was stated immediately after the inoculation, and the exponential phase was ended at 12h. The maximum dry cell concentration of 1.79g/L was observed.

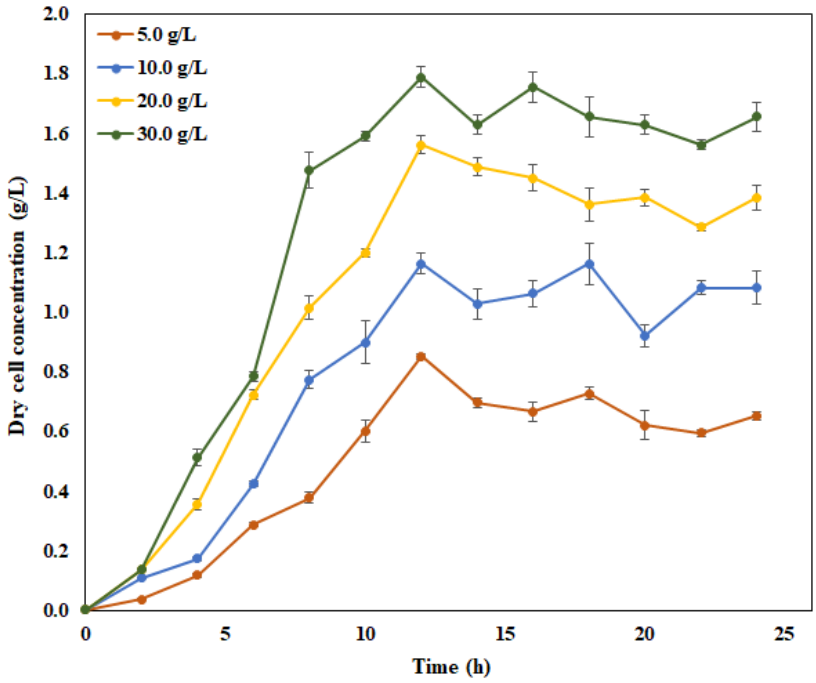

Figure 4-4 Experimental time histories of dry cell concentration (g/L) at an initial value of pH=6

When the initial pH of the reaction medium of batch reactor change to 7, a monotonic increase in microbial growth was observed, which was shown in Figure 4-5. In this figure, the time histories of microbial growth with the variation of initial glucose concentration with fixed initial pH were presented. In this case, the same growth pattern was observed for each initial glucose concentration. The lag phase of microbial growth initiated immediately whereas; the exponential phase stoped at 12h after inoculation. The maximum dry cell concentration of 1.96g/L was found when initial glucose concentration was 30g/L.

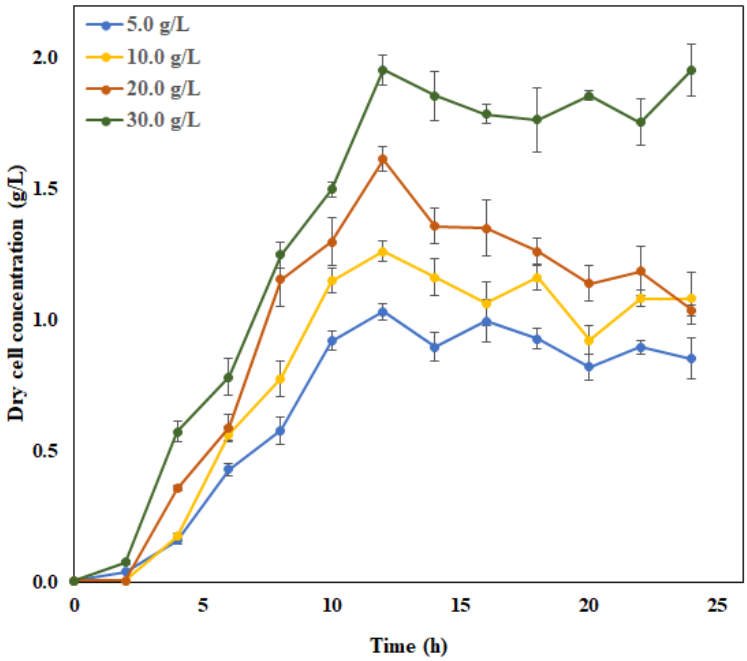

Figure 4-5 Experimental time histories of dry cell concentration (g/L) at an initial value of pH=7

As the pH of the reaction medium of batch reactor altered initially fro 7 to 8, a different scenario in microbial growth pattern was observed. In Figure 4-6, the time histories of the microbial growth rate at pH=8 at different initial glucose concentration were presented. In this case, the microbial growth rate decreased compared to pH=7 condition. Although the microbial growth pattern was similar to that of pH=7 condition, the maximum dry cell concentration lowered to 1.55g/L.

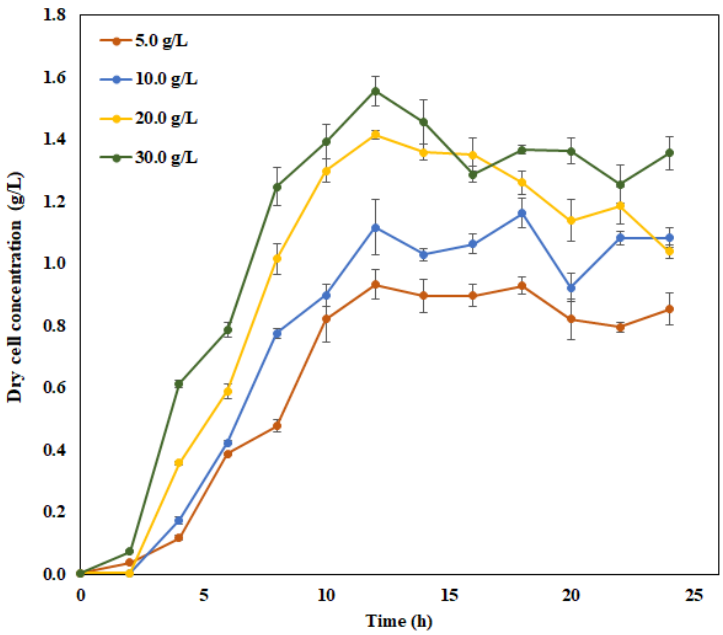

Figure 4-6 Experimental time histories of dry cell concentration (g/L) at an initial value of pH=8

4.1.6.2 Determination of Kinetic parameters

In the present experiments, at each initial pH, the substrate concentration was varied from 5g/L to 30g/L. For each combination of initial pH and substrate, the specific growth rate of microorganisms was determined. By using Equation (4.1), plots of 1/μ and 1/S were obtained at each initial pH. μ_{max} and k_s at each initial pH were determined by evaluating the intercepts and abscissas on Figure 4-7. The values of μ_{max} and k_s are provided in Table 4-2.

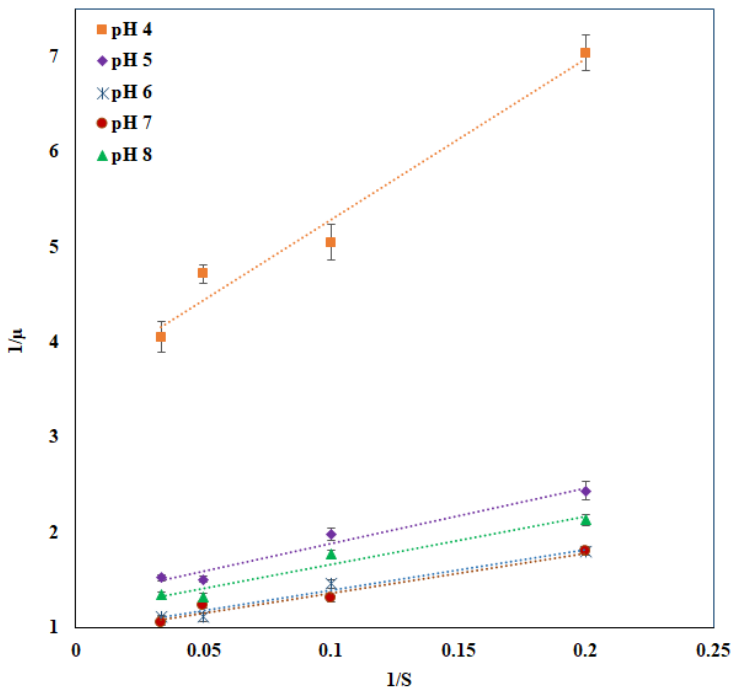

Figure 4-7 Determination of μ_{max}, and k_s at different initial pH

From Table 4-2, it can be observed that k_s, does not change in any systematic manner with the change of pH. Therefore, one can easily state there is inhibition due to substrate concentration. By plotting μ_{max} vs initial pH, it was found that μ_{max} became maximum when the value of initial pH is 6.7, which is considered as the optimum pH and the corresponding μ_{max} is optimum μ_{max},i.e. $\mu_{max,opt}$.

Table 4-2 Values of observed rate constants from experiments

Initial pH	μ_{max}	k_s
pH 4	0.278	4.70
pH 5	0.766	4.45
pH 6	1.042	4.47
pH 7	1.059	4.46
pH 8	0.864	4.35

Now plotting the values of $\mu_{max.N}$, which can be obtained from Equation (4.3) as a function of initial pH, a second-order correlation, as shown in Equation (4.5) was obtained. The plot of $\mu_{max.N}$ vs initial pH is shown in Figure 4-8. The values of second-order correlation constants along with other growth associated kinetic constants are provided in Table 4-3.

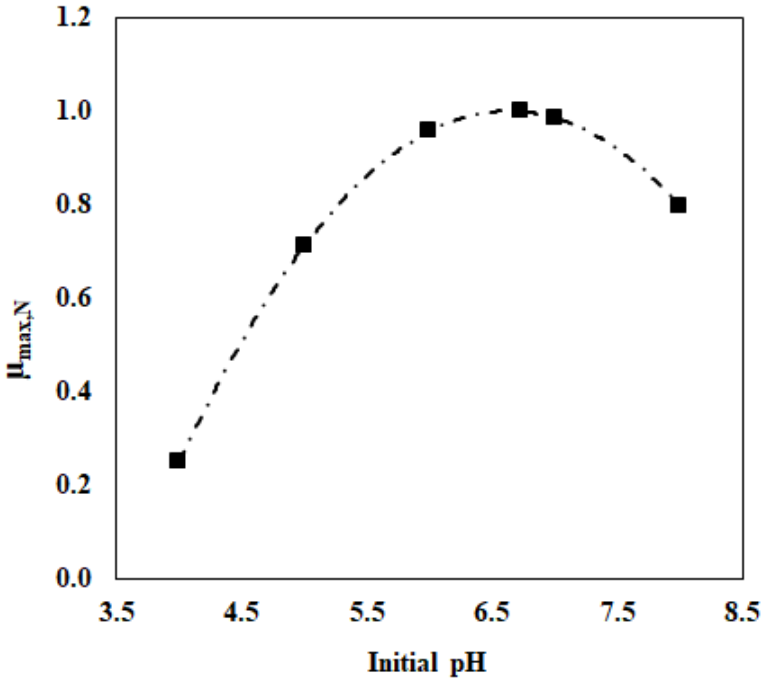

Figure 4-8 Variation of normalized $\mu_{max,N}$ with initial pH

Table 4-3 Values of kinetic parameters

Kinetic parameters	Values
$\mu_{max,opt}$ (h^{-1})	1.0775
K_S(gL^{-1})	4.5017
$Y_{X/S}$ (gg^{-1})	0.1
$Y_{p/X}$ (gg^{-1})	0.065
$Y_{p/S}$ (gg^{-1})	0.0065
A	-3.76195
B	1.4368
C	-0.10835

4.1.6.3 Sensitivity of pH through theoretical analysis

Time-trajectories of the sensitivity of system pH with respect to input variables D, D_1, S_0 and s_b have been plotted in Figure 4-9**.** From the analysis of the figure, it is clear that D, D_1 and s_b are the most influencing input variable with respect to pH sensitivity. This may be due to the fact that D, the dilution rate, affects the concentration of Lactic acid being generated by the biochemical reaction from the hydrodynamic point of view and D_1 and s_b regulate the rate of neutralization of the acid. On the other hand, S_0 plays a passive role regarding pH sensitivity because yield coefficient ($Y_{p/S}$) of Lactic acid with

respect to the substrate, glucose, is only 0.0065gg^{-1}, as reported in Table 4-3**.** Thus the input variables D, D_1 and s_b have been chosen for further experimental studies on parametric sensitivity.

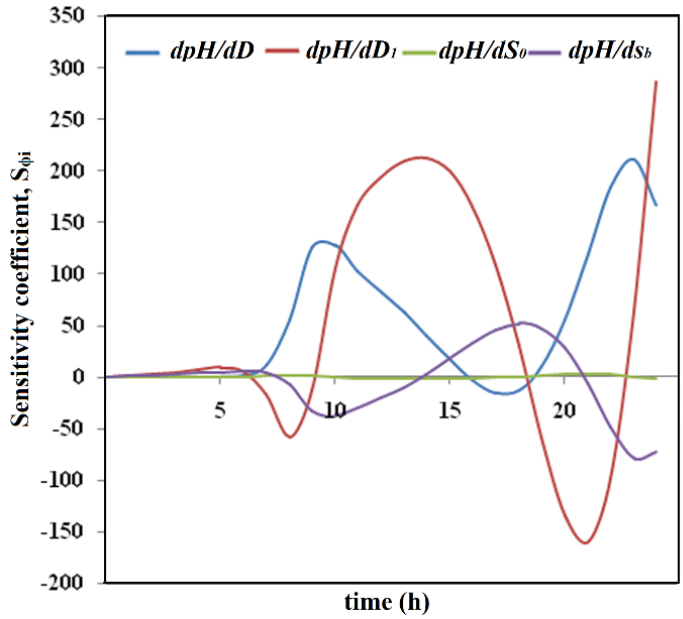

Figure 4-9 Time trajectories of Sensitivity variables, $S_{\varphi i}$

4.1.6.4 Critical multiplicity criterion and decision on experimental conditions

From the definition of multiplicity criterion (ω) described in the Mathematical analysis section, the critical value of ω is unity, and unique states will occur if ω ≥ 1 and otherwise, multiple steady states will be encountered. Based on this concept, the following conditions for conduction of experiments on parametric sensitivity of pH are reported in Table 4-4 with respect to D, D_1 and s_b.

Table 4-4 Summary of the results obtained from the present study

	s_b = 0.008M	D = 0.1 h^{-1}	D_1 = 0.007h^{-1} to D_1 = 0.008h^{-1}
Mutiplicity	D_1 = 0.008 h^{-1}	D = 0.1 h^{-1}	s_b = 0.007M to s_b = 0.008M
	D_1 = 0.008 h^{-1}	s_b = 0.008 M	D = 0.1h^{-1} to D = 0.12h^{-1}
	s_b = 0.002M	D = 0.1 h^{-1}	D_1 = 0.06h^{-1} to D_1 = 0.065h^{-1}
Uniqueness	D_1 = 0.06 h^{-1}	D = 0.1 h^{-1}	s_b = 0.002M to s_b = 0.003M
	D_1 = 0.06 h^{-1}	s_b = 0.002M	D = 0.08h^{-1} to D = 0.1h^{-1}

4.1.6.5 Experiments on parametric sensitivity

Effects of different parameters, namely D, D_1 and s_b on parametric sensitivity, have been studied by conducting experiments using the operating parameters satisfying either multiplicity (system with multiple steady-state) or uniqueness (system with single steady-state) criteria, as indicated in Table 4-

4. Initial conditions for all experiments in the CSTBR have been provided in Table 4-5. The concentration of glucose in the inlet MMRS medium has been maintained at 10 g/dm^3.

Table 4-5 Initial conditions for experiments on parametric sensitivity

Initial biomass concentration (gL^{-1})	0.004
Initial substrate concentration (gL^{-1})	10.0
Initial pH of the system	6.7
Initial lactic acid concentration (mM)	0.001
Initial concentration of sodium lactate (mM)	0.008

4.1.6.6 Numerical simulation

Model equations (4.8) to (4.12) were simultaneously solved using ODE23 of MATLAB-7 2010a for the conditions of input variables, either corresponding to unique or multiple steady-state regions. During the solution of equation (4.12), a very small value of the initial concentration of salt (s_A=0.001mM) and lactic acid (p=0.001mM) have been used, to avoid 'division by zero' situation.

4.1.6.7 Effect of D on sensitivity of system pH

The reactor was first operated with D= 0.1h^{-1}, D_1=0.008h^{-1} and s_b=0.008M. The system pH was recorded with a pH meter. The simulated and experimental patterns of the transient behaviour of pH under this condition have been shown in Figure 4-10. It has been observed that pH shows oscillatory behaviour and never stabilizes. After 50h, the pH has been observed to reach 7.23. Keeping the values of D_1 and s_b unaltered another experiment was conducted by setting D= 0.12h^{-1}.

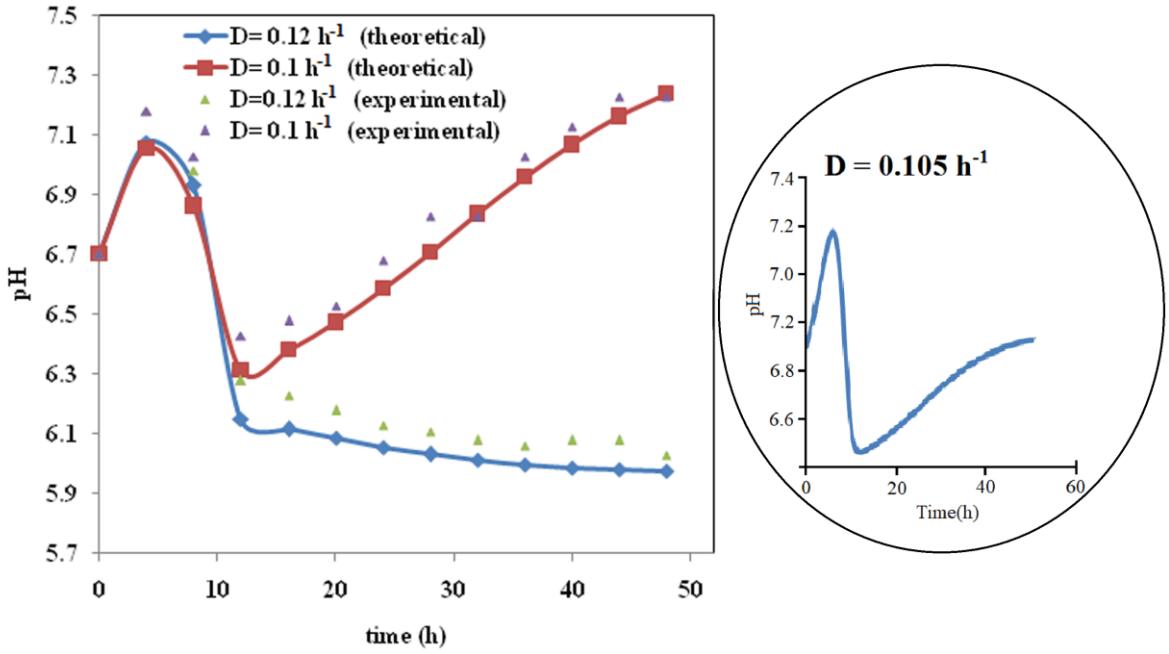

Figure 4-10 Simulated (lines) and experimental (Points) time histories of pH in the region of multiplicity with D as a parameter

From Figure 4-10, it is evident that although the transient goes through fluctuation up to 12h, it ultimately reaches almost a steady value of pH=6.1. After propagation of the same reaction time, i.e., 50h, the final pH has been observed to reach 5.97. Therefore, it is clear that the system shows parametric sensitivity, as evident from drastic change of behaviour of pH transient corresponding to a very small (16.6%) alteration in dilution rate in multiplicity region. Figure 4-11 depicts the simulated and experimental trends of time trajectories of pH at fixed values of D_1 =0.06 h^{-1} and s_b= 0.002M and two values of D=0.1h^{-1} and 0.08h^{-1}, judiciously selected in the region of the unique steady state. From the figure, it is evident that for D=0.1h^{-1}, the value of pH monotonically increases to 9.7 at 15h. When D's value was altered to 0.08h^{-1}, the same monotonic rising trend is observed with pH = 8.8 at 15h.

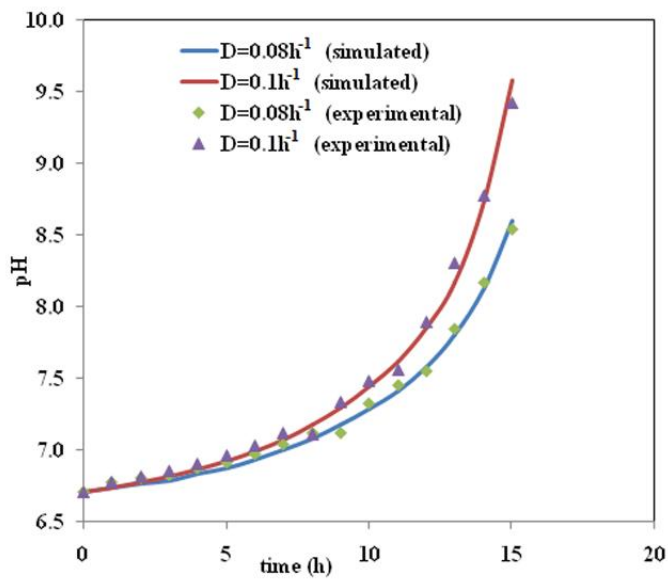

Figure 4-11: Simulated (lines) and experimental (Points) time histories of pH in the region of uniqueness with D as a parameter

Therefore, it may be inferred that in the unique steady states regime, there is a shooting tendency in pH. The experiments could not be run beyond 15h due to this abnormal overshoot in pH value. The occurrence of parametric sensitivity may be nullified if operating time is restricted to 13h. However, over a period from 13-15h, the system may be considered to show parametric sensitivity of pH with respect to D. Overall, the system may be considered to be moderately pH-sensitive with respect to D in the region of unique steady states. The agreement between the simulated and experimental values is satisfactory both in the regions of multiplicity and uniqueness as the coefficients of the nonlinear regression analysis (R^2) are 0.987, 0.991, 0.981 and 0.986 for D_1=0.045h^{-1}, 0.055h^{-1}, 0.06h^{-1} and 0.065h^{-} respectively.

4.1.6.8 Effect of D_1 on sensitivity of system pH

Figure 4-12 shows the simulated and experimental time histories of pH when D_1= 0.0045h^{-1} is set at D=0.1h^{-1} and s_b =0.008M. From the plot, it is clear that pH transient shows initial fluctuation and ultimately stabilizes at a steady-state value of 6.18 at 12h. After that, the pH remains almost constant (pH=6.15) even up to 48h. Next, the value of D_1 was changed to 0.0055$h^{-1,}$ keeping D and s_b unaltered. The analysis of the time trajectory of pH reveals that it always goes through fluctuations and at 48h, it reaches the value of 7.3, much different from that obtained with D_1= 0.0045h^{-1}. Absolutely different patterns of pH transients for a slight variation of D_1 from 0.0045h^{-1} to 0.0055h^{-1}, particularly beyond 12h, suggests that parametric sensitivity of pH with respect to D_1 exists in the region of multiplicity.

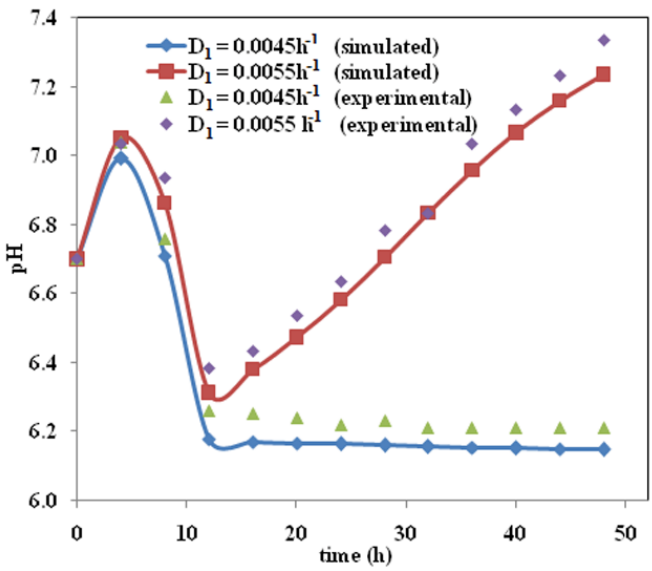

Figure 4-12 Simulated (lines) and experimental (Points) time histories of pH in the region of multiplicity with D_1 as a parameter

On the other hand, time-trajectories of pH shown in Figure 4-13 exhibits monotonically increasing pattern at both D_1=0.06h^{-1} and 0.065h^{-1} at fixed values of s_b= 0.002M and D=0.1h^{-1} in the region of unique steady states. Over 15h pH reaches the values of 9.7 and 10.5 respectively for D_1=0.06h^{-1} and 0.065h^{-1}. Thus the parametric sensitivity with respect to D_1 is moderately present in the unique steady-state region. Even in this case, the experiments could only be run up to 15h due to the problem of pH shooting. The analysis of Figures 4-12 and 4-13 reveals that simulated predictions agree well with the experimental results as the coefficients of the nonlinear regression analysis (R^2) are 0.987, 0.991, 0.981 and 0.986 for D_1=0.045h^{-1}, 0.055h^{-1}, 0.06h^{-1} and 0.065h^{-}respectively.

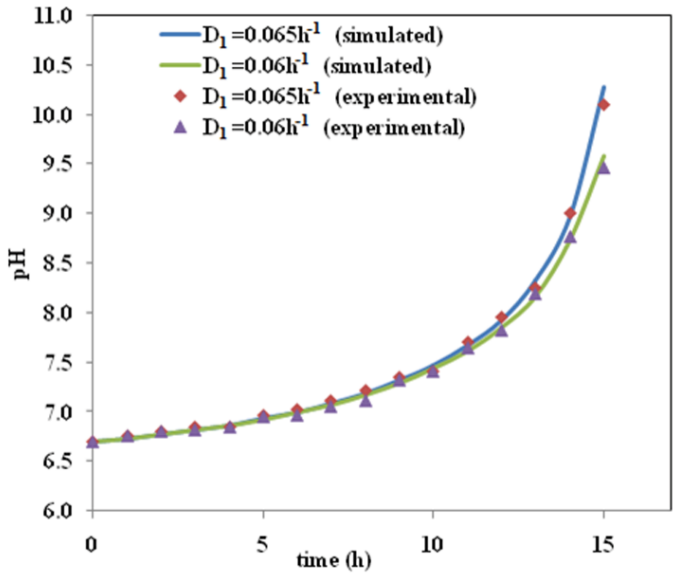

Figure 4-13 Simulated (lines) and experimental (Points) time histories of pH in the region of uniqueness with D_1 as a parameter

4.1.6.9 Effect of s_b on sensitivity of system pH

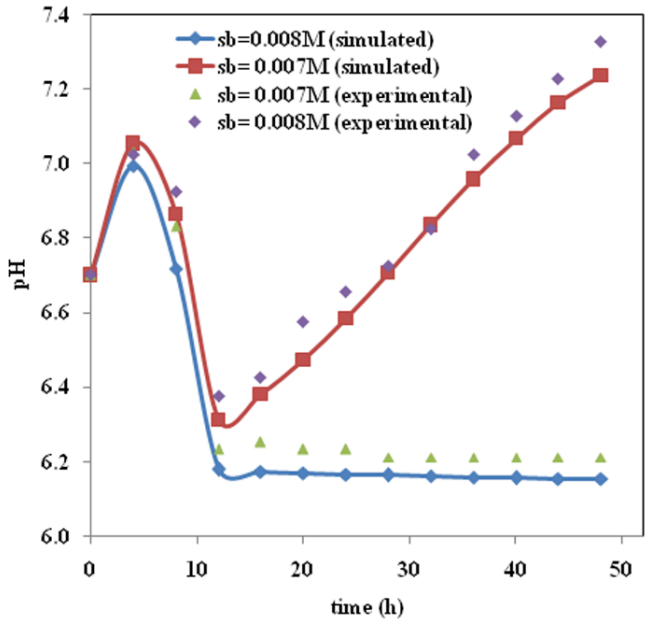

Figure 4-14 Simulated (lines) and experimental (Points) time histories of pH in the region of multiplicity with sb as a parameter

In Figure 4-14, the time trajectories of pH, as simulated using model equations (5.4) to (5.8) have been plotted along with their experimental counterparts for s_b= 0.007M and s_b= 0.008M and D_1=0.008h^{-1} and D=0.01h^{-1}. For both s_b= 0.007M and s_b= 0.008M the agreement between simulated and experimental results is satisfactory as the coefficients of the nonlinear regression analysis (R^2) are 0.988 and 0.985, respectively. As evident from Table 4-5, both sets of operating parameters fall under the region of multiple steady states. For s_b=0.007M, the pH trajectory passes through a fluctuating phase up to 12h after which steady state is attained, and pH remains almost constant at 6.18 to 6.15 even up to 48h. When the value of s_b is slightly altered to 0.008M, keeping other parameters constant, the pH-transient shows fluctuating behaviour throughout the operating period up to 48h. The value of pH at 48h is 7.3.

Since a very small change in sb completely alters the pH dynamics, the system appears to exhibit strong parametric sensitivity with respect to s_b in the region of multiplicity.

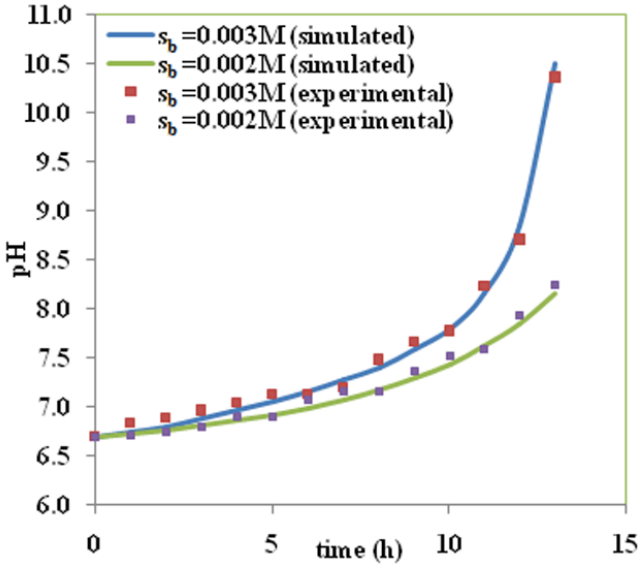

Figure 4-15 Simulated (lines) and experimental (Points) time histories of pH in the region of uniqueness with s_b as a parameter

In Figure 4-15, time-trajectories of pH are plotted using simulated and experimental data for two sets of operating parameters s_b= 0.002M and s_b= 0.003M and D_1=0.06 h^{-1}, D=0.1h^{-1} in the region of unique steady state. The trends of the plots clearly indicate that the pH increases monotonically to 8 and 10.5 over 15h, respectively, when s_b is set at 0.002M and 0.003M. Thus the parametric sensitivity of pH with respect to s_b is present even in the unique steady-state region. In all cases, the agreement between simulated and experimental results is satisfactory as the coefficients of the nonlinear regression analysis (R^2) are 0.982 and 0.989 for s_b= 0.003M and s_b= 0.002M.

In all cases, the agreement between simulated and experimental results is satisfactory. From the analysis of Figures 4-10 to 4–15, it may appear that the increasing trend of pH, in some cases, is due to overfeeding of base. However, the change of pH is not only a function of base dosage. The truth underlying the trend is that pH behaviour is affected by three main input parameters, namely D (dilution rate of nutrient stream), D_1 (dilution rate of base stream) and sb (concentration of base). According to the multiplicity criterion ω (difined in equation derived in the present investigation, unique steady-state condition prevails for a set of values of input parameters (D, D_1 and s_b)which correspond to an increased pH condition. The interesting features of Figures 4-10 to 4-15 show that the system is parametrically sensitive in both uniqueness and multiplicity regions.

4.1.6.10 Transient variation of sensitivity variable ($S_{\phi i}$)

In Figure 4-16 and 4-17, time course of theoretical (equations A.34 to A37) sensitivity of pH with respect to D, D_1, S_0 and s_b have been plotted at fixed values of D= 0.1h^{-1} and s_b=0.008M, S_0= 10gL^{-1} for D_1=0.0045h^{-1} and 0.0055h^{-1} respectively.

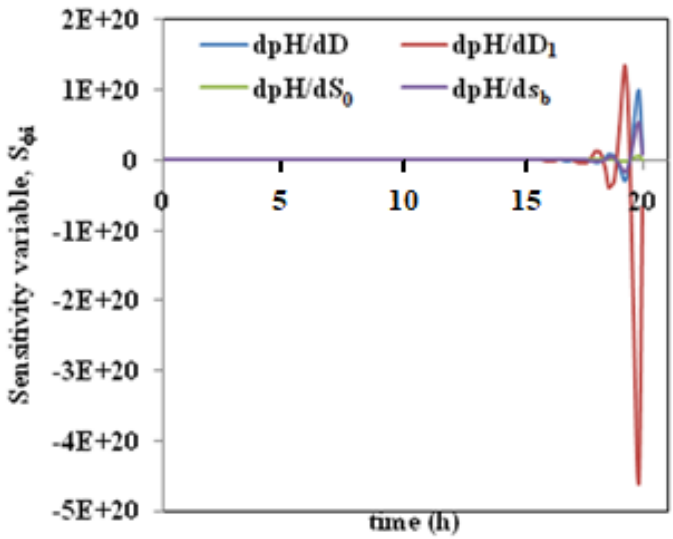

Figure 4-16 Time histories of all theoretical sensitivity variables in the region of multiplicity at D_1 =0.0045h^{-1} (D=0.1 h^{-1}; s_b = 0.008M)

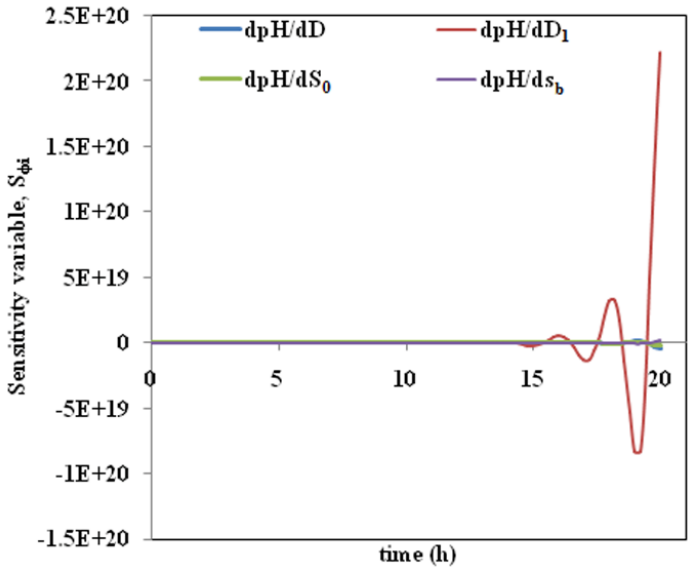

Figure 4-17 Time histories of all theoretical sensitivity variables in the region of multiplicity at D_1 =0.0055h^{-1} (D=0.1 h^{-1}; s_b = 0.008M)

According to the multiplicity criterion, i.e., $\omega<1$, both combinations of values of D, D_1 S_0 and s_b used in these figures fall under multiplicity region. From the analysis of figures, it appears that parametric sensitivity of pH exists for parameters, namely D, D_1 and s_b. Since the order of values of sensitivities is different for different parameters, sensitivities of pH against individual input variables have been plotted in Figures 4-18, 4-19 and 4-20 respectively for D, D_1 and s_b for the same set of values of D, D_1 and s_b available in Table 4-4. These figures vividly establish the existence of parametric sensitivity in the multiplicity region. Thus the theoretical prediction seems to reconfirm the experimental findings.

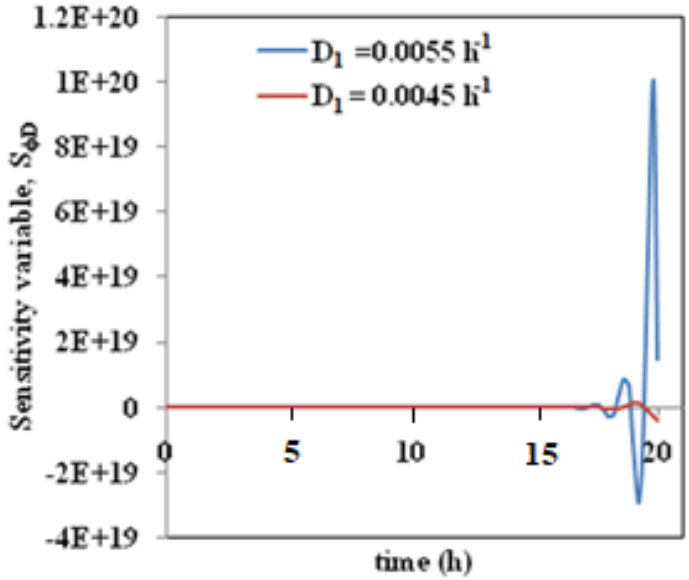

Figure 4-18 Time histories of theoretical sensitivity variable with respect to D in the region of multiplicity at D_1 =0.0045h^{-1} and D_1 =0.0055h^{-1}

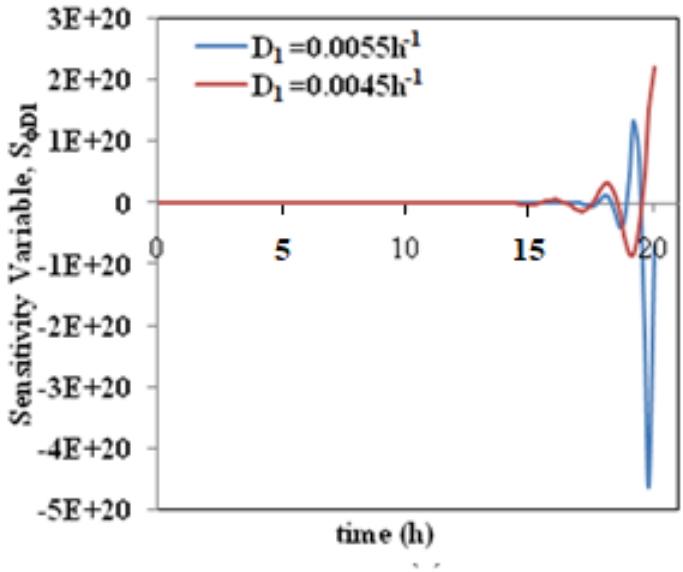

Figure 4-19 Time histories of theoretical sensitivity variable with respect to D_1 in the region of multiplicity at D_1 =0.0045$h^{-1}$and D_1 =0.0055h^{-1}

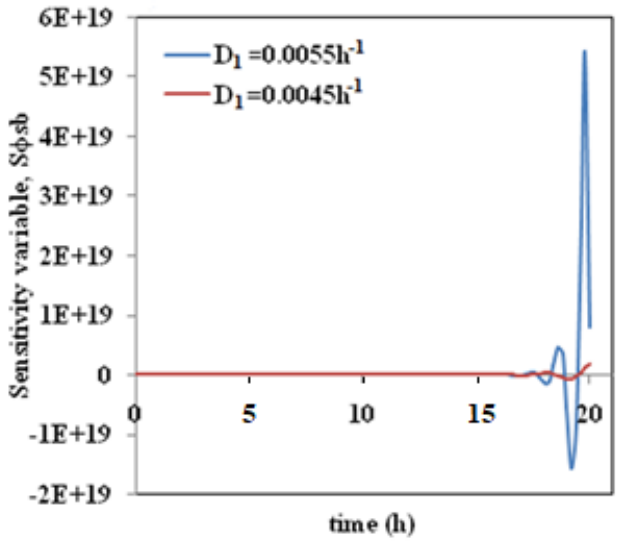

Figure 4-20 Time histories of theoretical sensitivity variable with respect to sb in the region of multiplicity at D_1 =0.0045h^{-1} (D=0.1h^{-1}; s_b = 0.008M) and D_1 =0.0055h^{-1} (D=0.1h^{-1}; s_b = 0.008M)

In Figures 4-21 and 4-22 the dynamic variation of theoretical sensitivities (equations A18 to A37) of pH with respect to D, D_1 and s_b respectively for D_1= 0.06h^{-1} and 0.065h^{-1} at fixed values of D=0.1h^{-1}, s_b=0.002M and S_0= 10gL^{-1} have been plotted. Both the combination relates to unique steady-state condition, ensuring ω>1.

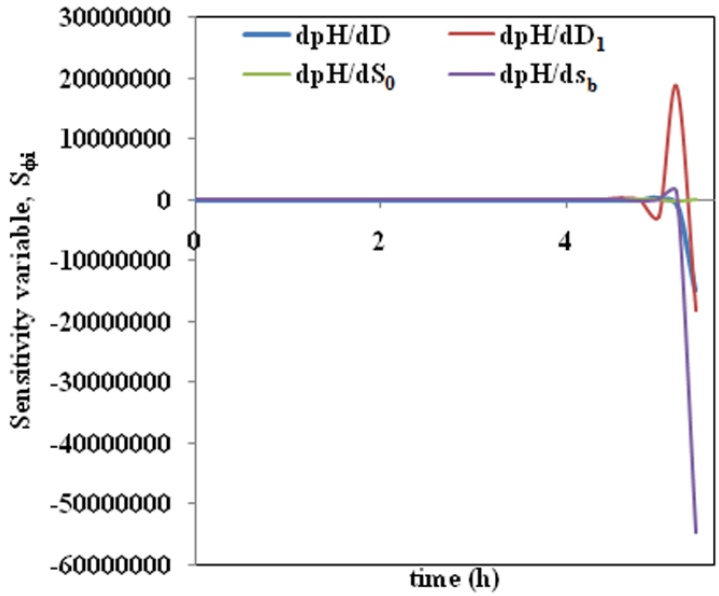

Figure 4-21 Time histories of all theoretical sensitivity variables in the region of uniqueness at D_1 =0.06h^{-1} (D=0.1h^{-1}; s_b = 0.002M)

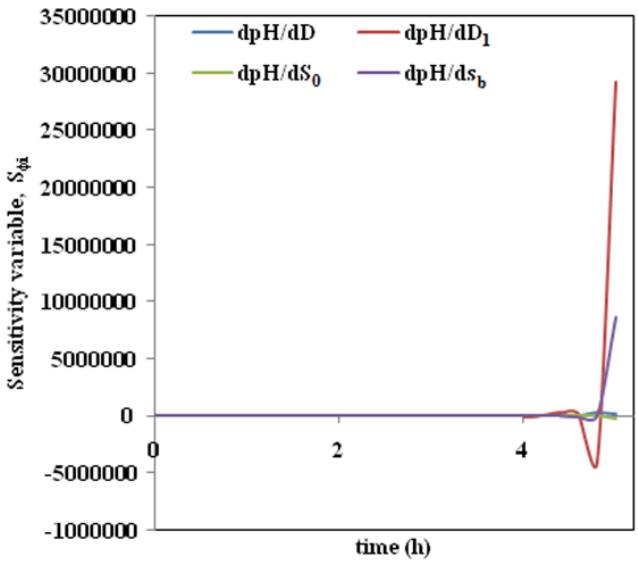

Figure 4-22 Time histories of all theoretical sensitivity variables in the region of uniqueness at D_1 =0.065h^{-1} (D=0.1h^{-1}; s_b = 0.002M)

Sensitivity against individual input vector has been shown in Figure 4-23 to 4-25 to elucidate the transient behaviour of sensitivity of all parameters and avoid confusion arising from the difference in the sensitivity of sensitivities against individual variables.

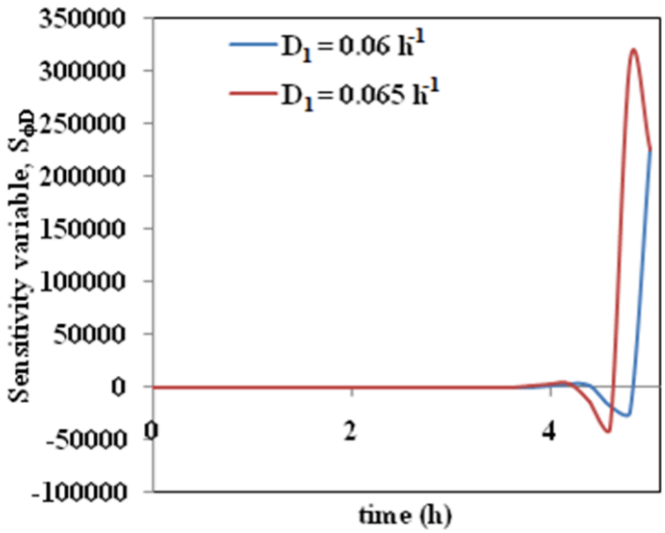

Figure 4-23 Time trajectories of theoretical sensitivity variable with respect to D in the region of uniqueness at D_1 =0.06h^{-1} (D=0.1h^{-1}; sb = 0.002M) and D_1 =0.065h^{-1} (D=0.1h^{-1}; sb = 0.002M)

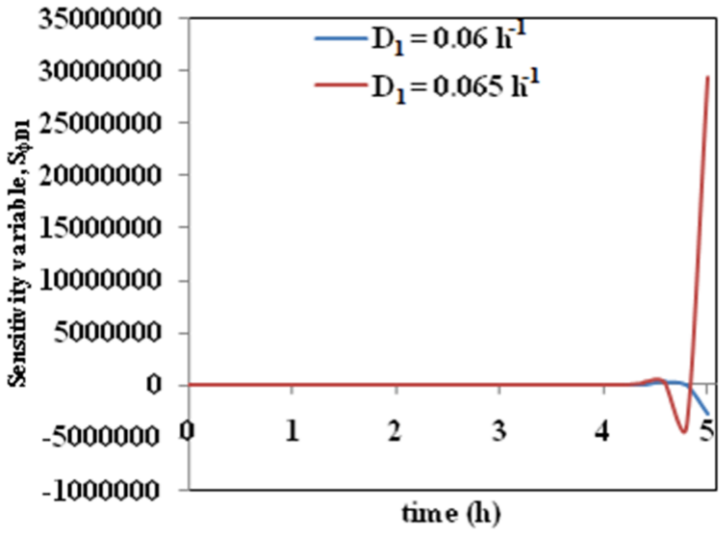

Figure 4-24 Time trajectories of theoretical sensitivity variable with respect to D_1 in the region of uniqueness at D_1 =0.06h^{-1} (D=0.1h^{-1}; sb = 0.002M) and D1 =0.065h^{-1} (D=0.1h^{-1}; sb = 0.002M)

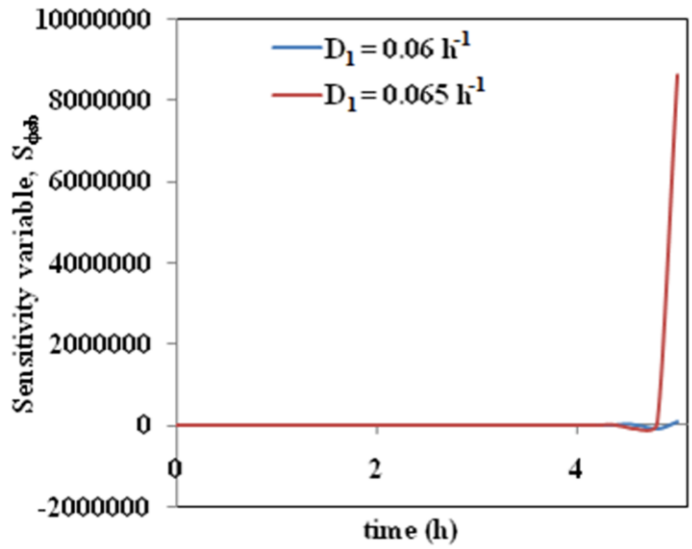

Figure 4-25 Time trajectories of theoretical sensitivity variable with respect to sb in the region of uniqueness at D_1 =0.06h^{-1} (D=0.1h^{-1}; sb = 0.002M) and D_1 =0.065h^{-1} (D=0.1h^{-1};sb= 0.002M)

All figures again confirm the occurrence of parametric sensitivity even in the region of the uniqueness of steady-state, although at a lower scale with respect to multiplicity region, as observed experimentally.

4.1.7 Discussion

The detailed analysis on multiplicity and parametric sensitivity under the present study reveals that similar to exothermic reactors, CSTBR handling the growth of pH-sensitive microorganisms, e.g., *Pediococcus acidilactici* understudy, is also parametrically sensitive irrespective of occurrence of the multiplicity of steady-state. Chemburkar et al. [118] observed that multiplicity co-occurs with parametric sensitivity during the studies on exothermic adiabatic CSTR. Besides the existence of strong parametric sensitivity in the region of multiplicity, it is also present moderately with respect to the dilution rate of feed stream(D) and alkaline stream (D_1) and firmly with regard to the concentration of NaOH in the alkaline stream (s_b) even in the unique steady state. Shooting tendency of pH dominates in

the region of uniqueness. Thus it may be inferred that the inherent bias of the system is to show parametric sensitivity and hence it is challenging to be operated with continuous feeding of base stream, for the control of pH. Although in multiple steady-state regions, a few conditions of input parameters correspond to stable pH values after 12h, which can be observed in Figures 4-10, 4-12 and 4-14. The operation at these conditions is also not recommended due to the presence of parametric sensitivity and multiplicity behaviour. On the other hand, due to the over-shooting tendency of pH in unique steady-state conditions, the operation of the CSTBR with pH control using continuous input of base stream seems to be impractical. Therefore, fed-batch type arrangement with an intermittent dosage of the base stream for the adjustment of pH, as adopted by many researchers [120,121] seems to be more judicious. crests

4.2 Case 2: Parametric sensitivity of CSTBRs for *lactobacillus casei*: Normalized sensitivity analysis

In this case, the CSTBR model of Das et al. 2016 [115] is adapted to describe the reactor's kinetics. In order to find out kinetic constants relating to this study, batch experiments were performed, and a calibrated model was used to conduct sensitivity analysis and highlight the sensitive parameter range and values for the considered variables.

The effect of pH on microbial growth was studied experimentally in a series of batch experiments. A lactic acid bacterium (LAB), *Lactobacillus casei*, was selected for the batch experiments. The initial pH of the growth medium was varied to determine pH's influence on the microbial growth rate. The information obtained from the batch experiments identified the optimum range of pH for the growth of LAB. Furthermore, the kinetic constants of the microbial growth model were also calculated.

A CSTBR operation model was developed by using the necessary information on the kinetic parameters of microbial growth, including their pH dependency. The mathematical model is able to predict time-dependent changes in the concentration of substrate, biomass, lactic acid, salt, and pH. The reactor pH remains constant by the use of a continuous flow of the alkaline stream. The model is then used to study normalized sensitivity concerning input variables; initial system pH, the dilution rate of the alkaline stream, and its concentration where pH-minimum (the lowest value of pH attain for a set of input variable) is an objective function. The sensitivity of the pH-minimum regarding the set of input parameters is examined, together with the determination of critical values of input parameters where a "pH-runaway" condition occurs. Lastly, the sensitivity analysis identified a parameter space, at which pH becomes simultaneously sensitive to small changes in input parameters. The following objectives were achieved in order to fulfil the overall aim of this case study.

a. To perform batch experiments using a lactic acid bacterium, *Lactobacillus casei*, to find out the optimum pH for microbial growth and other growth associated kinetic parameters;
b. To derive a generalized criterion for sensitivity by obtaining an objective sensitivity function for pH with respect to input variables;
c. To predict the critical value of input parameters and parameter space where the system becomes unstable and exhibits sensitive behaviour.

A series of batch experiments were conducted using *Lactobacillus casei*, as mentioned in Chapter 3.6.1.2. The detailed microbial growth kinetics and procedure of the kinetic parameter determination were similar to that of Case 1, which has been presented chapter 4.1.1. CSTBR process model s mentioned in the previous case study described in sections 4.1.2 and 4.1.3 is considered. However, the mass and molar balances (Eq (4.8) to (4.12)) are converted into the dimensionless form using the variables described in Table 4-6

Table 4-6 Definition of dimensionless variables

Parameter	Definition	Parameter	Definition	Parameter	Definition	Parameter	Definition
α	$\frac{X}{S_0 Y_{X/S}}$	U	$\frac{\mu}{D}$	R	$\frac{s_b M_b}{S_0}$	τ	tD
β	$\frac{S}{S_0}$	θ	$\frac{D_1}{D}$	L	$\frac{s_a M_c}{S_0}$	M_2	$\frac{M_c}{M_b}$
z	$\frac{pM_a}{S_0 Y_{p/S}}$	m	$\frac{\mu_{max}}{D}$	γ	$\frac{pH}{pH_0}$	n	$\frac{K_S}{S_0}$
b	$B.pH_0$	c	$C.pH_0^2$	M_1	$\frac{M_a Y_{p/S}}{M_b}$		

Therefore, the model equations in the non-dimensional form are as follows:

$$\frac{d\alpha}{d\tau} = (U - \theta - 1)\alpha \tag{4.37}$$

$$\frac{d\beta}{d\tau} = (1 - \beta) - U.\alpha - \theta.\beta \tag{4.38}$$

$$\frac{dz}{d\tau} = -z + U.\alpha - \theta(M_1 R + z) \tag{4.39}$$

$$\frac{dL}{d\tau} = (M_2 R - L)\theta - L \tag{4.40}$$

$$\frac{d\gamma}{d\tau} = \frac{1}{pH_0}\left[\frac{1}{L}\frac{dL}{d\tau} - \frac{1}{z}\frac{dz}{d\tau}\right] \tag{4.41}$$

On the other hand, the non-dimensional expression for the specific growth rate was expressed as:

$$U = \frac{m\beta}{n+\beta} I \tag{4.42}$$

Where,

$$I = A + B.\gamma + C.\gamma^2 \tag{4.43}$$

The differential equations (4.37) to (4.41) were solved numerically using the 4th order Runge-Kutta method using the following initial conditions. At,

$$\tau = 0; \gamma = 1;\ \alpha = \alpha_0;\ \beta = \beta_0; z = z_0\ ;\ L = L_0 \tag{4.44}$$

4.2.1 Normalized objective sensitivity analysis

The technique for analyzing the pH-sensitivity was selected as adopted by Morbedelli and Varma [122,123] and Dutta et al. [124]. In this case, the governing equations for pH and substrate concentration are written by dividing equation (4.41) by equation (4.38)

$$\frac{d\gamma}{d\beta} = \frac{\frac{R\cdot\theta}{pH_0}\left[\frac{M_2}{L} + \frac{M_1}{z} - \frac{U\cdot\alpha}{z\cdot R\cdot\theta}\right]}{1 - U.\alpha - (1+\theta)\beta} = g(\phi, \alpha, \beta, z, L, \gamma) \tag{4.45}$$

Where, ϕ is the vector of input parameters, namely, initial system pH (pH_0), the dilution rate of the alkaline stream (θ) and its concentration (R). Similarly, dividing equations (4.37),(4.39) and (4.40) by equation (4.38) the following equations are obtained as below.

$$\frac{d\alpha}{d\beta} = \frac{U.\alpha - (1+\theta)\alpha}{1 - U.\alpha - (1+\theta)\beta} \tag{4.46}$$

$$\frac{dz}{d\beta} = \frac{U.\alpha - (1+\theta).z - M_1.\theta.R}{1 - U.\alpha - (1+\theta)\beta} \tag{4.47}$$

$$\frac{dL}{d\beta} = \frac{M_2.\theta.R - (1+\theta).L}{1 - U.\alpha - (1+\theta)\beta} \tag{4.48}$$

With the following initial conditions,

$$pH = pH_0;\ \alpha = \alpha_0; z = z_0 \text{ and } L = L_0\ ;\ \beta = \beta_0 \tag{4.49}$$

By differentiating equation (4.45) with respect to parameter ϕ, the expression for first-order local sensitivity s_ϕ can be evaluated as,

$$\frac{ds_\phi}{d\beta} = \frac{dg}{d\phi} + \frac{dg}{d\gamma}.s_\phi \tag{4.50}$$

Where,

$$s_\phi = \frac{d\gamma}{d\phi} \tag{4.51}$$

Now taking

$$H = -\frac{dg}{d\gamma} \tag{4.52}$$

The adjoined equation from Equation (4.50) takes the following form:

$$\frac{dp_\beta}{d\beta} = H.p_\beta \text{ for } \beta \in (\beta_{0,}\beta^*) \tag{4.53}$$

Where,

$$p_\beta = \frac{\bar{s}_\phi(\beta)}{\bar{s}_\phi(0)} \tag{4.54}$$

And, β_0 in the value of initial substrate concentration (dimensionless) whereas β^* indicates the substrate concentration in the reactor at which $\gamma=\gamma_{min}$. The initial conditions of Equation (4.53) are

$$\text{At}, \beta = \beta_0;\ \rho = 1;\ \ s_\phi(0) = \frac{d\gamma}{d\phi_i} = 0 \tag{4.55}$$

Where,

ϕ_i is one element of the parameter vector, $\boldsymbol{\phi}$.

4.2.2 Calculation of sensitivities

The normalized objective sensitivities can be calculated as follows:

- Equations (4.46) to (4.48) and (4.53) were solved simultaneously with the help of initial conditions given in equations (4.49) and (4.55) until the γ reaches its minimum value. The corresponding values of ρ_β^* and β^* have been determined.
- $\bar{s}_\phi(0)$ given by equation (4.54) has been calculated using the value of ρ_β^* with the help of the following equation:

$$\bar{s}_\phi(0) = \frac{\bar{s}_\phi(\beta^*)}{\rho_{\beta^*}} = \frac{1}{\rho_{\beta^*}} \tag{4.56}$$

- The objective sensitivity is then evaluated by solving the following equation:

$$s^*_{\phi_i} = s_{\phi_i}(0).\bar{s}_\phi(0) + \int_{\beta_0}^{\beta^*} \sigma_i.\bar{s}_\phi(\beta)d\beta \tag{4.57}$$

Where,

$$\sigma_i = \frac{\partial g}{\partial \phi_i} \quad \text{for} \quad \beta \in (\beta_{0,} 1) \tag{4.58}$$

The expressions for σ_i and corresponding to each ϕ_i are provided in Table 4-7.

Table 4-7 Expressions of σi for various parameters ϕi, as defined in equation (4.57)

ϕ_i	σ_i
pH_0	$\frac{R.\theta\left[\frac{M_2}{L}+\frac{M_1}{z}-\frac{U\cdot\alpha}{z\cdot R\cdot\theta}\right]}{pH_0^2[U.\alpha+(1+\theta)\beta-1]}$
θ	$\frac{R.\theta.\beta\left[\frac{M_2}{L}+\frac{M_1}{z}-\frac{U\cdot\alpha}{z\cdot R\cdot\theta}\right]}{pH_0[U.\alpha+(1+\theta)\beta-1]^2}-\frac{R\left[\frac{M_2}{L}+\frac{M_1}{z}-\frac{U\cdot\alpha}{z\cdot R\cdot\theta}\right]}{pH_0[U.\alpha+(1+\theta)\beta-1]}-\frac{U\cdot\alpha}{\theta.z.pH_0[U.\alpha+(1+\theta)\beta-1]}$
R	$-\frac{\theta\left[\frac{M_2}{L}+\frac{M_1}{z}-\frac{U\cdot\alpha}{z\cdot R\cdot\theta}\right]}{pH_0[U.\alpha+(1+\theta)\beta-1]}-\frac{U\cdot\alpha}{R.z.pH_0[U.\alpha+(1+\theta)\beta-1]}$

4.2.3 Results

4.2.3.1 Influence of pH on microbial growth

In this study, the influence of initial pH on the microbial growth was studied by conducting batch experiments. The variation of initial pH was narrowed to 0.5 intervals compared to the previous case study where the interval was 1 to get a more accurate value of optimum pH. Similar kind of growth patterns was observed. However, there was a lag phase of 3h, and the exponential phase ended at 15h of incubation time. The detailed picture of the time history of dry cell concentrations was provided in the Appendix 3 section when pH at each batch reaction was varied initially.

4.2.3.2 Determination of kinetic parameters of *Lactobacillus casei* in batch culture

In the present experiments, at each initial pH, the substrate concentration was varied from 10g/L to 50g/L. For each combination of initial pH and substrate, the specific growth rate of microorganisms was determined. By using Equation (4.1), plots of 1/μ and 1/S were obtained at each initial pH. μ_{max} and k_s at each initial pH were determined by evaluating the intercepts and abscissas in Figure 4-26. The values of μ_{max} and k_s are provided in Table 4-8.

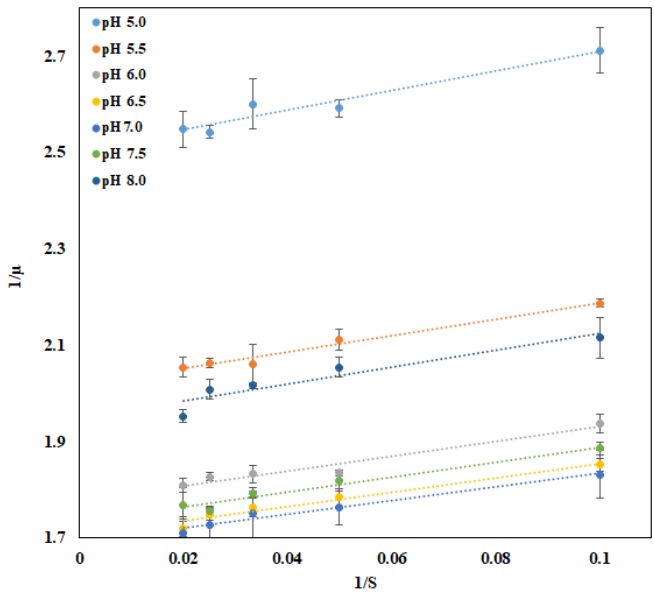

Figure 4-26 Determination of μ_{max} and k_s at different initial pH

From Table 4-8, it can be observed that k_s, does not change in any systematic manner with the change of pH. Therefore, one can easily state there is inhibition due to substrate concentration; in other words, a noncompetitive inhibition was observed. By plotting μ_{max} vs initial pH, it was found that μ_{max} became maximum when the value of initial pH is 6.75, which is considered as the optimum pH and the corresponding μ_{max} is optimum μ_{max},i.e. $\mu_{max,opt}$.

Table 4-8 Values of observed rate constants from experiments

Initial pH	μ_{max}	k_s
5.0	0.400	0.812
5.5	0.494	0.811
6.0	0.558	0.805
6.5	0.595	0.821
7.0	0.592	0.812
7.5	0.558	0.813
8.0	0.497	0.821

Now plotting the values of $\mu_{max.N}$, which can be obtained from Equation (4.3) as a function of initial pH, a second-order correlation, as shown in Equation (4.5) was obtained. The plot of $\mu_{max.N}$ vs initial pH is shown in Figure 4-27. The values of second-order correlation constants along with other growth associated kinetic constants are provided in Table 4-9.

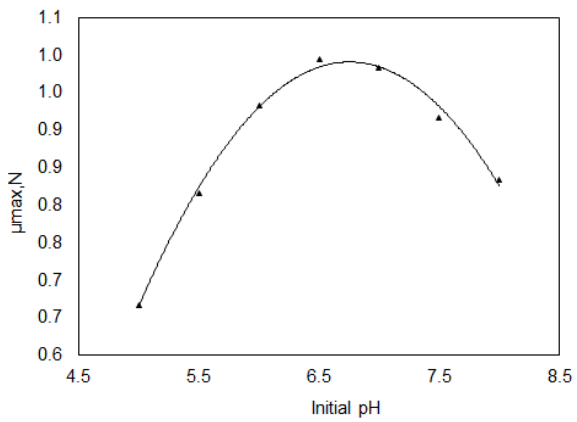

Figure 4-27 Variation of $\mu_{max,N}$ with respect to initial pH

Table 4-9 Values of kinetic parameters

Kinetic parameter	Value
$\mu_{max,opt}$ (h^{-1})	0.6
K_S (gL^{-1})	0.814
$Y_{X/S}$ ($g\ g^{-1}$)	0.238
$Y_{p/X}$ (gg^{-1})	3.36
$Y_{p/S}$ (gg^{-1})	0.8
A	-3.8507
B	1.434
C	-0.1062

4.2.3.3 pH sensitivity of a Continuous stirred tank bioreactor

The main objective of this analysis is to determine the parametric range of input variables at which the CSTBR system becomes vulnerable. The system behaviour is demonstrated in terms of normalized objective sensitivities coefficients as a function of input parameters. The mathematical model of the system consists of the Equations (4.45) – (4.48), (4.53). The equations (4.45) to (4.48) and (4.53) were simultaneously solved using Runga-Kutta 4th order method and equation (4.57) was solved using the trapezoidal numerical integration method. The results are illustrated in Figures 4-28 to 4-36. Figures 4-28 to 4-30, show normalized objective sensitivities of the pH-minimum, $S(\gamma^*, \phi_i)$, as a function of input parameters, i.e., dimensionless dilution rate of base feed stream (θ), the dimensionless concentration of base, (R) and initial pH (pH_0) of the system.

In Figure 4-28, S (γ^*, θ), S (γ^*, R), and S (γ^*, pH_0) are plotted against the dimensionless dilution rate of the base feed stream (θ). In this mathematical operation, the input parameter (θ) was varied in the range of 0 to 1, where the values of other input parameters pH_0 and R were kept constant at 6.75 and 0.8, respectively. As the value of θ reached 0.095, the system started showing sensitivity behaviour, and S

(γ^*, θ) and S (γ^*, R) started increasing, whereas S (γ^*, pH_0) started decreasing. At $\theta = 0.0195$, the values of sensitivity functions attained their maxima (for S (γ^*, θ) and S (γ^*, R)) and minima (S (γ^*, pH_0)). Further, for the increment of θ, the sensitivity functions S (γ^*, θ) and S (γ^*, R) were decreasing, and S (γ^*, pH_0) was increasing. This trend became near to 0 when θ reached a value of 0.295, and the system was again nonsensitive with respect to input parameter (θ). Therefore, the parameter range of θ is between 0.095 and 0.295, where the system becomes simultaneously sensitive. The value of θ at which the sensitivity functions attain their maxima and minima are defined as the critical value of θ.

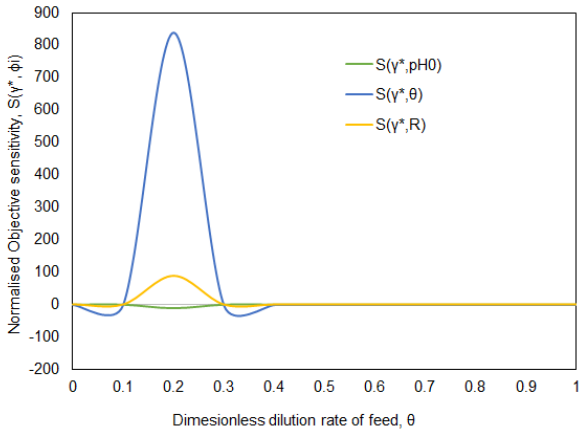

Figure 4-28 Normalized objective sensitivities S(γ,ϕi) as a function of θ*

Figure 4-29 shows the plots of S(γ^*,θ), S(γ^*,R), and S(γ^*,pH_0) versus the concentration of the base stream, (R). In this case, the dimensionless base stream concentration was varied in the range of 1 to 4 in order to observe the system behaviour in terms of sensitivity functions S(γ^*,θ), S(γ^*,R), and S(γ^*,pH_0), where the values of θ and pH_0 were kept constant at 0.3 and 6.75, respectively. The system starts showing sensitivity behaviour, and S(γ^*,θ) and S(γ^*,R) started increasing, whereas S(γ^*,pH_0) started decreasing from the beginning. This trend of the increment (for S(γ^*,θ) and S(γ^*,R)) descent (for S(γ^*,pH_0) was observed until R reached its value of 0.48. At this R = 0.48, sensitivity functions attained their maxima (for S(γ^*,θ) and S(γ^*,R)) and minima (S(γ^*,pH_0)) and became near to 0 when R reached a value of 0.865. The system was again nonsensitive with respect to input parameter R at this stage. Therefore, R's parameter range is between 0 and 0.865, where the system becomes simultaneously sensitive. The critical value of the dimensionless base stream concentration R_C is 0.48.

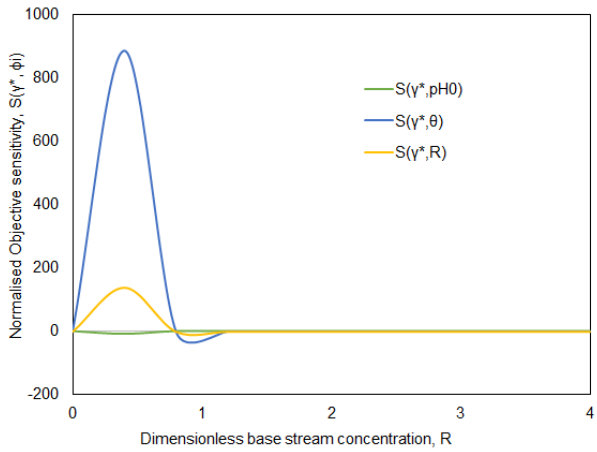

Figure 4-29 Normalized objective sensitivities S(γ,ϕi) as a function of R*

The system behaviour is also investigated in terms of sensitivity functions as a function of the initial pH (pH_0) of the system. The sensitivity functions S(γ*,θ), S(γ*,R), and S(γ*,pH_0) with respect to pH_0 are shown in Figure 4-30. Here, the pH_0 was varied in the range of 4 to 6 to observe the system behaviour in terms of sensitivity functions S(γ*,θ), S(γ*,R), and S(γ*,pH_0), where the values of θ and R were kept constant at 0.5 and 8, respectively. The system did not show any sensitivity for pH_0 from 4 to 4.42. As the value of pH_0 crossed 4.42, it started showing sensitivity behaviour, and S(γ*,θ) and S(γ*,R) started increasing, whereas S(γ*,pH_0) started decreasing. This movement of the increment (for S(γ*,θ) and S(γ*,R)) descent (for S(γ*,pH_0) was observed until pH_0 reached its value of 4.6. At this pH_0 = 4.6, sensitivity functions attained their maxima (for S(γ*,θ) and S(γ*,R)) and minima (S(γ*,pH_0)) and became near to 0 when pH_0 reached a value of 4.765. The system was again nonsensitive with respect to input parameter pH_0 at this stage. Therefore, the parameter range of pH_0 is between 4.42 and 4.765, where the system becomes simultaneously sensitive. The critical value of the initial system pH, pH_0 is 4.6.

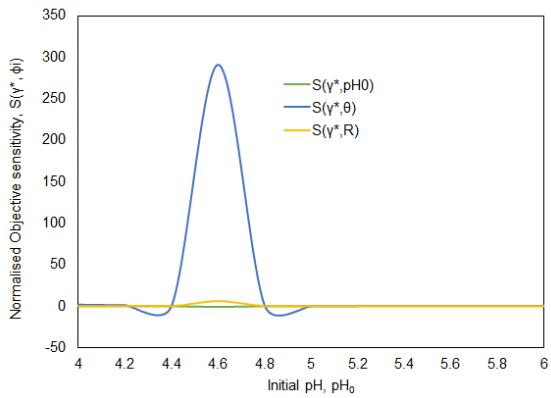

Figure 4-30 Normalized objective sensitivities S(γ,ϕi) as a function of pH_0*

Figures 4-31 and 4-32 show the nature of normalized objective sensitivity as a function of θ with the variation of R and pH_0, which is the combined effects of R and pH_0 on sensitivity function S(γ*, θ). The dimensionless input variables θ and R were varied to observe the behaviour of CSTBR in terms of the sensitivity coefficient, S(γ*, θ) with constant pH_0, which is presented in Figures 4-31. In this case, the range of θ and R was varied from 0 to 1 and 0 to 4, respectively. The parametric zone where the system found sensitivity is provided in Table 4-10. The sensitive function, S(γ*, θ), reached a maximum with a magnitude of 885 and the corresponding critical value of input variables is determined. The critical values of θ and R are provided in Table 4-10.

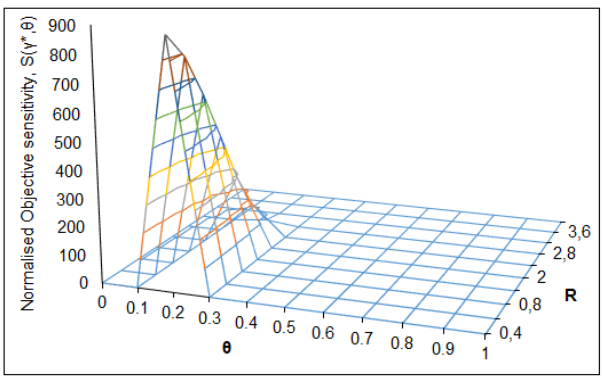

Figure 4-31 Normalized objective sensitivity S(γ, θ) as a function of parameters R and θ.*

The behaviour of CSTBR is presented in Figure 4-32 in terms of the sensitivity coefficient, S(γ*, θ). Figure 4-32 shows the variation of S(γ*, θ) with respect to the initial pH (pH_0) and θ. With a fixed value of R = 0.2, the θ and pH_0 were varied from 0 to 1 and 4.8 to 7.0, respectively. The sensitive zone for CSTBR operation for θ is 0.1 to 0.3, and for pH_0 the range is between 4.8 and 6. The sensitive function, S(γ*, θ), reached a maximum with a value of 735, and the corresponding critical values of input variables pH_0 and θ are determined. Table 4-10 provides the critical values of θ and pH_0 for this case.

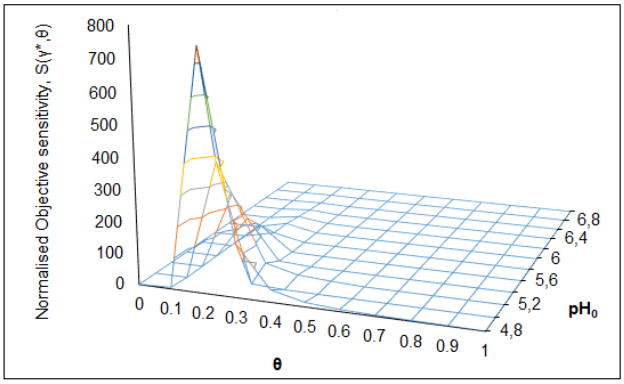

Figure 4-32 Normalized objective sensitivity S(γ, θ) as a function of parameters R and θ.*

The nature of normalized objective sensitivity as a function of R with the variation of θ and pH_0 have shown in Figures 4-33 and 4-34 to find out the influence of θ and pH_0 on the sensitivity function, S(γ*, R). Figure 4-33 shows the critical value of R and θ at a constant initial pH, pH_0 = 6.5, when S(γ*, R) attains its maximum. The system does not show any sensitive behaviour when θ goes beyond 0.7 and R = 0.75. The details of the input range and critical values of input parameters are given in Table 4-10.

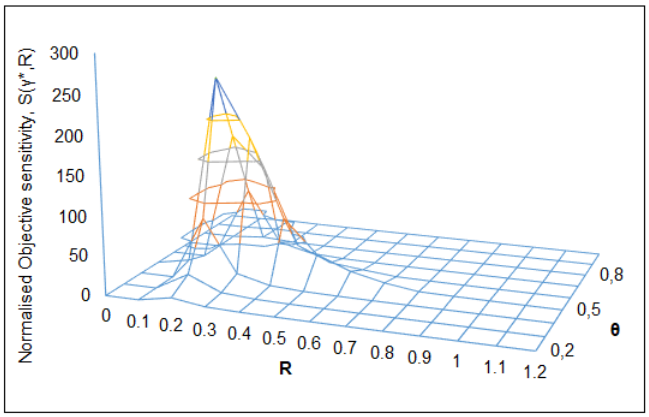

Figure 4-33 Normalized objective sensitivity S(γ, R) as a function of parameters R and θ.*

A similar trend occurred when pH_0 and R were the input variables. In this case, the range of R and pH_0 were varied from 0 to 3 and from 4 to 5, respectively. The influence of input parameters on sensitivity function S(γ*, R) is illustrated in Figure 4-34. The maximum value of sensitivity function S(γ*,R) is 245, and the corresponding critical values of R and pH_0 are provided in Table 4-10. The determined, sensitive region for CSTBR with respect to R and pH_0 is 0.2 to 1.4 and 4.2 to 4.6, respectively.

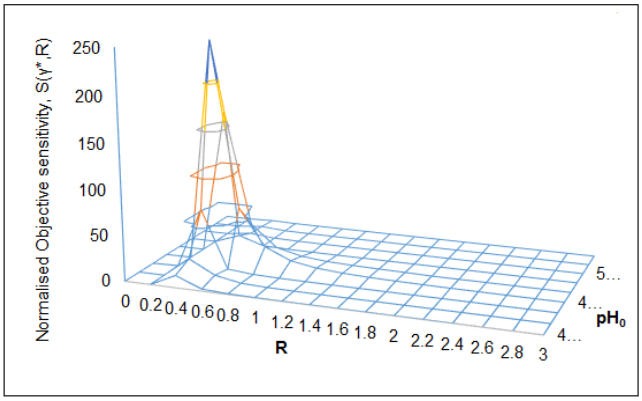

Figure 4-34 Normalized objective sensitivity S(γ, R) as a function of parameters R and pH_0.*

The behaviour of normalized objective sensitivity as a function of pH_0, S(γ*, pH_0) with the variation of R and θ are shown in Figures 4-35 and 4-36. The influences of R and pH_0 on S(γ*, pH_0) at a fixed value of θ = 0.7 are presented in Figure 4-35. The figure shows that the sensitivity function S(γ*, pH_0) exhibits sensitive behaviour in a negative direction. The S(γ*, pH_0) reached its lowest value of −7.8 when the R and pH_0 values are at 0.8 and 4.6, respectively. The sensitive region and critical values of input variables are presented in Table 4-10.

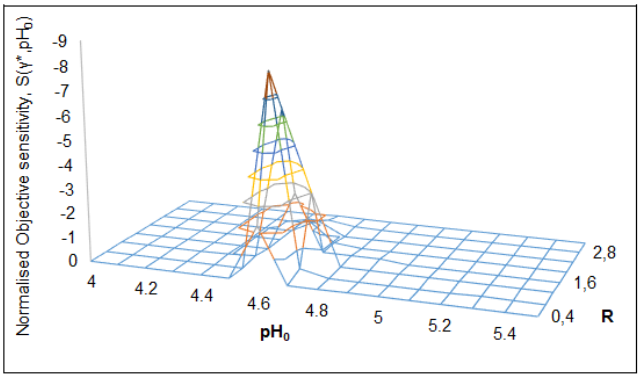

Figure 4-35 Normalized objective sensitivity S(γ, pH_0) as a function of parameters R and pH_0.*

Similar behaviour of sensitivity function, S(γ*, pH_0), was observed when pH_0 and θ were varied from 4 to 5.4 and 0 to 3, respectively, keeping R constant at 0.8. From the observation, it is found that the S(γ*, pH_0) reached its lowest value of −13.8 when the θ and pH_0 are at 0.5 and 4.6, respectively. The plot of normalized objective sensitivity S(γ*, pH_0) as a function of parameters R and θ are presented in Figure 4-36. The sensitive zone and the critical values of pH_0 and θ corresponding to S(γ*,pH_0) are provided in Table 4-10.

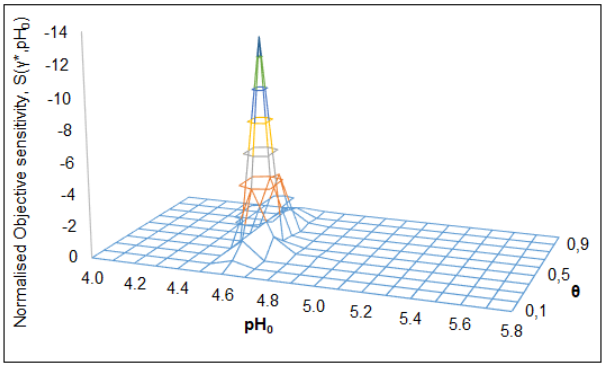

Figure 4-36 Normalized objective sensitivity $S(\gamma^*, pH_0)$ as a function of parameters pH_0 and θ

4.2.4 Discussions

The influence of initial pH on microbial growth is observed in the present case through batch experiments. It was found from the results, that initially when the experiments conducted within the initial pH range of 5.5 to 7.5, the microbial growth is not significantly affected. Therefore, the optimum value of pH is found to be within that range of 5.5 to 7.5, which is 6.75. However, as the initial pH went below or above that particular range, a considerable change in the microbial growth rate is observed. Therefore, the effects of pH on microbial growth are pragmatically observed.

On the other hand, from the sensitivity analysis of CSTBRs, it is found that the selected input parameters have a significant influence on the reactor operation. This analytical study provides a good insight into what extend these selected parameters can hinder the CSTBR operation. From Figures 4-28 to 4-36, it is observed that there is a zone where the system showed its undesirable behaviour in terms of sensitivity coefficients. The magnitude of the input parameters pH_0, θ, and R at which the normalized objective sensitivity attains maxima or minima are termed critical values. The critical values of pH_{0C}, θ_C, and R_C provide the boundary separating the stable pH system from an unstable pH system sometimes defined as the pH-runaway condition [115]. The magnitude of $S(\gamma^*,\theta)$, $S(\gamma^*,R)$, and $S(\gamma^*,pH_0)$ at critical points show that the influence of initial pH (pH_0) has less impact on the sensitivity behaviour compared to other input parameters, namely, R and θ.

Table 4-10 Different Critical values of input Parameters (From Figure 4-31 to 4-36)

Sensitivity Coefficients $S(\gamma^*, \phi_i)$	Figure	Variable Parameters (Critical Values)		Sensitive Zone of Input Variables		Fixed Parameters
$S(\gamma^*,\theta) = 885$	4-31	$\theta_C = 0.2$	$R_C = 0.4$	$\theta \rightarrow 0.1–0.3$	$R \rightarrow 0–2.4$	$pH_0 = 6.75$
$S(\gamma^*,\theta) = 735$	4-32	$\theta_C = 0.2$	$pH_{0C} = 4.8$	$\theta \rightarrow 0.1–0.3$	$pH_0 \rightarrow 4.8–6.0$	$R = 0.2$
$S(\gamma^*,R) = 285$	4-33	$R_C = 0.2$	$\theta_C = 0.5$	$R \rightarrow 0.1–0.75$	$\theta \rightarrow 0.05–0.7$	$pH_0 = 6.5$
$S(\gamma^*,R) = 245$	4-34	$R_C = 0.4$	$pH_{0C} = 4.6$	$R \rightarrow 0.2–1.4$	$pH_0 \rightarrow 4.2–4.6$	$\theta = 0.3$
$S(\gamma^*,pH_0) = –7.8$	4-35	$pH_0 = 4.6$	$R_C = 0.8$	$pH_0 \rightarrow 4.5–4.8$	$R \rightarrow 0.4–2.0$	$\theta = 0.7$
$S(\gamma^*,pH_0) = –13.8$	4-36	$pH_{0C} = 4.6$	$\theta_C = 0.5$	$pH_0 \rightarrow 4.45–4.85$	$\theta \rightarrow 0.25–0.75$	$R = 0.8$

Positive values of the objective normalized sensitivity of the pH-minimum with respect to input parameters θ and R indicate that the pH-minimum increases as the magnitude of these parameter increase. The negative value of objective normalized sensitivity of the pH-minimum with respect to pH_0 indicates that the pH-minimum increases as pH0 decreases. Thus, if the sensitivity is positive, the transition from a stable pH system to pH-runaway behaviour occurs as this parameter is increased. In contrast, if the sensitivity is negative, the same transformation occurs when the corresponding parameter is decreased.

4.3 Case 3: Kinetic modelling for determining inhibitory effects of products in the biohydrogen production process

In this case study, the inhibitory effects of hydrogen concentration in reactor headspace on fermentative hydrogen production from the acidogenesis of glucose by a bacterium, *Clostridium acetobutylicum*, were investigated experimentally in a batch reactor. A mathematical model to simulate and predict biological hydrogen production process was developed. The Monod model was modified to take inhibition kinetics on microbial growth into account. The modified model was then used to investigate the effect of hydrogen concentration on the microbial growth and hydrogen production rate.

In order to observe the effects of accumulated hydrogen in a batch reactor, a series of experiments were conducted by varying the initial hydrogen concentration in the reactor headspace. The details of the modelling and experimental procedure using a batch reactor for studying microbial growth kinetics of *Clostridium acetobutylicum* are provided in Chapter 3.

Kinetic modelling for defining inhibitory effects of accumulated hydrogen in the reactor headspace and the evaluation of growth associated kinetic constant of were described in sections 3.1.2.2 and 3.1.2.3 respectively.

The scheme of batch reactor operation and materials and equipment used for the reactor operation was described in detail in Section 3.4.1, and 3.4.3 provide the details of materials and equipment respectively

4.3.1.1 Effects of added H_2 in the reactor headspace

Effects of hydrogen concentration accumulated in the reactor headspace on microbial growth and hydrogen production were studied by conducting experiments in batch reactors. The results were shown in Figure 4-37 to 4-48. In these figures, the time history of biomass concentration and produced hydrogen concentration were showed when initial hydrogen concentration in the reactor headspace was varied. From these figures, it is clear that microbial growth, as well as hydrogen productivity, were greatly influenced by the presence of hydrogen in the reactor headspace.

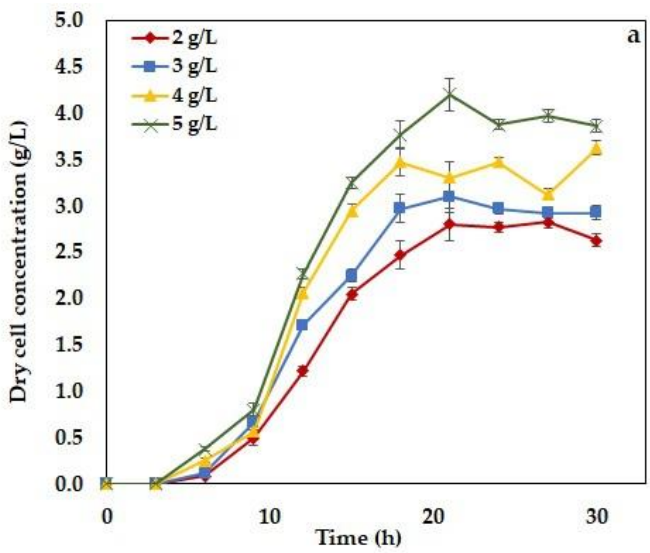

Figure 4-37 Experimental time histories of dry cell concentration with initial 0% H_2 in reactor headspace at different substrate concentration.

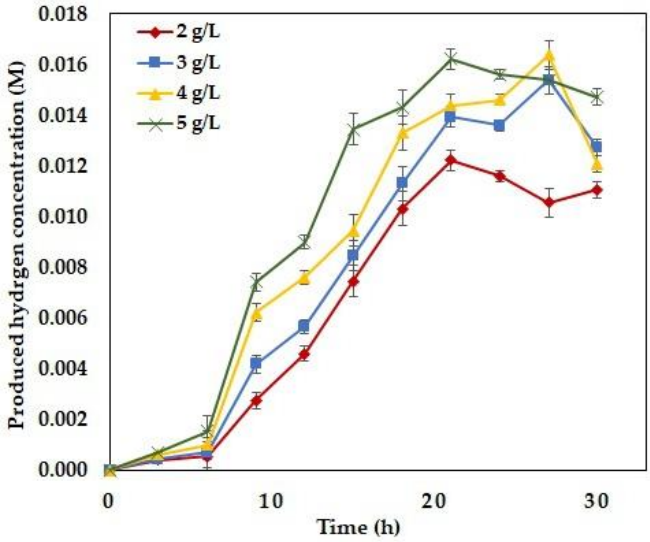

Figure 4-38 Experimental time histories of hydrogen concentration with an initial 0% H_2 in reactor headspace at different substrate concentration.

Initially, experiments were started when only argon gas was present in the reactor headspace, and initial glucose concentration in the liquid medium was varied in the range of 2g/L to 5g/L. At each variation of glucose, the microbial growth pattern and hydrogen production rate were observed for 30h. The time histories of microbial growth and hydrogen production rate were presented in Figure 4-37 and 4-38, respectively. From this figure, it is observed that microbial growth, as well as hydrogen production, was started immediately after 3h of reaction time. There was no significant lag phase of microbial growth detected. A stationary phase was started at 21h for every initial glucose concentration. The maximum productivity of hydrogen was 7.81 $mML^{-1}h^{-1}$ when initial glucose concentration in the liquid medium was 5g/L.

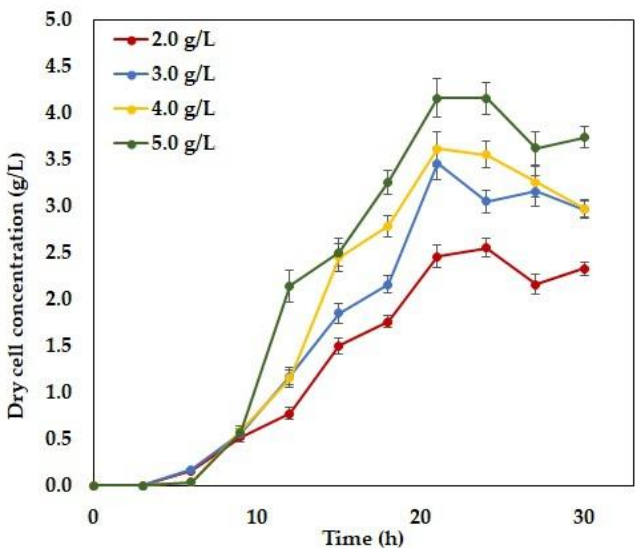

Figure 4-39 Experimental time histories of dry cell concentration with an initial 10% H_2 in reactor headspace at different substrate concentrations

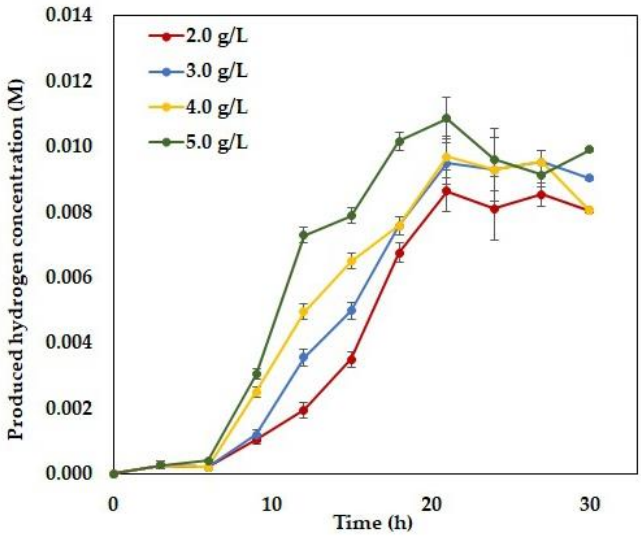

Figure 4-40 Experimental time histories of hydrogen concentration with an initial 10% H_2 in reactor headspace at different substrate concentrations

On the other hand, when 10% (v/v) of H_2 added to reactor headspace, microbial growth and hydrogen production started after 6h of incubation time, shown in Figures 4-39 and 4-40. Although there was no such difference in specific growth and hydrogen production observed for different initial substrate concentrations, the maximum hydrogen productivity decreased to 5.17 mML-1h-1, comparable to the 0% (v/v) added H_2 condition. The exponential phase of microbial growth ended at 21h, which was same as the previous condition.

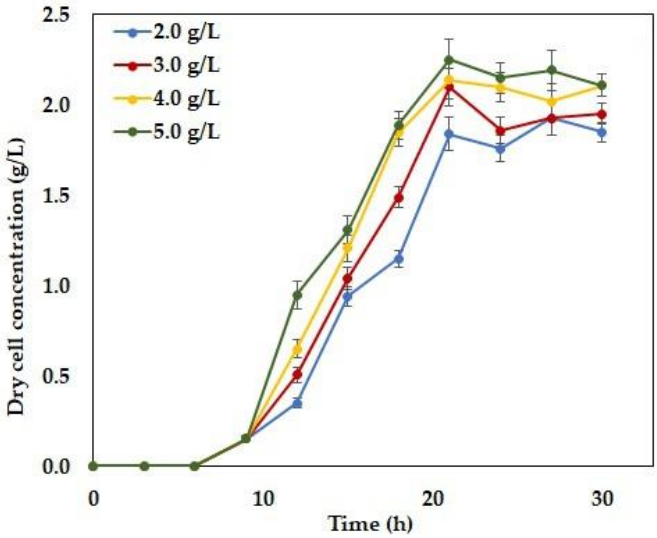

Figure 4-41 Experimental time histories of dry cell concentration with an initial 20% H_2 in reactor headspace at different substrate concentrations

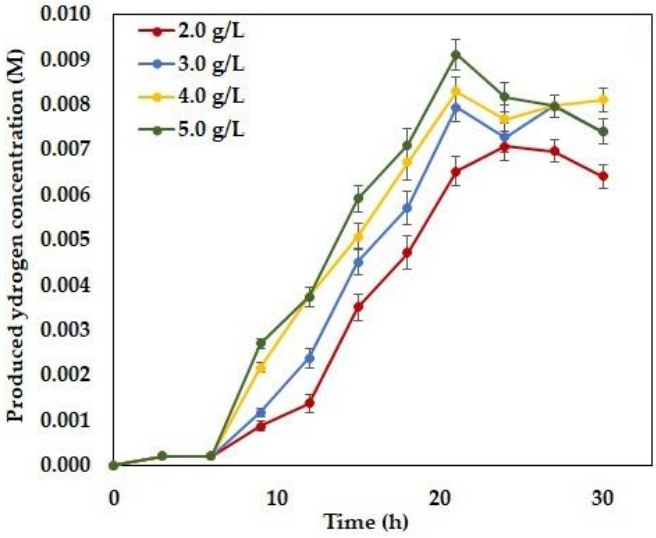

Figure 4-42 Experimental time histories of hydrogen concentration with an initial 20% H_2 in reactor headspace at different substrate concentrations

In the case of 20% (v/v) added H_2 in the reactor headspace, the hydrogen production rate as well as biomass production rate further decreased, which can be observed from Figure 4-41 and 4-42. In this condition, propagation of hydrogen production and bacterial growth was quite similar to that of 10% (v/v) added H_2 condition, where microbial growth reached its exponential phase at 6h and extended up to 21h. But in this condition, maximum hydrogen productivity decreased to 4.33 $mML^{-1}h^{-1}$.

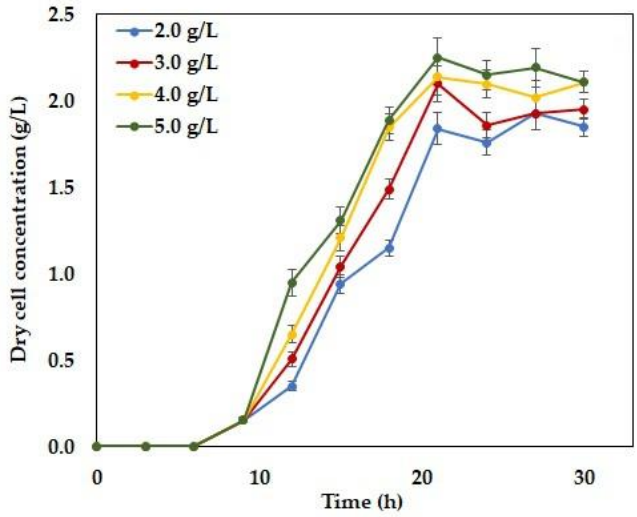

Figure 4-43 Experimental time histories of dry cell concentration with an initial 30% (v/v) H_2 in reactor headspace at different substrate concentrations

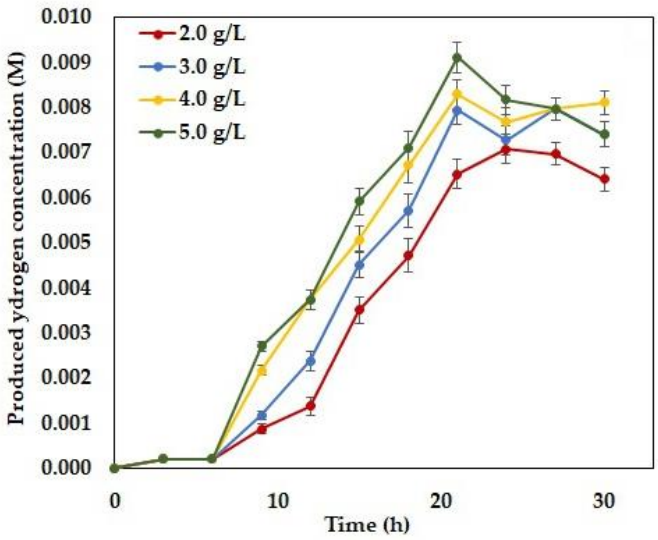

Figure 4-44 Experimental time histories of produced hydrogen concentration with an initial 30% (v/v) H_2 in reactor headspace at different substrate concentrations

A different phenomenon was observed when 30% (v/v) H_2 was added to the reactor headspace. In this case, the exponential phase of bacterial growth started after 6h of incubation time, but it extended to 24h where the stationary phase started. The time histories of dry cell concentration and produced hydrogen were presented in Figure 4-43 and 4-44. Monotonic decreases of microbial growth rate, and hydrogen production were observed where hydrogen productivity reduced to 3.075 $mML^{-1}h^{-1}$ when initial substrate concentration in liquid medium was 5g/L. Although, there was no such significant change in growth pattern observed for different substrate concentration in the liquid medium.

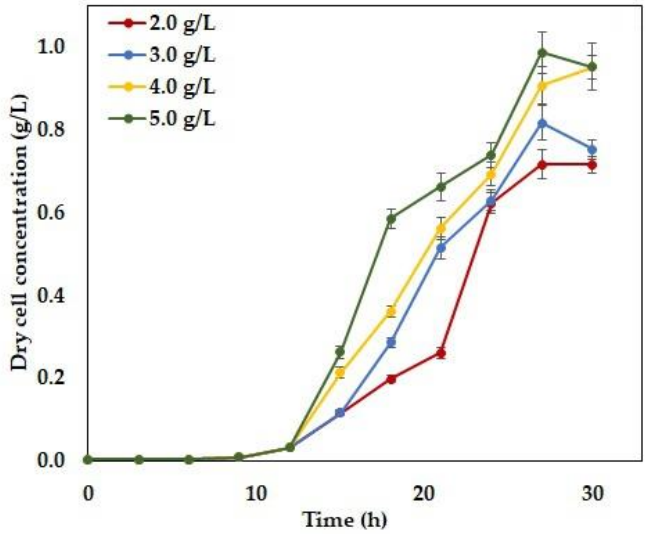

Figure 4-45 Experimental time histories of dry cell concentration with an initial 40% H_2 in reactor headspace at different substrate concentrations

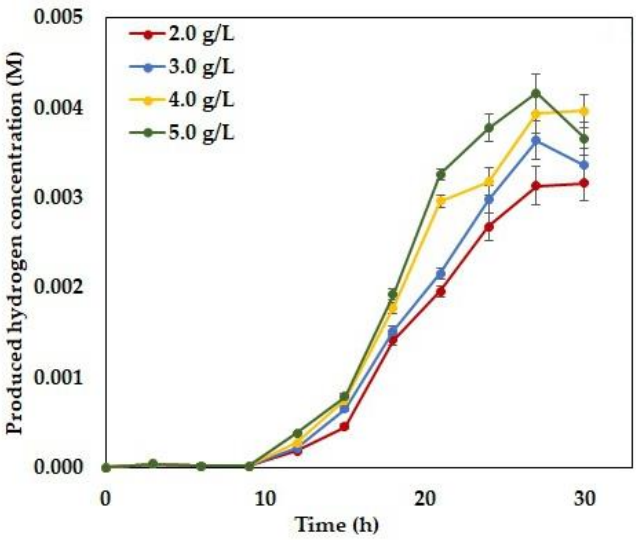

Figure 4-46 Experimental time histories of hydrogen concentration with an initial 40% H_2 in reactor headspace at different substrate concentrations

An extended lag phase in microbial growth was noticed as the quantity initially added H_2 increased from 30% (v/v) to 40% (v/v). At this condition, the exponential phase commenced at 12h of incubation time whereas, it extended until 27h. A sharp degradation in microbial growth, as well as biohydrogen production, were observed, which is demonstrated in Figure 4-45 and 4-46. There were no such effects of substrate concentration in liquid medium experience. The hydrogen productivity in this condition was estimated as 1.54 $mML^{-1}h^{-1}$ which is a sharp alteration compared to 30% (v/v) added H_2 condition.

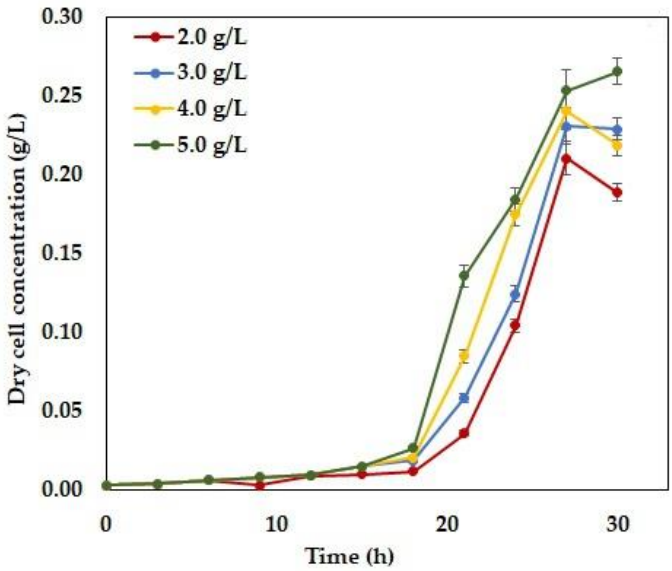

Figure 4-47 Experimental time histories of dry cell concentration with an initial 50% H_2 in reactor headspace at different substrate concentrations

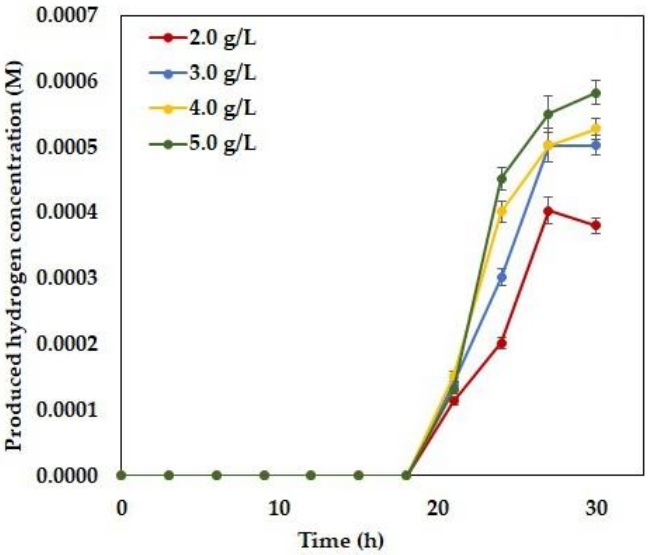

Figure 4-48 Experimental time histories of hydrogen concentration with an initial 50% H_2 in reactor headspace at different substrate concentrations

Furthermore, when 50%(v/v) H_2 was added to the reactor headspace, almost no growth condition was observed, shown in Figures 4-47 and 4-48. In this case, an extended lag phase with no microbial growth and hydrogen production was seen for 18h. A short period of exponential phase ended at 27h was noticed. Almost no hydrogen production condition with productivity of 0.19mML^{-1}h^{-1} was estimated.

4.3.1.2 Inhibition kinetics

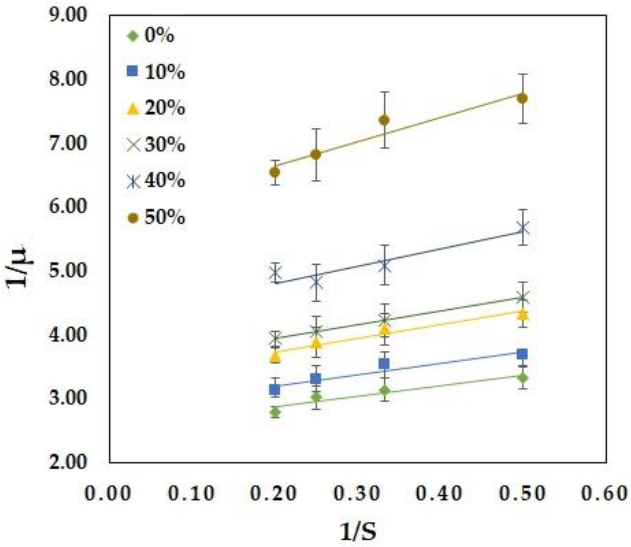

Figure 4-49 Determination of $\mu_{max,obs}$ and $k_{s,obs}$ at different initial concentrations of H_2

In the present investigation, a total of 24 experimental runs were conducted at different initial H_2 and substrate concentration. From each initially added H_2 concentration substrate concentration was varied from 2g/L to 5g/L. For each combination of initially H_2 concentration and substrate concentrations, specific growth rate microorganisms were determined. By using Equation (3.16), plots of 1/μ and 1/S were obtained at each initially added hydrogen in reactor headspace, which is demonstrated in Figure 4-49. $\mu_{max,obs}$ and ks,$_{obs}$ at each headspace H_2 concentration were determined by evaluating the intercepts and abscissas on Figure 4-49. The values of $\mu_{max,obs}$ and ks,$_{obs}$ are provided in Table 4-11.

Table 4-11 Values of observed rate constants from experiments

Initial H_2 concentration in reactor headspace (v/v)	$\mu_{max,obs}$	$ks_{,obs}$
0%	0.6209	0.6318
10%	0.5523	0.6395
20%	0.4792	0.6285
30%	0.4643	0.6141
40%	0.3695	0.6343
50%	0.2613	0.6521

From Table 4-11, it can be observed that $ks_{,obs}$ does not change in any systematic manner with the change of added hydrogen in the reactor headspace. Therefore, m=0 in Equation. (3.11) and 3.15), which infers the adopted model is a noncompetitive inhibition model and $ks_{,obs}$= ks which will be constant.

After determining values of $\mu_{max,obs}$ and $ks_{,obs}$ at different headspace H_2 concentration, constants in Equation. (3.11) can be evaluated by plotting $\ln(\mu_{max,obs})$ vs $\ln(1-H_2/ H_2^*)$ from Equation. (3.17) which is shown in Figure 4-50. Figure 4-50 gives the values of μ_{max} and n. As H_2^* was not identified from the experiments, a guessed value of 61.5 (v/v) H_2^* (24.74mM) was considered, which gives a straight line with R^2=0.9823. From Figure 4-47, the intercept and slope give the value of μ_{max}= 0.976 $h^{-1}$and n=0.4786.

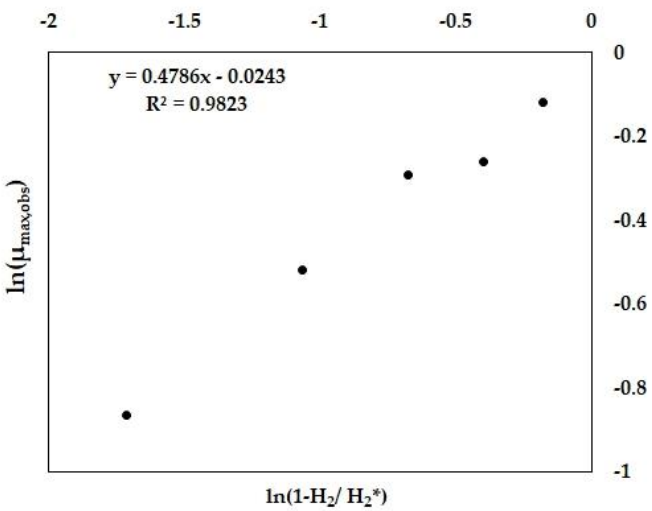

Figure 4-50 Determination of $u_{max,\,n}$ and H_2^* for product inhibition

4.3.2 Discussion

Initially, in the absence of H_2 in reactor headspace, the feed stream substrate concentration was varied from 2g/L to 5g/L. The production rates are high, and it significantly starts decreasing as the hydrogen

concentration start increasing gradually. When no hydrogen was initially added to the reactor, the growth phase started after 3h of reaction time and reached the stationary phase at 21h. For 10% added hydrogen condition, the exponential phase starts at 6h, and it went off until 21h. However, when 20% and 30% hydrogen added initially, the exponential phase started at 6h, and it goes until 24h. Further, on increasing hydrogen concentration by 40% of total headspace, lag phage elongated by 12h and growth phage started at 15h until 27h. No growth of microorganisms was observed pragmatically when 50% of reactor headspace filled with hydrogen initially. The specific growth rate of biomass decreases as the hydrogen concentration increases in the reactor headspace.

This increased hydrogen concentration reduces the glucose degradation efficiency of bacteria that results in lower hydrogen yield. Hydrogen yield gradually decreased along with specific growth rate from 1.11 to 0.56 mol/mol.glucose and 0.621±0.019h^{-1} to 0.261±0.021 h^{-1}, respectively. As the initial hydrogen concentration increases from 0.0 to 0.0161M, the hydrogen productivity reduction becomes faster when the initial hydrogen concentration altered from 0.0161M to 0.0201M. Therefore, the final partial pressure of hydrogen in the product gas declined and initially added hydrogen concentration increased. The effect of accumulated H_2 in reactor headspace on the specific growth rate, final hydrogen concentration and hydrogen yield was calculated by dividing the total amount hydrogen produced by the amount of glucose consumed are summarized in Table 4-12.

Table 4-12 Effects of added hydrogen on the specific growth rate, hydrogen production

Added hydrogen (M)/(v/v)	**Specific growth rate (h^{-1})**	**Hydrogen yield (mol-H_2/mol-glucose)**	**Final H_2 partial pressure (atm)**
0.0/(0%)	0.621±0.019	1.11±0.0026	0.280±0.015
$4.023*10^{-3}$(10%)	**0.552±0.028**	**1.01±0.0020**	**0.229±0.005**
$8.045*10^{-3}$(20%)	**0.479±0.029**	**0.92±0.0022**	**0.214±0.008**
$1.207*10^{-2}$(30%)	0.464±0.032	0.88±0.0016	0.165±0.013
$1.610*10^{-2}$(40%)	0.369±0.015	0.56±0.0010	0.094±0.005
$2.012*10^{-2}$(50%)	0.261±0.021	0.21±0.0010	0.0127±0.003

From the current analysis, it is inferred that as hydrogen concentration increases in the reactor headspace, it limits the mass transfer from the liquid to the gaseous phase. Therefore, liquid to gas transfer becomes a rate-limiting stage that controls microbial reactions. Subsequently, low microbial growth and less hydrogen production take place. On the other hand, high concentration of hydrogen affects hydrogenase, which activates the reversible oxidation of molecular hydrogen and the process become thermodynamically unfavourable for H_2 generation.

From this investigation, it is clear that the initial addition of hydrogen has an important influence on microbial growth, hydrogen yield and hydrogen production rate. Regarding non-competitive inhibition, substrate concentration does not affect the specific growth rate or rate of substrate utilization. In order

to sustain the hydrogen production at an optimal level, the accumulated hydrogen in reactor headspace should not be more than 8mM. The present study concludes that when 24.85mM hydrogen accumulated in the reactor headspace, reaction stops and no hydrogen is produced.

4.4 Case 4: Stability analysis of the biohydrogen production in a continuous bioreactor

The effect of process parameters in biological hydrogen production in a continuous stirred tank bioreactor (CSTBR) and how these parameters influence the stable bioreactor operation, was investigated in this case study. The substrate and/or product inhibits typically microbial growth in the process of biohydrogen production. An effort is made in order to examine the dynamic behaviour of a CSTBR subject to growth inhibition by the substrate and/or product. By the use of elementary principle bifurcation theory, the stability analysis was performed to demonstrate the dynamics of CSTBR model comprising steady-state multiplicity and hysteresis. A particular range of operating conditions where the non-washout steady-state solution is possible needed to be determined from this study. The results from this investigation can be used as strategies for selecting suitable operating conditions of similar bioreactor systems to avoid undesired instability and multiplicity.

4.4.1 Process model

A microbial population of hydrogen-producing bacteria is growing by consuming glucose in an ideal continuous stirred tank bioreactor. The schematic of the reactor setup is given in Figure 4-51.

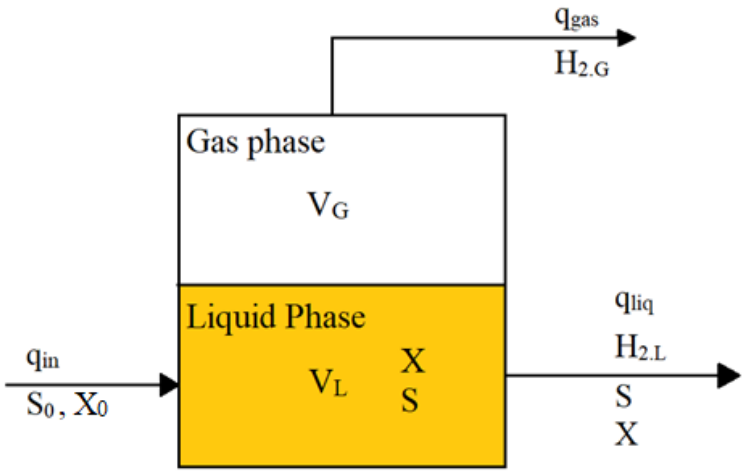

Figure 4-51 Schematic of reactor setup

The bacterial culture is assumed to increase its number and produce hydrogen during this metabolism period. The feed stream enters the reactor at a flow rate of q_{in} Lh^{-1}, and the concentrations of the substrate and bacterial cell in the feed stream are S_0 and X_0 gL^{-1}. The liquid phase and gaseous phase working volume of the reactor are V_L litre and V_G litre, respectively. The microbial reaction occurs in the liquid phase. The main products from the metabolism are hydrogen and several volatile fatty acids (VFA). A part of hydrogen produced in the liquid phase transfers to the gaseous phase, and the rest is leaving out with the effluent. The effluent contains glucose, produced bacterial cells, VFA, and hydrogen flow at a rate, q_{liq} Lh^{-1}. The fraction of hydrogen converting into the gaseous phase exits the reactor at a flow rate of q_{gas} Lh^{-1}. The material balance equations for different components, excluding VFAs are as below:

Biomass

$$\frac{dX}{dt} = D(X_0 - X) + \mu X \tag{4.59}$$

Substrate

$$\frac{dS}{dt} = D(S_0 - S) - \frac{1}{Y_{x/s}}\mu X \tag{4.60}$$

Liquid phase H_2

$$\frac{dH_{2.L}}{dt} = -D.H_{2.L} + Y_{H_{2.L}/x}\mu X - k_L a(H_{2.L} - H.R.T.H_{2.G}) \tag{4.61}$$

Gas phase H_2

$$\frac{dH_{2.G}}{dt} = k_L a(H_{2.L} - H.R.T.H_{2.G}) - D_2 H_{2.G} \tag{4.62}$$

This produced hydrogen exerts feedback inhibition on the growth of cells. For generality, the substrate itself, at high concentration is assumed toxic to growth. To understand the dynamic behaviour of this bioreactor system, kinetic expressions for microbial growth are needed. For that, the microbial growth kinetics from the previous case study, (Case 3) is considered, incorporating the substrate inhibition established by van Niel et al. [74]. Therefore, the specific growth rate for this case is described as follow:

$$\mu = \frac{\mu_{max}S}{K_S+S} \cdot \left(1 - \frac{S}{S^*}\right)^n \left(1 - \frac{H_{2.G}}{H^*_{2.G}}\right)^m \tag{4.63}$$

The values of kinetic constant also are used as in Case study 3. The kinetic constant and other operating constants are provided in Table 4-13.

Table 4-13 Values of kinetic and operating constants

Constants	Value	Constants	Value
$Y_{x/s}$	1.42 (g/g)	μ_{max}	0.976 h^{-1}
$Y_{H2.L/x}$	3.95 (mmol/g)	K_S	0.63 g/L
H	7.4×10^{-6} (mmol.L^{-1}.pa^{-1})	$H_{2.G}^*$	24.76 mmol.L^{-1}
R	8.314 (pa.L.mmol^{-1}.K^{-1})	$k_l a$	0.09 h^{-1}
T	303 K	**n**	0.4786
S^*	8.19, (g/L)	**m**	1.39

For the convenience of further study of stability and bifurcation analysis, the above equations 4.59 to 4.63 are converted into dimensionless forms as below;

$$\frac{dx_1}{d\tau} = d_1(x_{10} - x_1) + Ux_1 \tag{4.64}$$

$$\frac{dx_2}{d\tau} = d_1(x_{20} - x_2) - Ux_1 \tag{4.65}$$

$$\frac{dx_3}{d\tau} = -d_1x_3 + Ux_1 - K(x_3 - \alpha.x_4) \quad (4.66)$$

$$\frac{dx_4}{d\tau} = K(x_3 - \alpha.x_4) - d_2x_4 \quad (4.67)$$

The dimentionless form of specific growth rate is expressed as,

$$U = \frac{x_2}{1+x_2}\left(1 - \frac{x_2}{x_2^*}\right)^m \left(1 - \frac{x_4}{x_4^*}\right)^n \quad (4.68)$$

The definitions of different dimentionless variable are provided in the Table 4-14.

Table 4-14 Definition of dimensionless variables

Variable	Definition	Variable	Definition
x_1	$\frac{X}{K_S Y_{x/s}}$	x_2^*	$\frac{S^*}{K_S}$
x_2	$\frac{S}{K_S}$	τ	$t.\mu_{max}$
x_3	$\frac{H_{2.L}}{K_S Y_{x/s} Y_{H_{2.L}/x}}$	U	$\frac{\mu}{\mu_{max}}$
x_4	$\frac{H_{2.G}}{K_S Y_{x/s} Y_{H_{2.L}/x}}$	d_1	$\frac{D}{\mu_{max}}$
x_{10}	$\frac{X_0}{K_S Y_{x/s}}$	d_2	$\frac{D_2}{\mu_{max}}$
x_{20}	$\frac{s_0}{K_S}$	K	$\frac{k_L a}{\mu_{max}}$
x_4^*	$\frac{H_{2.G}^*}{K_S Y_{x/s} Y_{H_{2.L}/x}}$	α	$H.R.T$

A steady-state is supposed to be locally stable if the continuous system returns to the suitable steady state after a sufficiently small, but otherwise, arbitrary perturbation from the steady-state. Stability analysis of a nonlinear system is performed by examining a system's dynamic behaviour close to equilibrium. Thus, local stability of a steady-state for the reactor was analyzed by linearizing the differential equations (4.64 to 4.67) of the system around the steady-state in question and calculating the eigenvalues of the stability matrix (Jacobian matrix). The stability matrix of the linearized forms of the differential Equations (4.64 to 4.67) at the steady-state x_{1S}, x_{2S}, x_{3S} and x_{4S} are as follows:

$$A = \begin{bmatrix} a_{11} & a_{12} & a_{13} & a_{14} \\ a_{21} & a_{22} & a_{23} & a_{24} \\ a_{31} & a_{32} & a_{33} & a_{34} \\ a_{41} & a_{42} & a_{43} & a_{44} \end{bmatrix} \quad (4.69)$$

The eigenvalues of the matrix A, are the roots of the characteristic equation:

$$\lambda^4 + C_1\lambda^3 + C_2\lambda^2 + C_3\lambda + C_4 = 0 \tag{4.70}$$

These four eigenvalues can be all real, or one real and a complex conjugated pair with the following form:

$$\lambda = n \pm pi \tag{4.71}$$

where, n and p are real numbers, and i is imaginary, defined as the square root of −1. If the real parts of all the eigenvalues are negative, the steady-state is said to be locally asymptotically stable. In case one or some of the real parts of the eigenvalues are positive, the steady-state is unstable. If $p \neq 0$, the system will display oscillations after a perturbation. Depending on the sign of n, the oscillations may be damped or exponentially increasing. It is true for the linearized system, and the result is valid for the nonlinear system [Eqs. (4.64)– (4.67)] if the perturbation is sufficiently small.

4.4.2 Results and discussions

4.4.2.1 Multiplicity and stability analysis

The equations (Equations 4.64–4.67) model the process described in Figure 4.51 and are used to examine the possibility of occurrence of multiple steady states.

The model (Equations 4.64–4.67), were solved numerically by Runga-Kutta method using the initial value and particular operating condition, provided in Table 4-15 to obtain a steady-state solution. The obtained solution was used to examine the stability of the steady-state of bioreactor through bifurcation analysis. Bifurcation analysis can determine the region of the stable and unstable steady state of the dynamical system for operating parameters. The behaviour of the bioreactor system is suitably presented in continuity diagrams (Figures 4-52 to 4-55 and 4-57 to 4-60) demonstrating the progression of the steady-state solutions of the model with operating parameters. Among the operating parameters, feed dilution rate (d_1) and constant feed substrate concentration (x_{20}) were selected as bifurcation parameters in this case. The continuity diagrams are obtained using MATCONT, a numerical bifurcation package of MATLAB. High accuracy steps in the order of 10^{-8} were used to generate the continuity curves.

Table 4-15 Initial conditions and model parameters of equations 4.64 to 4.68

Initial conditions

x_1	x_2	x_3	x_4
0.1	6.0	0.0	0.0

Operating parameters				**Other model parameters**			
d_1	d_2	x_{10}	x_{20}	K	α	x_2^*	x_4^*
0.2	0.1	0.1	6.0	0.1	0.01864	13	7.007

Figures 4-52 to 4-55 show the steady-state dimensionless bacterial cell, substrate and product concentration in the reactor as functions of the feed dilution rate (d_1) keeping feed substrate concentration (x_{20}), initial bacterial cell concentration (x_{10}), dilution rate of gaseous effluent (d_2) and overall mass transfer coefficient (K) at constant.

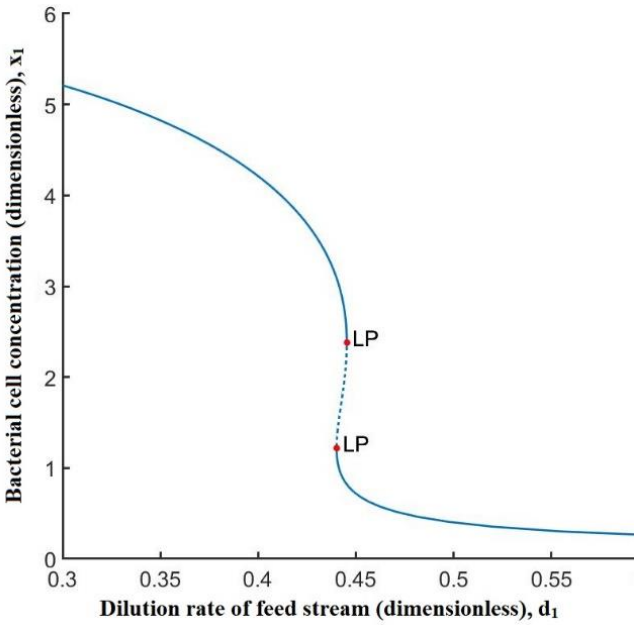

Figure 4-52 Steady-state dimensionless cell concentration (x_1) in CSTBR as function of feed stream dilution rate (d_1) at x_{20}=6

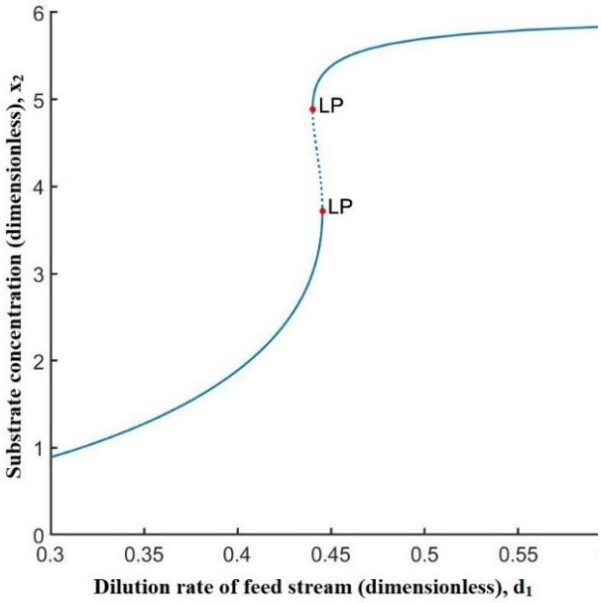

Figure 4-53 Steady-state dimensionless substrate concentration (x_2) in CSTBR as function of feed stream dilution rate (d_1) at x_{20}=6.

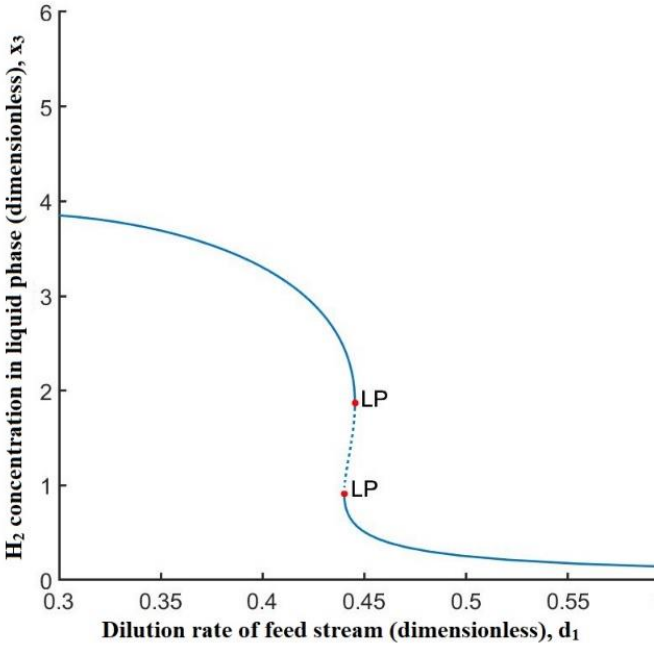

Figure 4-54 Steady-state dimensionless liquid phase H_2 concentration (x_3) in CSTBR as functions of feed stream dilution rate (d_1) at X_{20}=6

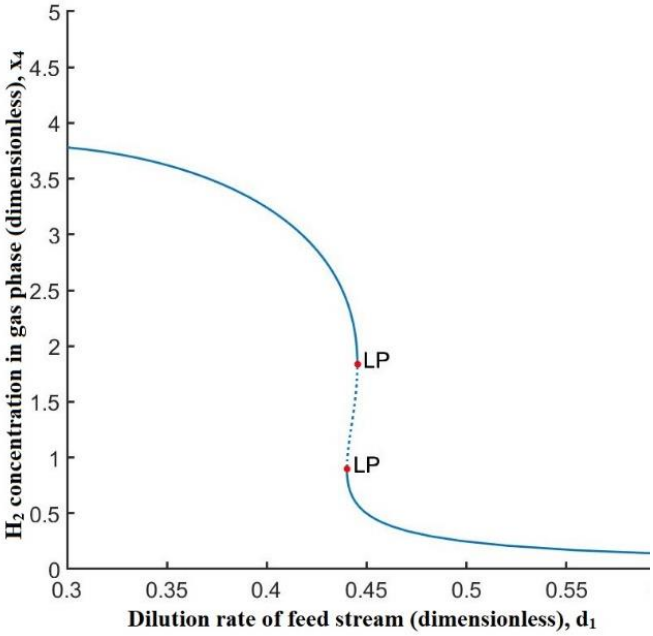

Figure 4-55 Steady-state dimensionless gas phase H_2 concentration (x_4) in CSTBR as functions of the dilution rate (d_1) at x_{20}=6

From these figures, it can be observed that the continuation diagram have three branches. Among these three branches, two branches are the stable-static branch (solid lines), connected by an unstable branch in the middle, which is demarcated by a dotted line. The points at which the stable changed to unstable steady states is demarcated as limit points (LP) in these figures. The two stable branches in these figures are connected to the unstable branch by two limit points (LP) where the feed stream dilution rates are

d_1=0.445 (x_1= 2.379, x_2= 3.72, x_3= 1.868, x_4= 1.833) and d_1=0.440 (x_1= 1217, x_2=4.833, x_3= 0.913, x_4= 0.8965) respectively. From the theory of stability analysis, in the region of unstable steady states, at least one eigenvalues of the characteristic equation of the Jacobian matrix must have a positive real part. In the present case, 4th eigenvalue becomes positive between d_1=0.445 and d_1=0.440, which is shown in Figure 4-56.

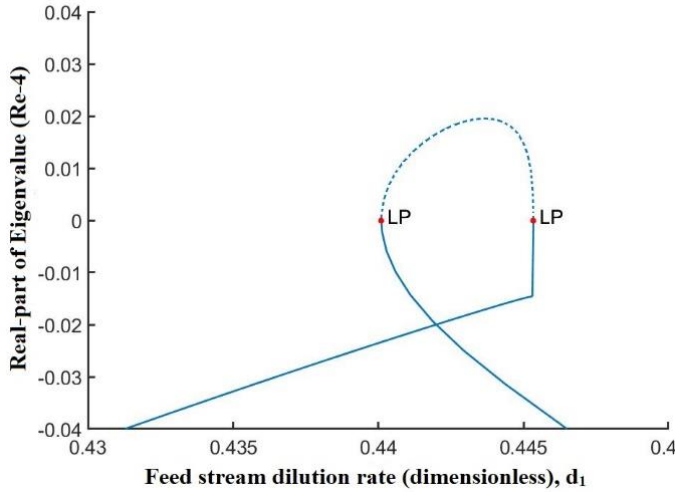

Figure 4-56 Eigenvalues of the stability matrix [Eq. (4.69)] for the steady-state solutions

The multiplicity of steady states occurs between these two limit points. In this region, there exist three steady-state solutions, and this kind of phenomenon is called hysteresis. If a sudden change in operating parameters, such as feed substrate concentration (x_{20}) or dilution rate of gas stream (d_2) occurs within this multiplicity region, irreversible effects on the system in terms of conversion can shift from high conversion (lower branch) to a low conversion (higher branch).

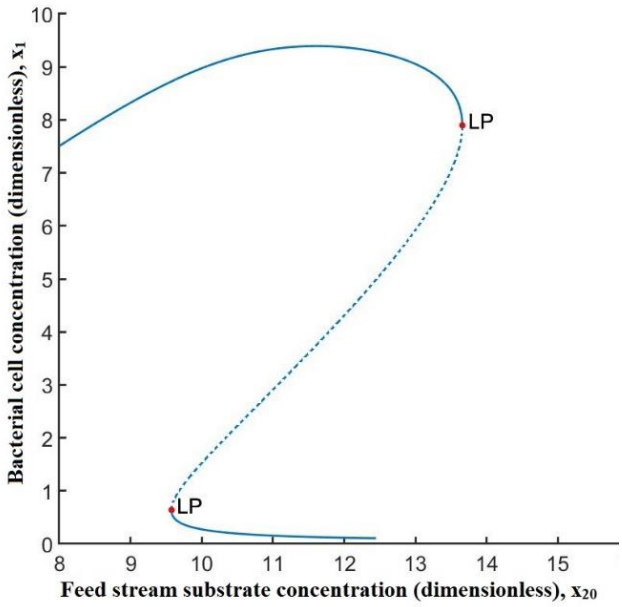

Figure 4-57 Steady-state dimensionless cell concentration (x_1) in CSTBR as functions of feed substrate concentration(x_{20})at d_1=0.2

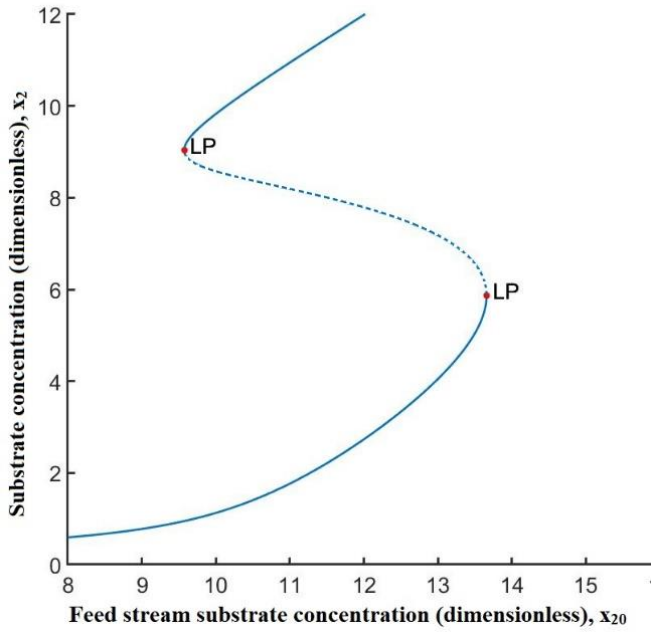

Figure 4-58 Steady-state dimensionless substrate concentration (x_2) in CSTBR as functions of feed substrate concentration(x_{20})at d_1=0.2

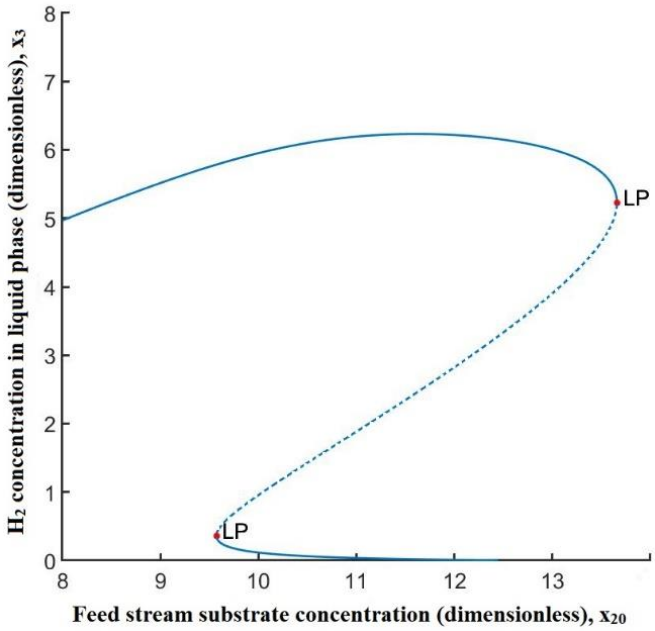

Figure 4-59 Steady-state dimensionless liquid phase H_2 concentration (x_3) in CSTBR as functions of feed substrate concentration(x_{20})at d_1=0.2

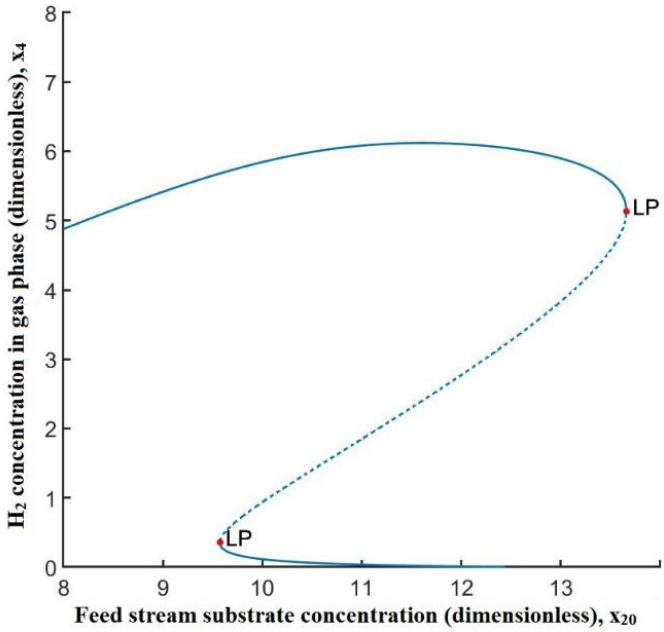

Figure 4-60 Steady-state dimensionless gas phase H_2 concentration (x_4) in CSTBR as functions of feed substrate concentration(x_{20})at d_1=0.2

The multiplicity of the steady-state solution of Equations (4.64)–(4.67) were also examined for cultures operated at a constant dilution rate (d_1=0.2)), initial bacterial cell concentration (x_{10}), dilution rate of gaseous effluent (d_2) and overall mass transfer coefficient (K) but with varied feed substrate concentration (x_{20}). The results are shown in Figures 4-54 to 4-57. Steady-state behaviour of the bacterial culture with respect to x_{20} is quite similar to that concerning the variation of dilution rate (d_1). In this case, also, multiplicity was observed in a specific range of feed substrate concentration (x_{20}). The branch between two limit points (LP) in Figures 4-54 to 4-57 represents a hysteresis loop similar to that in Figures 4-49 to 4-52. The feed substrate concentration at first limit point was x_{20} =9.572 (x_1= 0.637, x_2= 9.034, x_3= 0.36, x_4= 0.353) when the stable, steady-state (lower branch) bifurcated to unstable steady state. Likewise, at x_{20} =13.658 (x_1= 7.896, x_2= 5.862, x_3= 5.23, x_4= 5.133) the unstable steady-state transform its nature and the system became stable steady state (upper branch).

4.4.2.2 Effect of operating condition

In order to find out the range of these operating conditions for which the stability of steady-state changes its nature, the simulation was performed over the multiplicity or hysteresis zone. From the analysis, it is found that among all operating conditions, dimensionless dilution rate of feed stream (d_1) and gas stream (d_2) and dimensionless feed stream substrate concentration (x_{20}) influence bioreactor's steady-state behaviour.

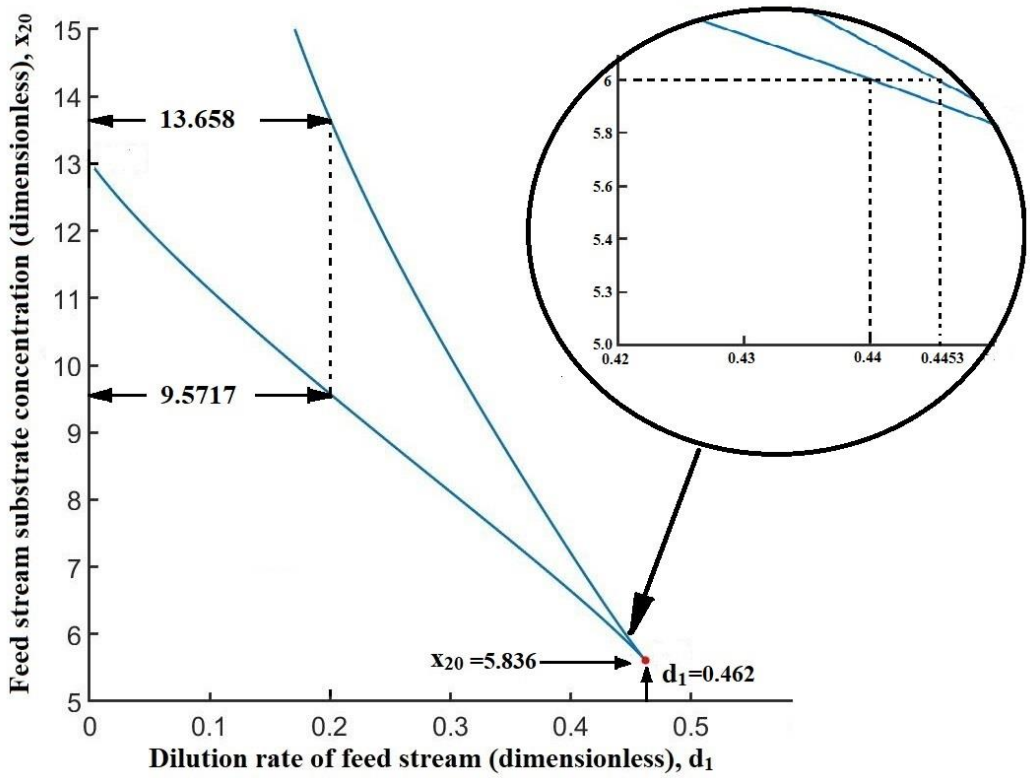

Figure 4-61 Two parameter continuation diagrams showing the effects of initial substrate concentration (x_{20}) on the limits of the hysteresis region

Figures 4-58 and 4-59 show the effects of operating conditions on the hysteresis region. Figure 4-58 shows the area of stability relating to operating parameters x_{20} and d_1. The two branches are representing the two limit points for different values of x_{20} and d_1. It can be observed that the thickness of the region between the two branches corresponds to instability. As feed substrate concentration (x_{20}) increases the thickness of instability increases. For an instant, at a constant value of d_1=0.2, the thickness of instability with respect to x_{20} is 4.086 (x20=13.658- x_{20}=9.572), which is presented in Figure 4-58 and can be observed in Figures 4-54 to 4-57. Furthermore, Figure 4-58 shows (Inset plot) that at a constant value of x_{20}=6.0, the width of instability with respect to d_1 is 0.0053 (d_1 = 0.4453- d_1 = 0.44) and can be seen in Figures 4-49 to 4-52. The width of instability for both the cases representing the length of the unstable branch between two Limit points as presented in Figures 4-49 to 4-57. However, the instability is only possible if the values of $x_{20} > 5.65$ and $d_1 < 0.467$, at which the two branches collapse.

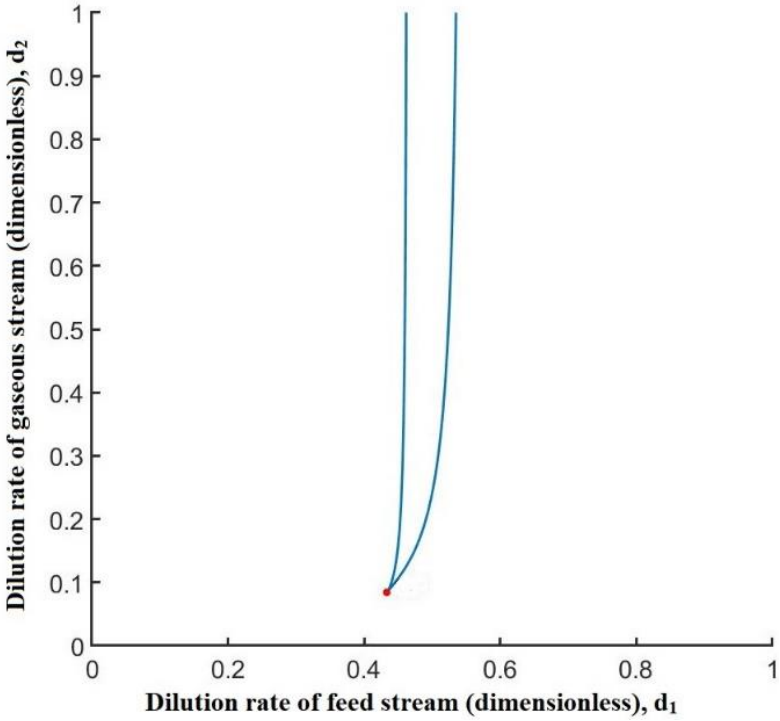

Figure 4-62 Two parameter continuation diagrams showing the effects of gaseous phase dilution rate (d_2) on the limits of the hysteresis region.

Similarly, the area of stability relating to operating parameters d_1 and d_2 represented in Figure 4-59. Here also, the two branches are representing the two limit points for different values of d_1, and d_2 and the region between the two branches corresponds to instability. As the dilution rate of the gaseous stream (d_2) increases the thickness of the instability region increases. Moreover, the range of instability increases with the increase of d_2. The region of instability collapse at d_1 = 0.417 and d_2=0.0612.

Observed results surmise the nonlinear phenomenon and parametrically sensitive behaviour of CSTBRs through bifurcation analysis. From this study, it can be stated that the model is capable of predicting the nonlinear phenomenon for a wide range of reactor kinetics and operating parameters, offering the model with a good deal of flexibility.

5 Conclusions

The present research study developed a mathematical model of continuous stirred tank bioreactors used for bioenergy conversion from biomass. It is expected that the investigation would contribute to bioreactor design and understanding factors that commonly influence productivity and reactors reliability. The reaction medium's pH and the partial pressure of gaseous product (H_2) are considered influencing factors for bioreactor operation to demonstrate the methodology. Whether it is a liquid or gaseous biofuel, acid is produced as one of the byproducts of microbial reactions. From this study, it is obtained that if the byproduct is acid, the pH of the reaction medium becomes acidic, which is not a favourable condition for microorganisms to growth at a specific limit. In the search for optimum pH condition for selected microbes, the experiments were conducted to find out the optimum pH and the other growth associated constants that characterize microbial growth. On the other hand, it is also observed that, if the main product of a bioprocess is a gas, then the pressure exerted by gaseous products inhibits the microbial reaction directly or indirectly. A series of experiments are conducted to investigate the effect of hydrogen concentration on microbial growth and hydrogen production rate. The methodology developed in this research is generic and can be implemented to find out other growth influencing parameters. A suitable bioreactor model can be established after finding out the objective variables that needed to be controlled.

The mathematical models for continuous stirred tank bioreactor (CSTBR) coupled with microbial growth reflecting influencing parameters are developed. Using the model, sensitivity analysis determines the parameter space of input variables for which the objective output variable will be uncontrollable. Multiplicity analysis can derive a dimensionless multiplicity criterion, to indicate a set of values of input parameters corresponding to multiple steady states. Furthermore, stability analysis was performed to demonstrate the dynamics of CSTBR model comprising steady-state multiplicity and hysteresis by using elementary principle bifurcation theory. A particular range of operating conditions where the non-washout steady-state solution is possible needed to be determined from this study. This methodology of finding out stability is suitable for predicting stable reactor operation in terms of the input variables.

Based on the research conducted in this thesis, the following specific conclusions are made.

5.1 Microbial growth kinetics

- It is established that microorganisms are the leading member of the bioreactor system, and it is essential to accrue information on microbial growth mechanisms and how the microbial activity is affected by the microenvironment of the growth medium. The experimental studies with two types of bacteria, *pediococcus acidilactic* and *lactobacillus casei* confirmed that for lactic acid type bacteria, the optimum value of pH for maximum microbial growth is at 6.7 - 6.75.
- However, the study found that despite the optimum pH value being similar for the two bacterias of the same type, the values of other kinetic parameters may be different for each strain of bacteria. Therefore, kinetic parameters defining the growth of certain bacteria should be determined prior to use the mathematical model for predicting control parameters for a reactor. These kinetic parameters can be determined by incorporating the influence of pH on microbial growth rate in the classical growth models such as the Monod model.

- Growth inhibition caused by hydrogen was examined through the acidogenesis of glucose by a bacterium, *clostridium acetobutylicum*. From the experiment, it was observed that hydrogen is an acute inhibitor if allowed to accumulate in reactor headspace. Initially, from 10% to 30% (v/v) hydrogen concentration, the microbial growth decreases linearly. As more hydrogen-filled the headspace, microbial activity was inhibited exponentially, particularly after 30% (v/v); the microbial growth critically affects the hydrogen production rate. When 50% of the reactor headspace was occupied by hydrogen, an extended lag phase in microbial growth observed and a much lower microbial growth and hydrogen production rate was also noticed. After 61.5% (v/v) of hydrogen accumulated in the reactor, no microbial growth was recorded, and thus the production of hydrogen ceased. Therefore, for optimal continuous production, the removal rate must be controlled in such a way that the reactor headspace does not accumulate gaseous produce more than 30% (v/v).
- Results also found that maximum specific growth rate (μ_{max}), substrate saturation constant (k_S), the critical concentration of hydrogen when microbial growth ceases (H_2^*) and degree of inhibition are 0.976 h^{-1}, 0.63 ± 0.01 g/L, 24.74 mM, and 0.4786, respectively.
- These results may be extended to similar bioenergy industries producing such as biobutanol where these kinds of phenomenon occur and employed for reactor safety and adaptation of control strategies

5.2 Mathematical modelling and stability analysis

- Unstructured mathematical models were developed using the fundamental knowledge about microbial and the related kinetic parameters. The steady-state stability analysis can provide the information on the favourable and avoidable condition for CSTBR operation, which can be incorporated in control strategies of reactors.
- The influences of process variables in a continuous stirred tank bioreactor (CSTBR) and how these parameters influence the stable bioreactor operation for biological hydrogen production are investigated in case study 4 using elementary principles bifurcation theory. The stability analysis was performed to demonstrate the dynamics of CSTBR model comprising steady-state multiplicity and hysteresis.
- The results establish that among all operating conditions, d_1, d_2, and x_{20} influence bioreactor's steady-state behaviour. In a particular range of d_1 (a dimensionless form of dilution rate of feed stream), from 0.44 to 0.4453, the CSTBR operation becomes unstable as it comes across multiple steady states condition. On the other hand, CSTBR enters to instability due to another essential operating parameter X_{20} (a dimensionless form of feed substrate concentration) when the operating region of X_{20} is 9.5717 to 13.658 steady-states of CSTBR system bifurcated to multiple steady states. The results also provide information on the limit of the hysteresis region in terms of operating variable that must be avoided for stable reactor operation.
- The developed kinetic model in case 3 is useful to determine the influences of products on bacterial growth and product formation rate for mesophilic bacteria. In the case of hydrogen-producing bacteria, other by-products, which form during metabolism are volatile fatty acid and influences the system pH and metabolic pathway. Therefore, the kinetic model should consider these factors along with the product inhibition. Stability analysis of steady states was analyzed in case 4 of a CSTBR used for biohydrogen production

5.3 Parametric sensitivity analysis

- It was observed that the system is parametrically sensitive to both regions of multiplicity and uniqueness of steady states. The theoretical trends of parametric sensitivity variables are also in

agreement with experimental findings. Since the overall system is parametrically sensitive for almost all input variables, namely D, D_1 and S_b, it is suggested to run the reactor in fed-batch mode with periodic adjustment of pH rather than control of system pH with a continuous base stream.

- The sensitivity analysis also examined a generalized criterion of parametric sensitivity through Normalized objective sensitivity. A generalized criterion of sensitivity, i.e., a precise domain of input parameters at which the CSTBR becomes sensitive can be determined from such analysis.
- pH was chosen as the objective function in the current study, for determining the generalized criteria. The sensitivity analysis was performed taking as a function of three dimensionless input variables, θ, R and pH_0. The sensitive region for CSTBR operation was determined in terms of sensitivity function, $S(\gamma^*,\phi_i)$ with respect to three selected input parameters. From the investigation, the identified sensitive zone of input parameters is; from 0.095 to 0.295 for θ, from 0 to 0.865 for R and from 4.42 to 4.765 for pH_0. On the other hand, the critical values of input parameters θ, R and pH_0 are 0.0195, 0.48 and 4.6, respectively.
- This investigation concludes, the approach implemented in the present study for defining a generalized criterion to find out a parametrically sensitive regime can be implemented for any other operating parameters, such as temperature, the concentration of metabolites and other by-products. Thus, in order to predict CSTBR performance and to develop control systems for the bio or biochemical processes, this mathematical model can be used as a design tool. The model can perform the stability analysis of a CSBTR and obtain parametric sensitivity regions of the process. Such quantitative analysis of CSTBRs will benefit in the selection of strategies for safe, controlled and economical utilization of CSTBRs.

5.4 General conclusions

- In order to design a continuous type of bioreactor, the maximum specific growth rate (μ_{max}) provides the guideline regarding the flow rate of the feed stream to restrict the washout condition. Knowledge of substrate saturation constant K_S values is required for modelling continuous cultures where K_S largely determines the steady-state concentration of unused growth rate-limiting nutrient. The value of K_S is an essential factor in the efficiency of conversion of substrate to biomass.
- In the field of bioenergy conversion, the information obtained from the present research study can contribute to the design and optimization of bioreactors such as bioethanol, and biomethanol production from biowaste. The methodology used here can also be implemented to find out additional growth influencing parameters such as temperature. The methods of parametric sensitivity and multiplicity analysis are useful in evaluating the design and control aspects of the bioreactors.

5.5 Recommendations for further work

The study identified some pathways for further work. There are more output variables other than pH and partial pressure need to be controlled for designing a continuous stirred tank bioreactors. These are temperature, the concentration of byproducts. The influence of the parameters on the microbial growth rate recommended studying further for designing a bioreactor through suitable kinetic modelling. In this research study influence of pH was investigated for lactic acid bacteria to get a general overview for pH influence of microbial growth rate. There are other kinds of bacterial such as thermophilic, hyperthermophile and mesophilic or anaerobic and aerobic used in industrial bioprocesses for bioenergy conversion. Therefore, it is recommended to compare the methods used in the present study for this type of bacteria. In the case of biohydrogen production, there are other metabolites such as volatile fatty acids (VFA) produce along with the hydrogen. These acids can alter the system pH, which can be

unfavourable for microorganisms and shift the metabolic pathway of microbial reactions. So, the influence of the concentration of VFA and adopt a kinetic model is recommended to study further. The validation of the model-predicted data with the experimental study where the model shows the critical value of input parameters for which the CSTBR becomes sensitive. The interaction between input parameters or the points corresponding to the limits of the region of instability is recommended to be investigated. Moreover, the impact of model kinetic parameters on system stability is the scope where further work is suggested.

References

1. Hein, K.R.G. Future energy supply in Europe - Challenge and chances. In Proceedings of the Fuel; 2005.

2. Chen, H.; Qiu, W. Key technologies for bioethanol production from lignocellulose. *Biotechnol. Adv.* 2010.

3. Pörtner, R.; Platas Barradas, O.; Frahm, B.; Hass, V.C. Advanced Process and Control Strategies for Bioreactors. In *Current Developments in Biotechnology and Bioengineering: Bioprocesses, Bioreactors and Controls*; 2017 ISBN 9780444636744.

4. Hawkes, F.R.; Hussy, I.; Kyazze, G.; Dinsdale, R.; Hawkes, D.L. Continuous dark fermentative hydrogen production by mesophilic microflora: Principles and progress. *Int. J. Hydrogen Energy* **2007**.

5. Zhang, T.; Mao, C.; Zhai, N.; Wang, X.; Yang, G. Influence of initial pH on thermophilic anaerobic co-digestion of swine manure and maize stalk. *Waste Manag.* **2015**, *35*, 119–126.

6. Wang, J.; Wan, W. Factors influencing fermentative hydrogen production: A review. *Int. J. Hydrogen Energy* **2009**, *34*, 799–811.

7. Adessi, A.; De Philippis, R. Photobioreactor design and illumination systems for H2 production with anoxygenic photosynthetic bacteria: A review. *Int. J. Hydrogen Energy* 2014.

8. Mao, C.; Feng, Y.; Wang, X.; Ren, G. Review on research achievements of biogas from anaerobic digestion. *Renew. Sustain. Energy Rev.* 2015.

9. Şentürk, E.; Ince, M.; Engin, G.O. The effect of transient loading on the performance of a mesophilic anaerobic contact reactor at constant feed strength. *J. Biotechnol.* **2012**.

10. Tauseef, S.M.; Abbasi, T.; Abbasi, S.A. Energy recovery from wastewaters with high-rate anaerobic digesters. *Renew. Sustain. Energy Rev.* 2013.

11. Bodkhe, S. Development of an improved anaerobic filter for municipal wastewater treatment. *Bioresour. Technol.* **2008**.

12. Zhang, L.; Zhang, B.; Zhu, X.; Chang, H.; Ou, S.; Wang, H. Role of bioreactors in microbial biomass and energy conversion. In *Green Energy and Technology*; 2018.

13. Ramkrishna, D.; Fredrickson, A.G.; Tsuchiya, H.M. Dynamics of microbial propagation: Models considering inhibitors and variable cell composition. *Biotechnol. Bioeng.* **1967**, *9*, 129–170.

14. Yano, T.; Koga, S. Dynamic behavior of the chemostat subject to product inhibition. *J. Gen. Appl. Microbiol.* **1973**, *19*, 97–114.

15. Agrawal, P.; Lee, C.; Lim, H.C.; Ramkrishna, D. Theoretical investigations of dynamic behavior of isothermal continuous stirred tank biological reactors. *Chem. Eng. Sci.* **1982**, *37*, 453–462.

16. Bruce, L.J.; Axford, D.B.; Ciszek, B.; Daugulis, A.J. Extractive fermentation by Zymomonas mobilis and the control of oscillatory behavior. *Biotechnol. Lett.* **1991**.

17. Ghommidh, C.; Vaija, J.; Bolarinwa, S.; Navarro, J.M. Oscillatory behaviour of Zymomonas in continuous cultures: A simple stochastic model. *Biotechnol. Lett.* **1989**.

18. Jöbses, I.M.L.; Egberts, G.T.C.; Luyben, K.C.A.M.; Roels, J.A. Fermentation kinetics of Zymomonas mobilis at high ethanol concentrations: Oscillations in continuous cultures. *Biotechnol. Bioeng.* **1986**.

19. Lee, K.J.; Skotnicki, M.L.; Tribe, D.E.; Rogers, P.L. Kinetic studies on a highly productive strain of Zymomonas mobilis. *Biotechnol. Lett.* **1980**.

20. Daugulis, A.J.; McLellan, P.J.; Li, J. Experimental investigation and modeling of oscillatory behavior in the continuous culture ofZymomonas mobilis. *Biotechnol. Bioeng.* **1997**, *56*, 99–105.

21. Skupin, P.; Metzger, M. Oscillatory behavior control in continuous fermentation processes. *IFAC-PapersOnLine* **2015**, *28*, 1114–1119.

22. Castelló, E.; Nunes Ferraz-Junior, A.D.; Andreani, C.; Anzola-Rojas, M. del P.; Borzacconi, L.; Buitrón, G.; Carrillo-Reyes, J.; Gomes, S.D.; Maintinguer, S.I.; Moreno-Andrade, I.; et al. Stability problems in the hydrogen production by dark fermentation: Possible causes and solutions. *Renew. Sustain. Energy Rev.* **2020**, *119*.

23. Garhyan, P.; Elnashaie, S.S.E.H.; Al-Haddad, S.M.; Ibrahim, G.; Elshishini, S.S. Exploration and exploitation of bifurcation/chaotic behavior of a continuous fermentor for the production of ethanol. *Chem. Eng. Sci.* **2003**, *58*, 1479–1496.

24. Abashar, M.E.E. Global bifurcation analysis of two-phase systems in continuous stirred tank reactors. *Kuwait J. Sci. Eng.* **2004**.

25. Abashar, M.E.E.; Elnashaie, S.S.E.H. Dynamic and chaotic behavior of periodically forced fermentors for bioethanol production. *Chem. Eng. Sci.* **2010**, *65*, 4894–4905.

26. Skupin, P.; Metzger, M. Stability analysis of the continuous ethanol fermentation process with a delayed product inhibition. *Appl. Math. Model.* **2017**, *49*, 48–58.

27. Cocaign-Bousquet, M.; Lindley, N.D. Pyruvate overflow and carbon flux within the central metabolic pathways of Corynebacterium glutamicum during growth on lactate. *Enzyme Microb. Technol.* **1995**.

28. Fiechter, A.; Seghezzi, W. Regulation of glucose metabolism in growing yeast cells. *J. Biotechnol.* 1992.

29. Streekstra, H.; Teixeira de Mattos, M.J.; Neijssel, O.M.; Tempest, D.W. Overflow metabolism during anaerobic growth of Klebsiella aerogenes NCTC 418 on glycerol and dihydroxyacetone in chemostat culture. *Arch. Microbiol.* **1987**.

30. Van Urk, H.; Mark, P.R.; Scheffers, W.A.; Van Dijken, J.P. Metabolic responses of Saccharomyces cerevisiae CBS 8066 and Candida utilis CBS 621 upon transition from glucose limitation to glucose excess. *Yeast* **1988**.

31. Zeng, A.P.; Deckwer, W.D. A model for multiproduct-inhibited growth of Enterobacter aerogenes in 2,3-butanediol fermentation. *Appl. Microbiol. Biotechnol.* **1991**.

32. Menzel, K.; Zeng, A.P.; Biebl, H.; Deckwer, W.D. Kinetic, dynamic, and pathway studies of glycerol metabolism by Klebsiella pneumoniae in anaerobic continuous culture: I. The phenomena and characterization of oscillation and hysteresis. *Biotechnol. Bioeng.* **1996**.

33. Lorencez, I. Puhar, E. Guerra, L. H. Fiechter, A. Modling with Product and Substrate Inhibition, and Stability Analysis for Growth of Methylomkonas clara : Growth of Methylomonas clara (II) :

J. Ferment. Technol. **1982**, *60*, 327–332.

34. Axelsson, J.P.; Munch, T.; Sonnleitner, B. Multiple steady states in continuous cultivation of yeast. In Proceedings of the IFAC Symposia Series; 1992.

35. Chung, J.D.; Stephanopoulos, G. On physiological multiplicity and population heterogeneity of biological systems. *Chem. Eng. Sci.* **1996**.

36. Bertucco, A.; Volpe, P.; Klei, H.E.; Anderson, T.F.; Sundstrom, D.W. The stability of activated sludge reactors with substrate inhibition kinetics and solids recycle. *Water Res.* **1990**, *24*, 169–176.

37. Ajbar, A.; Alhumaizi, K. Biodegradation of substitutable substrates in a continuous bioreactor with cell recycle: A study of static bifurcation. *Math. Comput. Model.* **2000**, *31*, 159–174.

38. Ajbar, A. Stability analysis of the biodegradation of mixed wastes in a continuous bioreactor with cell recycle. *Water Res.* **2001**, *35*, 1201–1208.

39. Ajbar, A.; AlAhmad, M.; Ali, E. On the dynamics of biodegradation of wastewater in aerated continuous bioreactors. *Math. Comput. Model.* **2011**, *54*, 1930–1942.

40. Amend, A.S.; Oliver, T.A.; Amaral-Zettler, L.A.; Boetius, A.; Fuhrman, J.A.; Horner-Devine, M.C.; Huse, S.M.; Welch, D.B.M.; Martiny, A.C.; Ramette, A.; et al. Macroecological patterns of marine bacteria on a global scale. *J. Biogeogr.* **2013**.

41. Lennon, J.T.; Jones, S.E. Microbial seed banks: The ecological and evolutionary implications of dormancy. *Nat. Rev. Microbiol.* 2011.

42. Zhalnina, K.; Dias, R.; de Quadros, P.D.; Davis-Richardson, A.; Camargo, F.A.O.; Clark, I.M.; McGrath, S.P.; Hirsch, P.R.; Triplett, E.W. Soil pH Determines Microbial Diversity and Composition in the Park Grass Experiment. *Microb. Ecol.* **2014**.

43. Bethke, C.M.; Sanford, R.A.; Kirk, M.F.; Jin, Q.; Flynn, T.M. The thermodynamic ladder in geomicrobiology. *Am. J. Sci.* **2011**.

44. Kemmitt, S.J.; Wright, D.; Goulding, K.W.T.; Jones, D.L. pH regulation of carbon and nitrogen dynamics in two agricultural soils. *Soil Biol. Biochem.* **2006**.

45. van Vuuren, H.J.J.; Meyer, L. Production of ethanol from sugar cane molasses by Zymomonas mobilis. *Biotechnol. Lett.* **1982**, *4*, 253–256.

46. Bajpai, P.K.; Margaritis, A. Effect of temperature and pH on immobilizedZymomonas mobilis for continuous production of ethanol. *Biotechnol. Bioeng.* **1986**, *28*, 824–828.

47. Lawford, H.; Holloway, P.; Ruggiero, A. Effect of pH on growth and ethanol production byZymomonas. *Biotechnol. Lett.* **1988**, *10*, 809–814.

48. Madi, N.S.; McNeil, B.; Harvey, L.M. Influence of Culture pH and Aeration on Ethanol Production and Pullulan Molecular Weight by Aureobasidium pullulans. *J. Chem. Technol. Biotechnol.* **1996**, *65*, 343–350.

49. Graves, T.; Narendranath, N. V.; Dawson, K.; Power, R. Effect of pH and lactic or acetic acid on ethanol productivity by Saccharomyces cerevisiae in corn mash. *J. Ind. Microbiol. Biotechnol.* **2006**, *33*, 469–474.

50. Kundiyana, D.K.; Bellmer, D.D.; Huhnke, R.L.; Wilkins, M.R.; Claypool, P.L. Influence of

temperature, pH and yeast on in-field production of ethanol from unsterilized sweet sorghum juice. *Biomass and Bioenergy* **2010**, *34*, 1481–1486.

51. Zhang, C.-M.; Jiang, L.; Mao, Z.-G.; Zhang, J.-H.; Tang, L. Effects of Propionic Acid and pH on Ethanol Fermentation by Saccharomyces cerevisiae in Cassava Mash. *Appl. Biochem. Biotechnol.* **2011**, *165*, 883–891.

52. Munasinghe, P.C.; Khanal, S.K. Biomass-derived syngas fermentation into biofuels: Opportunities and challenges. *Bioresour. Technol.* 2010.

53. Mohammadi, M.; Younesi, H.; Najafpour, G.; Mohamed, A.R. Sustainable ethanol fermentation from synthesis gas by Clostridium ljungdahlii in a continuous stirred tank bioreactor. *J. Chem. Technol. Biotechnol.* **2012**, *87*, 837–843.

54. Kennes, C.; Rene, E.R.; Veiga, M.C. Bioprocesses for air pollution control. *J. Chem. Technol. Biotechnol.* 2009.

55. Abubackar, H.N.; Veiga, M.C.; Kennes, C. Biological conversion of carbon monoxide: Rich syngas or waste gases to bioethanol. *Biofuels, Bioprod. Biorefining* 2011.

56. Abubackar, H.N.; Veiga, M.C.; Kennes, C. the bioconversion of carbon monoxide to ethanol and acetic acid by Clostridium autoethanogenum: *Bioresour. Technol.* **2012**, *114*, 518–522.

57. Cotter, J.L.; Chinn, M.S.; Grunden, A.M. Medium optimization for ethanol production with Clostridium autoethanogenum with carbon monoxide as sole carbon source. *Enzyme Microb. Technol.* **2009**.

58. Guo, Y.; Xu, J.; Zhang, Y.; Xu, H.; Yuan, Z.; Li, D. Medium optimization for ethanol production with Clostridium autoethanogenum with carbon monoxide as sole carbon source. *Bioresour. Technol.* **2010**.

59. Khanal, S.K.; Chen, W.H.; Li, L.; Sung, S. Biological hydrogen production: Effects of pH and intermediate products. *Int. J. Hydrogen Energy* **2004**, *29*, 1123–1131.

60. Hu, Z.H.; Yu, H.Q.; Zhu, R.F. Influence of particle size and pH on anaerobic degradation of cellulose by ruminal microbes. *Int. Biodeterior. Biodegrad.* **2005**.

61. Dinamarca, C.; Bakke, R. Process parameters affecting the sustainability of fermentative hydrogen production: A short-review. *Int. J. Energy Environ.* **2011**, *2*, 1076–1078.

62. Luo, G.; Karakashev, D.; Xie, L.; Zhou, Q.; Angelidaki, I. Long-term effect of inoculum pretreatment on fermentative hydrogen production by repeated batch cultivations: Homoacetogenesis and methanogenesis as competitors to hydrogen production. *Biotechnol. Bioeng.* **2011**.

63. Dabrock, B.; Bahl, H.; Gottschalk, G. Parameters affecting solvent production by Clostridium pasteurianum. *Appl. Environ. Microbiol.* **1992**.

64. Peiris, B.R.H.; Rathnasiri, P.G.; Johansen, J.E.; Kuhn, A.; Bakke, R. ADM1 simulations of hydrogen production. *Water Sci. Technol.* **2006**, *53*, 129–137.

65. Li, C.; Fang, H.H.P. Fermentative hydrogen production from wastewater and solid wastes by mixed cultures. *Crit. Rev. Environ. Sci. Technol.* 2007.

66. Lee, Y.J.; Miyahara, T.; Noike, T. Effect of pH on microbial hydrogen fermentation. *J. Chem. Technol. Biotechnol.* **2002**.

67. Luo, G.; Xie, L.; Zou, Z.; Zhou, Q.; Wang, J.Y. Fermentative hydrogen production from cassava stillage by mixed anaerobic microflora: Effects of temperature and pH. *Appl. Energy* **2010**.

68. De Gioannis, G.; Friargiu, M.; Massi, E.; Muntoni, A.; Polettini, A.; Pomi, R.; Spiga, D. Biohydrogen production from dark fermentation of cheese whey: Influence of pH. *Int. J. Hydrogen Energy* **2014**.

69. Van Ginkel, S.; Logan, B.E. Inhibition of Biohydrogen Production by Undissociated Acetic and Butyric Acids. *Environ. Sci. Technol.* **2005**, *39*, 9351–9356.

70. Guo, X.M.; Trably, E.; Latrille, E.; Carrre, H.; Steyer, J.P. Hydrogen production from agricultural waste by dark fermentation: A review. *Int. J. Hydrogen Energy* **2010**, *35*, 10660–10673.

71. Tang, G.-L.; Huang, J.; Sun, Z.-J.; Tang, Q.-Q.; Yan, C.-H.; Liu, G.-Q. Biohydrogen production from cattle wastewater by enriched anaerobic mixed consortia: Influence of fermentation temperature and pH. *J. Biosci. Bioeng.* **2008**, *106*, 80–87.

72. Angenent, L.T.; Karim, K.; Al-Dahhan, M.H.; Wrenn, B.A.; Domíguez-Espinosa, R. Production of bioenergy and biochemicals from industrial and agricultural wastewater. *Trends Biotechnol.* **2004**, *22*, 477–485.

73. Dong, L.; Zhenhong, Y.; Yongming, S.; Xiaoying, K.; Yu, Z. Hydrogen production characteristics of the organic fraction of municipal solid wastes by anaerobic mixed culture fermentation. *Int. J. Hydrogen Energy* **2009**, *34*, 812–820.

74. Van Niel, E.W.J.; Claassen, P.A.M.; Stams, A.J.M. Substrate and product inhibition of hydrogen production by the extreme thermophile, Caldicellulosiruptor saccharolyticus. *Biotechnol. Bioeng.* **2003**, *81*, 255–262.

75. Logan, B.E.; Oh, S.E.; Kim, I.S.; Van Ginkel, S. Biological hydrogen production measured in batch anaerobic respirometers. *Environ. Sci. Technol.* **2002**, *36*, 2530–2535.

76. Chang, S.; Li, J.; Liu, F.; Yu, Z. Effect of different gas releasing methods on anaerobic fermentative hydrogen production in batch cultures. *Front. Environ. Sci. Eng. China* **2012**, *6*, 901–906.

77. Esquivel-Elizondo, S.; Chairez, I.; Salgado, E.; Aranda, J.S.; Baquerizo, G.; Garcia-Peña, E.I. Controlled Continuous Bio-Hydrogen Production Using Different Biogas Release Strategies. *Appl. Biochem. Biotechnol.* **2014**, *173*, 1737–1751.

78. Oh, S.E.; Zuo, Y.; Zhang, H.; Guiltinan, M.J.; Logan, B.E.; Regan, J.M. Hydrogen production by Clostridium acetobutylicum ATCC 824 and megaplasmid-deficient mutant M5 evaluated using a large headspace volume technique. *Int. J. Hydrogen Energy* **2009**, *34*, 9347–9353.

79. Foglia, D.; Wukovits, W.; Friedl, A.; De Vrije, T.; Claassen, P.A.M. Fermentative hydrogen production: Influence of application of mesophilic and thermophilic bacteria on mass and energy balances. *Chem. Eng. Trans.* **2011**, *25*, 815–820.

80. Nguyen, T.A.D.; Han, S.J.; Kim, J.P.; Kim, M.S.; Sim, S.J. Hydrogen production of the hyperthermophilic eubacterium, Thermotoga neapolitana under N2sparging condition. *Bioresour. Technol.* **2010**, *101*, 38–41.

81. Bru, K.; Blazy, V.; Joulian, C.; Trably, E.; Latrille, E.; Quéméneur, M.; Dictor, M.-C. Innovative CO2 pretreatment for enhancing biohydrogen production from the organic fraction of municipal solid waste (OFMSW). *Int. J. Hydrogen Energy* **2012**, *37*, 14062–14071.

82. Kim, D.H.; Han, S.K.; Kim, S.H.; Shin, H.S. Effect of gas sparging on continuous fermentative hydrogen production. *Int. J. Hydrogen Energy* **2006**, *31*, 2158–2169.

83. Borja, R.; Sánchez, E.; Durán, M.M. Effect of the clay mineral zeolite on ammonia inhibition of anaerobic thermophilic reactors treating cattle manure. *J. Environ. Sci. Heal. - Part A Toxic/Hazardous Subst. Environ. Eng.* **1996**.

84. Beckers, L.; Hiligsman, S.; Masset, J.; Hamilton, C.; Thonart, P. Effects of hydrogen partial pressure on fermentative biohydrogen production by a chemotropic Clostridium bacterium in a new horizontal rotating cylinder reactor. *Energy Procedia* **2012**, *29*, 34–41.

85. Wang, J.; Wan, W. Kinetic models for fermentative hydrogen production: A review. *Int. J. Hydrogen Energy* **2009**, *34*, 3313–3323.

86. Zwietering, M.H.; Jongenburger, I.; Rombouts, F.M.; Van't Riet, K. Modeling of the bacterial growth curve. *Appl. Environ. Microbiol.* **1990**.

87. Wu, J.H.; Lin, C.Y. Biohydrogen production by mesophilic fermentation of food wastewater. *Water Sci. Technol.* **2004**.

88. Chen, C.C.; Lin, C.Y.; Lin, M.C. Acid-base enrichment enhances anaerobic hydrogen production process. *Appl. Microbiol. Biotechnol.* **2002**.

89. Fang, H.H.P.; Li, C.; Zhang, T. Acidophilic biohydrogen production from rice slurry. *Int. J. Hydrogen Energy* **2006**.

90. Cheong, D.Y.; Hansen, C.L. Bacterial stress enrichment enhances anaerobic hydrogen production in cattle manure sludge. *Appl. Microbiol. Biotechnol.* **2006**.

91. Chen, S. Der; Sheu, D.S.; Chen, W.M.; Lo, Y.C.; Huang, T.I.; Lin, C.Y.; Chang, J.S. Dark hydrogen fermentation from hydrolyzed starch treated with recombinant amylase originating from Caldimonas taiwanensis On1. *Biotechnol. Prog.* **2007**.

92. Zhang, T.; Liu, H.; Fang, H.H.P. Biohydrogen production from starch in wastewater under thermophilic condition. *J. Environ. Manage.* **2003**.

93. Lin, C.Y.; Wu, C.C.; Wu, J.H.; Chang, F.Y. Effect of cultivation temperature on fermentative hydrogen production from xylose by a mixed culture. *Biomass and Bioenergy* **2008**.

94. Mu, Y.; Wang, G.; Yu, H.Q. Kinetic modeling of batch hydrogen production process by mixed anaerobic cultures. *Bioresour. Technol.* **2006**.

95. Wang, J.; Wan, W. The effect of substrate concentration on biohydrogen production by using kinetic models. *Sci. China, Ser. B Chem.* **2008**, *51*, 1110–1117.

96. Nath, K.; Muthukumar, M.; Kumar, A.; Das, D. Kinetics of two-stage fermentation process for the production of hydrogen. *Int. J. Hydrogen Energy* **2008**.

97. Zheng, H.; Zeng, R.J.; Angelidaki, I. Biohydrogen production from glucose in upflow biofilm reactors with plastic carriers under extreme thermophilic conditions (700C). *Biotechnol. Bioeng.* **2008**.

98. Majizat, A.; Mitsunori, Y.; Mitsunori, W.; Michimasa, N.; Jun'ichiro, M. Hydrogen gas production from glucose and its microbial kinetics in anaerobic systems. In Proceedings of the Water Science and Technology; 1997.

99. Wang, B.; Wan, W.; Wang, J. Inhibitory effect of ethanol, acetic acid, propionic acid and butyric acid on fermentative hydrogen production. *Int. J. Hydrogen Energy* **2008**, *33*, 7013–7019.

100. Wang, Y.; Zhao, Q.-B.; Mu, Y.; Yu, H.-Q.; Harada, H.; Li, Y.-Y. Biohydrogen production with mixed anaerobic cultures in the presence of high-concentration acetate. *Int. J. Hydrogen Energy* **2008**, *33*, 1164–1171.

101. Liu, X.; Zhu, Y.; Yang, S.T. Construction and characterization of ack deleted mutant of Clostridium tyrobutyricum for enhanced butyric acid and hydrogen production. *Biotechnol. Prog.* **2006**.

102. Mu, Y.; Yu, H.Q.; Wang, G. A kinetic approach to anaerobic hydrogen-producing process. *Water Res.* **2007**.

103. Andreyeva, L.N.; Biryukov, V. V. Analysis of mathematical models of the effect of pH on fermentation processes and their use for calculating optimal fermentation conditions. *Biotechnol. Bioeng. Symp.* **1973**.

104. Lallai, A.; Mura, G.; Miliddi, R.; Mastinu, C. Effect of pH on growth of mixed cultures in batch reactor. *Biotechnol. Bioeng.* **1988**.

105. Giles, W.; Bisits, A.; Knox, M.; Madsen, G.; Smith, R. Kinetics of hydrogen production with continuous anaerobic cultures utilizing sucrose as the limiting substrate. *Appl. Microbiol. Biotechnol.* **2001**, *57*, 56–64.

106. Whang, L.M.; Hsiao, C.J.; Cheng, S.S. A dual-substrate steady-state model for biological hydrogen production in an anaerobic hydrogen fermentation process. *Biotechnol. Bioeng.* **2006**.

107. Chang, F.Y.; Lin, C.Y. Biohydrogen production using an up-flow anaerobic sludge blanket reactor. *Int. J. Hydrogen Energy* **2004**.

108. Lay, J.J. Biohydrogen generation by mesophilic anaerobic fermentation of microcrystalline cellulose. *Biotechnol. Bioeng.* **2001**.

109. Van Niel, E.W.J.; Budde, M.A.W.; De Haas, G.; Van der Wal, F.J.; Claassen, P.A.M.; Stams, A.J.M. Distinctive properties of high hydrogen producing extreme thermophiles, Caldicellulosiruptor saccharolyticus and Thermotoga elfii. In Proceedings of the International Journal of Hydrogen Energy; 2002.

110. Shuler, M.L.; Kargi, F. Bioprocess Engineering Basic Concepts Second Edition. *Adv. Chem. Eng.* **1991**.

111. Han, K.; Levenspiel, O. Extended monod kinetics for substrate, product, and cell inhibition. *Biotechnol. Bioeng.* **1988**, *32*, 430–447.

112. Bhattacharya, I.; Chakraborty, R.; Chowdhury, R. Intensification of Freeze-Drying Rate of Bacillus subtilis MTCC 2396 Using Tungsten Halogen Radiation: Optimization of Moisture Content and α-Amylase Activity. *Dry. Technol.* **2014**, *32*, 801–812.

113. Miller, G.L. Use of Dinitrosalicylic Acid Reagent for Determination of Reducing Sugar. *Anal. Chem.* **1959**.

114. Das, S.; Calay, R.K.; Chowdhury, R.; Nath, K.; Eregno, F.E. Product Inhibition of Biological Hydrogen Production in Batch Reactors. *Energies* **2020**, *13*, 1318.

115. Das, S.; Banerjee, A.; Chowdhury, R.; Bhattacharya, P.; Calay, R.K. Parametric sensitivity of

pH and steady state multiplicity in a continuous stirred tank bioreactor (CSTBR) using a lactic acid bacterium (LAB), Pediococcus acidilactici. *J. Chem. Technol. Biotechnol.* **2016**, *91*, 1431–1442.

116. Po, H.N.; Senozan, N.M. The Henderson-Hasselbalch equation: Its history and limitations. *J. Chem. Educ.* **2001**.

117. Parada, J.L.; Caron, C.R.; Medeiros, A.B.P.; Soccol, C.R. Bacteriocins from lactic acid bacteria: Purification, properties and use as biopreservatives. *Brazilian Arch. Biol. Technol.* **2007**.

118. De Vuyst, L.; Leroy, F. Bacteriocins from lactic acid bacteria: Production, purification, and food applications. In Proceedings of the Journal of Molecular Microbiology and Biotechnology; 2007.

119. Kauschus, W.; Demont, J.; Hartmann, K. On the steady states of continuous stirred tank reactors. *Chem. Eng. Sci.* **1978**, *33*, 1283–1285.

120. Guerra, N.P.; Pastrana, L. Modelling the influence of pH on the kinetics of both nisin and pediocin production and characterization of their functional properties. *Process Biochem.* **2002**.

121. Guerra, N.P.; Agrasar, A.T.; Macías, C.L.; Bernárdez, P.F.; Castro, L.P. Dynamic mathematical models to describe the growth and nisin production by Lactococcus lactis subsp. lactis CECT 539 in both batch and re-alkalized fed-batch cultures. *J. Food Eng.* **2007**.

122. Morbidelli, M.; Varma, A. A generalized criterion for parametric sensitivity: application to a pseudohomogeneous tubular reactor with consecutive or parallel reactions. *Chem. Eng. Sci.* **1989**, *44*, 1675–1696.

123. Morbidelli, M.; Varma, A. A generalized criterion for parametric sensitivity: Application to thermal explosion theory. *Chem. Eng. Sci.* **1988**, *43*, 91–102.

124. Dutta, S.; Chowdhury, R.; Bhattacharya, P. Parametric sensitivity in bioreactor: an analysis with reference to phenol degradation system. *Chem. Eng. Sci.* **2001**, *56*, 5103–5110.

Appendix 1

List of published articles relevant to the thesis

Paper 1

Parametric sensitivity of pH and steady statemultiplicity in a continuous stirred tankbioreactor (CSTBR) using a lactic acidbacterium (LAB), *Pediococcus acidilactici*

Subhashis Das, Rajnish Kaur Calay, Aritro Banerjee, Ranjana Chowdhury and Pinaki Bhattacharya

Journal of Chemical Technology and Biotechnology. Vol 91, Issue 5 pp 1431, 2016

Research Article

Received: 28 April 2015 Revised: 25 May 2015 Accepted article published: 1 June 2015 Published online in Wiley Online Library: 22 June 2015

(wileyonlinelibrary.com) DOI 10.1002/jctb.4740

Parametric sensitivity of pH and steady state multiplicity in a continuous stirred tank bioreactor (CSTBR) using a lactic acid bacterium (LAB), *Pediococcus acidilactici*

Subhashis Das,[a] Aritro Banerjee,[a] Ranjana Chowdhury,[a*] Pinaki Bhattacharya[b] and Rajnish Kaur Calay[c]

Abstract

BACKGROUND: A continuous stirred tank bioreactor (CSTBR) represents an open dynamic system with high probability to show nonlinear behavior such as parametric sensitivity and multiplicity of steady state. *A priori* determination of this behavior is needed to decide on the strategy of reactor operation.

RESULTS: The growth of a lactic acid bacterium, namely, *Pediococcus acidilactici* in a 2 L CSTBR is used to demonstrate the existence of parametric sensitivity of pH and the multiplicity of steady state in the system. A mathematical model has been developed and a dimensionless multiplicity criterion, ω, has been derived to indicate the set of values of input parameters corresponding to multiple steady states. Experiments have been conducted to study parametric sensitivity of pH with respect to input variables, namely, dilution rates and concentrations of nutrient and alkali stream for pH control in the regions of multiple and unique steady states. The CSTBR exhibited parametric sensitivity of pH over the entire region of operation under study. The experimental trends of parametric sensitivity of pH are also in agreement with those of theoretical parametric sensitivity of pH.

CONCLUSION: The nonlinear behavior of a CSTBR has been thoroughly portrayed in this article. The present study will add to the knowledge of control and operational strategies of CSTBRs.
© 2015 Society of Chemical Industry

Supporting information may be found in the online version of this article.

Keywords: bioreactors; control; dynamics; mathematical modelling

NOTATION

A, B, C	constant used in Equation (2)
D	dilution rate of substrate feed stream (h^{-1})
D_1	dilution rate of base stream (h^{-1})
J	Jacobian matrix
K_a	equilibrium dissociation constant for lactic acid
K_S	substrate saturation constant ($g\ L^{-1}$)
M_a	molecular weight of lactic acid ($g\ mol^{-1}$)
M_b	molecular weight of sodium hydroxide (NaOH) ($g\ mol^{-1}$)
M_c	molecular weight of sodium lactate acid ($g\ mol^{-1}$)
p	product concentration ($mol\ L^{-1}$)
s_A	concentration of sodium lactate ($mol\ L^{-1}$)
s_b	concentration of base (NaOH) ($mol\ L^{-1}$)
S	substrate concentration ($g\ L^{-1}$)
S_0	initial substrate concentration ($g\ L^{-1}$)
$S_{\phi i}$	sensitivity function
t	time (h)
X	concentration of microorganism ($g\ L^{-1}$)
$Y_{X/S}$	yield coefficient of biomass to substrate ($g\ g^{-1}$)
$Y_{p/X}$	yield coefficient of product to biomass ($g\ g^{-1}$)
$Y_{p/S}$	yield coefficient of product to substrate ($g\ g^{-1}$)
μ	specific growth rate (h^{-1})
Φ	vector

Dimensionless variables

$x = \frac{X}{S_0 Y_{X/S}}$	concentration of microorganism
$y = \frac{S}{S_0}$	substrate concentration
$z = \frac{pM_a}{S_0 Y_{p/S}}$	product concentration
$L = \frac{s_A M_c}{S_0}$	concentration of sodium lactate
$R = \frac{s_b M_b}{S_0}$	concentration of base (NaOH)
$\theta = \frac{\mu}{D}$	specific growth rate of microorganisms

* Correspondence to: Ranjana Chowdhury, Professor, Department of Chemical Engineering, Jadavpur University, India. E-mail: ranjana.juchem@gmail.com

a Department of Chemical Engineering, Jadavpur University, Kolkata 700032, India

b Department of Chemical Engineering, Heritage Institute of Technology, Kolkata 700107, India

c Department of Technology, Narvik University College, Lodve Langes gt. 2, P.O. Box 385, 8505 Narvik, Norway

 © 2015 Society of Chemical Industry

$\theta_1 = \frac{D_1}{D}$ dilution rate of base stream
$m = \frac{\mu_m}{D}$ maximum specific growth rate
$n = \frac{K_S}{S_0}$ substrate saturation constant
$\tau = tD$ time

Subscripts

max maximum
opt optimum
app apparent

INTRODUCTION

Industrially significant bioprocesses are complex and are sensitive to disturbances in process parameters. Previous investigators have shown that sensitivities of bioreactors are dependent on operating conditions.[1–5] This is particularly true for continuous stirred tank bioreactors (CSTBRs) which are actually open dynamic systems. In spite of this fact, CSTBRs are the most extensively used reactors for continuous production of products in large quantities due to their high flexibility. Due to open dynamics and nonlinear nature of growth kinetics of microbes, CSTBRs are susceptible to multiplicity of steady states and parametric sensitivity. Although studies on multiplicity and parametric sensitivity of non-isothermal and non-adiabatic CSTRs[6–18] are well advanced and it is now possible to predict *a priori* the criteria of runaway condition of conventional chemical reactors, more research studies are required for bioreactors, CSTBRs in particular.

The slow progress of research on revealing non-linear dynamics of bioreactors may be mainly due to the fact that the mechanisms behind the growth of microorganisms and generation of metabolic products, and their correlation with conditions of operating variables are not well understood in many cases. It is well known that one of the most important output variables in bioreactors is the system pH. When a product generated in the reactor is either an acid or a base, it alters the pH. Parametrically sensitive behavior of pH, i.e. a large change in pH in response to a small perturbation in one or more of the input variables is likely to occur. In a CSTBR, pH is usually controlled by the streams of either base or acid. Analogous to thermal runaway in an exothermic reaction, pH may become extremely sensitive and uncontrollable. Since the pH-sensitive microorganisms cease to grow beyond a particular range of pH the CSTBR becomes vulnerable to destabilize and this may be termed a pH runaway condition of bioreactors.

In the literature, a few pioneering research studies have been reported on sensitivity analysis of product yields in enzymatic and microbial CSTBRs.[19,20] Comparatively more studies have been focused on multiplicity of steady states in CSTBRs and batch type stirred tank reactors.[1,2,21,22] These studies are mainly concerned with the occurrence of multiplicity of steady states with respect to product generation in CSTBRs and other bioreactors. However, from the literature review it is clear that information on the parametric sensitivity of pH in bioreactors is scarce. Dutta *et al.*[21] analyzed the parametric sensitivity of pH in batch reactors using phenol degrading bacteria by applying generalized sensitivity criterion proposed by Mobidelli and Verma.[15,16,23] However, effort should also be made to investigate the parametric sensitivity of pH in CSTBRs. During studies on nth order irreversible exothermic reactions in a non-adiabatic CSTR, Chemburkar *et al.*[24] showed that there exists a distinct relationship between parametric sensitivity of temperature and multiplicity of steady states. However, no such article dealing simultaneously with both parametric sensitivity of pH and multiplicity of steady states in CSTBRs is currently available. Since *a priori* determination of both phenomena, i.e. parametric sensitivity and multiplicity may save the CSTBRs from 'out of control situations', such studies are also required for bioreactors. The experimental verifications of parametric sensitivity in both multiple and unique steady regions is also lacking for CSTBRs. Continuous stirred tank bioreactors using lactic acid bacteria (LAB) may serve as an important and interesting system from the perspective of studies on parametric sensitivity of pH and multiplicity of steady states. There is an antagonistic relationship between the generation of lactic acid and growth of LABs. The growth rates of many LABs decrease as pH is lowered due to formation of lactic acid. Since LAB cultures are gaining increased popularity for their probiotic nature (i.e. antimicrobial activity against pathogen), it is essential to have expert knowledge on pH sensitivity as well as on the presence of multiplicity of steady states in CSTBRs using LABs.

Motivated by the research gap discussed above, the present article intends to study the parametric sensitivity of system pH and multiplicity of steady states of a CSTBR meant for the production of the anti-pathogenic bacteriocin called pediocin from the LAB, *Pediococcus acidilactici*. The present work has three objectives: one is to derive a simple dimensionless steady state multiplicity criterion for the CSTBR following the technique adopted by Kauschus *et al.*[25] in connection with adiabatic CSTR operation. This requires fundamental knowledge on the kinetic parameters of microbial growth including their dependence on pH and subsequent development of an unstructured mathematical model using dimensionless variables. The criterion should be able to identify the set of values of input variables which lead to multiple steady states. The second objective of the paper is to derive an expression for theoretical sensitivity functions of pH with respect to different input variables, namely dilution rates of nutrient and base streams and concentrations of substrate and base stream for pH control. The third objective of the study is to conduct experiments to study the parametric sensitivity for sets of input parameters belonging to the regimes of multiple and unique steady states as determined using multiplicity criterion. The experimental and simulated transient behaviors of pH are also analyzed and compared to verify the existence of parametric sensitivity under both multiple and unique steady state conditions. Studies of this kind have never been conducted for LABs and it is expected that the knowledge-base gained through the holistic approach of a study incorporating both parametric sensitivity and multiplicity of steady states will aid in the selection of strategies for safe, controlled and economic utilization of CSTBRs using LABs.

MATERIALS AND METHODS

Materials

The following materials were used for the present investigation:

Microorganism

Pediococcus acidilactici (NCIM-2292) were procured from NCIM, Pune, India.

Chemicals

Beef extract, peptone, yeast extract, Tween 80, di-potassium hydrogen phosphate, sodium acetate, tri-ammonium citrate, manganese sulphate, magnesium sulphate, glucose, 3,5-dinitro salicylic acid, sodium hydroxide and sodium potassium tartrate were procured from Merck Specialities Private Limited, India.

 © 2015 Society of Chemical Industry

Table 1. MRS composition in 100 mL solution

Components	Amount (g)
Peptone	1.0
Beef extract	0.8
Yeast extract	0.4
Glucose	2.0
Sodium acetate trihydrate	0.5
Polysorbate 80 (also known as Tween 80)	0.1
Dipotassium hydrogen phosphate	0.2
Triammonium citrate	0.2
Magnesium sulfate heptahydrate	0.02
Manganese sulfate tetrahydrate	0.005

Equipments

A BOD incubator shaker (G. B. Enterprises, Kolkata, India), autoclave (G. B. Enterprises, Kolkata, India), centrifuge (Plasto Craft Industries Pvt. Ltd, India), fermenter (B. Braun Biotech International), peristaltic pump (Enertech electronics Pvt. Ltd, india), UV-visible spectrophotometer (Varian. India), Shimadzu Corporation Reverse Phase HPLC (Model no: CBM-Ro A) and pH meter (Sartorious, PB-11) were used.

Methods

Batch mode experiments

The bacterial strain was maintained in de Man, Rogosa and Sharpe (MRS) medium. The composition of MRS medium is provided in Table 1. The growth kinetics of *Pediococcus acidilactici* were determined by conducting batch experiments in Erlenmeyer flasks using 50 mL modified MRS (MMRS) medium. The temperature was maintained at the optimum value of 37°C. Initial pH was varied in the range 4.0–8.0. At each initial pH experiments were conducted by varying initial glucose concentration of MMRS medium in the range 5.0–30.0 g L^{-1}. The concentrations of all components other than glucose in MMRS medium were always same as those of the MRS medium. At each initial substrate concentration the microbial growth pattern was studied for 24 h. Samples were withdrawn at 2 h intervals during incubation. The biomass concentration of each sample was determined using a spectrophotometric method[26] and glucose concentration was determined using the DNS method.[27] Each sample was centrifuged at 10000 rpm and the supernatant was analyzed for lactic acid using HPLC.

Determination of growth kinetics

The growth kinetics of *Pediococcus acidilactici* were determined using a classical Monod type growth model. The kinetic parameters of the Monod model were determined using the initial specific growth rate at each initial glucose concentration obtained at each initial pH (pH = 4, 5, 6, 7, 8). The Monod equation is as follows:

$$\mu = \frac{\mu_{max} S}{K_S + S} \tag{1}$$

By making double reciprocal plots of μ versus S (not shown), the values of μ_{max} and K_s at each pH were determined. From analysis of the results, it appears that although K_s remains constant for all pH, the value of μ_{max} varies with pH and is maximum at pH = 6.7. This may be considered the optimum pH. The values of $\mu_{max,opt}$ and K_s are provided in Table 2.The values of normalized μ_{max} i.e. $\mu_{max,N}$ are plotted in Fig. 1 as a function of initial pH and a second-order correlation was obtained as follows:

Table 2. Values of kinetic parameters

Kinetic parameter	Value
$\mu_{max,opt}$ (h^{-1})	1.0775
K_S(g L^{-1})	4.5017
$Y_{X/S}$ (g g^{-1})	0.1
$Y_{p/X}$ (g g^{-1})	0.065
$Y_{p/S}$ (g g^{-1})	0.0065
A	−3.76195
B	1.4368
C	−0.10835

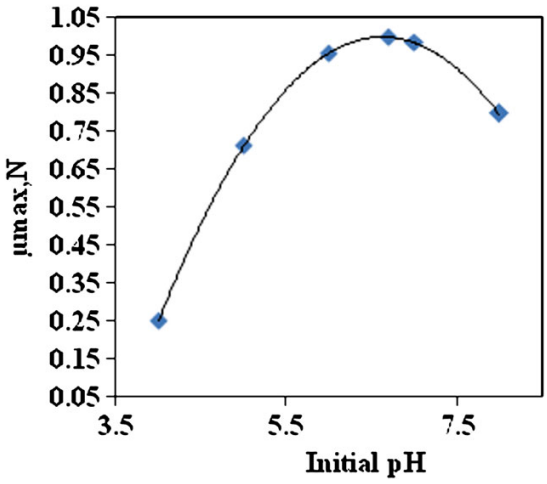

Figure 1. Variation of normalized $\mu_{max,N}$ with initial pH.

$$\mu_{max,N} = A + BpH + CpH^2 \tag{2}$$

where

$$\mu_{max,N} = \frac{\mu_{max}}{\mu_{max,opt}} \tag{3}$$

therefore, Equation (1) reduces to

$$\mu = \frac{\mu_{max,opt}\left(A + BpH + CpH^2\right) S}{K_S + S} \tag{4}$$

The correlation is similar to that obtained by Lallai *et al.*[28] and Datta *et al.*[21] The values of A, B and C are also provided in Table 2.

Reactor setup

Experiments were conducted in a 2 L B. Braun bioreactor. The volume of the growth medium in the bioreactor was kept at 1 L, initial pH was kept at the optimum value of 6.7 and the system temperature was maintained constant at 37°C. Using a peristaltic pump, the bioreactor was fed continuously with sterile modified MRS (MMRS) medium. An alkaline (NaOH) stream was fed to the reactor continuously to maintain the optimum pH. The flow-sheet of the reactor set up is shown in Fig. 2. Based on the multiplicity criterion defined in the theoretical analysis section, the flow rate and glucose concentration of the MMRS feed stream and the inlet

 © 2015 Society of Chemical Industry

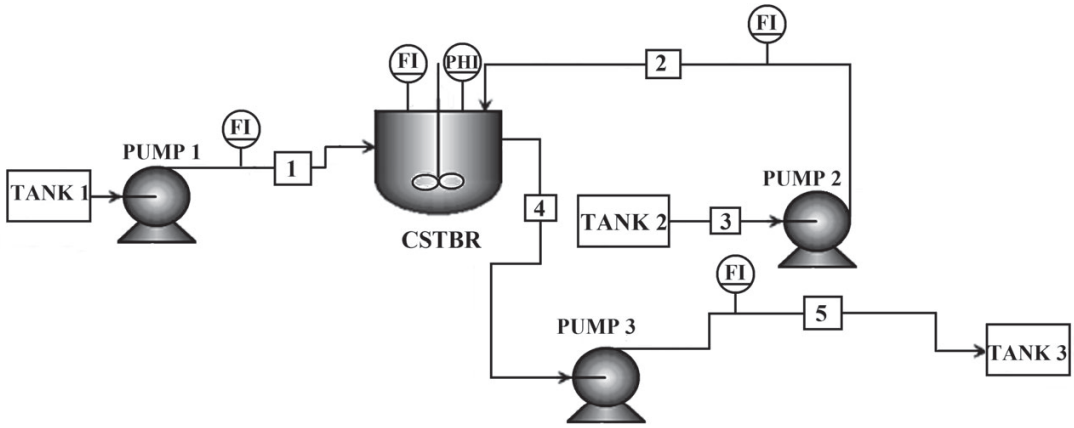

TANK 1: Feed tank, TANK 2: Base dosing tank, TANK 3: Effluent tank, FI: Rotameter, PHI: pH

Figure 2. Experimental set up.

flow rate and strength of the alkaline stream were selected, so that sensitivity may be analyzed in the regions showing uniqueness and multiplicity of steady state. Bioreactor samples were analyzed for biomass concentration and lactic acid. The pH was recorded continuously.

MATHEMATICAL ANALYSIS

Reactions

The biochemical reaction occurring in the system may be represented as follows:

$$X + \text{Glucose} \rightarrow nX + CH_3CH(OH)COOH\ (\text{Lactic acid}) + \text{Pediocin} \quad (5)$$

The desired product is pediocin and its formation is influenced by the system pH.[32] To control pH, NaOH was fed to the system. The acid-base neutralization reaction may be written as follows,

$$CH_3CH(OH)COOH + NaOH \rightarrow CH_3CH(OH)COONa + H_2O \quad (6)$$

The pH is correlated with the concentrations of salt and lactic acid according to the Henderson-Hasselbalch equation[29] as follows

$$pH = pK_a + \log \frac{s_A}{p} \quad (7)$$

where K_a = equilibrium dissociation constant for lactic acid, s_A and p are molar concentrations of sodium lactate and lactic acid, respectively.

Mathematical model

The continuous bioreactor set-up is represented schematically in Fig. 3. The mathematical model for the CSTBR was developed using the following assumptions:

1. The bioreactor is stirred uniformly, i.e. concentration within the reactor is spatially uniform.
2. Temperature effect of the reaction is negligible.

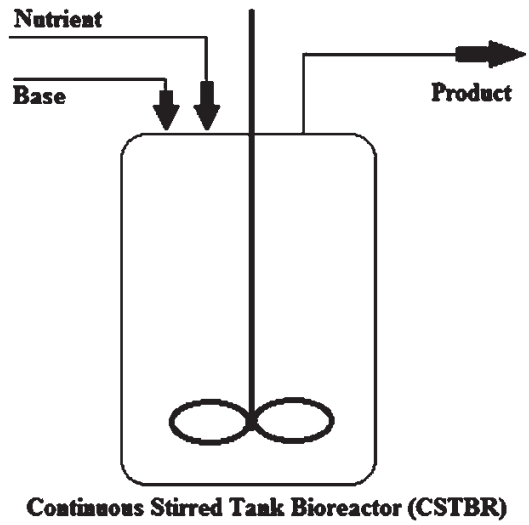

Figure 3. Schematic diagram of the CSTBR.

The differential mass and mole balance equations for different components, namely biomass, substrate, lactic acid and sodium lactate are as follows:

Mass balance equations:

Biomass:

$$\frac{dX}{dt} = (\mu - D - D_1)X \quad (8)$$

Substrate:

$$\frac{dS}{dt} = D(S_0 - S) - D_1 S - \frac{1}{Y_{X/S}}\mu X \quad (9)$$

Mole balance equations:

Lactic acid:

$$\frac{dp}{dt} = -Dp + \frac{Y_{P/X}\mu X}{M_a} - D_1(s_b + p) \quad (10)$$

 © 2015 Society of Chemical Industry

Sodium lactate:

$$\frac{ds_A}{dt} = D_1\left(s_b - s_A\right) - Ds_A \tag{11}$$

pH dynamics:
Differentiating Equation (7), with respect to time,

$$\frac{dpH}{dt} = \frac{1}{s_A}\frac{ds_A}{dt} - \frac{1}{p}\frac{dp}{dt} \tag{12}$$

The values of K_a, $Y_{X/S}$, $Y_{p/X}$ are provided in Table 2.

Since bacteriocin is a growth related product,[30,31] influence of the sensitivity of pH towards formation of bacteriocin is expected to be similar to that of biomass. For simplicity of the model, mass balance of bacteriocin has been excluded from the mathematical analysis.

Generalized criterion for multiplicity

In dimensionless form, the system Equations (8) to (12) may be written as follows:

$$\frac{dx}{d\tau} = \left(\theta - \theta_1 - 1\right)x \tag{13}$$

$$\frac{dy}{d\tau} = (1 - y) - \theta x - \theta_1 y \tag{14}$$

$$\frac{dz}{d\tau} = -z + \theta x - \theta_1\left(\frac{M_a}{M_b Y_{p/s}}R + z\right) \tag{15}$$

$$\frac{dL}{d\tau} = \left(\frac{M_c}{M_b}R - L\right)\theta_1 - L \tag{16}$$

$$\frac{dpH}{d\tau} = \frac{1}{L}\frac{dL}{d\tau} - \frac{1}{z}\frac{dz}{d\tau} \tag{17}$$

and

$$\theta = \frac{my}{n + y}H \tag{18}$$

where
$x = \frac{X}{S_0 Y_{X/S}}; y = \frac{S}{S_0}; z = \frac{pM_a}{S_0 Y_{p/s}}; R = \frac{s_b M_b}{S_0}; L = \frac{s_A M_c}{S_0}; \tau = tD; \theta = \frac{\mu}{D}; \theta_1 = \frac{D_1}{D}; m = \frac{\mu_m}{D}; n = \frac{K_S}{S_0}$
and

$$H = A + BpH + CpH^2 \tag{19}$$

At steady-state, the left-hand sides of Equations (13)–(17) become zero. After further mathematical operations the following condition with respect to pH is obtained:

$$\ln\left(\alpha + \beta pH + \gamma pH^2\right) = -\frac{pH}{2.303} \tag{20}$$

where
$\alpha = \left(M + n(1 + mMA) - p_m\right)\frac{K_a}{p_m}$, $\beta = (nmMB)\frac{K_a}{p_m}$ and $\gamma = (nmMC)\frac{K_a}{p_m}$

Details of the mathematical operations are provided in the Supplementary material. Equation (20) may be represented in the following form:

$$f(pH, \alpha, \beta, \gamma) = \ln\left(\alpha + \beta pH + \gamma pH^2\right) + \frac{pH}{2.303} = 0 \tag{21}$$

The multiplicity of solutions of the transcendental Equation (21) is dependent only on the values of α, β and γ. The number of solution is obtained as the number of intersecting points of function f (pH α β and γ) with the abscissa of pH–f system of coordinate. This may be obtained by setting

$$\frac{\partial f}{\partial pH} = 0 \tag{22}$$

This leads to the following roots

$$pH_{1/2} = \frac{4.606\gamma + \beta}{2\gamma}\left(-1 \pm \sqrt{1 - \omega}\right) \tag{23}$$

where

$$\omega = \frac{4\gamma(2.303\beta + \alpha)}{(4.606\gamma + \beta)^2} \tag{24}$$

For higher value of ω (>1), the radicand in Equation (24) is negative. Using the same principles, as cited by Kauschus *et al.*,[25] one steady-state at the most is obtainable for $\omega \geq 1$ and more than one steady states are possible for $\omega < 1$. Therefore, it is understandable that the nature of steady states is extremely influenced by ω and hence the values of α, β and γ.

Theoretical parametric sensitivity analysis

The parametric sensitivity analysis is done on the basis of the differential Equations (8)–(12).

The generalized form of the model equations is as follows:

$$\frac{\mathbf{dy}}{\mathbf{dx}} = F(x, \mathbf{y}, \phi) \tag{25}$$

where, y is a vector of dependent variables. In the present investigation 'y' may be concentrations of biomass, substrate, product and salt, **x** is an independent variable namely time, and ϕ represents the vector of input parameters of the system.

The first order local sensitivity or simply local sensitivity with respect to vector ϕ is given by,

$$s_{j\phi_i} = \frac{d\mathbf{y}_j\left(t, \phi_i\right)}{d\phi_i} \tag{26}$$

j = any output variable
i = any input vector

By differentiating Equation (26), the following equation, is obtained

$$\frac{ds_{\phi_i}}{dt} = Js_{\phi_i} + \frac{\partial F\left(t, \mathbf{y}, \phi_i\right)}{\partial \phi_i} \tag{27}$$

where J is the Jacobian matrix of the system. The initial conditions for the above Equation (27) is, $s_{\phi i} = 0$ at $t = 0$. For the CSTBR under consideration,

$y_1 = X$, $y_2 = S$, $y_3 = p$, $y_4 = s_A$, $y_5 = \text{pH}$, $\phi_1 = D$, $\phi_2 = D_1$, $\phi_3 = s_b$, $\phi_4 = S_0$, $F_1 = dX/dt$, $F_2 = dS/dt$, $F_3 = dp/dt$, $F_4 = ds_A/dt$ and $F_5 = dpH/dt$

The dynamic equations for the parametric sensitivity in a CSTBR for any variable y_i becomes,

$$\frac{d}{dt}\left[s_{j\phi i}\right] = \left[\frac{\partial F_j}{\partial X}\frac{\partial F_j}{\partial S}\frac{\partial F_j}{\partial p}\frac{\partial F_j}{\partial s_A}\frac{\partial F_j}{\partial pH}\right]\left[\frac{dX}{d\phi_i}\frac{dS}{d\phi_i}\frac{dp}{d\phi_i}\frac{ds_A}{d\phi_i}\frac{dpH}{d\phi_i}\right]^T + \left[\frac{\partial F_1}{\partial \phi_i}\frac{\partial F_2}{\partial \phi_i}\frac{\partial F_3}{\partial \phi_i}\frac{\partial F_4}{\partial \phi_i}\frac{\partial F_5}{\partial \phi_i}\right]^T \tag{28}$$

 © 2015 Society of Chemical Industry

Equation (28) may be written with respect to D as follows:

$$\frac{d}{dt}\left[\frac{dX}{dD}\right] = \left[\frac{\partial F_1}{\partial X}\ \frac{\partial F_1}{\partial S}\ \frac{\partial F_1}{\partial p}\ \frac{\partial F_1}{\partial s_A}\ \frac{\partial F_1}{\partial pH}\right]\left[\frac{dX}{dD}\ \frac{dS}{dD}\ \frac{dp}{dD}\ \frac{ds_A}{dD}\ \frac{dpH}{dD}\right]^T + \left[\frac{\partial F_1}{\partial D}\right] \quad (29)$$

$$\frac{d}{dt}\left[\frac{dS}{dD}\right] = \left[\frac{\partial F_2}{\partial X}\ \frac{\partial F_2}{\partial S}\ \frac{\partial F_2}{\partial p}\ \frac{\partial F_2}{\partial s_A}\ \frac{\partial F_2}{\partial pH}\right]\left[\frac{dX}{dD}\ \frac{dS}{dD}\ \frac{dp}{dD}\ \frac{ds_A}{dD}\ \frac{dpH}{dD}\right]^T + \left[\frac{\partial F_2}{\partial D}\right] \quad (30)$$

$$\frac{d}{dt}\left[\frac{dp}{dD}\right] = \left[\frac{\partial F_3}{\partial X}\ \frac{\partial F_3}{\partial S}\ \frac{\partial F_3}{\partial p}\ \frac{\partial F_3}{\partial s_A}\ \frac{\partial F_3}{\partial pH}\right]\left[\frac{dX}{dD}\ \frac{dS}{dD}\ \frac{dp}{dD}\ \frac{ds_A}{dD}\ \frac{dpH}{dD}\right]^T + \left[\frac{\partial F_3}{\partial D}\right] \quad (31)$$

$$\frac{d}{dt}\left[\frac{ds_A}{dD}\right] = \left[\frac{\partial F_4}{\partial X}\ \frac{\partial F_4}{\partial S}\ \frac{\partial F_4}{\partial p}\ \frac{\partial F_4}{\partial s_A}\ \frac{\partial F_4}{\partial pH}\right]\left[\frac{dX}{dD}\ \frac{dS}{dD}\ \frac{dp}{dD}\ \frac{ds_A}{dD}\ \frac{dpH}{dD}\right]^T + \left[\frac{\partial F_4}{\partial D}\right] \quad (32)$$

$$\frac{d}{dt}\left[\frac{dpH}{dD}\right] = \left[\frac{\partial F_5}{\partial X}\ \frac{\partial F_5}{\partial S}\ \frac{\partial F_5}{\partial p}\ \frac{\partial F_5}{\partial s_A}\ \frac{\partial F_5}{\partial pH}\right]\left[\frac{dX}{dD}\ \frac{dS}{dD}\ \frac{dp}{dD}\ \frac{ds_A}{dD}\ \frac{dpH}{dD}\right]^T + \left[\frac{\partial F_5}{\partial D}\right] \quad (33)$$

The overall set of dynamic equations for the parametric sensitivities of different output variables with respect to all input variables are provided in the Supplementary material.

All symbols used in the theoretical analysis are described in the section Notation.

RESULTS AND DISCUSSION

Sensitivity of pH through theoretical analysis

Time-trajectories of sensitivity of system pH with respect to input variables D, D_1, S_0 and s_b are plotted in Fig. 4. From analysis of the figure, it is clear that D, D_1 and s_b are the most influencial input variables with respect to pH sensitivity. This may be due to the fact that D, the dilution rate, affects the concentration of lactic acid being generated by the biochemical reaction from the hydrodynamic point of view and D_1 and s_b regulate the rate of neutralization of the acid. On the other hand S_0 plays a passive role regarding pH sensitivity because yield coefficient ($Y_{p/S}$) for lactic acid with respect to substrate, glucose, is only 0.0065 g g^{-1}, as reported in Table 2. Thus the input variables D, D_1 and s_b were chosen for further experimental studies on parametric sensitivity.

Table 3. Initial conditions for experiments on parametric sensitivity

Initial biomass concentration (g L^{-1})	0.004
Initial substrate concentration (g L^{-1})	10.0
Initial pH of system	6.7
Initial lactic acid concentration (mmol L^{-1})	0.001
Initial concentration of sodium lactate (mmol L^{-1})	0.008

Critical multiplicity criterion and decision on experimental conditions

From the definition of multiplicity criterion (ω) described in the Mathematical analysis section, the critical value of ω is unity and unique states will occur if $\omega \geq 1$ and otherwise, multiple steady states will be encountered. Based on this concept, the following conditions for conduction of experiments on parametric sensitivity of pH are reported in Table 3 with respect to D, D_1 and s_b.

Experiments on parametric sensitivity

Effects of different parameters, namely D, D_1 and s_b on parametric sensitivity were studied by conducting experiments using the operating parameters satisfying either multiplicity or uniqueness criteria, as indicated in Table 3. Initial conditions for all experiments

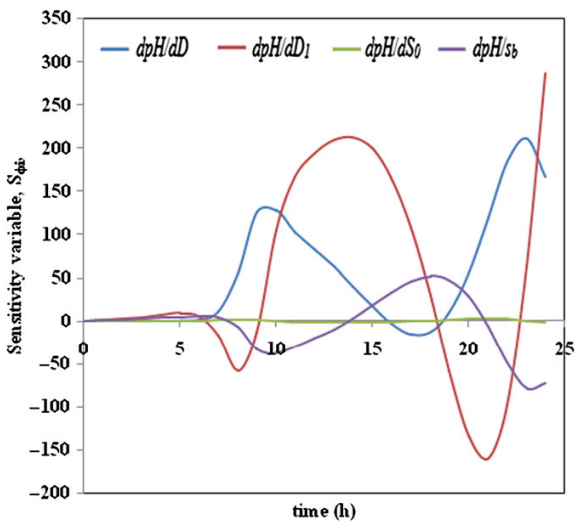

Figure 4. Time trajectories of sensitivity variables, $S_{\phi i}$.

Table 4. Summary of the results obtained from the present study

Mutiplicity	$s_b = 0.008$ mol L^{-1} $D_1 = 0.008$ h^{-1} $D_1 = 0.008$ h^{-1}	$D = 0.1$ h^{-1} $D = 0.1$ h^{-1} $s_b = 0.008$ mol L^{-1}	$D_1 = 0.007$ h^{-1} to $D_1 = 0.008$ h^{-1} $s_b = 0.007$ to 0.008 mol L^{-1} $D = 0.1$ h^{-1} to $D = 0.12$ h^{-1}
Uniqueness	$s_b = 0.002$M $D_1 = 0.06$ h^{-1} $D_1 = 0.06$ h^{-1}	$D = 0.1$ h^{-1} $D = 0.1$ h^{-1} $s_b = 0.002$ mol L^{-1}	$D_1 = 0.06$h^{-1} to $D_1 = 0.065$ h^{-1} $s_b = 0.002$ to 0.003mol L^{-1} $D = 0.08$ h^{-1} to $D = 0.1$ h^{-1}

 © 2015 Society of Chemical Industry

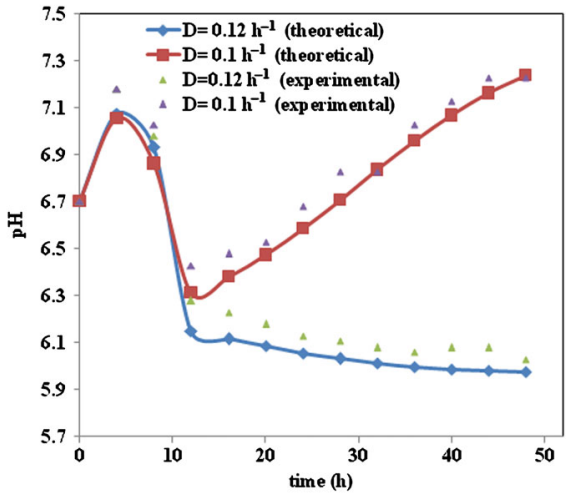

Figure 5. Simulated (lines) and experimental (points) time histories of pH in the region of multiplicity with D as a parameter.

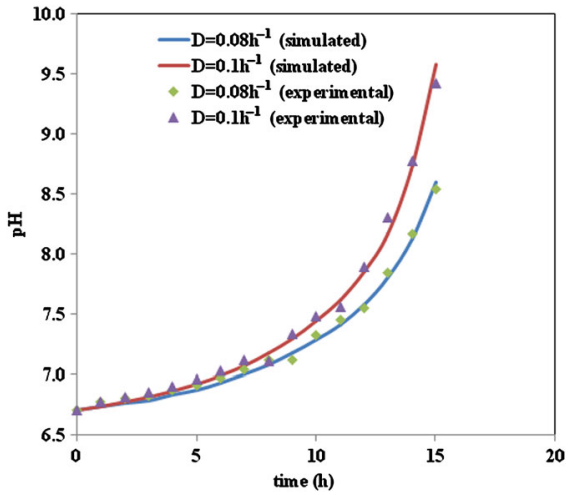

Figure 6. Simulated (lines) and experimental (points) time histories of pH in the region of uniqueness with D as a parameter.

in the CSTBR are provided in Table 4. The concentration of glucose in the inlet MMRS medium was maintained at 10 g L^{-1}.

Numerical simulation

Model Equations (8)–(12) were solved simultaneously using ODE23 of MATLAB-7 2010a for the conditions of input variables, either corresponding to unique or multiple steady state regions. During the solution of Equation (12), very small values of initial concentration of salt ($s_A = 0.001$ mmol L^{-1}) and lactic acid ($P = 0.001$ mmol L^{-1}) were used, to avoid a 'division by zero' situation.

Effect of D on sensitivity of system pH

The reactor was first operated with $D = 0.1$ h^{-1}, $D_1 = 0.008$ h^{-1} and $s_b = 0.008$ mol L^{-1}. The system pH was recorded with a pH meter. The simulated and experimental patterns of transient behavior of pH under this condition are shown in Fig. 5. It is observed that pH shows oscillatory behavior and never stabilizes. After 50 h, pH reached 7.23. Keeping the values of D_1 and s_b unaltered another experiment was conducted setting $D = 0.12$ h^{-1}. From Fig. 5, it is evident that although the transient fluctuates for up to 12 h, it ultimately reaches a steady value of pH = 6.1. After the reaction time of 50 h, the final pH reached 5.97. Therefore, it is clear that the system shows parametric sensitivity, as is evident from the drastic change in behavior of pH for a very small (16.6%) alteration in dilution rate in the multiplicity region. The inset of Fig. 5 shows oscillatory behavior at $D = 0.105$ h^{-1}. Figure 6 shows simulated and experimental trends of time trajectories of pH at fixed values of $D_1 = 0.06$ h^{-1} and $s_b = 0.002$ mol L^{-1} and two values of $D = 0.1$ h^{-1} and 0.08 h^{-1}, judiciously selected in the region of unique steady state. From the figure, it is evident that for $D = 0.1$ h^{-1}, pH monotonically increases to 9.7 at 15 h. When the value of D was altered to 0.08 h^{-1}, the same monotonic rise was observed, with pH = 8.8 at 15 h. Therefore, it may be inferred that in the unique steady states regime, there is an overshoot in pH. The experiments could not be run beyond 15 h due to this abnormal overshoot in pH value. The occurrence of parametric sensitivity may be nullified if operating time is restricted to 13 h. However,

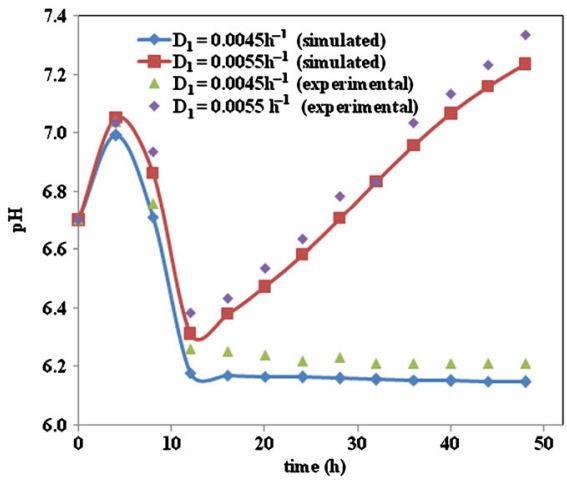

Figure 7. Simulated (lines) and experimental (points) time histories of pH in the region of multiplicity with D_1 as a parameter.

over the period from 13–15 h, the system may be considered to show parametric sensitivity of pH with respect to D. Overall, the system may be considered to be moderately pH sensitive with respect to D in the region of unique steady states. The agreement between the simulated and experimental values is satisfactory in both the regions of multiplicity and uniqueness.

Effect of D_1 on sensitivity of system pH

Figure 7 shows the simulated and experimental time histories of pH when $D_1 = 0.0045$ h^{-1} is set at $D = 0.1$ h^{-1} and $s_b = 0.008$ mol L^{-1}. From the plot, it is clear that pH shows initial fluctuation and ultimately stabilizes at a steady state value of 6.18 after 12 h. Thereafter, pH remains almost constant (pH = 6.15) up to 48 h. Next the value of D_1 was changed to 0.0055 h^{-1} keeping D and s_b unaltered. The time trajectory of pH reveals that it always fluctuates and at 48 h it reaches a value of 7.3, much

 © 2015 Society of Chemical Industry

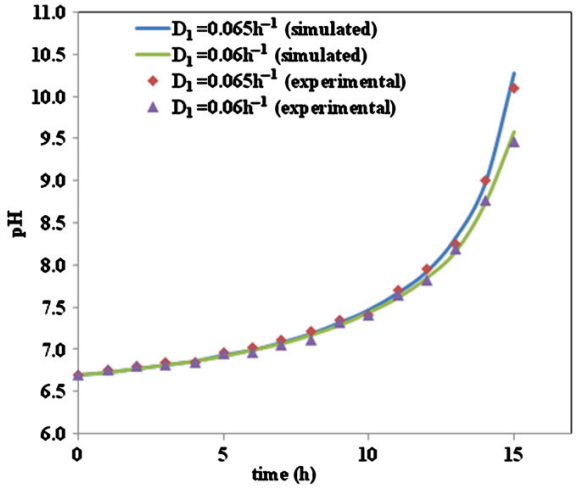

Figure 8. Simulated (lines) and experimental (points) time histories of pH in the region of uniqueness with D_1 as a parameter.

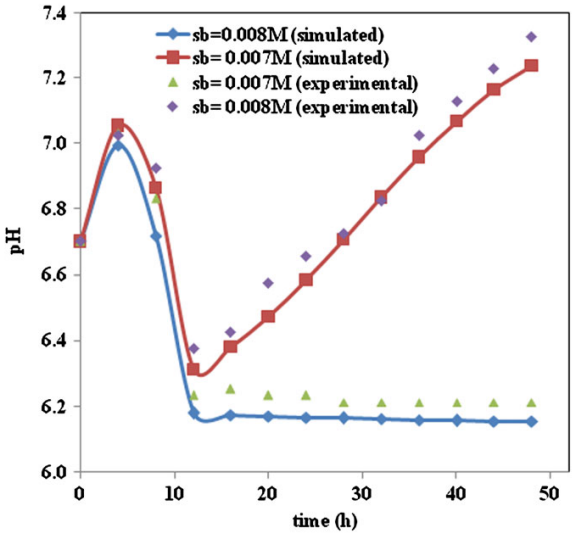

Figure 9. Simulated (lines) and experimental (points) time histories of pH in the region of multiplicity with s_b as a parameter.

different from that obtained with $D_1 = 0.0045$ h^{-1}. Absolutely different patterns of pH behaviour for slight variations of D_1 from 0.0045 h^{-1} to 0.0055 h^{-1}, particularly beyond 12 h, suggests that parametric sensitivity of pH with respect to D_1 exists in the region of multiplicity. On the other hand, time-trajectories of pH shown in Fig. 8 exhibit monotonically increasing pattern at both $D_1 = 0.06$ h^{-1} and 0.065 h^{-1} at fixed values of $s_b = 0.002$ mol L^{-1} and $D = 0.1$ h^{-1} in the region of unique steady states. Over 15 h pH reaches 9.7 and 10.5, respectively, for $D_1 = 0.06$ h^{-1} and 0.065 h^{-1}. Thus the parametric sensitivity with respect to D_1 is moderately present in the unique steady state region. Even in this case, the experiments could only be run up to 15 h due the problem of pH overshoot. The analysis of Figs 6 and 7 reveals that simulated predictions agree well with experimental results.

Effect of s_b on sensitivity of system pH

In Fig. 9, the time trajectories of pH, simulated using model Equations (8)–(12) are plotted along with their experimental counterparts for $s_b = 0.007$ mol L^{-1} and $s_b = 0.008$ mol L^{-1} and $D_1 = 0.008$ h^{-1} and $D = 0.01$ h^{-1}. As is evident from Table 4, both sets of operating parameters fall under the region of multiple steady states. For $s_b = 0.007$ mol L^{-1} the pH trajectory passes through a fluctuating phase up to 12 h after which steady state is attained and pH remains almost constant at 6.18 to 6.15 up to 48 h. When the value of s_b is slightly altered to 0.008 mol L^{-1}, keeping other parameters constant, pH shows fluctuating behavior throughout the operating period up to 48 h. The value of pH at 48 h is 7.3. Since the pH dynamics is completely altered by a very small change in s_b, the system appears to exhibit strong parametric sensitivity with respect to s_b in the region of multiplicity. In Fig. 10 time-trajectories of pH are plotted using simulated and experimental data for two sets of operating parameters $s_b = 0.002$ mol L^{-1} and $s_b = 0.003$ mol L^{-1} and $D_1 = 0.06$ h^{-1}, $D = 0.1$ h^{-1} in the region of unique steady state. The trends in the plots clearly indicate that pH increases monotonically to 8 and 10.5, respectively, over 15 h when s_b is set at 0.002 mol L^{-1} and 0.003 mol L^{-1}. Thus the parametric sensitivity of pH with respect to s_b is present even in the unique steady state region.

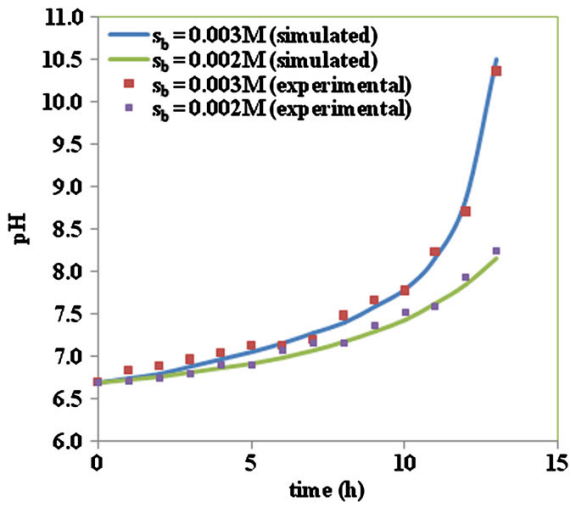

Figure 10. Simulated (lines) and experimental (points) time histories of pH in the region of uniqueness with s_b as a parameter.

In all cases the agreement between simulated and experimental results is satisfactory. From the analysis of Figs 5–10, it may appear that the increasing trend of pH, in some cases, is due to overfeeding of base. However, the change of pH is not only a function of base dosage. The truth underlying the trend is that pH behaviour is affected by three main input parameters, namely D (dilution rate of nutrient stream), D_1 (dilution rate of base stream) and s_b (concentration of base). According to the multiplicity criterion ω derived in the present investigation, unique steady state condition prevails for a set of values of input parameters (D, D_1 and s_b) which correspond to an increased pH condition. The interesting features of Figs 5–10 show that the system is parametrically sensitive in both uniqueness and multiplicity regions.

 © 2015 Society of Chemical Industry

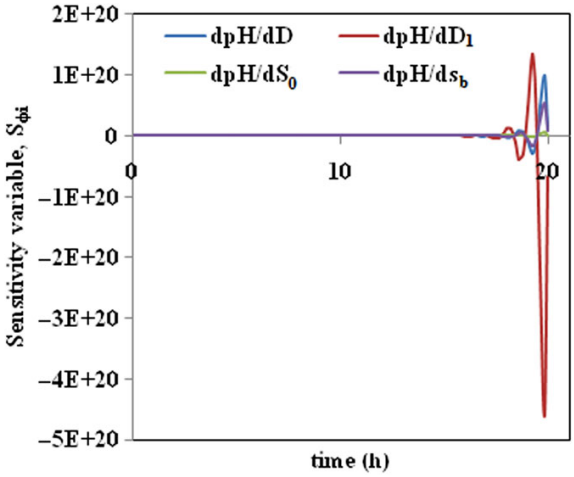

Figure 11. Time trajectories of all theoretical sensitivity variables in the region of multiplicity at $D_1 = 0.0045\ h^{-1}$ ($D = 0.1\ h^{-1}$; $s_b = 0.008\ mol\ L^{-1}$).

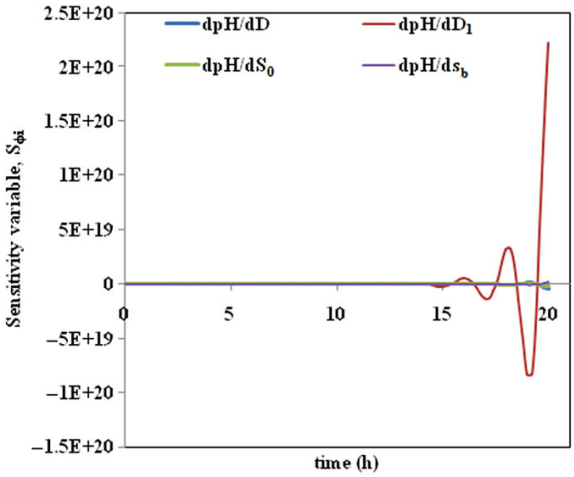

Figure 12. Time trajectories of all theoretical sensitivity variables in the region of multiplicity at $D_1 = 0.0055\ h^{-1}$ ($D = 0.1\ h^{-1}$; $s_b = 0.008\ mol\ L^{-1}$).

Transient variation of sensitivity variable ($S_{\phi i}$)

In Figs 11 and 12, the time course of theoretical (Equations (A.34) to (A37), Supplementary material) sensitivity of pH with respect to D, D_1, S_0 and s_b are plotted at fixed values of $D = 0.1\ h^{-1}$ and $s_b = 0.008\ mol\ L^{-1}$, $S_0 = 10\ g\ L^{-1}$ for $D_1 = 0.0045\ h^{-1}$ and $0.0055\ h^{-1}$, respectively. According to the multiplicity criterion, i.e. $\omega < 1$, both combinations of values of D, D_1 S_0 and s_b used in these figures fall into the multiplicity region. From analysis of the figures it appears that parametric sensitivity of pH exists for the parameters D, D_1 and s_b. Since the order of values of sensitivities are different for different parameters, sensitivities of pH to individual input variables are plotted in Fig. 13(a), 13(b) and 13(c), respectively, for D, D_1 and s_b for the same set of values of D, D_1 and s_b used in Figs 10 and 11. These figures vividly establish the existence of parametric sensitivity in the multiplicity region. Thus the theoretical prediction seems to reconfirm the experimental findings.

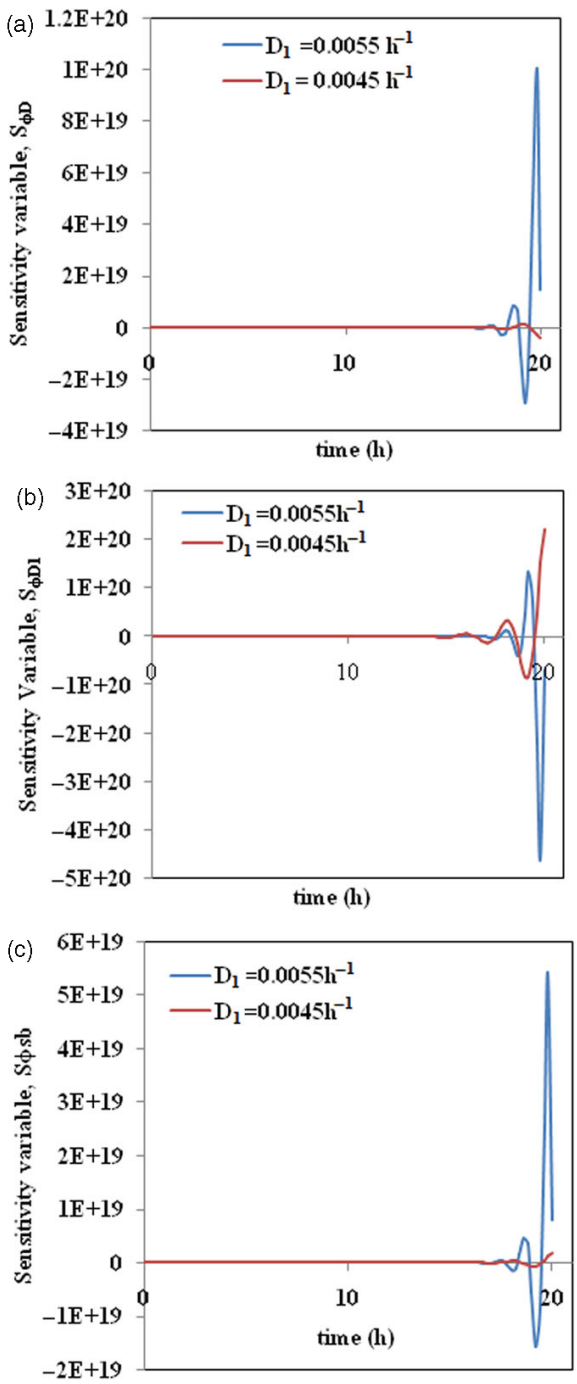

Figure 13. (a) Time trajectories of theoretical sensitivity variable with respect to D in the region of multiplicity at $D_1 = 0.0045\ h^{-1}$ ($D = 0.1\ h^{-1}$; $s_b = 0.008\ mol\ L^{-1}$) and $D_1 = 0.0055\ h^{-1}$ ($D = 0.1\ h^{-1}$; $s_b = 0.008\ mol\ L^{-1}$). (b)Time trajectories of theoretical sensitivity variable with respect to D_1 in the region of multiplicity at $D_1 = 0.0045\ h^{-1}$ ($D = 0.1\ h^{-1}$; $s_b = 0.008\ mol\ L^{-1}$) and $D_1 = 0.0055\ h^{-1}$ ($D = 0.1\ h^{-1}$; $s_b = 0.008\ mol\ L^{-1}$). (c) Time trajectories of theoretical sensitivity variable with respect to s_b in the region of multiplicity at $D_1 = 0.0045\ h^{-1}$ ($D = 0.1\ h^{-1}$; $s_b = 0.008\ mol\ L^{-1}$) and $D_1 = 0.0055\ h^{-1}$ ($D = 0.1\ h^{-1}$; $s_b = 0.008\ mol\ L^{-1}$)

 © 2015 Society of Chemical Industry

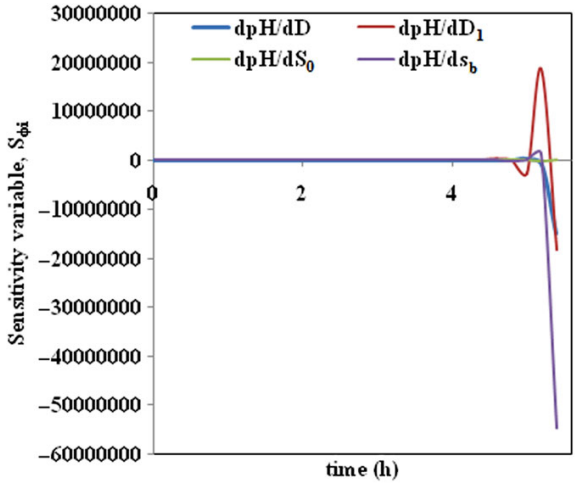

Figure 14. Time trajectories of all theoretical sensitivity variables in the region of uniqueness at $D_1 = 0.06\ h^{-1}$ ($D = 0.1\ h^{-1}$; $s_b = 0.002$ mol L^{-1}).

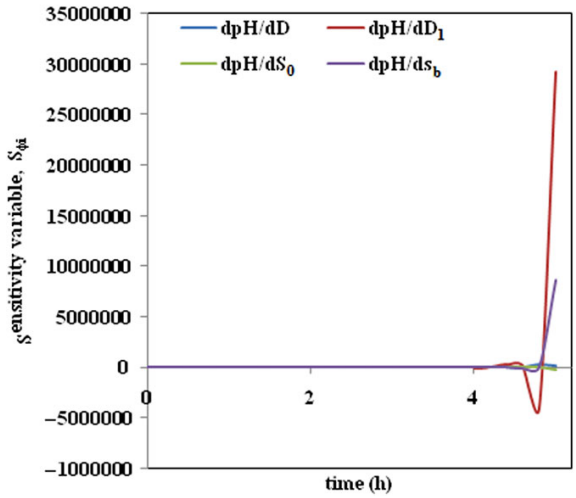

Figure 15. Time trajectories of all theoretical sensitivity variables in the region of uniqueness at $D_1 = 0.065\ h^{-1}$ ($D = 0.1\ h^{-1}$; $s_b = 0.002$ mol L^{-1}).

Figures 14 and 15 show the dynamic variation of theoretical sensitivities (Equations (A.34) to (A.37)) of pH with respect to D, D_1 and s_b respectively for $D_1 = 0.06\ h^{-1}$ and $0.065\ h^{-1}$ at fixed values of $D = 0.1\ h^{-1}$, $s_b = 0.002$ mol L^{-1} and $S_0 = 10$ g L^{-1}. Both combinations correspond to unique steady state conditions ensuring $\omega > 1$. Sensitivity against individual input vector is shown in Fig. 16(a), 16(b) and 16(c) to elucidate the transient behavior of sensitivity of all parameters and to avoid confusion arising due to differences in dimension of values of sensitivities against individual variables. All figures again confirm the occurrence of parametric sensitivity even in the region of uniqueness of steady state, although at a lower scale with respect to the multiplicity region, as observed experimentally.

Overall analysis indicates that the multiplicity region is a sub-set of the parametrically sensitive zone. The series of figures (Figs 11–16) clearly indicates that sensitivity passes through peaks and

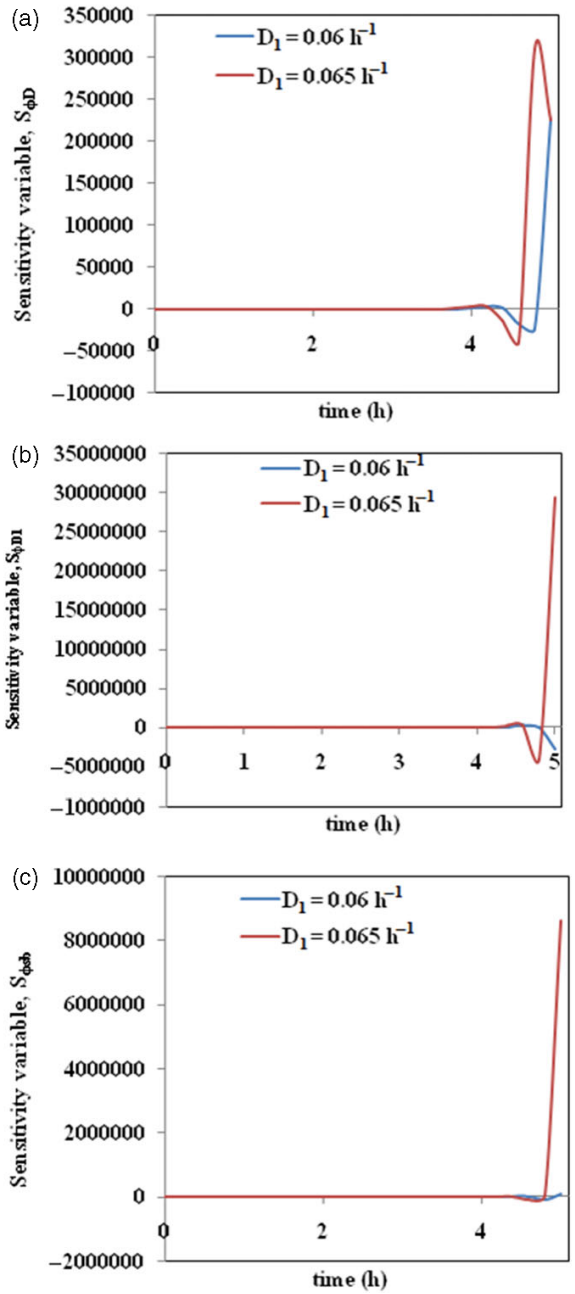

Figure 16. (a) Time trajectories of theoretical sensitivity variable with respect to D in the region of uniqueness at $D_1 = 0.06\ h^{-1}$ ($D = 0.1\ h^{-1}$; $s_b = 0.002$ mol L^{-1}) and $D_1 = 0.065\ h^{-1}$ ($D = 0.1\ h^{-1}$; $s_b = 0.002$ mol L^{-1}). (b) Time trajectories of theoretical sensitivity variable with respect to D_1 in the region of uniqueness at $D_1 = 0.06\ h^{-1}$ ($D = 0.1\ h^{-1}$; $s_b = 0.002$ mol L^{-1}) and $D_1 = 0.065\ h^{-1}$ ($D = 0.1\ h^{-1}$; $s_b = 0.002$ mol L^{-1}). (c) Time trajectories of theoretical sensitivity variable with respect to s_b in the region of uniqueness at $D_1 = 0.06\ h^{-1}$ ($D = 0.1\ h^{-1}$; $s_b = 0.002$ mol L^{-1}) and $D_1 = 0.065\ h^{-1}$ ($D = 0.1\ h^{-1}$; $s_b = 0.002$ mol L^{-1}).

 © 2015 Society of Chemical Industry

crests as time propagates. This information will be particularly useful for implementation of a control scheme and not for the exact design of controllers for the bioreactor. The controller design will definitely need determination of the classically defined open-loop eigenvalue and stability criterion based on system equations.

Suggested operational strategy

The detailed analysis of multiplicity and parametric sensitivity in the present study reveals that, similar to exothermic reactors, CSTBR handling the growth of pH-sensitive microorganisms, e.g. *Pediococcus acidilactici*, is also parametrically sensitive irrespective of the occurrence of a multiplicity of steady state. As observed by Chemburkar *et al.*,[24] during studies on an exothermic adiabatic CSTR, multiplicity occurs simultaneously with parametric sensitivity. Besides the existence of strong parametric sensitivity in the region of multiplicity, it is also present moderately with respect to D and D_1 and strongly with respect to s_b in the region of unique steady state. An overhoot tendency of pH dominates in the region of uniqueness. Thus it may be inferred that the inherent tendency of the system is to show parametric sensitivity and hence it is very difficult to operate with a continuous feed of base stream to control pH. Although in the multiple steady state region, a few conditions of input parameters correspond to stable values of pH after 12 h, operation at these conditions is not recommended due to the presence of parametric sensitivity and multiplicity behavior. On the other hand, due to the overshoot tendency of pH in unique steady state conditions, operation of the CSTBR with pH control using a continuous input of base stream seems to be impractical. Therefore, fed batch type arrangement with intermittent dosage of base stream for the adjustment of pH, as adopted by many researchers,[32,33] seems to be more judicious.

CONCLUSION

In the present investigation a multiplicity criterion for a CSTBR using *pediococcus acidilactici* was developed. Theoretical equations for the parametric sensitivity functions of system pH were also developed. Experiments were conducted both in the regions of multiple and unique steady states to investigate the effects of different parameters on parametric sensitivity of pH. Experimental data fit well with the model predictions. It was observed that the system is parametrically sensitive both in the regions of multiplicity and uniqueness of steady states. The theoretical trends of parametric sensitivity variable, $S_{\phi i}$ are also in agreement with experimental findings. Similar to the case of adiabatic CSTRs for exothermic reaction, the multiplicity region is a sub-set of the parametrically sensitive regime. Since the overall system is parametrically sensitive for almost all input variables, namely D, D_1 and s_b it is suggested to run the reactor in fed batch mode with intermittent adjustment of pH rather than control of system pH with a continuous base stream.

Supporting Information

Supporting information may be found in the online version of this article.

REFERENCES

1 Sadana A, Kulkarni BD and Ramachandrana P, Criteria for multiplicity for complex biochemical reactions. *Chem Eng Commun* **7**:389–394 (1980).
2 Patnaik PR, Dynamic sensitivity of a chemostat for a microbial reaction with substrate and product inhibition. *Appl Math Model* **18**:620–627 (1994).
3 Keesman KL, Stigter JD. Optimal parametric sensitivity control for the estimation of kinetic parameters in bioreactors. *Math Biosci* **179**: 95–111 (2002).
4 Guerra NP, Agrasar AT, Macías CL, Bernárdez PF and Castro LP, Dynamic mathematical models to describe the growth and nisin production by *Lactococcus lactis* subsp. *lactis* CECT 539 in both batch and re-alkalized fed-batch cultures. *J Food Eng* **82**:103–113 (2007).
5 Romero JA and Navarro JL, Improved efficiency in sensitivity calculations for bioreactor models. *Comput Chem Eng* **33**:903–910 (2009).
6 Bilous O and Amundson. NR, Chemical reactor stability and sensitivity-II. Effect of parameters on sensitivity of empty tubular reactors. *AIChE J* **2**:117–126 (1956).
7 Adler J and Enig JW, The critical conditions in thermal explosion theory with reactant consumption. *Combust Flame* **8**:97–103 (1964).
8 Uppal A, Ray H and Poore AB, On the dynamic behavior of continuous stirred tank reactors. *Chem Eng Sci* **29**:967–985 (1974).
9 Balakotaiah V and Luss D, Analysis of the multiplicity patterns of a CSTR. *Chem Eng Commun* **13**:111–132 (1981).
10 Morbidelli M and Varma A, Parametric sensitivity and runaway in tubular reactors. *AIChE J* **28**:705–713 (1982).
11 Boddington T, Gray P, Kordylewski W and Scott SK, Thermal explosions with extensive reactant consumption: a new criterion for criticality. *Proc R Soc London* **A390**:13–30 (1983).
12 Barkelew CH, Stability of chemical reactors. *Chem Eng Progr Symp* **55**:37 (1959).
13 Morbidelli M and Varma A, On parametric sensitivity and runaway criteria of pseudohomogeneous tubular reactors. *Chem Eng Sci* **40**:2165–2168 (1985).
14 Morbidelli M and Varma A, A generalized criterion for parametric sensitivity: application to thermal explosion theory. *Chem Eng Sci* **43**:91–201 (1988).
15 Morbidelli M and Varma A, Parametric sensitivity in fixed-bed reactors: the role of interparticle transfer resistances. *AIChE J* **32**:97–306 (1986).
16 Morbidelli M and Varma A, Parametric sensitivity and runaway in fixed bed catalytic reactors. *Chem Eng Sci* **41**:1063–1071 (1986).
17 Jayakumar NS, Agrawal A, Hashim MA and Sahua JN, Experimental and theoretical investigation of parametric sensitivity and dynamics of a continuous stirred tank reactor for acid catalyzed hydrolysis of acetic anhydride. *Comput Chem Eng* **35**:1295–1303 (2011).
18 Jiang J, Jiang J, Pan Y, Wang R and Tang P, Investigation on thermal runaway in batch reactors by parametric sensitivity analysis. *Chem Eng Technol* **34**:1521–1528 (2011).
19 Sayar NA, Chen BG, Lye GJ and Woodley JM, Modelling and simulation of a transketolase mediated reaction: sensitivity analysis of kinetic parameters. *Biochem Eng J* **47**:1–9 (2009).
20 Sayar NA, Chen BG, Lye GJ and Woodley JM, Process modelling and simulation of a transketolase mediated reaction: analysis of alternative modes of operation. *Biochem Eng J* **47**:10–18 (2009).
21 Dutta S, Chowdhury R and Bhattacharya P, Parametric sensitivity in bioreactor: an analysis with reference to phenol degradation system. *Chem Eng Sci* **56**:5103–5110 (2001).
22 Dutta S, Chowdhury R and Bhattacharya P, Stability and response of bioreactor: an analysis with reference to microbial reduction of SO_2. *Chem Eng J* **133**:343–354 (2007).
23 Morbidelli M and Varma A, A generalized criterion for parametric sensitivity: application to a pseudohomogeneous tubular reactor with consecutive or parallel reactions. *Chem Eng Sci* **44**:675–1696 (1989).
24 Chemburkar RM, Morbidelli M and Varma A, Parametric sensitivity of a CSTR. *Chem Eng Sci* **41**:1647–1654 (1986).
25 Kaushus W, Demont J and Hartmann K, On the steady states of continuous stirred tank reactors. *Chem Eng Sci* **33**:1283–1285 (1978).
26 Bhattacharya I, Chowdhury R and Chakraborty R, Intensification of freeze-drying rate of *Bacillus subtilis* MTCC 2396 using tungsten halogen radiation: optimization of moisture content and α-amylase activity. *Drying Technol* **32**:801–812 (2014).
27 Miller GL, Use of dinitrosalicylic acid reagent for determination of reducing sugar. *Anal Chem* **31**:426–428 (1959).
28 Lallai A, Mura G, Milidd R and Mastinu C, Effect of pH on growth of mixed cultures in batch reactor. *Biotechnol Bioeng* **31**:130–134 (1988).

 © 2015 Society of Chemical Industry

29 Atkins P and de Paula J, *Atkins' Physical Chemistry*, Vol. 1. Oxford University Press (2002).
30 Parada JL, Caron CR, Medeiros ABP and Soccol CR, Bacteriocins from lactic acid bacteria: purification, properties and use as biopreservatives. *Brazilian Arch Biol Technol* **50**:521–542 (2007).
31 Vuyst LD and Leroy F, Bacteriocins from lactic acid bacteria: production, purification, and food applications. *J Mol Microbiol Biotechnol* **13**:194–199 (2007).
32 Guerra NP and Pastrana L, Modelling the influence of pH on the kinetics of both nisin and pediocin production and characterization of their functional properties. *Process Biochem* **37**:1005–1015 (2002).
33 Guerra NP, Agrasar AT, Macías CL, Bernárdez PF and Castro LP, Dynamic mathematical models to describe the growth and nisin production by *Lactococcus lactis* subsp. *lactis* CECT 539 in both batch and re-alkalized fed-batch cultures. *J Food Eng* **82**:103–113 (2007).

 © 2015 Society of Chemical Industry

Paper 2

Parametric Sensitivity of CSTBRs for *Lactobacillus casei*: Normalized Sensitivity Analysis

Subhashis Das, Rajnish Kaur Calay and Ranjana Chowdhury

ChemEngineering 4.2 (2020): 41

chemengineering

MDPI

Article

Parametric Sensitivity of CSTBRs for *Lactobacillus casei*: Normalized Sensitivity Analysis

Subhashis Das [1,*], Rajnish Kaur Calay [1] and Ranjana Chowdhury [2]

[1] Faculty of Engineering Science and Technology, UiT- The Arctic University of Norway, 8514 Narvik, Norway; rajnish.k.calay@uit.no

[2] Department of Chemical Engineering, Jadavpur University, Kolkata 700032, India; ranjana.juchem@gmail.com

* Correspondence: das.subhashis@gmail.com

Received: 30 April 2020; Accepted: 18 June 2020; Published: 18 June 2020

check for updates

Abstract: In this paper, a sensitivity analysis of a continuous stirred tank bioreactor (CSTBR) was conducted to determine a parametrically sensitive regime. The growth of a lactic acid bacterium, namely, *Lactobacillus casei*, in a pH-controlled CSTBR was considered as a process model. Normalized objective sensitivities of the minimum pH were determined with respect to input parameters. A generalized criterion for sensitivity was defined for determining the parametric range of three input variables, i.e., dilution rate base stream (θ), base concentration (R), and initial pH (pH_0) for maintaining optimal pH range in the reactor. The system exhibits sensitive behavior for θ, R, and pH_0, from 0.095 to 0.295, 0 to 0.865, and 4.42 to 4.77, respectively. The critical values of θ, R, and pH_0 are 0.0195, 0.48, and 4.6, respectively. The mathematical model can also be used to determine a parametrically sensitive regime for other important parameters, namely, temperature, the concentration of metabolites, and other byproducts. The mathematical tool can also be used in bioreactor design and the improvement of control strategies.

Keywords: bioreactor; mathematical modeling; sensitivity analysis; control

1. Introduction

Continuous stirred tank reactors are the most widely used reactors for continuous and large scale production in many industries due to their high flexibility. For the production of bioenergy vectors (e.g., biogas, biohydrogen, bioethanol) continuous type systems are also preferred. The reactors used for bioprocesses are termed as continuous stirred type bioreactors (CSTBR).

The biochemical processes in CSTBR can be mathematically described as a set of ordinary differential equations, which explicitly or implicitly provide the relationship between the system behavior and input parameters. The system behavior is defined by the output or dependent variables that change in time or space. Whereas input parameters contain the physicochemical parameters, the initial conditions, and operating conditions of the system. When the output variables of a system change drastically with a small variation of input parameters, the specific range of that input parameter is called parametric sensitivity region of the system. Once a biochemical system undergoes through this parametric sensitivity region, its performance becomes unpredictable because outputs change sharply with a small variation of the input variable. For all chemical and biological processes, there exists a parametric range within which a process becomes unstable and unreliable, where even small variations in parameters abruptly change the performance. Thus, it is important to investigate a change in the behavior of a system with respect to any change in parameters. Such a study is called parametric sensitivity analysis [1]. In the context of chemical reactors, Bilous and Amundson [2] first introduced this concept of parametric sensitivity and runaway (where the system becomes unstable).

However, the parametric sensitivity studies for bioprocesses in CSTBR are limited. It is essential to have sufficient information on the kinetics of microbial growth and product output for better control and optimization of CSTBRs.

Many research articles are available on parametric sensitivity in non-isothermal and non-adiabatic chemical reactors [3,4] that discuss the occurrence of multiple steady states. These studies are suitable to predict a priori criteria for parametric sensitivity based upon which any possible steady-state regime of the reactor can be identified. On the other hand, research on the nonlinear dynamics behavior of CSTBRs is limited due to the complex mechanism of microbial growth and generation of secondary metabolic products. Moreover, in many cases, the influence of operating conditions on microbial growth which directly affect CSTBR operation is not adequately understood.

In CSTBRs, the growth of microorganisms is subjected to vary due to the influence of some operating variables, such as temperature, dissolved oxygen, and pH value [5–8]. Among these variables, pH plays a vital role in exerting a significant impact on various aspects of bioprocesses where fermentation is involved. The microbial cultures have an optimum pH range which is the most favorable condition for their growth [9,10]. The product that is produced in a process can be either an acid or a base, pH; therefore, pH is also a critical output variable. If the pH value of the microbial growth medium goes beyond the optimum pH range, the microbial growth could be hindered. Some comprehensive studies have been reported on the occurrence of multiple steady states for CSTBRs and other similar bioreactors [11,12].

Dutta et al. [12] investigated the parametric sensitivity of pH using a generalized sensitivity criterion proposed by Morbidelli and Verma [3,13] in a batch type bioreactor used for a phenol degradation system. However, information on the parametric sensitivity of CSTBRs is not widely available in the literature. Das et al. [14] defined a criterion, denoted as "pH-runaway" condition of CSTBR, which stated, pH-sensitive microorganisms stop growing when pH of the growth medium goes beyond its optimum range, and CSTBR operation becomes vulnerable. In their study, growth of lactic acid bacteria (LAB), namely, *Pediococcus acidilactici* with a continuous NaOH dosing for maintaining the pH system, was studied in a CSTBR. The parametric sensitivity of pH was observed in both unique and multiple steady-state conditions for a particular set of input variables. However, the parametric range of input variables that simultaneously affect the CSTBR operation cannot be predicted by their model. Moreover, a generalized criterion for sensitivity, independent of the topology of pH contour for recognizing the extent of parameters, where a CSTBR exhibits sensitive behavior, is not available in the literature.

Therefore, the focus of this study is to develop a mathematical model of CSTBR and derive an expression for normalized sensitivity function to determine parameter space and the critical value of input parameters where the system becomes unstable. The general methodology presented here can be modified to study the influence of other variables on microbial growth and can be used as a useful tool to design control strategies in CSTBRs.

2. Methodology

In this paper, the CSTBR bioprocess model of Das et al. [14] is adapted to describe the kinetics within the reactor. In order to to obtain kinetic constants relating to this study, batch experiments were performed and a calibrated model was used to conduct sensitivity analysis and highlight the sensitive parameter range and values for the considered variables.

The influence of pH on microbial growth was examined experimentally in a number of batch experiments. A lactic acid bacterium (LAB), *Lactobacillus casei*, was selected for these experiments. The initial pH of the reaction medium was varied to determine the impact of pH on the microbial growth rate. The data obtained from these batch experiments identified the optimum range of pH for the growth of LAB. From the data, the kinetic constants for the microbial growth model were also obtained.

By using the necessary knowledge on the kinetic parameters of microbial growth, including their dependence on pH, a model of CSTBR operation was developed. The mathematical model is capable of predicting time-dependent changes in the concentration of substrate, biomass, lactic acid, salt, and pH. The reactor pH is kept constant by assuming a continuous flow of the alkaline stream. The model is then used to analyze normalized sensitivity with respect to input variables; initial system pH, the dilution rate of the alkaline stream, and its concentration where pH-minimum (the lowest value of pH attain for a set of input variable) is an objective function. The sensitivity of the pH-minimum with respect to the vector of input parameters is investigated, along with the determination of critical values of input parameters where a "pH-runaway" condition occurs. Finally, the sensitivity analysis identified a parameter space, where pH becomes simultaneously sensitive to small changes in input parameters. The following objectives were achieved in order to fulfill the overall aim of the paper.

- Perform batch experiments using a lactic acid bacterium, *Lactobacillus casei*, to find out the optimum pH for microbial growth and other growth associated kinetic parameters;
- Derive a generalized criterion for sensitivity by obtaining an objective sensitivity function for pH with respect to input variables;
- Predict the critical value of input parameters and parameter space where the system becomes unstable and exhibits sensitive behavior.

2.1. Experimental Analysis

The details of the materials and equipment used for the batch experiments are provided in Table 1. A probiotic bacterium, *Lactobacillus casei* (LAB), is chosen, which is commonly used in dairy and pharmaceutical industries [15,16]. LAB is a gram-positive and facultative anaerobic bacterium. The pure stock culture was maintained separately at 37 °C in de Man Rogosa and Sharpe (MRS) medium for 18 h. After 18 h, the stock culture was kept at 4 °C. For the batch experiment, the composition of MRS medium is modified, and the composition of modified MRS (mMRS) is provided in Table 2.

2.1.1. Modified MRS Culture Preparation

The mMRS was prepared by varying the glucose concentration from 10 gL^{-1} to 50 gL^{-1}. The pH of each glucose concentration was varied from 5 to 8, using 2N HCl and 2M NaOH. In order to make the prepared mMRS media sterile, it was autoclaved at 121 °C for 15 min.

2.1.2. Batch Experiment

The incubating batch experiments were performed in 150 mL Erlenmeyer flasks using 50 mL modified MRS (mMRS) media. The temperature for all experiments was maintained at 37 °C. The experiment was started by adding 1% inoculum of LAB in mMRS media of 50 mL volume for every initial pH and glucose concentration. The flasks were then agitated at 60 rpm at 37 °C for 24 h. The carbon source (glucose) concentration was varied from 10.0 gL^{-1} to 50.0 gL^{-1}. At each glucose concentration, experiments were conducted by varying initial pH in the range of 5.0 to 8.0. The microbial growth kinetics were studied for 24 h. Each experimental run was repeated three times to confirm the statistical accuracy of the results.

2.1.3. Assessment

Samples were withdrawn at an interval of 2 h during incubation. After centrifuging at 10,000 rpm, the supernatant was passed through a 0.22-micron filter for analyzing lactic acid concentration with the help of HPLC (Agilent 1260 series Agilent Technologies India Pvt Ltd., New Delhi, India). The mobile phase was 5 mM sulphuric acid with a flow rate of 0.6 mL/min at 35 °C, and the stationary phase was a Hypersil gold column. The cell biomass concentration of each sample was analyzed using a spectrophotometer (Perkin Elmer LAMBDA 850+ UV/Vis, India) at a wavelength of 600 nm. Cell dry weight was measured by withdrawing 5 mL of sample and centrifuging it at 10,000 rpm for 20 min.

The supernatant is collected separately, and the pellet is dried at 100 °C to construct a standard calibration curve of cell biomass vs. optical density. The collected supernatant was also analyzed to determine the reduced sugar concentration using the dinitrosalicylic (DNS) acid reagent through spectrophotometry at 540 nm [5,17].

Table 1. Details of materials and equipment used for the batch study.

Microorganism	***Lactobacillus casei* (NCIM 5303) (Procured from the National Chemical Laboratory, Pune, India [18])**
Chemicals for DNS method (Merck Specialties Private Limited, India)	3,5-dinitro salicylic acid, sodium hydroxide, sodium potassium tartrate
Equipment	a. A BOD incubator shaker (G. B. Enterprises, Kolkata, India); b. Autoclave (G. B. Enterprises, Kolkata, India) Centrifuge (Plasto Craft Industries Pvt. Ltd., India); c. Fermenter (B. Braun Biotech International); d. Peristaltic pump (Enertech Electronics Pvt. Ltd., India); e. UV-visible spectrophotometer (Varian, India); f. Shimadzu Corporation Reverse Phase HPLC (Model no: CBM-Ro A); g. pH meter (Sartorius, PB-11).

Table 2. Man Rogosa and Sharpe (MRS) composition in 100 mL solution.

Components	Amount (g)
Peptone	1.0
Beef extract	0.8
Yeast extract	0.4
Glucose	2.0
Sodium acetate trihydrate	0.5
Polysorbate 80 (also known as Tween 80)	0.1
Dipotassium hydrogen phosphate 0.2	0.2
Triammonium citrate	0.2
Magnesium sulfate heptahydrate	0.02
Manganese sulfate tetrahydrate	0.05

2.2. *Theoretical Analysis*

2.2.1. Kinetics Modeling

The most popular and simplest model, the Monod model, which describes the microbial reaction of microbial growth within a single substrate, was considered. The Monod equation is as follows:

$$\mu = \frac{\mu_{max} S}{K_S + S}, \quad (1)$$

where,

μ specific microbial growth rate, (h^{-1})
μ_{max} maximum specific microbial growth rate, (h^{-1})
K_S substrate saturation constant (Monod constant) (gL^{-1})
S substrate (glucose) concentration (gL^{-1})

Kinetic parameters of the Monod model were determined using the initial specific growth rate at each initial glucose concentration obtained at each initial pH. Equation (1) can be linearized in the

form of Equation (2) to find out the kinetic parameters (μ_{max} and K_s) by making double reciprocal plots of μ versus S at each initial pH.

$$\frac{1}{\mu} = \frac{K_S}{\mu_{max} S} + \frac{1}{\mu_{max}}. \tag{2}$$

Regression analysis can be used to find the best fit for a straight line on a plot of $1/\mu$ vs. 1/S, and the values of μ_{max} and K_S are determined. The variation of μ_{max} with initial pH would determine an optimum value of pH at which μ_{max} is maximum, thus, describing optimum conditions for the microbial growth. By plotting the values of normalized μ_{max}, i.e., $\mu_{max,N}$ vs. initial pH, a second-order correlation, similar to that obtained by Lallai et al. [19] and Datta et al. [12], is then obtained, as given in Equation (3)

$$\mu_{max,N} = \left(A + B \cdot pH + C \cdot pH^2\right), \tag{3}$$

where

$$\mu_{max,N} = \frac{\mu_{max}}{\mu_{max,opt}}, \tag{4}$$

where, $\mu_{max,opt}$, μ_{max} at optimum pH.

Therefore, Equation (1) can be written as

$$\mu = \frac{\mu_{max,opt}\left(A + B{\cdot}pH + C{\cdot}pH^2\right)S}{K_S + S}. \tag{5}$$

This correlation defines the influence of pH on the specific microbial growth rate. A, B, and C are the second-order polynomial constants, and their values can be determined by nonlinear regression analysis of the experimental data. The mathematical model is used to design bioreactors and offer the necessary information to adopt control strategies for reactor operations. The mathematical model is based on conservation equations of mass or molar balance for each component in the process and simulates the kinetics of the bioprocess in a reactor. For quantitative prediction, the kinetic constants may be obtained experimentally.

2.2.2. Mathematical Modeling of CSTBRs

A continuous stirred tank bioreactor (CSTBR) as described by Das et al. [14] in which the feed conditions contain the glucose at a flow rate of F_1 (Lh^{-1}) and the glucose concentration of glucose is S_0 (gL^{-1}) was considered in this present study. The feed condition is sterile, which indicates that the feed is not containing any microbial cell. An alkaline stream containing aqueous NaOH fed to the bioreactor at a flow rate of F_2 (Lh^{-1}) and the concentration of NaOH is s_b (M) for controlling pH of the reaction medium. The volume of the bioreactor is V (L), and X (gL^{-1}) and S (gL^{-1}) are the cell and substrate (glucose) concentrations in the output stream, respectively. The detailed reaction scheme is shown in Figure 1.

The primary biochemical reaction in the CSTBR is described in Equation (6),

$$X + \text{Glucose} \rightarrow nX + CH_3CH(OH)COOH\ (\text{Lactic acid}) + \text{Caseicin}. \tag{6}$$

In the above biochemical reaction, bacterial cell, X is growing by utilizing glucose as a substrate, and the main byproduct is lactic acid. The optimum pH for microbial growth is maintained by continuously feeding the alkaline stream (NaOH) to the CSTBR. The acid-neutralizing reaction is taking place, as shown in Equation (7).

$$CH_3CH(OH)COOH + NaOH \rightarrow CH_3CH(OH)COONa + H_2O. \tag{7}$$

By knowing the concentration of NaOH and the salt (sodium lactate), the pH of the solution medium can be calculated using the Henderson–Hasselbalch equation [20] as shown in Equation (8).

$$pH = pK_a + \log \frac{s_A}{p}, \tag{8}$$

where,

K_i the equilibrium dissociation constant for lactic acid
s_A molar concentration of sodium lactate (M)
p molar concentrations of lactic acid (M)

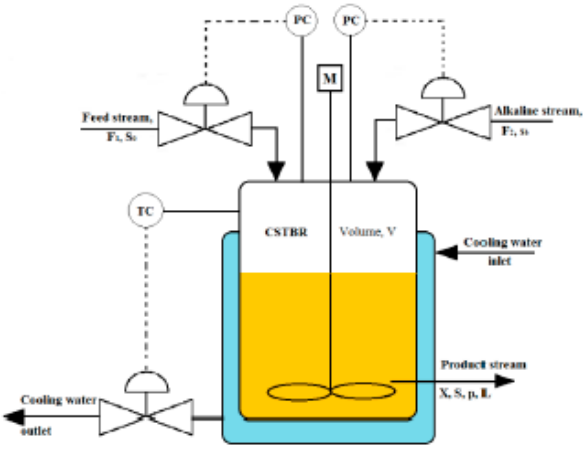

Figure 1. Schematic of the bioreactor setup.

The unsteady-state mass, molar, and pH balance are established in the following manner:
The mass balances are given by

$$\frac{dX}{dt} = (\mu - D - D_1)X, \tag{9}$$

$$\frac{dS}{dt} = D(S_0 - S) - D_1 S - \frac{1}{Y_{\frac{X}{S}}}\mu X, \tag{10}$$

where,

$D = F_1/V$, dilution rate of the glucose feed stream (h^{-1})
$D_1 = F_2/V$, dilution rate of the alkaline stream (h^{-1})
$Y_{X/S}$ yield coefficient for cell ($g.g^{-1}$)
t time (h)

The Mole Balances are given as

$$\frac{dp}{dt} = -Dp + \frac{Y_{\frac{p}{X}}\mu X}{M_a} - D_1(s_b + p), \tag{11}$$

$$\frac{ds_A}{dt} = D_1(s_b - s_A) - Ds_A, \tag{12}$$

where,
$Y_{p/S}$ yield coefficient for product ($g.g^{-1}$)

M_a Molecular weight of lactic acid ($g.mol^{-1}$)

The pH balance is obtained by differentiating Equation (8), and given as

$$\frac{dpH}{dt} = \frac{1}{s_A}\frac{ds_A}{dt} - \frac{1}{p}\frac{dp}{dt}. \tag{13}$$

The mass and molar balances were suitably transformed into the dimensionless form using the variables described in Table 3.

Table 3. Definitions of the dimensionless variable used in the model.

Parameter	Definition	Parameter	Definition
α	$X/(S_0Y_{X/S})$	U	μ/D
β	S/S_0	θ	D_1/D
z	$pM_a/(S_0Y_{P/S})$	m	μ_{max}/D
R	s_bM_b/S_0	n	K_S/S_0
L	s_aM_c/S_0	b	$B.pH_0$
γ	pH/pH_0	c	$C.pH_0^2$
τ	tD	M_1	$M_aY_{P/S}/M_b$
M_2	M_c/M_b		

Therefore, the model equations in the non-dimensional form are as follows:

$$\frac{d\alpha}{d\tau} = (U - \theta - 1)\alpha, \tag{14}$$

$$\frac{d\beta}{d\tau} = (1 - \beta) - U.\alpha - \theta.\beta, \tag{15}$$

$$\frac{dz}{d\tau} = -z + U.\alpha - \theta(M_1R + z), \tag{16}$$

$$\frac{dL}{d\tau} = (M_2R - L)\theta - L, \tag{17}$$

$$\frac{d\gamma}{d\tau} = \frac{1}{pH_0}\left[\frac{1}{L}\frac{dL}{d\tau} - \frac{1}{z}\frac{dz}{d\tau}\right]. \tag{18}$$

On the other hand, the non-dimensional expression for the specific growth rate can be expressed as

$$U = \frac{m\beta}{n + \beta}I, \tag{19}$$

where,

$$I = A + B.\gamma + C.\gamma^2. \tag{20}$$

The differential Equations (14)–(18) can be solved numerically using the 4th order Runge–Kutta method using the following initial conditions. At

$$\tau = 0; \gamma = 1; \alpha = \alpha_0; \beta = \beta_0; z = z_0; L = L_0. \tag{21}$$

2.2.3. Sensitivity Analysis

For analyzing the pH-sensitivity, the method adopted by Morbedelli and Varma [3,13] and Dutta et al. [12] is considered. In this case, the governing equations for pH and the substrate concentration are written by dividing Equation (18) by Equation (15)

$$\frac{d\gamma}{d\beta} = \frac{\frac{R\cdot\theta}{pH_0}\left[\frac{M_2}{L} + \frac{M_1}{z} - \frac{U\cdot\alpha}{z\cdot R\cdot\theta}\right]}{1 - U.\alpha - (1 + \theta)\beta} = g(\phi, \alpha, \beta, z, L, \gamma), \tag{22}$$

where ϕ is the vector of input parameters, namely, initial system pH (pH_0), the dilution rate of the alkaline stream (θ), and its concentration (R). Similarly, dividing Equations (14), (16), and (17) by Equation (15), the following equations are obtained as below.

$$\frac{d\alpha}{d\beta} = \frac{U.\alpha - (1+\theta)\alpha}{1 - U.\alpha - (1+\theta)\beta}, \tag{23}$$

$$\frac{dz}{d\beta} = \frac{U.\alpha - (1+\theta).z - M_1.\theta.R}{1 - U.\alpha - (1+\theta)\beta}, \tag{24}$$

$$\frac{dL}{d\beta} = \frac{M_2.\theta.R - (1+\theta).L}{1 - U.\alpha - (1+\theta)\beta}. \tag{25}$$

With the following initial conditions,

$$pH = pH_0;\ \alpha = \alpha_0; z = z_0 \text{ and } L = L_0\ ;\ \beta = \beta_0. \tag{26}$$

By differentiating Equation (22) with respect to parameter ϕ, the expression for first-order local sensitivity s_ϕ can be evaluated as

$$\frac{ds_\phi}{d\beta} = \frac{dg}{d\phi} + \frac{dg}{d\gamma}.\ s_\phi. \tag{27}$$

The adjoined equation from Equation (27) takes the following form:

$$\frac{dp_\beta}{d\beta} = H.p_\beta \ \text{ for } \beta \in \left(\beta_0, \beta^*\right), \tag{28}$$

where,

$$H = -\frac{dg}{d\gamma} \tag{29}$$

and

$$p_\beta = \frac{\overline{s}_\phi(\beta)}{\overline{s}_\phi(0)}. \tag{30}$$

Furthermore, β_0 indicates the value of initial substrate concentration (dimensionless), whereas β^* indicates the substrate concentration in the reactor at which $\gamma = \gamma_{min}$. The initial conditions of Equation (28) are

$$\text{At, } \beta = \beta_0;\ \rho = 1;\ s_\phi\ (0) = \frac{d\gamma}{d\phi_i} = 0, \tag{31}$$

where, ϕ_i is one element of the parameter vector, $\boldsymbol{\phi}$.

2.2.4. Calculation of Sensitivities

The normalized objective sensitivities can be evaluated as follows:

- Equations (22)–(25) and (28) are solved simultaneously with the help of initial conditions given in Equations (26) and (31) until the γ reaches its minimum value. The corresponding values of $\rho_\beta{}^*$ and β^* wre determined;
- $\overline{s}_\phi(0)$ given by Equation (30) was calculated using the value of $\rho_\beta{}^*$ with the help of the following equation:

$$\overline{s}_\phi(0) = \frac{\overline{s}_\phi(\beta^*)}{\rho_{\beta^*}} = \frac{1}{\rho_{\beta^*}}; \tag{32}$$

- The objective sensitivity is then evaluated by solving the following equation:

$$s^*_{\phi_i} = s_{\phi_i}(0).\overline{s}_\phi(0) + \int_{\beta_0}^{\beta^*} \sigma_i.\overline{s}_\phi(\beta)d\beta, \tag{33}$$

where,

$$\sigma_i = \frac{\partial g}{\partial \phi_i} \text{ for } \beta \in (\beta_0, 1). \tag{34}$$

The expressions for σ_i and corresponding values for each ϕ_i are provided in Table 4.

Table 4. Expressions of σ_i for various parameters ϕ_i, as defined in equation (33).

ϕ_i	σ_i
pH_0	$\frac{R.\theta\left[\frac{M_2}{L}+\frac{M_1}{x}-\frac{U.\alpha}{x.R.\theta}\right]}{pH_0^2[U.\alpha+(1+\theta)\beta-1]}$
θ	$\frac{R.\theta.\beta\left[\frac{M_2}{L}+\frac{M_1}{x}-\frac{U.\alpha}{x.R.\theta}\right]}{pH_0[U.\alpha+(1+\theta)\beta-1]^2}-\frac{R\left[\frac{M_2}{L}+\frac{M_1}{x}-\frac{U.\alpha}{x.R.\theta}\right]}{pH_0[U.\alpha+(1+\theta)\beta-1]}-\frac{U.\alpha}{\theta.x.pH_0[U.\alpha+(1+\theta)\beta-1]}$
R	$-\frac{\theta\left[\frac{M_2}{L}+\frac{M_1}{x}-\frac{U.\alpha}{x.R.\theta}\right]}{pH_0[U.\alpha+(1+\theta)\beta-1]}-\frac{U.\alpha}{R.x.pH_0[U.\alpha+(1+\theta)\beta-1]}$

3. Results

3.1. Determination of Kinetic Parameters of Lactobacillus Casei in Batch Culture

At each initial pH, the maximum specific growth rate (μ_{max}) and substrate saturation constant (K_S) are determined using Equation (2). The values of normalized μ_{max}, i.e., $\mu_{max.N}$ are plotted as a function of initial pH, is shown in Figure 2. As observed from Figure 2, at pH = 6.75, (μ_{max}) reaches the maximum value, which is considered as the optimum pH for the microbial growth.

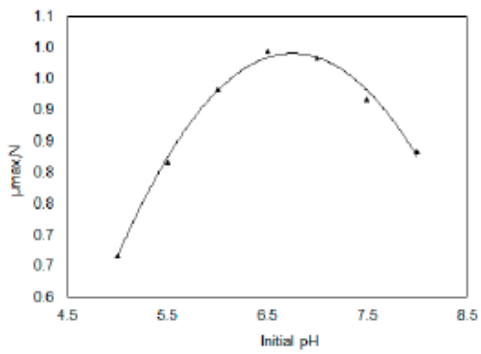

Figure 2. Variation of $\mu_{max.N}$ with respect to initial pH.

The maximum specific growth rate (μ_{max}) at optimum pH is denoted as $\mu_{max,\,opt}$. A second-order correlation is obtained, as specified in Equation (3). The different values of the constants of Equation (3) and other kinetic constants evaluated from the experiments are provided in Table 5.

Table 5. Values of kinetic parameters.

Kinetic Parameter	Value
$\mu_{max,opt}$ (h^{-1})	0.6
K_S (gL^{-1})	0.08144
$Y_{X/S}$ (gg^{-1})	0.238
$Y_{P/X}$ (gg^{-1})	3.36
$Y_{P/S}$ (gg^{-1})	0.8
A	−3.8507
B	1.434
C	−0.1062

3.2. pH Sensitivity of a Continuous Stirred Tank Bioreactor

The main objective of this analysis is to determine the parametric range of input variables at which the CSTBR system becomes vulnerable. The system behavior is demonstrated in terms of normalized objective sensitivities coefficients as a function of input parameters. The mathematical model of the system consists of the Equations (22)–(25), (28), and (33). The Equations (22)–(25) and (28) were simultaneously solved using Runga–Kutta 4th order method, and Equation (33) is solved using the trapezoidal numerical integration method. The results are illustrated in Figures 3–11. Figures 3–5 show normalized objective sensitivities of the pH-minimum, $S(\gamma^*, \phi_i)$, as a function of the input parameters, i.e., dimensionless dilution rate of base feed stream (θ), the dimensionless concentration of base, (R) and initial pH (pH_0) of the system.

In Figure 3, $S(\gamma^*, \theta)$, $S(\gamma^*, R)$, and $S(\gamma^*, pH_0)$ are plotted against the dimensionless dilution rate of the base feed stream (θ). In this mathematical operation, the input parameter (θ) was varied in the range of 0 to 1, where the values of other input parameters pH_0 and R were kept constant at 6.75 and 0.8, respectively. As the value of θ reached 0.095, the system started showing sensitivity behavior, and $S(\gamma^*, \theta)$ and $S(\gamma^*, R)$ started increasing, whereas $S(\gamma^*, pH_0)$ started decreasing. At $\theta = 0.0195$, the values of sensitivity functions attained their maxima (for $S(\gamma^*, \theta)$ and $S(\gamma^*, R)$) and minima ($S(\gamma^*, pH_0)$). Further, for the increment of θ, the sensitivity functions $S(\gamma^*, \theta)$ and $S(\gamma^*, R)$ were decreasing, and $S(\gamma^*, pH0)$ was increasing. This trend became near to 0 when θ reached a value of 0.295 and the system was again nonsensitive with respect to input parameter (θ). Therefore, the parameter range of θ is between 0.095 and 0.295, where the system becomes simultaneously sensitive. The value of θ at which the sensitivity functions attain their maxima and minima are defined as the critical value of θ.

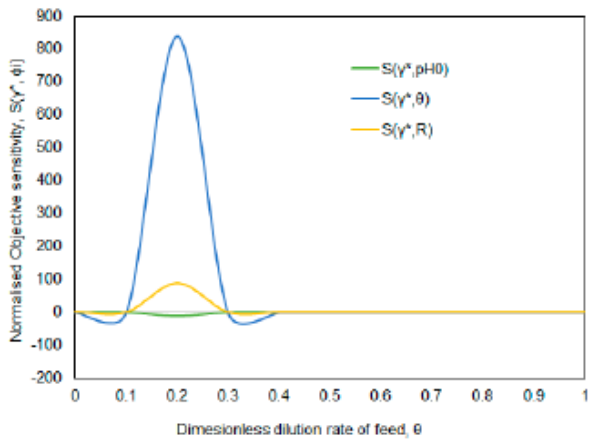

Figure 3. Normalized objective sensitivities $S(\gamma^*,\phi_i)$ as a function of base stream dilution rate θ.

Figure 4 shows the plots of $S(\gamma^*,\theta)$, $S(\gamma^*,R)$, and $S(\gamma^*,pH_0)$ versus the concentration of the base stream, (R). In this case, the dimensionless base stream concentration was varied in the range of 1 to 4 in order to observe the system behavior in terms of sensitivity functions $S(\gamma^*,\theta)$, $S(\gamma^*,R)$, and $S(\gamma^*,pH_0)$, where the values of θ and pH_0 were kept constant at 0.3 and 6.75, respectively. The system starts showing sensitivity behavior, and $S(\gamma^*,\theta)$ and $S(\gamma^*,R)$ started increasing, whereas $S(\gamma^*,pH_0)$ started decreasing from the beginning. This trend of the increment (for $S(\gamma^*,\theta)$ and $S(\gamma^*,R)$) descent (for $S(\gamma^*,pH_0)$ was observed until R reached its value of 0.48. At this R = 0.48, sensitivity functions attained their maxima (for $S(\gamma^*,\theta)$ and $S(\gamma^*,R)$) and minima ($S(\gamma^*,pH_0)$) and became near to 0 when R reached a value of 0.865. The system was again nonsensitive with respect to input parameter R at this stage. Therefore, the parameter range of R is between 0 and 0.865, where the system becomes simultaneously sensitive. The critical value of the dimensionless base stream concentration R_C is 0.48.

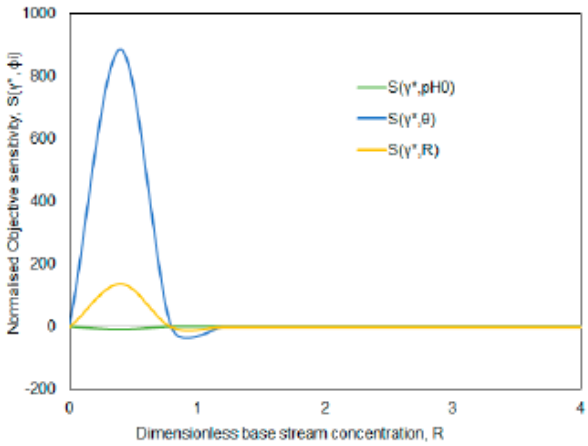

Figure 4. Normalized objective sensitivities S(γ*,ϕi) as a function of base concentration R.

The system behavior is also investigated in terms of sensitivity functions as a function of the initial pH (pH_0) of the system. The sensitivity functions S(γ*,θ), S(γ*,R), and S(γ*,pH_0) with respect to pH_0 are shown in Figure 5. Here, the pH_0 was varied in the range of 4 to 6 to observe the system behavior in terms of sensitivity functions S(γ*,θ), S(γ*,R), and S(γ*,pH_0), where the values of θ and R were kept constant at 0.5 and 8, respectively. The system did not show any sensitivity for pH_0 from 4 to 4.42. As the value of pH_0 crossed 4.42, it started showing sensitivity behavior, and S(γ*,θ) and S(γ*,R) started increasing, whereas S(γ*,pH_0) started decreasing. This movement of the increment (for S(γ*,θ) and S(γ*,R)) descent (for S(γ*,pH_0) was observed until pH_0 reached its value of 4.6. At this pH_0 = 4.6, sensitivity functions attained their maxima (for S(γ*,θ) and S(γ*,R)) and minima (S(γ*,pH_0)) and became near to 0 when pH_0 reached a value of 4.765. The system was again nonsensitive with respect to input parameter pH_0 at this stage. Therefore, the parameter range of pH_0 is between 4.42 and 4.765, where the system becomes simultaneously sensitive. The critical value of the initial system pH, pH_0 is 4.6.

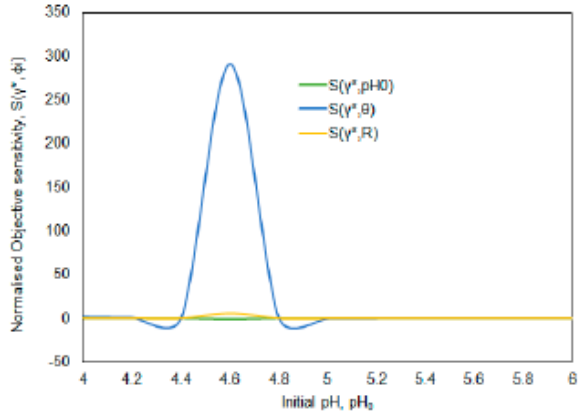

Figure 5. Normalized objective sensitivities S(γ*,ϕi) as a function of initial pH (pH_0) of the system.

Figures 6 and 7 show the nature of normalized objective sensitivity as a function of θ with the variation of R and pH_0, which is the combined effects of R and pH_0 on sensitivity function S(γ*, θ). The dimensionless input variables θ and R were varied to observe the behavior of CSTBR in terms of the

sensitivity coefficient, $S(\gamma^*, \theta)$ with constant pH_0, which is presented in Figure 6. In this case, the range of θ and R was varied from 0 to 1 and 0 to 4, respectively. The parametric zone where the system found sensitivity is provided in Table 6. The sensitive function, $S(\gamma^*, \theta)$, reached a maximum with a magnitude of 885 and the corresponding critical value of input variables is determined. The critical values of θ and R are provided in Table 6.

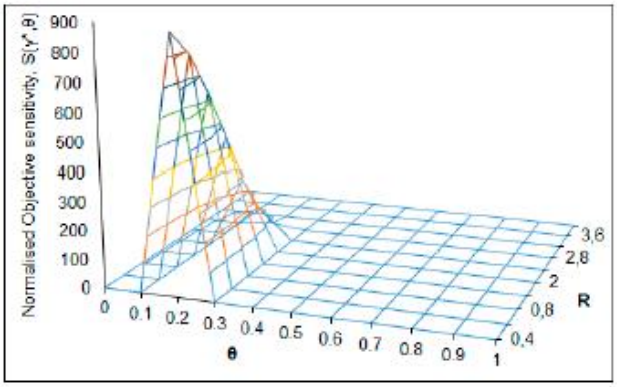

Figure 6. Normalized objective sensitivity $S(\gamma^*, \theta)$ as a function of parameters R and dilution rate base stream (θ).

The behavior of CSTBR is presented in Figure 7 in terms of the sensitivity coefficient, $S(\gamma^*, \theta)$. Figure 7 shows the variation of $S(\gamma^*, \theta)$ with respect to the initial pH (pH_0) and θ. With a fixed value of R = 0.2, the θ and pH_0 were varied from 0 to 1 and 4.8 to 7.0, respectively. The sensitive zone for CSTBR operation for θ is 0.1 to 0.3, and for pH_0 the range is between 4.8 and 6. The sensitive function, $S(\gamma^*, \theta)$, reached a maximum with a value of 735, and the corresponding critical values of input variables pH_0 and θ are determined. Table 6 provides the critical values of θ and pH_0 for this case.

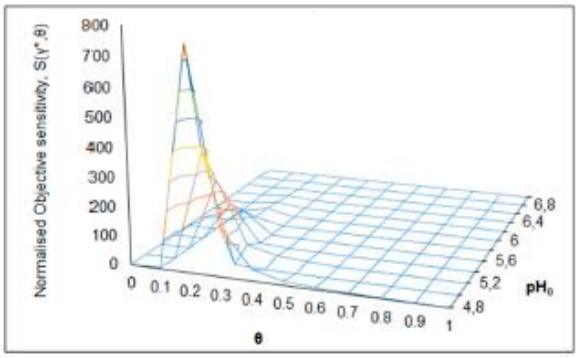

Figure 7. Normalized objective sensitivity $S(\gamma^*, \theta)$ as a function of parameters R and θ.

The nature of normalized objective sensitivity as a function of R with the variation of θ and pH_0 have shown in Figures 8 and 9 to find out the influence of θ and pH_0 on the sensitivity function, $S(\gamma^*, R)$. Figure 8 shows the critical value of R and θ at a constant initial pH, $pH_0 = 6.5$, when $S(\gamma^*, R)$ attains its maximum. The system does not show any sensitive behavior when θ goes beyond 0.7 and R = 0.75. The details of the input range and critical values of input parameters are given in Table 6.

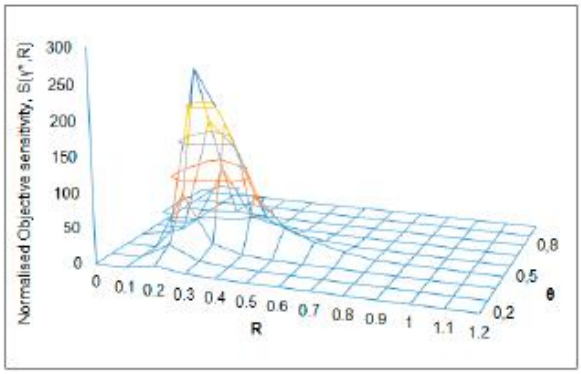

Figure 8. Normalized objective sensitivity $S(\gamma^*, R)$ as a function of parameters R and θ.

A similar trend occurred when pH_0 and R were the input variables. In this case, the range of R and pH_0 were varied from 0 to 3 and from 4 to 5, respectively. The influence of input parameters on sensitivity function $S(\gamma^*, R)$ are illustrated in Figure 9. The maximum value of sensitivity function $S(\gamma^*,R)$ is 245, and the corresponding critical values of R and pH_0 are provided in Table 6. The determined sensitive region for CSTBR with respect to R and pH_0 is 0.2 to 1.4 and 4.2 to 4.6, respectively.

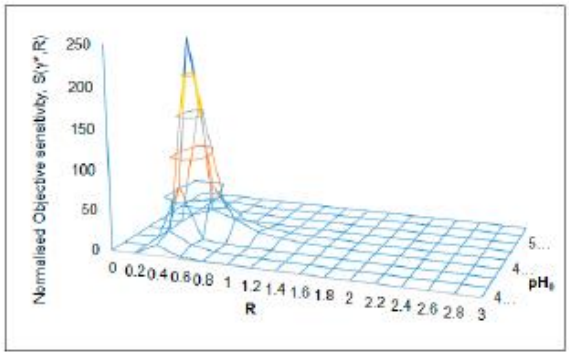

Figure 9. Normalized objective sensitivity $S(\gamma^*, R)$ as a function of parameters R and pH_0.

The behavior of normalized objective sensitivity as a function of pH_0, $S(\gamma^*, pH_0)$ with the variation of R and θ are shown in Figures 10 and 11. The influences of R and pH_0 on $S(\gamma^*, pH_0)$ at a fixed value of $\theta = 0.7$ are presented in Figure 10. From the figure, it can be observed that the sensitivity function $S(\gamma^*, pH_0)$ exhibit sensitive behavior in a negative direction. The $S(\gamma^*, pH_0)$ reached its lowest value of −7.8 when the R and pH_0 values are at 0.8 and 4.6, respectively. The sensitive region and critical values of input variables are presented in Table 6.

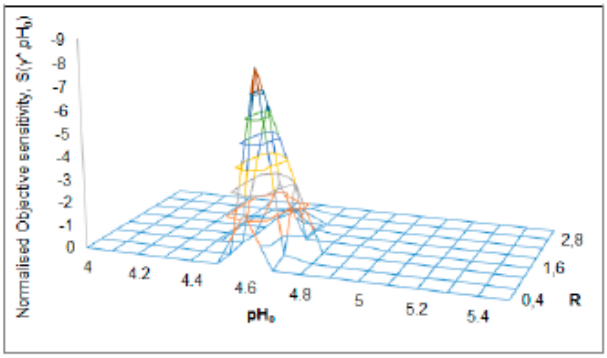

Figure 10. Normalized objective sensitivity S(γ*, pH0) as a function of parameters R and pH_0.

Similar behavior of sensitivity function, S(γ*, pH_0), was observed when pH_0 and θ were varied from 4 to 5.4 and 0 to 3, respectively, keeping R constant at 0.8. From the observation, it is found that the S(γ*, pH_0) reached its lowest value of −13.8 when the θ and pH_0 are at 0.5 and 4.6, respectively. The plot of normalized objective sensitivity S(γ*, pH_0) as a function of parameters R and θ is presented in Figure 11. The sensitive zone and the critical values of pH_0 and θ corresponding to S(γ*,pH_0) are provided in Table 6.

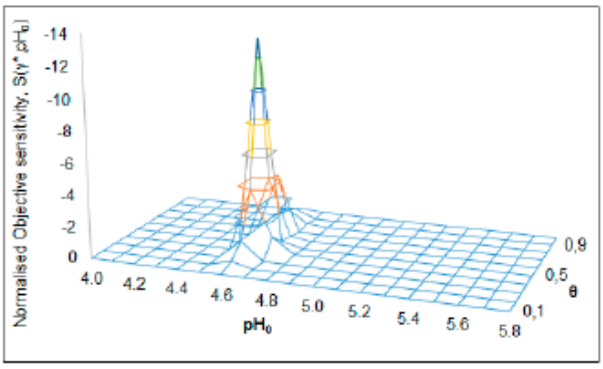

Figure 11. Normalized objective sensitivity S(γ*, pH_0) as a function of parameters pH_0 and θ.

Table 6. Different critical values of input parameters (from Figures 6–11).

Sensitivity Coefficients S(γ*, ϕ_i)	Variable Parameters (Critical Values)		Sensitive Zone of Input Variables		Fixed Parameters
S(γ*,θ) = 885 (Figure 6)	$\theta_C = 0.2$	$R_C = 0.4$	θ → 0.1–0.3	R → 0–2.4	$pH_0 = 6.75$
S(γ*,θ) = 735 (Figure 7)	$\theta_C = 0.2$	$pH_{0C} = 4.8$	θ → 0.1–0.3	pH_0 → 4.8–6.0	R = 0.2
S(γ*,R) = 285 (Figure 8)	$R_C = 0.2$	$\theta_C = 0.5$	R → 0.1–0.75	θ → 0.05–0.7	$pH_0 = 6.5$
S(γ*,R) = 245 (Figure 9)	$R_C = 0.4$	$pH_{0C} = 4.6$	R → 0.2–1.4	pH_0 → 4.2–4.6	θ = 0.3
S(γ*,pH_0) = −7.8 (Figure 10)	$pH_0 = 4.6$	$R_C = 0.8$	pH_0 → 4.5–4.8	R → 0.4–2.0	θ = 0.7
S(γ*,pH_0) = −13.8 (Figure 11)	$pH_{0C} = 4.6$	$\theta_C = 0.5$	pH_0 → 4.45–4.85	θ → 0.25–0.75	R = 0.8

4. Discussions

The influence of initial pH on microbial growth is observed in the present study through batch experiments. From the results, it is observed that initially, when the experiments conducted within the initial pH range of 5.5 to 7.5, the microbial growth is not significantly affected. Therefore, the optimum value of pH is found to be within that range of 5.5 to 7.5, which is 6.75. However, as the initial pH went

below or above that particular range, a considerable change in the microbial growth rate is observed. Therefore, the effects of pH on microbial growth are pragmatically observed.

On the other hand, from the sensitivity analysis of CSTBRs, it is found that the selected input parameters have significant influence for reactor operation. This analytical study provides a good insight at what extend these selected parameters can hinder the CSTBR operation. From Figures 3–11, it is observed that there is a zone where the system showed its undesirable behavior in terms of sensitivity coefficients. The magnitude of the input parameters pH_0, θ, and R at which the normalized objective sensitivity attain their maxima or minima are termed as critical values. The critical values of pH_{0C}, θ_C, and R_C provide the boundary separating the stable pH system from an unstable pH system sometimes defined as the pH-runaway condition [14]. The magnitude of $S(\gamma^*,\theta)$, $S(\gamma^*,R)$, and $S(\gamma^*,pH_0)$ at critical points show that the influence of initial pH (pH_0) has less impact on the sensitivity behavior compared to other input parameters, namely, R and θ.

Positive values of the objective normalized sensitivity of the pH-minimum with respect to input parameters θ and R indicate that the pH-minimum increases as the magnitude of these parameter increase. The negative value of objective normalized sensitivity of the pH-minimum with respect to pH_0 indicates that the pH-minimum increases as pH_0 decreases. Thus, if the sensitivity is positive, the transition from a stable pH system to pH-runaway behavior occurs as this parameter is increased. In contrast, if the sensitivity is negative, the same transition occurs when the corresponding parameter is decreased.

5. Conclusions

This paper presents the behavior of a CSTBR using lactic acid bacteria, namely, *L. casei*, through parametric sensitivity analysis. From the batch experiments, one can certainly observe that the microbial growth profoundly depends on the system pH. The parametric range of inputs for maintaining optimal pH range conductive for the microbial growth during reactor operation is determined. The impact of input parameters, which are directly involved in maintaining the pH of the system, is observed by determining normalized objective sensitivity of pH. A generalized criterion of sensitivity, i.e., a specific range of input parameters at which the CSTBR becomes sensitive. In the present study, pH was selected as the objective function for determining the generalized criteria. The sensitivity analysis was conducted with respect to three dimensionless input variables, dilution rate θ; base concentration, R, and initial pH, pH_0. The sensitive operating zone for CSTBR was determined in terms of sensitivity function, $S(\gamma^*,\phi_i)$, with respect to three selected input parameters. From the investigation, the sensitive zone of input parameters is from 0.095 to 0.295 for θ, from 0 to 0.865 for R, and from 4.42 to 4.765 for pH_0. Whereas, the critical values of input parameters θ, R, and pH_0 are 0.0195, 0.48, and 4.6, respectively. From this investigation, it can be concluded that the methodology implemented in the present study to define a generalized criterion to determine a parametrically sensitive regime can also be applied for any other output parameters, namely, temperature, the concentration of metabolites, and other byproducts. Thus, this mathematical model can be used as a design tool to predict CSTBR behavior and to develop control systems for the CSTBR operations.

Author Contributions: Conceptualization, S.D., R.C., and R.K.C.; formal analysis, S.D.; investigation, S.D., R.K.C., and R.C.; methodology, S.D. and R.C.; supervision, R.K.C. and R.C.; writing—original draft, S.D.; writing—review & editing, R.C. All authors have read and agreed to the published version of the manuscript.

Funding: The publication charges for this article have been funded by a grant from the publication fund of UiT The Arctic University of Norway.

Acknowledgments: The authors wish to thank the Department of Chemical Engineering, Jadavpur University, Kolkata, India, for providing laboratory facilities for this study.

Conflicts of Interest: The authors declare no conflict of interest.

References

1. Varma, A.; Morbidelli, M.; Wu, H. *Parametric Sensitivity in Chemical Systems*; Cambridge University Press: New York, NY, USA, 1999; ISBN 13-978-0-521-62171-7.
2. Bilous, O.; Amundson, N.R. Chemical reactor stability and sensitivity: II. Effect of parameters on sensitivity of empty tubular reactors. *AIChE J.* **1956**, *2*, 117–126. [CrossRef]
3. Morbidelli, M.; Varma, A. A generalized criterion for parametric sensitivity: Application to thermal explosion theory. *Chem. Eng. Sci.* **1988**, *43*, 91–102. [CrossRef]
4. Chemburkar, R.; Morbidelli, M.; Varma, A. Parametric sensitivity of a CSTR. *Chem. Eng. Sci.* **1986**, *41*, 1647–1654. [CrossRef]
5. Das, S.; Calay, R.K.; Chowdhury, R.; Nath, K.; Eregno, F.E. Product Inhibition of Biological Hydrogen Production in Batch Reactors. *Energies* **2020**, *13*, 1318. [CrossRef]
6. Latif, M.A.; Mehta, C.M.; Batstone, D.J. Influence of low pH on continuous anaerobic digestion of iste activated sludge. *Water Res.* **2017**, *113*, 42–49. [CrossRef] [PubMed]
7. Valle, B.; Aramburu, B.; Remiro, A.; Arandia, A.; Bilbao, J.; Gayubo, A.G. Optimal conditions of thermal treatment unit for the steam reforming of raw bio-oil in a continuous two-step reaction system. *Chem. Eng. Trans.* **2017**, *58*. [CrossRef]
8. Waki, M.; Yasuda, T.; Fukumoto, Y.; Béline, F.; Magrí, A. Treatment of swine istewater in continuous activated sludge systems under different dissolved oxygen conditions: Reactor operation and evaluation using modelling. *Bioresour. Technol.* **2018**, *250*, 574–582. [CrossRef] [PubMed]
9. Sayar, N.A.; Chen, B.H.; Lye, G.J.; Woodley, J.M. Modelling and simulation of a transketolase mediated reaction: Sensitivity analysis of kinetic parameters. *Biochem. Eng. J.* **2009**, *47*. [CrossRef]
10. Sayar, N.A.; Chen, B.H.; Lye, G.J.; Woodley, J.M. Process modelling and simulation of a transketolase mediated reaction: Analysis of alternative modes of operation. *Biochem. Eng. J.* **2009**, *47*, 10–18. [CrossRef]
11. Dutta, S.; Chowdhury, R.; Bhattacharya, P. Stability and response of bioreactor: An analysis with reference to microbial reduction of SO2. *Chem. Eng. J.* **2007**, *133*, 343–354. [CrossRef]
12. Dutta, S.; Chowdhury, R.; Bhattacharya, P. Parametric sensitivity in bioreactor: An analysis with reference to phenol degradation system. *Chem. Eng. Sci.* **2001**, *56*, 5103–5110. [CrossRef]
13. Morbidelli, M.; Varma, A. A generalized criterion for parametric sensitivity: Application to a pseudohomogeneous tubular reactor with consecutive or parallel reactions. *Chem. Eng. Sci.* **1989**, *44*, 1675–1696. [CrossRef]
14. Das, S.; Banerjee, A.; Chowdhury, R.; Bhattacharya, P.; Calay, R.K. Parametric sensitivity of pH and steady state multiplicity in a continuous stirred tank bioreactor (CSTBR) using a lactic acid bacterium (LAB), Pediococcus acidilactici. *J. Chem. Technol. Biotechnol.* **2016**, *91*, 1431–1442. [CrossRef]
15. Cats, A.; Kuipers, E.J.; Bosschaert, M.A.R.; Pot, R.G.J.; Vandenbroucke-Grauls, C.M.J.E.; Kusters, J.G. Effect of frequent consumption of a Lactobacillus casei-containing milk drink in Helicobacter pylori-colonized subjects. *Aliment. Pharmacol. Ther.* **2003**, *17*, 429–435. [CrossRef] [PubMed]
16. De Vrese, M. Effects of probiotic bacteria on gastrointestinal symptoms, Helicobacter pylori activity and frequency and duration of antibiotics-induced diarrhoea. *Gastroenterology* **2003**, *124*, A560. [CrossRef]
17. Miller, G.L. Use of Dinitrosalicylic Acid Reagent for Determination of Reducing Sugar. *Anal. Chem.* **1959**, *31*, 426–428. [CrossRef]
18. Pandey, A.; Koruri, S.S.; Chowdhury, R.; Bhattacharya, P. Prebiotic influence of plantago ovata on free and microencapsulated l. Casei-growth kinetics, antimicrobial activity and microcapsules stability. *Int. J. Pharm. Pharm. Sci.* **2016**, *8*, 89–97.
19. Lallai, A.; Mura, G.; Miliddi, R.; Mastinu, C. Effect of pH on growth of mixed cultures in batch reactor. *Biotechnol. Bioeng.* **1988**, *31*, 130–134. [CrossRef] [PubMed]
20. Po, H.N.; Senozan, N.M. The Henderson-Hasselbalch equation: Its history and limitations. *J. Chem. Educ.* **2001**, *78*, 1499. [CrossRef]

© 2020 by the authors. Licensee MDPI, Basel, Switzerland. This article is an open access article distributed under the terms and conditions of the Creative Commons Attribution (CC BY) license (http://creativecommons.org/licenses/by/4.0/).

Paper 3

Product Inhibition of Biological Hydrogen Production in Batch Reactors

Subhashis Das, Rajnish Kaur Calay, Ranjana Chowdhury and Kaustav Nath

Energies. 2020; Vol 13, Issue 6 pp 1318

energies

MDPI

Article

Product Inhibition of Biological Hydrogen Production in Batch Reactors

Subhashis Das [1,*], Rajnish Kaur Calay [1], Ranjana Chowdhury [2], Kaustav Nath [3] and Fasil Ejigu Eregno [1]

1 Faculty of Engineering Science and Technology, UiT-The Arctic University of Norway, 8514 Narvik, Norway; rajnish.k.calay@uit.no (R.K.C.); fasil.e.eregno@uit.no (F.E.E.)
2 Department of Chemical Engineering, Jadavpur University, Kolkata 700032, India; ranjana.juchem@gmail.com
3 Department of Biotechnology, Indian Institute of Technology, Kharagpur 721302, India; knstar.nath8@gmail.com
* Correspondence: das.subhashis@gmail.com or subhashis.das@uit.no

Received: 20 February 2020; Accepted: 10 March 2020; Published: 12 March 2020

Abstract: In this paper, the inhibitory effects of added hydrogen in reactor headspace on fermentative hydrogen production from acidogenesis of glucose by a bacterium, *Clostridium acetobutylicum*, was investigated experimentally in a batch reactor. It was observed that hydrogen itself became an acute inhibitor of hydrogen production if it accumulated excessively in the reactor headspace. A mathematical model to simulate and predict biological hydrogen production process was developed. The Monod model, which is a simple growth model, was modified to take inhibition kinetics on microbial growth into account. The modified model was then used to investigate the effect of hydrogen concentration on microbial growth and production rate of hydrogen. The inhibition was moderate as hydrogen concentration increased from 10% to 30% (*v/v*). However, a strong inhibition in microbial growth and hydrogen production rate was observed as the addition of H_2 increased from 30% to 40% (*v/v*). Practically, an extended lag in microbial growth and considerably low hydrogen production rate were detected when 50% (*v/v*) of the reactor headspace was filled with hydrogen. The maximum specific growth rate (μ_{max}), substrate saturation constant (ks), a critical hydrogen concentration at which microbial growth ceased (H_2*) and degree of inhibition were found to be 0.976 h^{-1}, 0.63 ± 0.01 gL, 24.74 mM, and 0.4786, respectively.

Keywords: hydrogen; reactor headspace; product inhibition; kinetic modelling; *clostridium acetobutylicum*

1. Introduction

Hydrogen energy is considered one of the most promising energy storage hubs and carriers of energy harvested from renewable energy sources. Hydrogen fuel cell technology, particularly, has the potential to replace fossil fuel-based internal combustion engine mainly used in the transport sector [1]. Hydrogen is the most abundant element, but it does not exist in its molecular form and has to be produced using different technologies, such as by electrolysis from water, steam reforming, and gasification of fossil fuel. All of these technologies are energy-intensive. For example, 1 kg of hydrogen (specific energy of 40 kWh/kg) requires 50–55 kWh of electricity by electrolysis of water, which is 70–80% efficient. Therefore, exploring energy-efficient hydrogen production methods from renewable sources are necessary. Biological and thermochemical processes can convert various types of biomass such as agriculture, forest sector, and bio-waste directly into hydrogen. Biological processes for hydrogen production are more environment-friendly and consume less energy compared to

thermochemical processes [2]. When using bio-waste, the production of hydrogen becomes even more cost-effective due to the utilization of low-cost waste biomass as feedstock.

The available paths of biohydrogen are typically categorized as either photo fermentation (PF) or dark fermentation (DF). PF is carried out by nonoxygenic photosynthetic bacteria, which use sunlight and biomass to produce hydrogen. DF, however, takes place under anaerobic conditions. Carbohydrate-rich biomasses, along with industrial wastes, can be used as the feedstock of DF for hydrogen production [3]. The yield of hydrogen is higher in the PF process, although there are studies [4–7] that establish that treatment capacity of organic waste and hydrogen production rate of DF is better than the PF.

Considering the potential of DF, a detailed investigation is required for scaling up the technology into industrial scale. The most critical issue that needs to be addressed is increasing the production of hydrogen, which depends on the activity of microorganisms. Production of hydrogen quantitively and qualitatively strongly depend on the metabolic pathway of microorganisms. The metabolic pathway of microorganism in DF often deviates due to the influence of certain physicochemical parameters such as substrate composition, culture pH, or concentration of byproducts of reaction medium. On the other hand, there are various research studies [7–14] that have identified the dark fermentation process parameters that influence the production of hydrogen, such as the optimal functionality of the microorganisms, hydraulic retention time, temperature, and the partial pressure of hydrogen of reaction processes. Therefore, it is possible to enrich hydrogen productivity by improving approaches to metabolic pathway control.

The primary pathway in the dark fermentation is the breakdown of carbohydrate-rich substrates to H_2 and other intermediate products such as volatile fatty acids (VFAs) and alcohols by the use of bacteria. There are a few kinds of anaerobic mesophilic or thermophilic bacteria such as genus *Clostridium*, which can produce hydrogen at a high rate, in the course of their metabolism. During fermentative hydrogen production, polysaccharides are hydrolyzed into simpler saccharides. These simpler sugars are easily taken up by hydrogen-producing bacteria (HPB) and enter the 'Embden-Meyerhof-Parnas' pathway to produce pyruvate and nicotinamide adenine dinucleotide (NADH). NADH becomes NAD^+ by donating electrons to the electron transport chain and H^+ is transported across the membrane. The major products are further formed from pyruvate and these are mainly short-chain fatty acids (e.g., acetate, butyrate, lactate) as well as alcohols (e.g., butanol, ethanol). Among these products, lactate, butanol, and ethanol have the only contribution to re-oxidized NADH. As the reactions proceed, CO_2 formed from other metabolic reactions and increases its concentration in the liquid medium. The excess CO_2 in liquid culture reacts with pyruvate using NADH to produce succinate and oxidize NADH by reducing H^+. The product formation from pyruvate is shown in Figure 1.

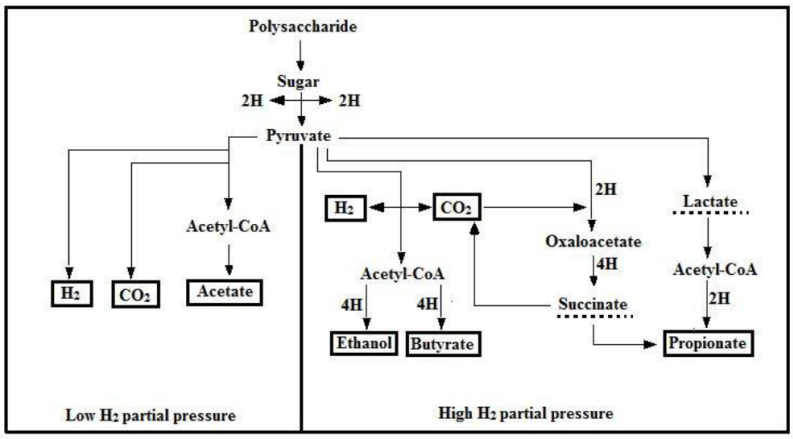

Figure 1. Metabolic pathway of H_2 formation.

On the other hand, hydrogenase, an enzyme that catalyzes the reversible oxidation of molecular hydrogen during fermentative hydrogen production, is often affected by the H_2 concentration in liquid culture. At higher H_2 partial pressure in liquid broth, the reduction of ferredoxin, which mediates electron transfer, takes place and the reduction of a proton to H_2 becomes thermodynamically less favourable, which results in a reduction of H_2 formation.

Numerous research articles have shown the inhibitory effects of hydrogen concentration in terms of partial pressure in the reactor [7–9] and these articles explain how to overcome these inhibitory effects to improve H_2 productivity. On the way to decrease partial pressure to improve H_2 productivity, several strategies were employed such as continuous gas release [6–8], larger headspace volume [9], vacuum stripping [13], or sparging with an inert gas like N_2 or CO_2 [15,16].

Different kinetic models describe the fermentation process of hydrogen production [17–19]. These models depend on physicochemical parameters and microbial environment within the reactor. Usually, these models are developed considering the effects of substrate concentration, pH, and temperature on the hydrogen production process. Kinetic models are also used to design reactors and provide proper information to adopt control strategies for hydrogen production processes. On the other hand, kinetic models are useful to describe the inhibitory effects of substrate, temperature, pH, dilution rate (in case of the continuous process), and soluble metabolites, which are generated during DF [18]. However, models that describe the effects of hydrogen accumulated in the headspace of a batch reactor on microbial growth and hydrogen production are limited. Therefore, the present study investigates the influence of hydrogen on microbial growth and evaluates how the produced hydrogen hinders the rate of production of hydrogen. The main aim of the study is to experimentally examine the adverse of produced hydrogen on microbial growth and adopted mathematical models to predict the production rate hydrogen batch reactors.

2. Materials and Methods

In order to achieve the objective, first, a series of experiments were performed in a batch reactor. A hydrogen-producing bacterium *Clostridium acetobutylicum*, which is strictly anaerobic, was selected in the present study where glucose was the sole nutrient for microbial growth. In the batch reactor operation, the headspace gas concentration, and the nutrient concentration, were varied to observe the effect of hydrogen, accumulated in the headspace on microbial growth and hydrogen production rate. Observing the nature of the batch reaction suitable microbial reaction kinetics was adopted secondly. Furthermore, the kinetic parameters were determined by using experimental data. The experimental procedure is described below.

2.1. Experiments

2.1.1. Inoculum

A pure lyophilized strain of *Clostridium Acetobutylicum* (NCIM 2337) was procured from National chemical laboratory (NCL), Pune, India. Cooked meat (CM) medium containing beef extract 45 g/L, glucose 2 g/L, peptone 20 g/L, NaCl 5 g/L was used for the growth of lyophilized bacterial culture at 37 °C for 72 h.

2.1.2. Reactor Setup for Batch Experiment

Batch experiments were conducted in 250 mL cork fitted Erlenmeyer flask having an outlet port at the bottom. A cork was fitted to a glass tube and connected to a gas measuring tube for gas sampling. The batch experimental setup is shown in Figure 2a and the whole system is presented schematically in Figure 2b.

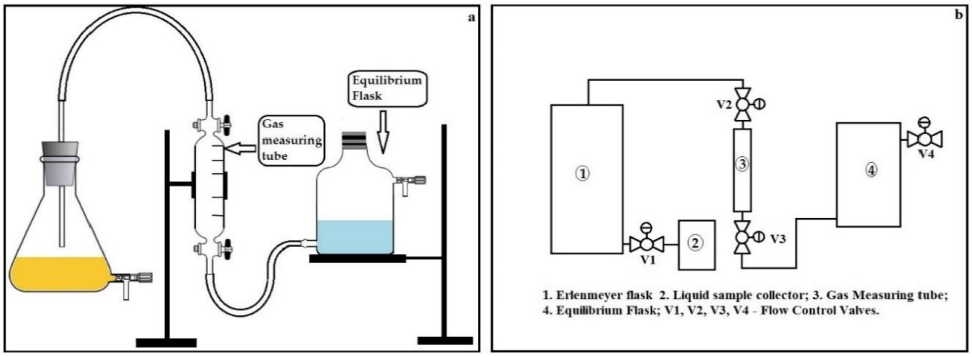

Figure 2. Experimental setup for batch test (**a**); schematic diagram of the experimental setup (**b**).

An Erlenmeyer flask was half filled with the CM medium along with 1% (*v/v*) of inoculum into the medium then remaining void was filled completely with the CM medium. The flask was then firmly sealed with the cork and 150 mL of argon gas was passed through the flask by a glass tube for displacing the CM media from the bottom of the flask. Thus, the flask was left with 100 mL of CM medium with bacterial culture and 150 mL headspace was occupied by a mixture of argon and hydrogen. The whole setup was then kept in the incubator at maintaining the temperature of 37 °C and pH of 7.2, which are the ideal conditions for this bacteria. Initial hydrogen concentration in the reactor headspace were varied in the range of 0% (*v/v*) to 50% (*v/v*). Initially, H_2 experiments were performed by varying glucose concentration of the modified CM medium in the range of 2 g/L to 5 g/L. At each initial substrate concentration, microbial growth pattern was observed for 30 h. An interval of 3 h samples were collected. The produced gas was accumulated in the reactor headspace and was taken out from the flask using a gas sampling tube, connected with the flask for examining the gas composition after each interval. Each experimental run was repeated three times to ensure the repeatability and the statistical accuracy of the results.

2.1.3. Sample Collection and Analysis

The biomass concentration of each sample was determined in terms of optical density with a spectrophotometer at 600 nm wavelength. Each liquid sample was centrifuged at 10,000 rpm and the supernatant was collected in order to find out the reducing sugar concentration using the dinitrosalicylic (DNS) acid reagent [20]. Next, 100 mL of gas was collected after every 3 h interval from the headspace of batch reactor using a gas sampling tube. Collected gas was then passed through an ORSAT apparatus for the removal of CO_2 gas present in the gas sample. Furthermore, the remaining gas composition was analyzed by gas chromatography. On a molecular sieve column (13×, 180 cm by 1/4 inch, 60–80 mesh), the gases were separated where argon was the carrier gas at 100 °C. A 406 Packard GC equipped with a thermal conductivity detector (TCD, 100 mA) was used to measure hydrogen concentration.

2.2. Kinetic Modelling

Herein, we consider the Monod model, which is the most popular and simplest model for describing the microbial reaction of microbial growth within a single substrate. The reaction kinetics are expressed as:

$$\text{Substrate(S)} \xrightarrow{\text{Cell(X)}} \text{more Cells(X)} + \text{Product } (H_2) \tag{1}$$

the rate of reaction will be:

$$r_c = \frac{dX}{dt} = \frac{\mu_{max} S}{k_S + S} X \tag{2}$$

where, r_c is the microbial growth rate, ($gL^{-1}h^{-1}$); X is the dry cell concentration, (gL^{-1}); t is time, (h); μ_{max} is the maximum specific growth rate of cells, (h^{-1}); S is the substrate concentration, (gL^{-1}); and k_s is the Monod constant or substrate saturation constant, (gL^{-1}).

The inhibition in microbial growth occurs typically due to the excess presence of substrate, product, or other inhibitory substance in the cell growth medium. Hans and Levenspiel [21] express the inhibition of microbial growth model as:

$$\frac{dX}{dt} = \mu_{max}\left(1 - \frac{H_2}{H_2^*}\right)^n \left(\frac{S \cdot X}{S + k_s\left(1 - \frac{X}{X^*}\right)^m}\right) \tag{3}$$

where, H_2* is the critical molar concentration of hydrogen at which microbial reaction ceases, (M); n is the degree of inhibition; and m is the degree of inhibition.

Evaluation of the Constants

Taking inhibition of microbial growth Equation (3) into account, Equation (2) can be expressed as a generalized Monod model:

$$\mu = \frac{\mu_{max,obs} \cdot S}{k_{s,obs} + S} \tag{4}$$

where, μ is the pecific microbial growth rate (h^{-1}) and $_{obs}$ is the experimentally observed value.

$$\mu = \frac{1}{X} \cdot \frac{dX}{dt} \tag{5}$$

$$\mu_{max,obs} = \mu_{max}\left(1 - \frac{H_2}{H_2^*}\right)^n \tag{6}$$

$$k_{s,obs} = k_s\left(1 - \frac{X}{X^*}\right)^m \tag{7}$$

By reciprocating Equation (4),

$$\frac{1}{\mu} = \frac{k_{s,obs}}{\mu_{max,obs}} \cdot \frac{1}{S} + \frac{1}{\mu_{max,obs}} \tag{8}$$

plots of $1/\mu$ and $1/S$ can be obtained at each initially added hydrogen in reactor headspace, which is shown in the Figure 3. $\mu_{max,obs}$ and $k_{s,obs}$ at each headspace H_2 concentration can be determined by evaluating the intercepts and abscissas on Figure 3.

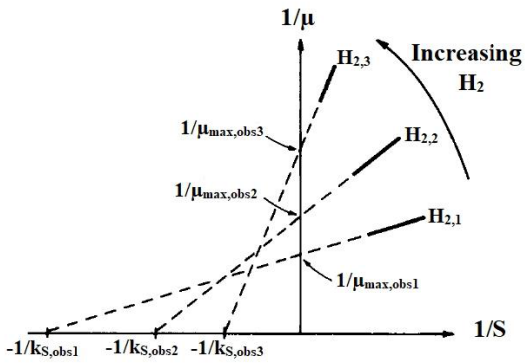

Figure 3. Evaluation procedure of $\mu_{max,obs}$ and $k_{s,obs}$ at various concentration of inhibitor; Reproduced with permission from Keehyun Han and Octave Levenspiel, Biotechnology & Bioengineering; published by John Wiley and Sons, 2004 [21].

After determining values of $\mu_{max,obs}$ and $k_{s,obs}$ at different headspace H_2 concentration, constants in Eqation (3) can be evaluated. On taking logarithms of Eqation (5) i.e.,

$$\ln\left(\mu_{max,obs=}\right) = n \cdot \ln\left(1 - \frac{H_2}{H_2^*}\right) + \ln\left(\mu_{max}\right) \tag{9}$$

a plot of $\ln(\mu_{max,obs})$ and $\ln(1-H_2/H_2^*)$ gives the values of μ_{max} and n. If the values of H_2^* is not identified from the experiments then a guessed value of H_2^* have to be has to be considered. A corrected value of H_2^* can be determined until a straight line is obtained which is shown in Figure 4.

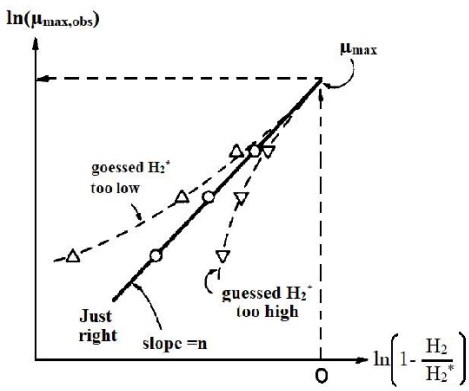

Figure 4. Evaluation procedure of μ_{max}, n and H_2^* for product inhibition; Reproduced with permission from Keehyun Han and Octave Levenspiel, Biotechnology & Bioengineering; published by John Wiley and Sons, 2004 [21].

3. Results

3.1. Effects of Added H_2 in the Reactor Headspace

Effects of hydrogen concentration accumulated in the reactor headspace on microbial growth and hydrogen production were studied by conducting experiments in batch reactor. The results were shown in Figures 5–10. In these figures, the time history of biomass concentration and produced hydrogen concentration were showed when initial hydrogen concentration in the reactor headspace

was varied. From these figures, it is clear that microbial growth as well as hydrogen productivity were greatly influenced by the presence of hydrogen in the reactor headspace.

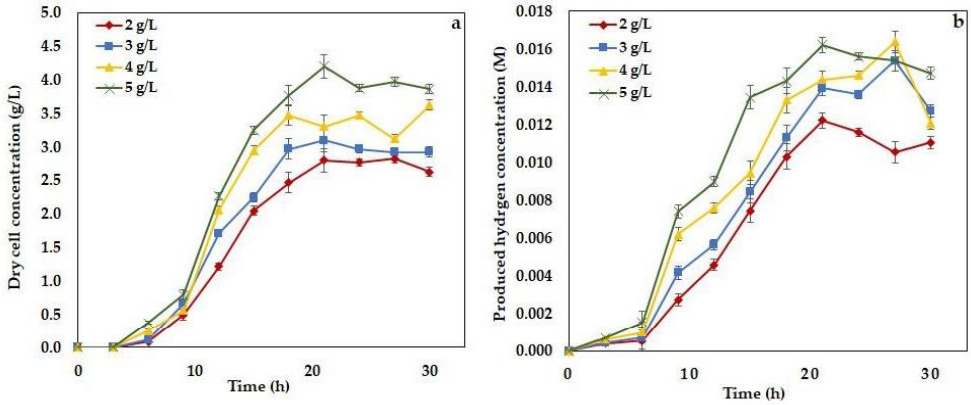

Figure 5. Experimental time histories of dry cell concentration (a) and hydrogen concentration (b) with initial 0% H_2 in reactor headspace at different substrate concentration.

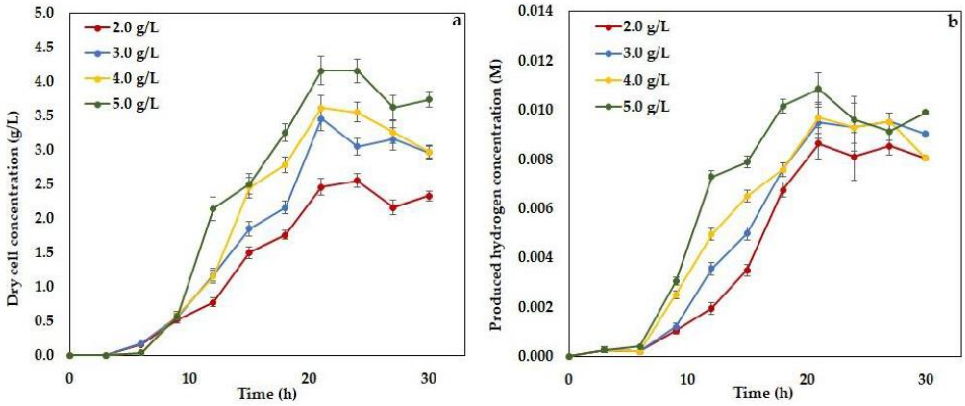

Figure 6. Experimental time histories of dry cell concentration (a) and hydrogen concentration (b) with initial 10% H_2 in reactor headspace at different substrate concentration.

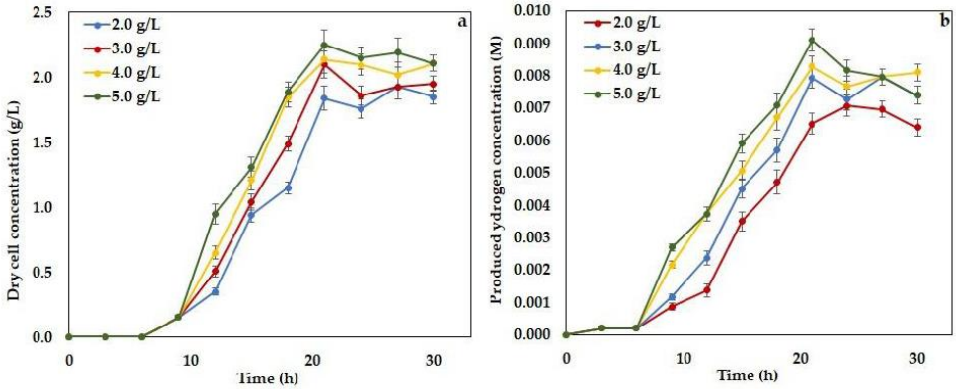

Figure 7. Experimental time histories of dry cell concentration (a) and hydrogen concentration (b) with initial 20% H_2 in reactor headspace at different substrate concentration.

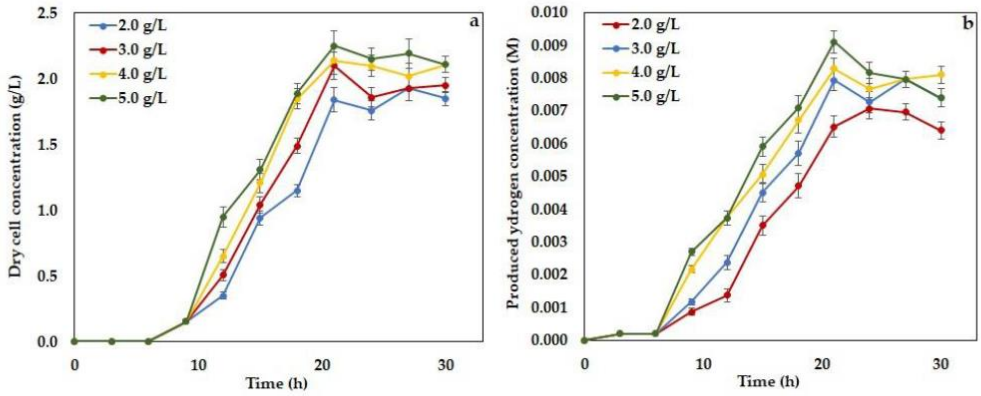

Figure 8. Experimental time histories of dry cell concentration (a) and produced hydrogen concentration (b) with initial 30% (*v*/*v*) H_2 in reactor headspace at different substrate concentration.

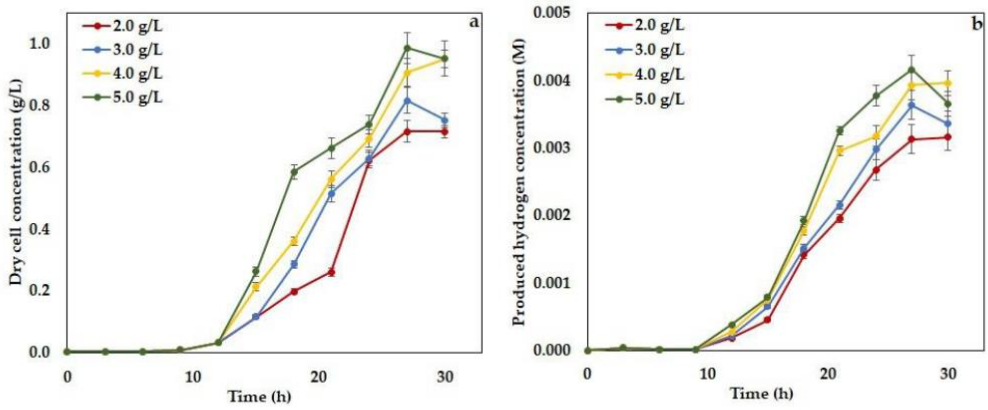

Figure 9. Experimental time histories of dry cell concentration (a) and hydrogen concentration (b) with initial 40% H_2 in reactor headspace at different substrate concentration.

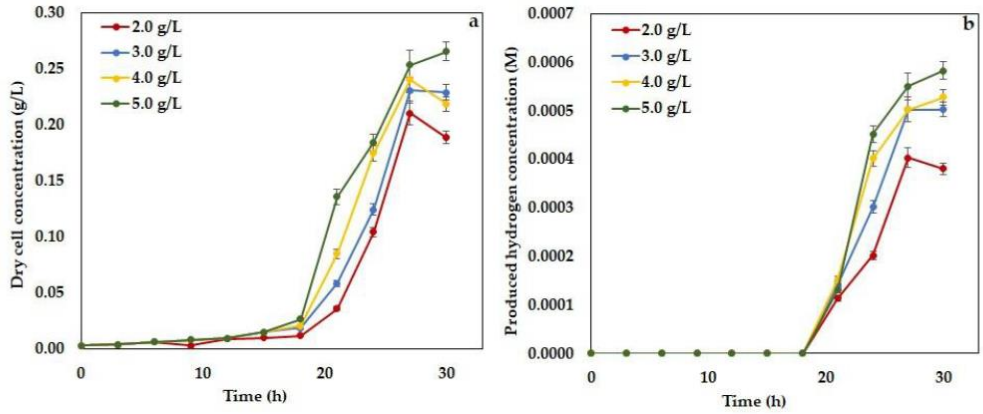

Figure 10. Experimental time histories of dry cell concentration (a) and hydrogen concentration (b) with initial 50% H_2 in reactor headspace at different substrate concentration.

Initially, experiments were started when argon gas was present in the reactor headspace and initial glucose concentration in the liquid medium was varied in the range of 2 g/L to 5 g/L. At each variation of glucose, the microbial growth pattern and hydrogen production rate were observed for 30 h. The time histories of microbial growth and hydrogen production rate were presented in Figure 5. From this figure, it is observed that microbial growth, as well as hydrogen production, was started immediately after 3 h of reaction time. There was no significant lag phase of microbial growth detected. A stationary phase was started at 21 h for every initial glucose concentration. The maximum productivity of hydrogen was 7.81 $mML^{-1}h^{-1}$ when initial glucose concentration in the liquid medium was 5 g/L.

On the other hand, when 10% (*v/v*) of H_2 added to reactor headspace, microbial growth and hydrogen production started after 6 h of incubation time, which is shown in Figure 6. Although there was no such difference in specific growth and hydrogen production observed for different initial substrate concentration, the maximum hydrogen productivity decreased to 5.17 $mML^{-1}h^{-1}$, which is comparable to the 0% (*v/v*) added H_2 condition. The exponential phase of microbial growth ended at 21 h which was same as the previous condition.

In the case of 20% (*v/v*) added H_2 in the reactor headspace, the hydrogen production rate as well as biomass production rate further decreased, which can be observed from Figure 7. In this condition, propagation of hydrogen production and bacterial growth was quite similar to that of 10% (*v/v*) added H_2 condition, where microbial growth reached at its exponential phase at 6 h and it extended up to 21 h. However, in this condition, maximum hydrogen productivity decreased to 4.33 $mML^{-1}h^{-1}$.

A different phenomenon was observed when 30% (*v/v*) H_2 was added to the reactor headspace. In this case, exponential phase of bacterial growth started after 6 h of incubation time but it extended to 24 h where the stationary phase started. The time histories of dry cell concentration and produced hydrogen were presented in Figure 8. Monotonic decreases of microbial growth rate and hydrogen production were observed where hydrogen productivity reduced to 3.075 $mML^{-1}h^{-1}$ when initial substrate concentration in liquid medium was 5 g/L. However, there was no such significant change in growth pattern observed for different substrate concentration in liquid medium.

An extended lag phase in microbial growth was noticed as the quantity initially added H_2 increased from 30% (*v/v*) to 40% (*v/v*). At this condition, the exponential phase commenced at 12 h of incubation time and extended until 27 h. A sharp degradation in microbial growth, as well as biohydrogen production, were also observed (Figure 9). There were no such effects of substrate concentration in liquid medium experience. The hydrogen productivity in this condition was estimated as 1.54 $mML^{-1}h^{-1}$, which is a sharp alteration compared to 30% (*v/v*) added H_2 condition.

Furthermore, when 50% (*v/v*) H_2 was added to the reactor headspace, almost no growth condition was observed which is presented in Figure 10. In this case, an extended lag phase with no microbial growth and hydrogen production was seen for 18 h. A short period of exponential phase ended at 27 h was noticed. Almost no hydrogen production condition with productivity of 0.19 $mML^{-1}h^{-1}$ was estimated.

3.2. Inhibition Kinetics

In the present investigation, a total of 24 experimental runs were conducted at different initial H_2 and substrate concentration. Each initially added H_2 concentration and substrate concentration, and was varied from 2 g/L to 5 g/L. For each combination of H_2 concentration and substrate concentration, specific growth rate microorganisms were determined. By using Equation (8), plots of $1/\mu$ and $1/S$ were obtained at each initially added hydrogen in reactor headspace, which is demonstrated in Figure 11. $\mu_{max,obs}$ and $k_{s,obs}$ at each headspace H_2 concentration were determined by evaluating the intercepts and abscissas on Figure 3. The values of $\mu_{max,obs}$ and $k_{s,obs}$ are provided in the Table 1.

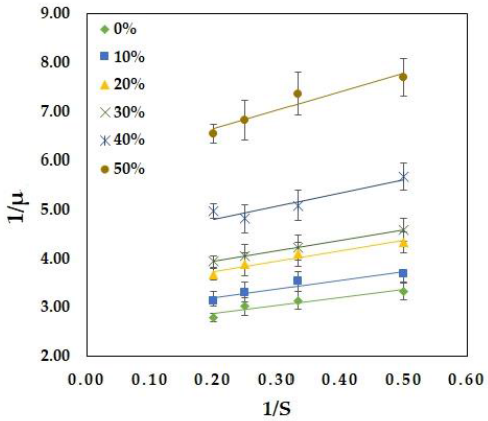

Figure 11. Determination of $\mu_{max,obs}$ and $k_{s,obs}$ at different initial concentration of H_2.

Table 1. Values of observed rate constants from experiments.

Initial H_2 Concentration in Reactor Headspace (*v/v*)	$\mu_{max,obs}$	$k_{s,obs}$
0%	0.6209	0.6318
10%	0.5523	0.6395
20%	0.4792	0.6285
30%	0.4643	0.6141
40%	0.3695	0.6343
50%	0.2613	0.6521

From Table 1, it can be observed that $k_{s,obs}$ does not change in any systematic manner with the change of added hydrogen in the reactor headspace. Therefore, m = 0 in Equation (7), which infers the adopted model is a noncompetitive inhibition model and $k_{s,obs}$ = ks which will be constant.

After determining values of $\mu_{max,obs}$ and $k_{s,obs}$ at different headspace H_2 concentration, constants in Equation (3) can be evaluated by plotting $\ln(\mu_{max,obs})$ vs $\ln(1-H_2/H_2^*)$ from Equation (9), which is shown in Figure 12. Figure 12 gives the values of μ_{max} and n. As H_2^* was not identified from the experiments, a guessed value of 61.5 (*v/v*) H_2^* (24.74 mM) was considered, which gives a straight line with $R^2 = 0.9823$. From Figure 12, the intercept and slope give the value of $\mu_{max} = 0.976\ h^{-1}$ and n = 0.4786.

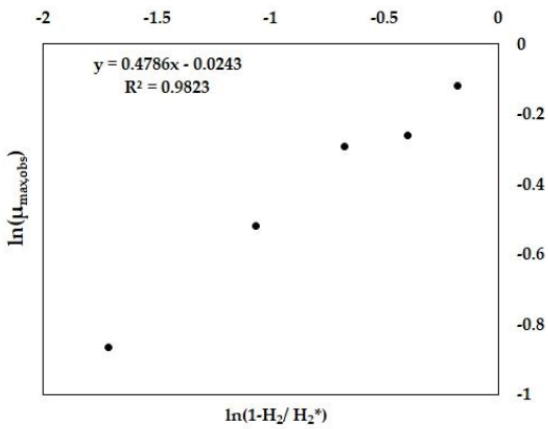

Figure 12. Determination of μ_{max}, n, and H_2^* for product inhibition.

4. Discussion

Initially, when there was no hydrogen present in the headspace and the reactor substrate concentration varied from 2 g/L to 5 g/L, the production rates were high and it significantly decreased as the hydrogen concentration increased gradually. When no hydrogen was added to the reactor, the growth phase started after 3 h of incubation time and reached the stationary phase at 21 h. For the 10% added hydrogen condition, the exponential phase started at 6 h and it went until 21 h. On the other hand, when 20% and 30% hydrogen were added, the exponential phase started at 6 h and went until 24 h. Further, when increasing hydrogen concentration by 40% of total headspace, the lag phase elongated by 12 h and the growth phase started at 15 h until 27 h. Almost no growth of bacteria was observed when 50% of the reactor headspace filled with hydrogen. The specific growth rate of biomass decreased as the hydrogen concentration increased in the reactor headspace.

This increased hydrogen concentration reduced the glucose degradation efficiency of bacteria, resulting in a lower hydrogen yield. Hydrogen yield gradually decreased along with specific the growth rate from 1.11 to 0.56 mol/mol.glucose and 0.621 ± 0.019 h^{-1} to 0.261 ± 0.021 h^{-1}, respectively. As the initial hydrogen concentration increases from 0.0 to 0.0161 M, the hydrogen productivity depletion becomes more rapid when the initial hydrogen concentration altered from 0.0161 M to 0.0201 M. Thus, the final partial pressure of hydrogen in the product gas declined and initially added hydrogen concentration increased. The effect of added hydrogen in the reactor on the specific microbial growth rate, final hydrogen concentration and hydrogen yield were calculated by dividing the total amount hydrogen produced by the amount of glucose consumed are summarized in Table 2.

Table 2. Effects of added hydrogen on specific growth rate, hydrogen production.

Added Hydrogen (M)/(*v*/*v*)	Specific Growth Rate (h^{-1})	Hydrogen Yield (mol-H_2/mol-glucose)	Final H_2 Partial Pressure (atm)
0.0/(0%)	0.621 ± 0.019	1.11 ± 0.0026	0.280 ± 0.015
4.023×10^{-3} (10%)	0.552 ± 0.028	1.01 ± 0.0020	0.229 ± 0.005
8.045×10^{-3} (20%)	0.479 ± 0.029	0.92 ± 0.0022	0.214 ± 0.008
1.207×10^{-2} (30%)	0.464 ± 0.032	0.88 ± 0.0016	0.165 ± 0.013
1.610×10^{-2} (40%)	0.369 ± 0.015	0.56 ± 0.0010	0.094 ± 0.005
2.012×10^{-2} (50%)	0.261 ± 0.021	0.21 ± 0.0010	0.0127 ± 0.003

From the current study, it is apparent to see that as hydrogen concentration increases in the reactor headspace, it restricts the mass transfer from the liquid to the gaseous phase. Thus, liquid to gas transfer becomes a rate-limiting step that dominates microbial reactions. Consequently, low microbial growth and less hydrogen production occur. On the other hand, hydrogenase, which mobilizes the reversible oxidation of molecular hydrogen, is affected by a high concentration of hydrogen and the process becomes thermodynamically unfavorable for H_2 formation.

From this analysis, it is clear that the initial addition of hydrogen has a significant impact on microbial growth, hydrogen yield, and hydrogen productivity. As per non-competitive inhibition is concerned, substrate concentration neither influences specific growth rate nor substrate utilization. In order to maintain the hydrogen production at an optimal level, the accumulated hydrogen in reactor headspace should not be more than 8 mMol. It can also be concluded from the present study that when 24.85 mMol hydrogen accumulated in the reactor headspace, reaction stopped and no hydrogen was produced.

5. Conclusions

Growth inhibition caused by hydrogen was examined through the acidogenesis of glucose by a bacterium, *Clostridium acetobutylicum*. Until now, the research showed that the inhibition is caused by H_2 present in the liquid medium, whereas kinetic models are developed to describe how that inhibition kinetically related to hydrogen production rate but not microbial growth rate. This study

presented the kinetic model that describes how the microbial growth inhibited H_2 in the reactor headspace. The experiments were conducted in a batch reactor to observe the effects of hydrogen accumulated in the reactor headspace on hydrogen production from acidogenesis of glucose by a bacterium, *Clostridium acetobutylicum*. The concluding remarks can be made based on the data of the experiments and prediction of the kinetic model.

A nonlinear and non-competitive inhibition model described the inhibition kinetics of initially added hydrogen concentration on microbial growth and hydrogen production. The maximum specific growth rate (μ_{max}), substrate saturation constant (ks) critical added hydrogen concentration at which microbial growth ceased (H_2*), and degree of inhibition were found to be 0.976 h^{-1}, 0.63 ± 0.01 g/L, 24.74 mM, and 0.4786, respectively. It was observed from the experiment that hydrogen could be an acute inhibitor if allowed to accumulate in reactor headspace. From 10% to 30% (*v/v*) concentration of hydrogen concentration, the microbial growth was decreased linearly. However, as more hydrogen was added in the headspace, microbial activity was inhibited exponentially, particularly after 30% (*v/v*), where there was a potent inhibition in microbial growth and hydrogen production rate. Practically, an extended lag phase in microbial growth and considerably low microbial growth and hydrogen production rate was detected when 50% of total reactor headspace filled with hydrogen. After 61.5% (*v/v*) (i.e., 24.74 mM) of hydrogen accumulated in the reactor, no microbial growth took place and production of hydrogen and microbial growth ceased. Furthermore, different process industries such as biohydrogen and biobutanol production can use the results obtained from the present study for reactor safety and adaptation of control strategies where these kinds of phenomenon occur.

Author Contributions: Conceptualization, S.D., R.C. and R.K.C.; Formal analysis, K.N.; Investigation, S.D., R.C. and R.C.; Methodology, R.C. and K.N.; Supervision, R.K.C. and R.C.; Writing—original draft, S.D.; Writing—review & editing, R.C. and F.E.E. All authors have read and agreed to the published version of the manuscript.

Funding: The publication charges for this article have been funded by a grant from the publication fund of UiT The Arctic University of Norway.

Acknowledgments: The authors wish to thank the Department of Chemical Engineering, Jadavpur University, Kolkata, India, for providing laboratory facilities for this study.

Conflicts of Interest: The authors declare no conflict of interest.

References

1. Offer, G.J.; Howey, D.; Contestabile, M.; Clague, R.; Brandon, N.P. Comparative analysis of battery electric, hydrogen fuel cell and hybrid vehicles in a future sustainable road transport system. *Energy Policy* **2010**, *38*, 24–29. [CrossRef]
2. Sivagurunathan, P.; Kumar, G.; Bakonyi, P.; Kim, S.H.; Kobayashi, T.; Xu, K.Q.; Lakner, G.; Tóth, G.; Nemestóthy, N.; Bélafi-Bakó, K. A critical review on issues and overcoming strategies for the enhancement of dark fermentative hydrogen production in continuous systems. *Int. J. Hydrog. Energy* **2016**, *41*, 3820–3836. [CrossRef]
3. Das, D.; Veziroglu, T. Advances in biological hydrogen production processes. *Int. J. Hydrog. Energy* **2008**, *33*, 6046–6057. [CrossRef]
4. Zhang, T.; Jiang, D.; Zhang, H.; Jing, Y.; Tahir, N.; Zhang, Y. Comparative study on bio-hydrogen production from corn stover: Photo-fermentation, dark-fermentation and dark-photo co-fermentation. *Int. J. Hydrog. Energy* **2020**, *45*, 3807–3814. [CrossRef]
5. Hay, J.X.W.; Wu, T.Y.; Juan, J.C.; Md. Jahim, J. Biohydrogen production through photo fermentation or dark fermentation using waste as a substrate: Overview, economics, and future prospects of hydrogen usage. *Biofuels Bioprod. Biorefin.* **2013**, *7*, 334–352. [CrossRef]
6. Eker, S.; Sarp, M. Hydrogen gas production from waste paper by dark fermentation: Effects of initial substrate and biomass concentrations. *Int. J. Hydrog. Energy* **2017**, *42*, 2562–2568. [CrossRef]
7. Levin, D.B.; Pitt, L.; Love, M. Biohydrogen production: Prospects and limitations to practical application. *Int. J. Hydrog. Energy* **2004**, *29*, 173–185. [CrossRef]
8. Guo, X.M.; Trably, E.; Latrille, E.; Carrre, H.; Steyer, J.P. Hydrogen production from agricultural waste by dark fermentation: A review. *Int. J. Hydrog. Energy* **2010**, *35*, 10660–10673. [CrossRef]

9. Oh, S.E.; Zuo, Y.; Zhang, H.; Guiltinan, M.J.; Logan, B.E.; Regan, J.M. Hydrogen production by *Clostridium acetobutylicum* ATCC 824 and megaplasmid-deficient mutant M5 evaluated using a large headspace volume technique. *Int. J. Hydrog. Energy* **2009**, *34*, 9347–9353. [CrossRef]
10. Logan, B.E.; Oh, S.E.; Kim, I.S.; Van Ginkel, S. Biological hydrogen production measured in batch anaerobic respirometers. *Environ. Sci. Technol.* **2002**, *36*, 2530–2535. [CrossRef]
11. Chang, S.; Li, J.; Liu, F.; Yu, Z. Effect of different gas releasing methods on anaerobic fermentative hydrogen production in batch cultures. *Front. Environ. Sci. Eng. China* **2012**, *6*, 901–906. [CrossRef]
12. Esquivel-Elizondo, S.; Chairez, I.; Salgado, E.; Aranda, J.S.; Baquerizo, G.; Garcia-Peña, E.I. Controlled Continuous Bio-Hydrogen Production Using Different Biogas Release Strategies. *Appl. Biochem. Biotechnol.* **2014**, *173*, 1737–1751. [CrossRef] [PubMed]
13. Foglia, D.; Wukovits, W.; Friedl, A.; De Vrije, T.; Claassen, P.A.M. Fermentative hydrogen production: Influence of application of mesophilic and thermophilic bacteria on mass and energy balances. *Chem. Eng. Trans.* **2011**, *25*, 815–820.
14. Rafieenia, R.; Pivato, A.; Schievano, A.; Lavagnolo, M.C. Dark fermentation metabolic models to study strategies for hydrogen consumers inhibition. *Bioresour. Technol.* **2018**, *267*, 445–457. [CrossRef]
15. Kim, D.-H.; Shin, H.-S.; Kim, S.-H. Enhanced H2 fermentation of organic waste by CO2 sparging. *Int. J. Hydrog. Energy* **2012**, *37*, 15563–15568. [CrossRef]
16. Nguyen, T.A.D.; Han, S.J.; Kim, J.P.; Kim, M.S.; Sim, S.J. Hydrogen production of the hyperthermophilic eubacterium, Thermotoga neapolitana under N2sparging condition. *Bioresour. Technol.* **2010**, *101*, 38–41. [CrossRef]
17. Saady, N.M.C. Homoacetogenesis during hydrogen production by mixed cultures dark fermentation: Unresolved challenge. *Int. J. Hydrog. Energy* **2013**, *38*, 13172–13191. [CrossRef]
18. Wang, J.; Wan, W. Kinetic models for fermentative hydrogen production: A review. *Int. J. Hydrog. Energy* **2009**, *34*, 3313–3323. [CrossRef]
19. Bundhoo, M.A.Z.; Mohee, R. Inhibition of dark fermentative bio-hydrogen production: A review. *Int. J. Hydrog. Energy* **2016**, *41*, 6713–6733. [CrossRef]
20. Miller, G.L. Use of Dinitrosalicylic Acid Reagent for Determination of Reducing Sugar. *Anal. Chem.* **1959**, *31*, 426–428. [CrossRef]
21. Han, K.; Levenspiel, O. Extended monod kinetics for substrate, product, and cell inhibition. *Biotechnol. Bioeng.* **1988**, *32*, 430–447. [CrossRef] [PubMed]

© 2020 by the authors. Licensee MDPI, Basel, Switzerland. This article is an open access article distributed under the terms and conditions of the Creative Commons Attribution (CC BY) license (http://creativecommons.org/licenses/by/4.0/).

Appendix 2

Following the mathematical analysis provided under steady state,

$$\frac{dx}{d\tau} = 0 \tag{A1}$$

Therefore eq.(4.13)

$$\theta = \theta_1 + 1 \tag{A2}$$

Using eq. (4.18)

$$\theta_1 + 1 = \frac{my_s}{n+y_s} H \tag{A3}$$

Hence,

$$y_s = \frac{n(\theta_1 + 1)}{mH - (\theta_1 + 1)} \tag{A4}$$

And,

$$x_s = \left[\frac{1}{\theta_1 + 1} - \frac{n(\theta_1 + 1)}{mH - (\theta_1 + 1)}\right] \tag{A5}$$

Under steady state eq. (4.15)

$$0 = -z + \theta x - \theta_1 \left(\frac{M_a}{M_b Yp_{/s}} R + z\right) \tag{A6}$$

Defining

$$p_m = \frac{\theta_1}{(\theta_1 + 1)} \frac{M_a}{M_b Yp_{/s}} R \tag{A7}$$

$$\theta x = (\theta_1 + 1)(z + p_m) \tag{A8}$$

$$pH = -\log K_a + \log \frac{L_s}{Z_s} \frac{M_a}{M_c} \frac{1}{Yp_{/s}} \tag{A9}$$

Under steady state,

$$z_s = \frac{L_s M_a}{M_c K_a Yp_{/s}} e^{-\frac{pH}{2.303}} \tag{A10}$$

From eq. (4.16).

$$L_s = \frac{\theta_1}{\theta_1 + 1} \frac{M_c}{M_b} R = \frac{M_c}{M_a} Yp_{/s} p_m \tag{A11}$$

$$z_s = \frac{p_m}{K_a} e^{-\frac{pH}{2.303}} \tag{A12}$$

On replacement of x_S, y_S and z_S in eq. (A.8), using equations (A.4), (A.5) and (A.12) respectively, and the following correlation is obtained

$$\frac{m*\frac{n(\theta_1+1)}{mH-(\theta_1+1)}}{n+\frac{n(\theta_1+1)}{mH-(\theta_1+1)}}*H*\left(\frac{1}{(\theta_1+1)}-\frac{n(\theta_1+1)}{mH-(\theta_1+1)}\right)=(\theta_1+1)(z_s+p_m) \quad \text{(A13)}$$

On simplification, the above equation reduces to

$$\left(\frac{1}{(\theta_1+1)}+\frac{n}{1-\frac{mH}{(\theta_1+1)}}\right)=z_s+p_m \quad \text{(A14)}$$

By Taylor series expansion of $\left(1-\frac{mH}{\theta_1+1}\right)^{-1}$ and neglecting higher terms,

$$\frac{1}{(\theta_1+1)}+n\left(1+\frac{mH}{(\theta_1+1)}\right)=p_m\left(1+\frac{1}{K_a}e^{-\frac{pH}{2.303}}\right) \quad \text{(A15)}$$

Incorporating, $M=\frac{1}{\theta_1+1}$ and substituting $H=A+BpH+CpH^2$ in equation (A.15)

$$\left(M+n(1+Mm(A+BpH+CpH^2)-p_m)\frac{K_a}{p_m}\right)=e^{-\frac{pH}{2.303}} \quad \text{(A16)}$$

Defining the constants,

$\alpha=(M+n(1+mMA)-p_m)\frac{K_a}{p_m}$, $\beta=(nmMB)\frac{K_a}{p_m}$ and $\gamma=(nmMC)\frac{K_a}{p_m}$

$$e^{-\frac{pH}{2.303}}=\alpha+\beta pH+\gamma pH^2 \quad \text{(A17)}$$

Sensitivity trajectories

$$\frac{d}{dt}\left(\frac{\partial X}{\partial D}\right)=\left(\frac{\mu_m S(A+BpH+CpH^2)}{K_s+S}-D-D_1\right)\times\left(\frac{\partial X}{\partial D}\right)+\left[\frac{\mu_m X.K_s(A+BpH+CpH^2)}{(K_s+S)^2}\right]\times\left(\frac{\partial S}{\partial D}\right)+\left[\frac{\mu_m S.X(B+2CpH)}{K_s+S}\right]\times\left(\frac{\partial pH}{\partial D}\right)-X \quad \text{(A18)}$$

$$\frac{d}{dt}\left(\frac{\partial X}{\partial D_1}\right)=\left(\frac{\mu_m S(A+BpH+CpH^2)}{K_s+S}-D-D_1\right)\times\left(\frac{\partial X}{\partial D_1}\right)+\left[\frac{\mu_m X.K_s(A+BpH+CpH^2)}{(K_s+S)^2}\right]\times\left(\frac{\partial S}{\partial D_1}\right)+\left[\frac{\mu_m S.X(B+2CpH)}{K_s+S}\right]\times\left(\frac{\partial pH}{\partial D_1}\right)-X \quad \text{(A19)}$$

$$\frac{d}{dt}\left(\frac{\partial X}{\partial S_0}\right)=\left(\frac{\mu_m S(A+BpH+CpH^2)}{K_s+S}-D-D_1\right)\times\left(\frac{\partial X}{\partial S_0}\right)+\left[\frac{\mu_m X.K_s(A+BpH+CpH^2)}{(K_s+S)^2}\right]\times\left(\frac{\partial S}{\partial S_0}\right)+\left[\frac{\mu_m S.X(B+2CpH)}{K_s+S}\right]\times\left(\frac{\partial pH}{\partial S_0}\right) \quad \text{(A20)}$$

$$\frac{d}{dt}\left(\frac{\partial X}{\partial S_b}\right)=\left(\frac{\mu_m S(A+BpH+CpH^2)}{K_s+S}-D-D_1\right)\times\left(\frac{\partial X}{\partial S_b}\right)+\left[\frac{\mu_m X.K_s(A+BpH+CpH^2)}{(K_s+S)^2}\right]\times\left(\frac{\partial S}{\partial S_b}\right)+\left[\frac{\mu_m S.X(B+2CpH)}{K_s+S}\right]\times\left(\frac{\partial pH}{\partial S_b}\right) \quad \text{(A21)}$$

$$\frac{d}{dt}\left(\frac{\partial S}{\partial D}\right) = -\left(\frac{\mu_m S K_s(A+BpH+CpH^2)}{(K_s+S)^2 Y_{X/S}}\right) \times \left(\frac{\partial X}{\partial D}\right) - \left[D + D_1 + \frac{\mu_m X.K_s(A+BpH+CpH^2)}{(K_s+S)^2}\right] \times \left(\frac{\partial S}{\partial D}\right) - \left[\frac{\mu_m SX(B+2CpH)}{(K_s+S)Y_{X/S}}\right] \times \left(\frac{\partial pH}{\partial D}\right) + (S_0 + S) \quad \text{(A22)}$$

$$\frac{d}{dt}\left(\frac{\partial S}{\partial D_1}\right) = -\left(\frac{\mu_m S K_s(A+BpH+CpH^2)}{(K_s+S)^2 Y_{X/S}}\right) \times \left(\frac{\partial X}{\partial D_1}\right) - \left[D + D_1 + \frac{\mu_m X.K_s(A+BpH+CpH^2)}{(K_s+S)^2}\right] \times \left(\frac{\partial S}{\partial D_1}\right) - \left[\frac{\mu_m SX(B+2CpH)}{(K_s+S)Y_{X/S}}\right] \times \left(\frac{\partial pH}{\partial D_1}\right) - S \quad \text{(A23)}$$

$$\frac{d}{dt}\left(\frac{\partial S}{\partial S_0}\right) = -\left(\frac{\mu_m S K_s(A+BpH+CpH^2)}{(K_s+S)^2 Y_{X/S}}\right) \times \left(\frac{\partial X}{\partial S_0}\right) - \left[D + D_1 + \frac{\mu_m X.K_s(A+BpH+CpH^2)}{(K_s+S)^2}\right] \times \left(\frac{\partial S}{\partial S_0}\right) - \left[\frac{\mu_m SX(B+2CpH^2)}{(K_s+S)Y_{X/S}}\right] \times \left(\frac{\partial pH}{\partial S_0}\right) + D \quad \text{(A24)}$$

$$\frac{d}{dt}\left(\frac{\partial S}{\partial S_b}\right) = -\left(\frac{\mu_m S K_s(A+BpH+CpH^2)}{(K_s+S)^2 Y_{X/S}}\right) \times \left(\frac{\partial X}{\partial S_b}\right) - \left[D + D_1 + \frac{\mu_m X.K_s(A+BpH+CpH^2)}{(K_s+S)^2}\right] \times \left(\frac{\partial S}{\partial S_b}\right) - \left[\frac{\mu_m SX(B+2CpH^2)}{(K_s+S)Y_{X/S}}\right] \times \left(\frac{\partial pH}{\partial S_b}\right) \quad \text{(A25)}$$

$$\frac{d}{dt}\left(\frac{\partial p}{\partial D}\right) = \left(\frac{Y_{P/X}\mu_m S(A+BpH+CpH^2)}{M_a \times (K_s+S)}\right) \times \left(\frac{\partial X}{\partial D}\right) + \left[\frac{Y_{P/X}\mu_m X.K_s(A+BpH+CpH^2)}{M_a(K_s+S)}\right] \times \left(\frac{\partial S}{\partial D}\right) - [D + D_1] \times \left(\frac{\partial p}{\partial D}\right) + \left[\frac{Y_{P/X}\mu_m SX(B+2CpH)}{M_a(K_s+S)}\right] \times \left(\frac{\partial pH}{\partial D}\right) - p \quad \text{(A26)}$$

$$\frac{d}{dt}\left(\frac{\partial p}{\partial D_1}\right) = \left(\frac{Y_{P/X}\mu_m S(A+BpH+CpH^2)}{M_a \times (K_s+S)}\right) \times \left(\frac{\partial X}{\partial D_1}\right) + \left[\frac{Y_{P/X}\mu_m X.K_s(A+BpH+CpH^2)}{M_a(K_s+S)}\right] \times \left(\frac{\partial S}{\partial D_1}\right) - [D + D_1] \times \left(\frac{\partial p}{\partial D_1}\right) + \left[\frac{Y_{P/X}\mu_m SX(B+2CpH)}{M_a(K_s+S)}\right] \times \left(\frac{\partial pH}{\partial D_1}\right) - (s_b + p) \quad \text{(A27)}$$

$$\frac{d}{dt}\left(\frac{\partial p}{\partial S_0}\right) = \left(\frac{Y_{P/X}\mu_m S(A+BpH+CpH^2)}{M_a \times (K_s+S)}\right) \times \left(\frac{\partial X}{\partial S_0}\right) + \left[\frac{Y_{P/X}\mu_m X.K_s(A+BpH+CpH^2)}{M_a(K_s+S)}\right] \times \left(\frac{\partial S}{\partial S_0}\right) - [D + D_1] \times \left(\frac{\partial p}{\partial S_0}\right) + \left[\frac{Y_{P/X}\mu_m SX(B+2C\times p)}{M_a(K_s+S)}\right] \times \left(\frac{\partial pH}{\partial S_0}\right) \quad \text{(A28)}$$

$$\frac{d}{dt}\left(\frac{\partial p}{\partial S_b}\right) = \left(\frac{Y_{P/X}\mu_m S(A+BpH+CpH^2)}{M_a \times (K_s+S)}\right) \times \left(\frac{\partial X}{\partial S_b}\right) + \left[\frac{Y_{P/X}\mu_m X.K_s(A+BpH+CpH^2)}{M_a(K_s+S)}\right] \times \left(\frac{\partial S}{\partial S_b}\right) - [D + D_1] \times \left(\frac{\partial p}{\partial S_0}\right) + \left[\frac{Y_{P/X}\mu_m SX(B+2C\times p)}{M_a(K_s+S)}\right] \times \left(\frac{\partial pH}{\partial S_0}\right) - D_1 \quad \text{(A29)}$$

$$\frac{d}{dt}\left(\frac{\partial s_A}{\partial D}\right) = -[D + D_1] \times \left(\frac{\partial s_A}{\partial D}\right) - s_A \quad \text{(A30)}$$

$$\frac{d}{dt}\left(\frac{\partial s_A}{\partial D_1}\right) = -[D + D_1] \times \left(\frac{\partial s_A}{\partial D_1}\right) - (s_b - s_A) \quad \text{(A31)}$$

$$\frac{d}{dt}\left(\frac{\partial s_A}{\partial S_0}\right) = -[D + D_1] \times \left(\frac{\partial s_A}{\partial S_0}\right) \tag{A32}$$

$$\frac{d}{dt}\left(\frac{\partial s_A}{\partial S_b}\right) = -[D + D_1] \times \left(\frac{\partial s_A}{\partial S_b}\right) \tag{A33}$$

$$\frac{d}{dt}\left(\frac{\partial pH}{\partial D}\right) = \left(\frac{Y_{P/X}\mu_m S(A+BpH+CpH^2)}{M_a \times (K_s+S)p}\right) \times \left(\frac{\partial X}{\partial D}\right) - \left[\frac{Y_{P/X}\mu_m X.K_s(A+BpH+CpH^2)}{M_a(K_s+S)^2 p}\right] \times \left(\frac{\partial S}{\partial D}\right) + \left[\frac{1}{p^2}\frac{dp}{dt} + \frac{1}{p}(D + D_1)\right] \times \left(\frac{\partial p}{\partial D}\right) - \left[\frac{1}{s_A^2}\frac{ds_A}{dt} + \frac{1}{s_A}(D + D_1)\right] \times \left(\frac{\partial s_A}{\partial D}\right) - \left[\frac{Y_{P/X}\mu_m SX(B+2CpH)}{M_a(K_s+S)p}\right] \times \left(\frac{\partial pH}{\partial D}\right) \tag{A34}$$

$$\frac{d}{dt}\left(\frac{\partial pH}{\partial D_1}\right) = \left(\frac{Y_{P/X}\mu_m S(A+BpH+CpH^2)}{M_a \times (K_s+S)p}\right) \times \left(\frac{\partial X}{\partial D_1}\right) - \left[\frac{Y_{P/X}\mu_m X.K_s(A+BpH+CpH^2)}{M_a(K_s+S)^2 p}\right] \times \left(\frac{\partial S}{\partial D_1}\right) + \left[\frac{1}{p^2}\frac{dp}{dt} + \frac{1}{p}(D + D_1)\right] \times \left(\frac{\partial p}{\partial D_1}\right) - \left[\frac{1}{s_A^2}\frac{ds_A}{dt} + \frac{1}{s_A}(D + D_1)\right] \times \left(\frac{\partial s_A}{\partial D_1}\right) - \left[\frac{Y_{P/X}\mu_m SX(B+2CpH)}{M_a(K_s+S)p}\right] \times \left(\frac{\partial pH}{\partial D_1}\right) + \frac{1}{p}(s_b + p) \tag{A35}$$

$$\frac{d}{dt}\left(\frac{\partial pH}{\partial S_0}\right) = \left(\frac{Y_{P/X}\mu_m S(A+BpH+CpH^2)}{M_a \times (K_s+S)p}\right) \times \left(\frac{\partial X}{\partial S_0}\right) - \left[\frac{Y_{P/X}\mu_m X.K_s(A+BpH+CpH^2)}{M_a(K_s+S)^2 p}\right] \times \left(\frac{\partial S}{\partial S_0}\right) + \left[\frac{1}{p^2}\frac{dp}{dt} + \frac{1}{p}(D + D_1)\right] \times \left(\frac{\partial p}{\partial S_0}\right) - \left[\frac{1}{s_A^2}\frac{ds_A}{dt} + \frac{1}{s_A}(D + D_1)\right] \times \left(\frac{\partial s_A}{\partial S_0}\right) - \left[\frac{Y_{P/X}\mu_m SX(B+2CpH)}{M_a(K_s+S)p}\right] \times \left(\frac{\partial pH}{\partial S_0}\right) \tag{A36}$$

$$\frac{d}{dt}\left(\frac{\partial pH}{\partial S_b}\right) = \left(\frac{Y_{P/X}\mu_m S(A+BpH+CpH^2)}{M_a \times (K_s+S)p}\right) \times \left(\frac{\partial X}{\partial S_b}\right) - \left[\frac{Y_{P/X}\mu_m X.K_s(A+BpH+CpH^2)}{M_a(K_s+S)^2 p}\right] \times \left(\frac{\partial S}{\partial S_b}\right) + \left[\frac{1}{p^2}\frac{dp}{dt} + \frac{1}{p}(D + D_1)\right] \times \left(\frac{\partial p}{\partial S_b}\right) - \left[\frac{1}{s_A^2}\frac{ds_A}{dt} + \frac{1}{s_A}(D + D_1)\right] \times \left(\frac{\partial s_A}{\partial S_b}\right) - \left[\frac{Y_{P/X}\mu_m SX(B+2CpH)}{M_a(K_s+S)p}\right] \times \left(\frac{\partial p}{\partial S_b}\right) \tag{A37}$$

The components of matrix A in equation 4.69

$$a_{11} = \frac{x_2\left(1-\frac{x_4}{x_4^*}\right)^n\left(1-\frac{x_2}{x_2^*}\right)^m}{X_2+1} - d_1$$

$$a_{12} = \frac{x_1\left(1-\frac{x_2}{x_2^*}\right)^m\left(1-\frac{x_4}{x_4^*}\right)^n}{x_2+1} - \frac{x_1x_2\left(1-\frac{x_2}{x_2^*}\right)^m\left(1-\frac{x_4}{x_4^*}\right)^n}{(x_2+1)^2} - \frac{m\cdot x_1x_2\left(1-\frac{x_4}{x_4^*}\right)^n\left(1-\frac{x_2}{x_2^*}\right)^{m-1}}{x_2^*(x_2+1)}$$

$$a_{13} = 0$$

$$a_{14} = -\frac{n.x_1.x_2\left(1-\frac{x_4}{x_4^*}\right)^{(n-1)}\left(1-\frac{x_2}{x_2^*}\right)^m}{x_4^*(x_2+1)}$$

$$a_{21} = -\frac{X_2\left(1-\frac{x_4}{x_4^*}\right)^n\left(1-\frac{x_2}{x_2^*}\right)^m}{X_2+1}$$

$$a_{22} = \frac{X_1X_2\left(1-\frac{x_2}{x_2^*}\right)^m\left(1-\frac{x_4}{x_4^*}\right)^n}{(X_2+1)^2} - \frac{X_1\left(1-\frac{x_2}{x_2^*}\right)^m\left(1-\frac{x_4}{x_4^*}\right)^n}{X_2+1} - d_1 + \frac{m\cdot X_1X_2\left(1-\frac{x_4}{x_4^*}\right)^n\left(1-\frac{x_2}{x_2^*}\right)^{m-1}}{x_2^*(X_2+1)}$$

$$a_{23} = 0$$

$$a_{24} = \frac{n.X_1.X_2\left(1-\frac{x_4}{x_4^*}\right)^{(n-1)}\left(1-\frac{x_2}{x_2^*}\right)^m}{x_4^*(X_2+1)}$$

$$a_{31} = \frac{X_2\left(1-\frac{x_4}{x_4^*}\right)^n\left(1-\frac{x_2}{x_2^*}\right)^m}{X_2+1}$$

$$a_{32} = \frac{X_1\left(1-\frac{x_2}{x_2^*}\right)^m\left(1-\frac{x_4}{x_4^*}\right)^n}{X_2+1} - \frac{X_1X_2\left(1-\frac{x_2}{x_2^*}\right)^m\left(1-\frac{x_4}{x_4^*}\right)^n}{(X_2+1)^2} - \frac{m\cdot X_1X_2\left(1-\frac{x_4}{x_4^*}\right)^n\left(1-\frac{x_2}{x_2^*}\right)^{m-1}}{x_2^*(X_2+1)}$$

$$a_{33} = -d_1 - K$$

$$a_{34} = K.\alpha - \frac{n.X_1.X_2\left(1-\frac{x_4}{x_4^*}\right)^{(n-1)}\left(1-\frac{x_2}{x_2^*}\right)^m}{x_4^*(X_2+1)}$$

$$a_{41} = 0$$

$$a_{42} = 0$$

$$a_{43} = K$$

$$a_{41} = -d_2 - K.$$

Appendix 3

The time history of dry cell concentrations of *Lactobacillus casei* when pH at each batch reaction was varied initially.

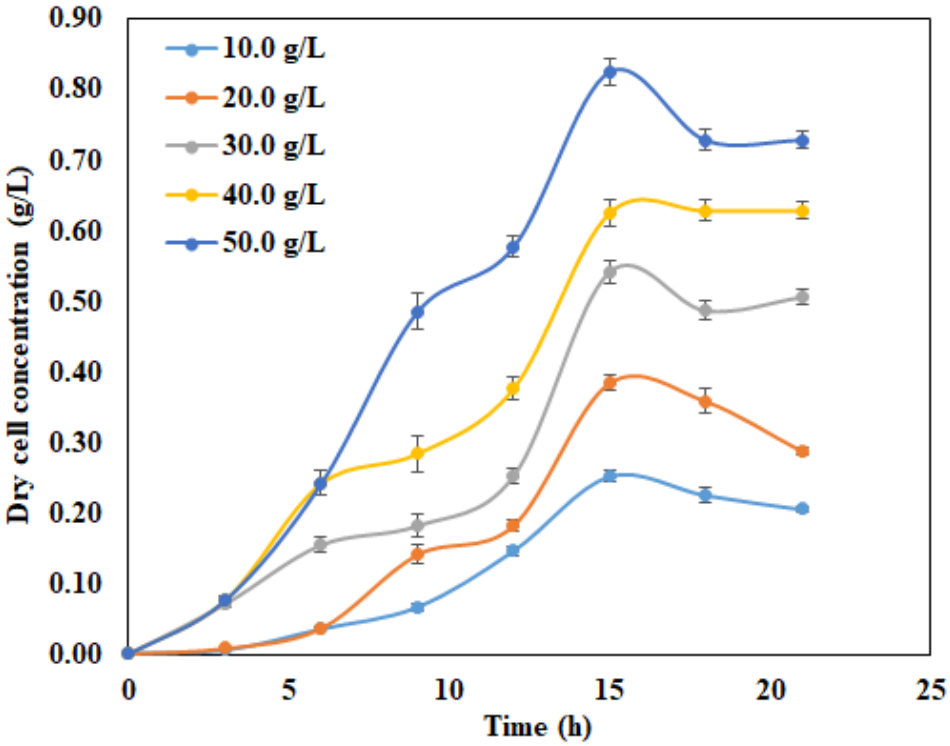

Figure A-1 Experimental time histories of dry cell concentration (g/L) at an initial value of pH=5

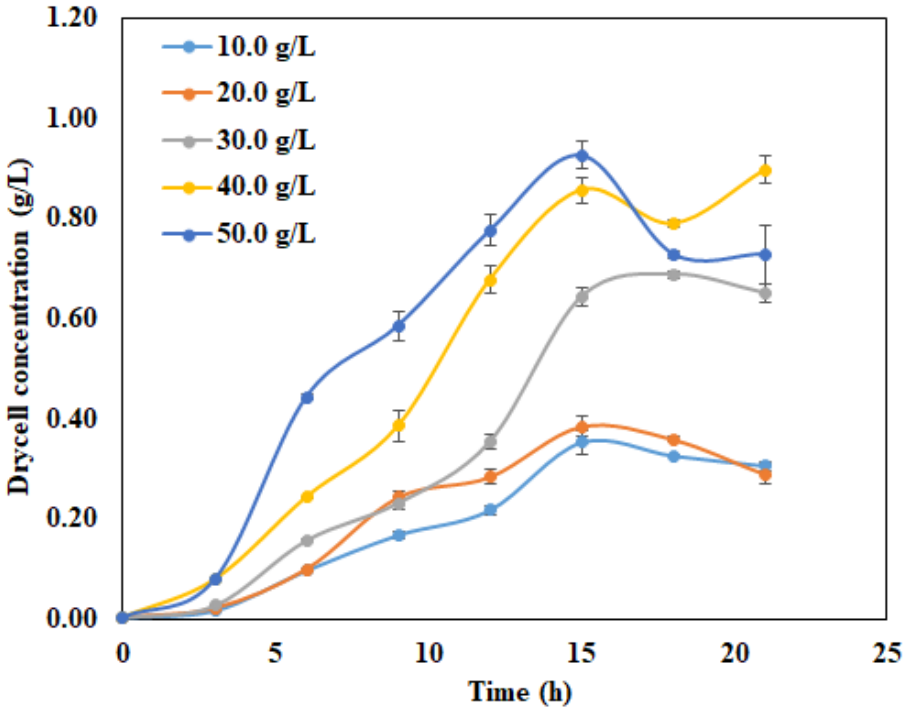

Figure A-2 Experimental time histories of dry cell concentration (g/L) at an initial value of pH=5.5

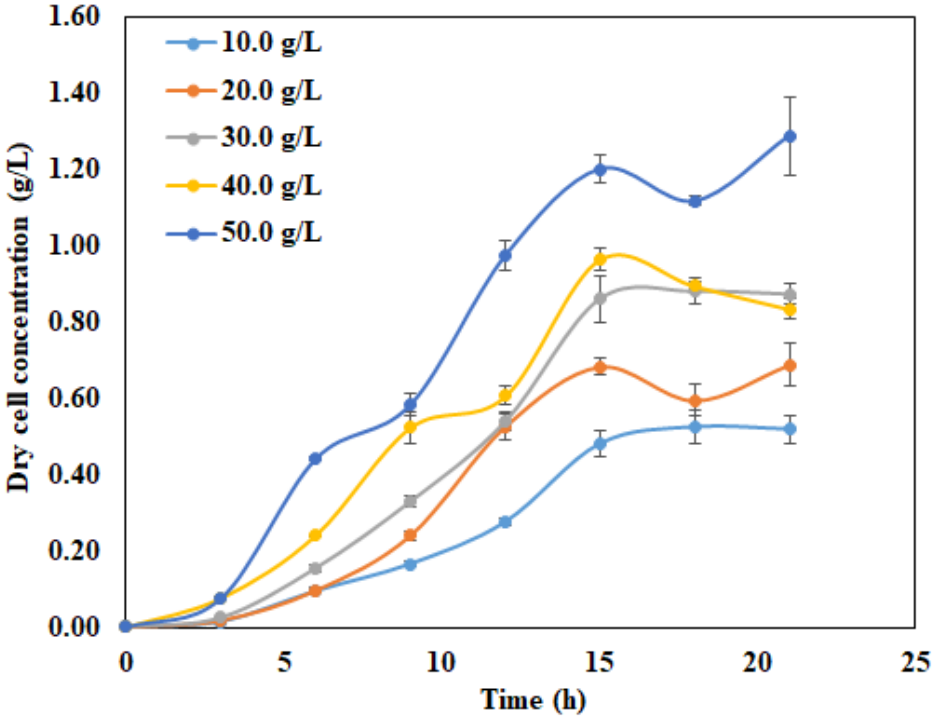

Figure A-3 Experimental time histories of dry cell concentration (g/L) at an initial value of pH=6.0

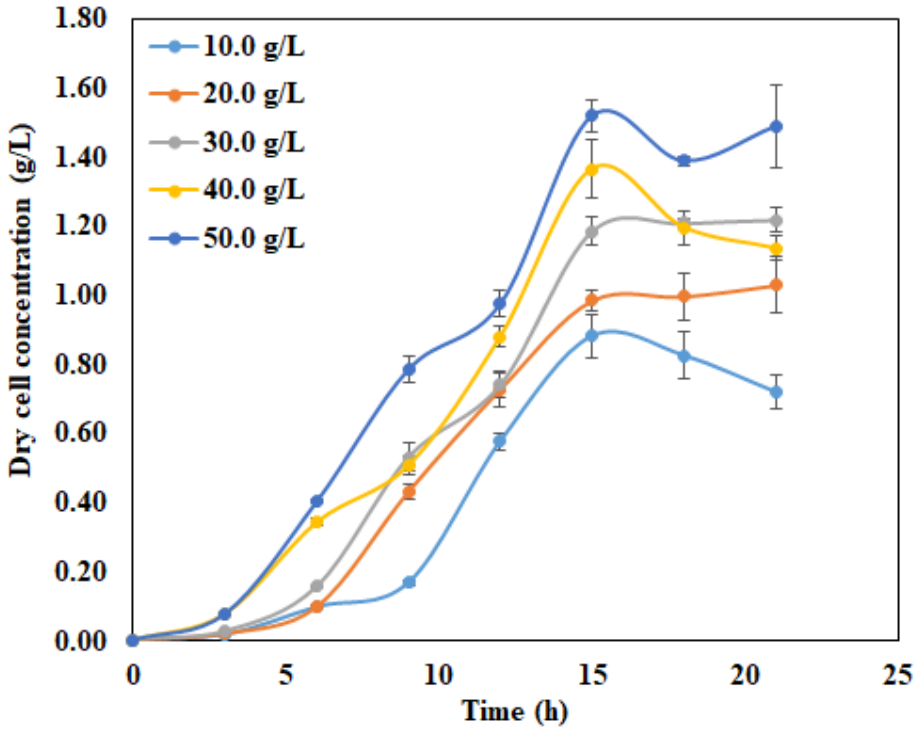

Figure A-4 Experimental time histories of dry cell concentration (g/L) at an initial value of pH=6.5

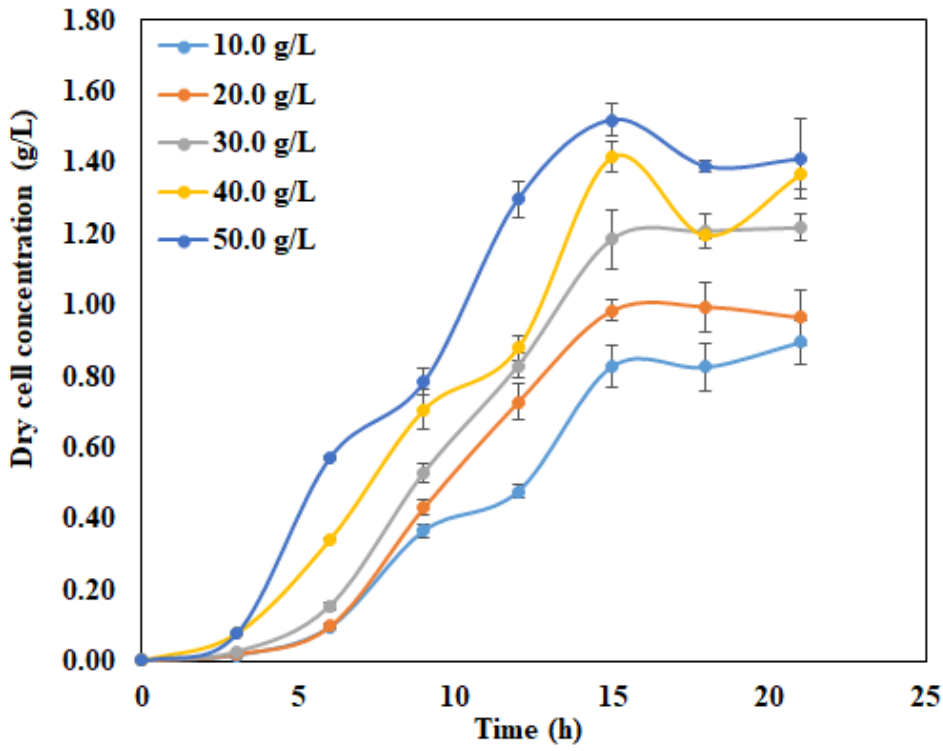

Figure A-5 Experimental time histories of dry cell concentration (g/L) at an initial value of pH=7.0

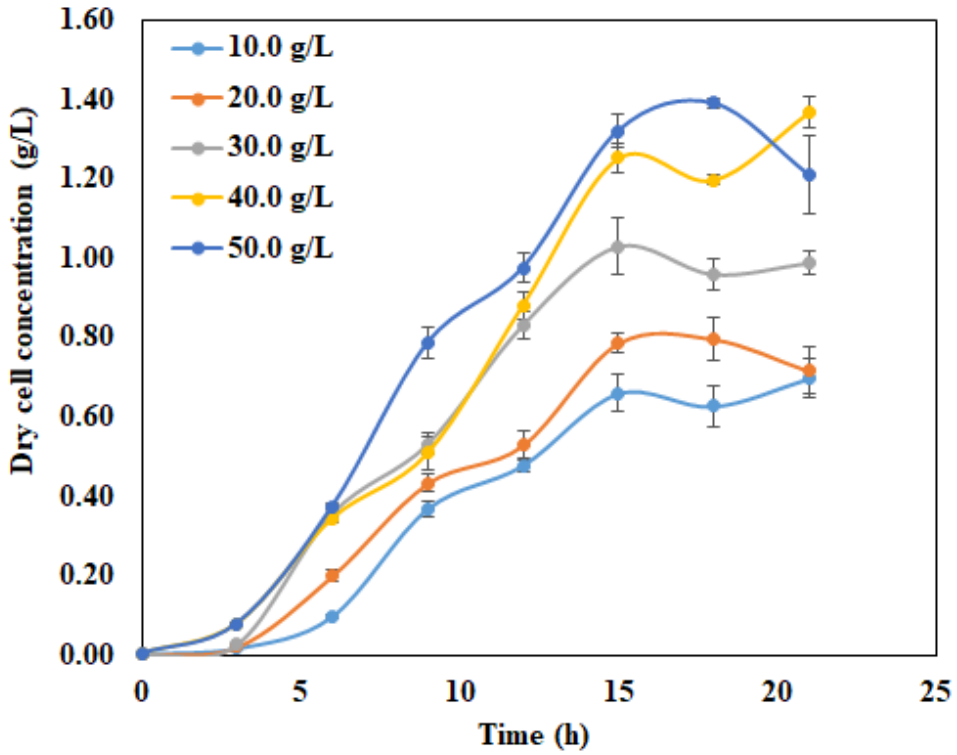

Figure A-6 Experimental time histories of dry cell concentration (g/L) at an initial value of pH=7.5

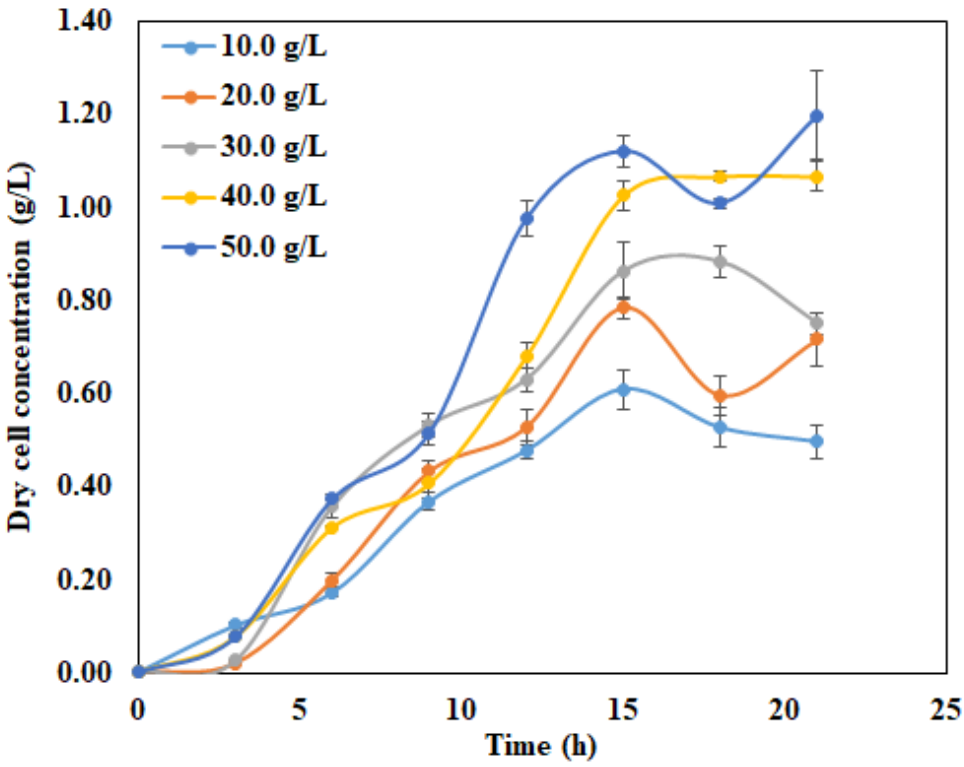

Figure A-7 Experimental time histories of dry cell concentration (g/L) at an initial value of pH=8.0